FY22 NRL DOD HPCMP ANNUAL REPORTS

U.S. NAVAL RESEARCH LABORATORY

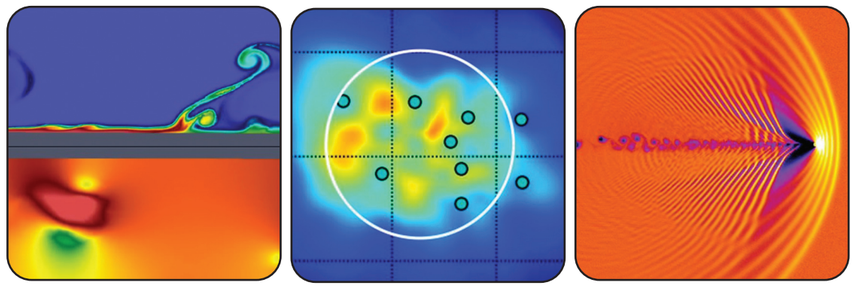
FY22 NRL DoD High Performance Computing Modernization Program Annual Reports

Edited by
Bonnie J. Assad

Prepared by
Beth A. Howell

Center for Computational Science
Information Technology Division

November 1, 2023



Distribution Statement A. Approved for public release. Distribution unlimited.

REVIEWED AND APPROVED
NRL/PU/5594--23-673
IR-5594-23-1-U
November 2023

Center for Computational Science
Information Technology Division

Introduction

This book is a compilation of reports on all the work accomplished by NRL scientists, engineers, and their collaborators using the DoD High Performance Computing Modernization Program's (HPCMP) resources for fiscal year 2022. The reports encompass work performed by researchers at all three NRL sites: Washington, DC, Stennis Space Center, Mississippi, and Monterey, California.

These reports are categorized according to the primary Computational Technology Area (CTA) as specified by the HPCMP and include resources at the DOD Supercomputing Resource Centers (DSRC) as well as the Affiliated Resource Centers (ARC). This volume includes three indices for ease of reference: an author index, a site index, and an NRL hierarchical index of reports from the branches and divisions in the Laboratory.

THIS PAGE INTENTIONALLY LEFT BLANK

Table of Contents

Computational Structural Mechanics (CSM)

Atomistic Simulations of Structural Materials 2
E. Antillon
U.S. Naval Research Laboratory, Washington, DC

Computational Analysis of Warfighter Brain Injury and Protective Equipment 4
X.G. Tan and R.N. Saunders
U.S. Naval Research Laboratory, Washington, DC

Stochastic Methods for Uncertainty Quantification in Computational Mechanics 6
L.P. Kuna,[2] K. Teferra,[1] and R.N. Saunders[1]
[1] U.S. Naval Research Laboratory, Washington, DC
[2]National Research Council Postdoctoral Research Associate, U. S. Naval Research Laboratory, Washington, DC

Geometric, Constitutive and Loading Complexities in Structural Materials 8
S.A. Wimmer,[1] R.N. Saunders,[1] A. Arcari,[1] L.P. Kuna,[2] and J.G. Michopoulos[1]
[1]U.S. Naval Research Laboratory, Washington, DC
[2] National Research Council Postdoctoral Associate, U.S. Naval Research Laboratory, Washington, DC

Computational Fluid Dynamics (CFD)

Simulations of Laser-plasma Interactions and the Radiation Hydrodynamics of High-velocity Laser-accelerated Matter 12
J.W. Bates and K. Obenschain
U.S. Naval Research Laboratory, Washington, DC

Modeling of Detonations in Jet Fuel Sprays 14
V.N. Gamezo[1] and A.Y. Poludnenko[2]
[1]U.S. Naval Research Laboratory, Washington, DC
[2]University of Connecticut, Storrs, CT

Airbreathing Combustion for Hypersonics 16
G. Goodwin
U.S. Naval Research Laboratory, Washington, DC

Multidimensional Chemically Reacting Fluid Dynamics with Application to Flameless Combustors 18
R.F. Johnson
U.S. Naval Research Laboratory, Washington, DC

High-Fidelity CFD Simulations of High-Speed Flows in Realistic Atmospheric Conditions.....20
D.A. Kessler, R.F. Johnson, A.M. Hess, and B.T. Bojko
U.S. Naval Research Laboratory, Washington, DC

Jet Noise Reduction Studies.....22
Y. Khine
U.S. Naval Research Laboratory, Washington, DC

Numerical Investigation of Advanced Military Aircraft Noise Reduction Concepts.....24
J. Liu
U.S. Naval Research Laboratory, Washington, DC

Aircraft Engine Noise Reduction Technology.....26
J. Liu
U.S. Naval Research Laboratory, Washington, DC

Numerical Simulations of Turbulence Impact on Optical Signal Transmission and Near-Surface Turbulence.....28
S. Matt
U.S. Naval Research Laboratory, Stennis Space Center, MS

Predicting Fluid-Structure Interaction for Military Applications.....30
D.R. Mott and Y. Khine
U.S. Naval Research Laboratory, Washington, DC

Developing a Shallow Water Environmental Database for Nearshore Operations ..32
A.M. Penko, K. Edwards, S. Harrison, R. Phillip, S. Schoenauer, and J. Veeramony
U.S. Naval Research Laboratory, Stennis Space Center, MS

Detonations with Multi-Phase Flows for Propulsion.....34
D.A. Schwer
U.S. Naval Research Laboratory, Washington, DC

Direct Numerical Simulation of Fluid-Sediment Wave Bottom Boundary Layer.....36
S. Schoenauer,[1] A.M. Penko,[1] J.A. Simeonov,[1] I. Adams,[2] S.P. Bateman,[1] J. Calantoni,[1] K. Edwards,[1] W. Kearney,[3] R. Phillip,[1] and J. Veeramony[1]
[1]U.S. Naval Research Laboratory, Stennis Space Center, MS
[2]National Research Council Postdoctoral Fellow, Stennis Space Center, MS
[3]American Society for Engineering Education Postdoctoral Fellow, Stennis Space Center, MS

Numerical Simulations of Noise Generated by Non-Circular Advanced Military Aircraft Nozzles.....38
K. Viswanath and R. Ramamurti
U.S. Naval Research Laboratory, Washington, DC

Towards Simulation of Solid Fuel Combustion using Detailed and Reduced Order Modeling Approaches 40
B.T. Bojko
U.S. Naval Research Laboratory, Washington, DC

Simulations of the Ionosphere/Plasmasphere/Thermosphere System 42
J. Krall,[1] and J.D. Huba[2]
[1]*U.S. Naval Research Laboratory, Washington, DC*
[2]*Syntek Technologies, Fairfax, VA*

Applications of FEFLO Incompressible Flow Solver 44
R. Ramamurti
U.S. Naval Research Laboratory, Washington, DC

Mitigation of Blasts in Enclosures 46
D.A. Schwer
U.S. Naval Research Laboratory, Washington, DC

Computational Biology, Chemistry, and Materials Science (CCM)

Multiple Length and Time Scale Simulations of Material Properties 50
N. Bernstein
U.S. Naval Research Laboratory, Washington, DC

Surfaces and Interfaces in Oxides and Semiconductors 52
C.S. Hellberg
U.S. Naval Research Laboratory, Washington, DC

Marine Biofilm Metaproteomics 54
W.J. Hervey and G.J. Vora
U.S. Naval Research Laboratory, Washington, DC

Synthetic Biology for Military Environments 56
W.J. Hervey, S.M. Colston, J.R. Compton, D.H. Leary, Z. Wang, L.J. Bird, T. Tschirhart, and G.J. Vora
U.S. Naval Research Laboratory, Washington, DC

New Method for Calculation of Solid-Phase Heat of Formation Using Intermolecular Interactions in Crystal Structures 58
I.D. Giles and G.H. Imler
U.S. Naval Research Laboratory, Washington, DC

Materials for Energy Storage and Generation 60
M. Johannes
U.S. Naval Research Laboratory, Washington, DC

DFT-Calculated IR Absorption Spectra for PFAS Molecules.....62
S. Lambrakos and A. Shabaev
U.S. Naval Research Laboratory, Washington, DC

Calculation of Materials Properties Via Density Functional Theory and Its Extensions.....64
J.L. Lyons
U.S. Naval Research Laboratory, Washington, DC

Materials Properties of Surfaces and Two-dimensional Systems.....66
M. Phillips
U.S. Naval Research Laboratory Voluntary Emeritus Program, Washington, DC

Numerical Studies of Semiconductor Nanostructures.....68
T.L. Reinecke[1] and I. Welland[2]
[1]U.S. Naval Research Laboratory, Washington DC
[2]National Research Council Postdoctoral Research Associate, U.S. Naval Research Laboratory, Washington DC

First-principles Simulations of Condensed-phase Decomposition of Energetic Materials.....70
I.V. Schweigert
U.S. Naval Research Laboratory, Washington, DC

Crystal Properties of Explosives from Quantum Molecular Dynamics 72
I.V. Schweigert
U.S. Naval Research Laboratory, Washington, DC

Molecular and Quantum Dynamics of Biomolecule-nanostructure Interaction 74
K. Whitener
U.S. Naval Research Laboratory, Washington, DC

Point Defects and Interfaces in Two-Dimensional Materials 76
D. Wickramaratne
U.S. Naval Research Laboratory, Washington, DC

Computation of Refractive Indices and Birefringence in Novel Polyimide Optical Polymers.....78
G. Kushto and A. Rosenberg
U.S. Naval Research Laboratory, Washington, DC

Atomistic Simulations of Navy-relevant Materials.....80
D. Fragiadakis
U.S. Naval Research Laboratory, Washington, DC

Engineering Phase Change Materials for Neuromorphic Photonic Applications 82
J.G. Champlain[1] and K.A. Cooley[2]
[1]U.S. Naval Research Laboratory, Washington, DC
[2]National Research Council Postdoctoral Research Associate, U.S. Naval Research Laboratory, Washington, DC

DFT Studies of Small Molecule Adsorption on Monolayer Transition Metal Dichalcogenide Films 84
F.K. Perkins[1] and C.H. Sharp[2]
[1]U.S. Naval Research Laboratory, Washington, DC; [2]National Research Council Postdoctoral Research Associate, U.S. Naval Research Laboratory, Washington, DC

Computational Electromagnetics and Acoustics (CEA)

Pinched-beam Diode Particle in Cell Simulations 88
J.C. Foster,[1] S.B. Swanekamp,[2] and P.E. Adamson[2]
[1]Air Force Institute of Technology, Wright-Patterson AFB, OH
[2]U.S. Naval Research Laboratory, Washington, DC

Parallel Cylindrical Reflex Triode (CTR) Particle in Cell (PIC) Simulations 90
I.M. Rittersdorf, B.V. Weber, S.B. Swanekamp, and P.E. Adamson
U.S. Naval Research Laboratory, Washington, DC

Small-Slope Approximation (SSA) Rough-Surface Backscattering Analysis 92
J. Alatishe
U.S. Naval Research Laboratory, Washington, DC

Acoustic Parameter Variability over an Ocean Reanalysis (AVORA).....94
J.P. Fabre
U.S. Naval Research Laboratory, Stennis Space Center, MS

Simulation of Passively Model-Locked and Frequency-Modulated Intraband Cascade Laser Frequency Combs 96
M. Povolotskyi,[1] I. Vurgaftman,[2] and J.R. Meyer[2]
[1]Jacobs, Hanover MD
[2]U.S. Naval Research Laboratory, Washington DC

Molecular Dynamics Simulations and Electric Micro-field Distribution in Two-component Plasmas.....98
G.M. Petrov
U.S. Naval Research Laboratory, Washington, DC

Low Grazing Angle Radar Backscatter.....100
J.V. Toporkov, M.A. Sletten, and J.D. Ouelette
U.S. Naval Research Laboratory, Washington, DC

Underwater Electrical Impedance Tomography 102
G.R. Gatling and E.M. Tejero
U.S. Naval Research Laboratory, Washington, DC

Climate Weather Ocean Modeling (CWO)

Coupled Ocean-Wave-Air-Ice Prediction System.....106
R. Allard,[1] T. Campbell,[1] E. Douglass,[1] K. Edwards,[1] D. Hebert,[1] T. Jensen,[1] A. Rydbeck,[1] T. Smith,[1] J. Veeramony,[1] and M. Phelps[2]
[1]Naval Research Laboratory, Stennis Space Center, MS
[2]Peraton, Inc., Stennis Space Center, MS

Multi-scale Characterization and Prediction of the Global Atmosphere from Ground to the Edge of Space using Next-Generation Navy Modeling Systems.....108
C.A. Barton, S.D. Eckermann, J.F. Kelly, M.A. Herrera, K.W. Hoppel, D.D. Kuhl, D.R. Allen, J. Ma, and T. Rhodes
[1]U.S. Naval Research Laboratory, Washington DC

COAMPS-TC® Tropical Cyclone Rapid Intensification Prediction 110
J.D. Doyle
U.S. Naval Research Laboratory, Monterey, CA

Turbulent Mixing in NCOM and HYCOM.....112
Y. Fan
U.S. Naval Research Laboratory, Stennis Space Center, MS

Coupled Ocean-Wave-Air-Ice Prediction System.....114
T. Jensen,[1] A. Rydbeck,[1] H. Wijesekera,[1] C. Luecke,[1] D. Wang,[1] M. Flatau,[2] and T. Campbell[1]
[1]U.S. Naval Research Laboratory, Stennis Space Center, MS
[2]U.S. Naval Research Laboratory, Monterey, CA

Bio-Optical Modeling and Forecasting 116
J.K. Jolliff, S. Ladner, and T. Smith
U.S. Naval Research Laboratory, Stennis Space Center, MS

Investigation and Implementation of GPU Capability to Next Generation Weather Prediction Code, NEPTUNE.....118
Y. Khine
U.S. Naval Research Laboratory, Washington, DC

Coastal Mesoscale Modeling 120
W.A. Komaromi and P.A. Reinecke
U.S. Naval Research Laboratory, Monterey, CA

Eddy-Resolving Global/Basin-Scale Ocean Modeling – Artic OSSE.....122
E. Douglass
U.S. Naval Research Laboratory, Stennis Space Center, MS

Eddy-Resolving Global/Basin-Scale Ocean Modeling – Global Ocean Reanalysis 124
E.J. Metzger and L. Zamudio
U.S. Naval Research Laboratory, Stennis Space Center, MS

Eddy-Resolving Global/Basin-Scale Ocean Modeling – Internal Tides 126
J.F. Shriver, R.W. Helber, and E.J. Metzger
U.S. Naval Research Laboratory, Stennis Space Center, MS

Eddy-Resolving Global/Basin-Scale Ocean Modeling – Large Scale Prediction.....128
E.J. Metzger and L. Zamudio
U.S. Naval Research Laboratory, Stennis Space Center, MS

Eddy-Resolving Global/Basin-Scale Ocean Modeling – Sea Ice Assimilation 130
D. Hebert,[1] J. May,[1] T. Townsend,[1] M. Phelps[2]
[1]U.S. Naval Research Laboratory, Stennis Space Center, MS
[2]Peraton, Inc., Stennis Space Center, MS

Eddy-Resolving Global/Basin-Scale Ocean Modeling – South China Sea 132
E.J. Metzger and Z. Yu
U.S. Naval Research Laboratory, Stennis Space Center, MS

Eddy-Resolving Global/Basin-Scale Ocean Modeling – Winter Convective Mixing 134
P. Thoppil
U.S. Naval Research Laboratory, Stennis Space Center, MS

Rogue Wave Probability Estimator for WAVEWATCH III®.....136
M. Orzech
U.S. Naval Research Laboratory, Stennis Space Center, MS

Dynamics of Coupled Models 138
I. Shulman, B. Penta, and S. Cayula
U.S. Naval Research Laboratory, Stennis Space Center, MS

Ocean Data Assimilation – Deterministic and Predictability of Mid-Frequency Acoustic Ducts 140
J.J. Osborne,[1] C.M. Amos,[2] and G.A. Jacobs[1]
[1]U.S. Naval Research Laboratory, Stennis Space Center, MS
[2]American Society for Engineering Education, Stennis Space Center, MS

Ocean Data Assimilation – GHOST and Multi-Scale/Multi-Physics 142
J. D'Addezio,[1] G. Jacobs,[1] C. Barron,[1] L. Smedstad,[1] S. Smith,[1] J. Crout,[3] R. Linzell,[3] I. Souopgui,[2] M. Carrier,[1] C. DeHaan,[4] and H. Ngodock[1]
[1]U.S. Naval Research Laboratory, Stennis Space Center, MS
[2]University of New Orleans, Stennis Space Center, MS
[3] Peraton Inc., Stennis Space Center, MS

Ocean Data Assimilation – NCODA-4DVAR.....144
M. Carrier,[1] S. Smith,[1] J. D'Addezio,[1] H. Ngodock,[1] J. Osborne,[1] I. Souopgui,[2] V. Montiforte,[3] C. Amos,[3] and C. Rowley[1]
[1]U. S. Naval Research Laboratory, Stennis Space Center, MS
[2] University of New Orleans, Stennis Space Center, MS
[3]American Society for Engineering Education, Stennis Space Center, MS

Ocean Data Assimilation – NCODAv5 and ALPS.....146
J. D'Addezio,[1] S. Smith,[1] G. Jacobs,[1] M. Carrier,[1] J. Osborne,[1] I. Souopgui,[2] H. Ngodock,[1] V. Montiforte,[3] and C. Rowley[1]
[1]U.S. Naval Research Laboratory, Stennis Space Center, MS
[2] University of New Orleans, Stennis Space Center, MS
[3]American Society for Engineering Education, Stennis Space Center, MS

Ocean Data Assimilation 148
S. Smith,[1] J. D'Addezio,[1] J. Osborne,[1] I. Souopgui,[2], V. Montiforte,[3] M. Carrier,[1] G. Panteleev,[1] T. Townsend,[1] C. Amos,[3] S. DeRada,[1] L. Smedstad,[1] M. Phelps,[4] J. May,[1] R. Linzell,[4] E. Carr,[4] H. Ngodock,[1] and C. Rowley[1]
[1]U.S. Naval Research Laboratory, Stennis Space Center, MS
[2] University of New Orleans, Stennis Space Center, MS
[3]American Society for Engineering Education, Stennis Space Center, MS
[4] Peraton, Inc. Stennis Space Center, MS

Data Assimilation Studies Project 150
J. Tsu and W.F. Campbell
U.S. Naval Research Laboratory, Monterey, CA

Atmospheric Process Studies 152
T. Whitcomb,[1] N. Barton,[2] J. Christophersen,[3] W. Crawford,[1] M. Flatau,[1] K. Hansen,[3] M. Janiga,[1] M. Liu,[2] J. McLay,[1] J. Moskaitis,[1] C. Reynolds,[1] J. Ridout,[1] S. Rushley,[3] K. Viner,[2] S. Yang,[1] G. Carl,[4] and W. Davis[5]
[1]U.S. Naval Research Laboratory, Monterey, CA
[2]Departed/Retired from Naval Research Laboratory, Monterey, CA
[3]National Research Council, Monterey, CA
[4]SAIC, Monterey, CA
[5]DeVine Consulting, Monterey, CA

Signal Image Processing (SIP)

Applying Physics-based Machine Learning to Navy Problems 156
L.N. Smith
U.S. Naval Research Laboratory, Washington, DC

Space and Astrophysical Science (SAS)

Electromagnetic Pulses from Hypervelocity Impacts on Spacecraft 160
A. Fletcher
U.S. Naval Research Laboratory, Washington, DC

Global Kinetic Simulations of Space Plasma Waves and Turbulence 162
A. Fletcher
U.S. Naval Research Laboratory, Washington, DC

Modeling Propagation of Ionospheric Disturbances Initiated by Magnetospheric Substorms 164
J. Haiducek and J. Helmboldt
U.S. Naval Research Laboratory, Washington, DC

Navy Ionosphere Model for Operations 166
S.E. McDonald,[1] C.A. Metzler,[1] F. Sassi,[1] J.L. Tate,[2] M.R. Burleigh,[1] D. Hodyss[1]
[1]*U.S. Naval Research Laboratory, Washington, DC*
[2]*Computational Physics, Inc., Springfield, VA*

Searches for Millisecond Pulsars and Pulsar Emission Modeling.....168
P.S. Ray[1] and J. Deneva[2]
[1]*U.S. Naval Research Laboratory, Washington, DC*
[2]*George Mason University, Fairfax, VA*

Dynamic Phenomena in the Solar Atmosphere.....170
J.E. Unverferth
National Research Council Postdoctoral Fellow, U.S. Naval Research Laboratory, Washington, DC

Particle-in-Cell Simulations of Plasma Waves and Turbulence.....172
A.R. Soto-Chavez
U.S. Naval Research Laboratory, Washington, DC

Thermosphere & Ionosphere Numerical Models and Ensemble Methods 174
D.P. Drob, M. Jones, and J. Emmert
U.S. Naval Research Laboratory, Washington, DC

Other (OTH)

Simulation of High Energy-Radiation Environments 178
J. Finke and W. Duvall
U.S. Naval Research Laboratory, Washington, DC

Author Index 181

Division Index.....184

Site Index 187

CSM

Computational Structural Mechanics

CSM covers the high-resolution multidimensional modeling of materials and structures subjected to a broad range of loading conditions including quasistatic, dynamic, electromagnetic, shock, penetration, and blast. It also includes the highly interdisciplinary research area of materials design, where multiscale modeling from atomistic scale to macroscale is essential. CSM encompasses a wide range of engineering problems in solid mechanics, such as material or structural response to time- and history-dependent loading, large deformations, fracture propagation, shock wave propagation, isotropic and anisotropic plasticity, frequency response, and nonlinear and heterogeneous material behaviors. High-performance computing for CSM addresses the accurate numerical solution of conservation equations, equations of motion, equations of state, and constitutive relationships to model simple or complex geometries and material properties, subject to external boundary conditions and loads. CSM is used for basic studies in continuum mechanics, stress analysis for engineering design studies, predicting structural and material response to impulsive loads, and modeling response of heterogeneous embedded sensors/devices. DoD application areas include conventional underwater explosion and ship response, structural acoustics, coupled field problems, space debris, propulsion systems, structural analysis, total weapon simulation, weapon systems' lethality/survivability (e.g., aircraft, ships, submarines, and tanks), theater missile defense lethality analyses, optimization techniques, and real-time, large-scale soldier- and hardware-in-the-loop ground vehicle dynamic simulation.

Title: Atomistic Simulations of Structural Materials
Author(s): E. Antillon
Affiliation(s): U.S. Naval Research Laboratory, Washington, DC
CTA: CSM

Computer Resources: HPE SGI 8600 [AFRL, OH]; Cray XC40/50 [ERDC, MS]

Research Objectives: The objective is to understand atomistic processes that are responsible for mechanical strength and phase stability in structural materials, specifically steel alloys.

Methodology: Due to a large content of iron in the alloys of interest, spin-polarized calculations using density functional codes are necessary. We make use of Vienna Ab initio Simulation Package (VASP) to perform first-principles calculations that capture energetics and magneto-volume coupling of the system self-consistently. However, this approach is computationally intensive and limited to system on the order of 100 atoms or less. To explore larger systems, we make use of a molecular dynamic code (LAMMPS) that makes use of effective interatomic potentials to approximate energies and forces on similar systems. While this approach is less rigorous, it is much less computationally intensive and we can afford to simulate millions of atoms, which is necessary to capture long-range interaction between extensive defects (dislocations) and local defects (solutes, precipitates).

Results: We apply our computational resources to study a novel nanoprecipitate strengthened austenitic steel alloy: Fe-17.7Mn-10.0Ni-5.0Al-4.7Cr-4.0Cu-0.48C (wt.%), which has been shown (by our collaborators in Code 6356) to provide exceptional strength compared to current austenitic and ferritic steels used today for naval applications. We have carried out a series of atomistic-level calculations to calculate properties relevant to strength and phase stability that include bulk energies, point defects, and elastic properties of ordered and disordered phases relevant to the above system. Our atomistic results are validated against experiment by comparing the contribution of solute-solution to the overall yield strength of the alloy. For example, critical yield stresses can be predicted using an effective solute-solution strengthening model due to Varvenne et al., which uses solute “misfit volumes” as input parameters. While such parameters can be difficult to estimate experimentally, they can be measured straightforwardly using ab initio calculations. Figure 1 shows various predictions on resolved shear stress using different methods to estimate the input misfit volumes. The circle markers illustrate the yield stress using misfit volumes obtained using a reference from bulk-metallic glasses, the square markers make use of a high-throughput synthesis experiment on a high-entropy alloy to correlate volume changes due to various species, and the triangle markers make use of misfit volumes obtained using first-principles calculations. It is clear that the use of high-fidelity atomistic calculations can provide accurate measurements of material properties that are relevant to understanding strengthening mechanisms in highly complex alloys.

DoD Impact/Significance: The objectives above have immediate relevance for military interests. The problems of designing superior steel alloys are relevant to designing surface and underwater naval vessels. First-principles methods and surrogate methods using interatomic potentials provide necessary input parameters to connect modeling approaches at various length scales. Such a framework opens the possibility to combine computational and experimental methods to accelerate material discovery and to improve material performance for naval applications.

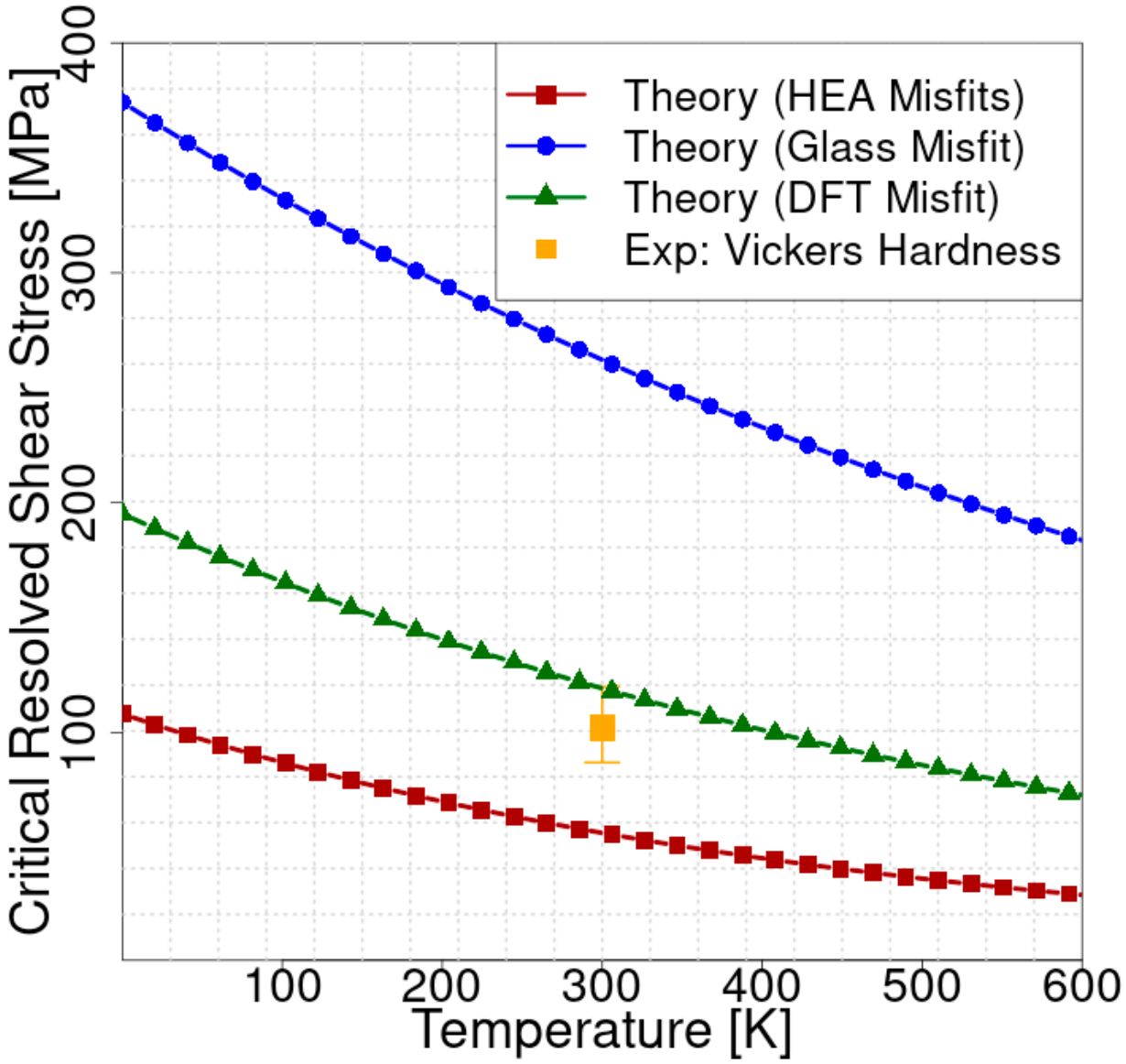


Figure 1. Comparison of predicted critical shear stress using various estimates of the misfit volumes as described in the text, and experimental measurement using an empirical relation between yield stress and Vickers harness.

Title: Computational Analysis of Warfighter Brain Injury and Protective Equipment
Author(s): X.G. Tan and R.N. Saunders
Affiliation(s): U.S. Naval Research Laboratory, Washington, DC
CTA: CSM

Computer Resources: HPE SGI 8600 [AFRL, OH], [NAVY, MS]; Cray Shasta [NAVY, MS]

Research Objectives: The research objective of this project is developing methods to prevent and mitigate injury to warfighters. This involves computational analysis of ballistic/blunt impacts on personal protective equipment (PPE) and blast-induced traumatic brain injury (TBI). Computational methods such as finite-element analysis are used to conduct the simulation analysis. The use of HPC resources is vitally important to this project due to the high fidelity of the models of interest. A typical model to analyze traumatic brain injury requires approximately 24 hours on 216 CPUs. One of the primary outcomes of this research will be the accumulation of a significant number of simulations that will be used to construct the correspondence relationship between humans and animals and to optimize the design of protective equipment.

Methodology: The project uses finite-element methods extensively, but the work is not restricted to finite-element methodologies. Nonlinear material mechanical constitutive response features are highlighted in much of the work performed. Implicit and explicit solution methods are used as appropriate. The primary finite-element codes used are Abaqus, CoBi and CTH. User subroutines are used for specialized material constitutive response when applicable. Multiphysics analysis is used to capture the fluid/acoustic-structure interaction, thermomechanical and electromagneto-mechanical effects. Typically, Abaqus/Viewer, ParaView, VisIt, IDL, Matlab are used for visualization of results in formats such as VTU and HDF5, including animation. For model development, the project typically uses CUBIT, ABAQUS/CAE, Simpleware, IDL, and in-house code. Large run times and large model sizes are often required for the multiphysics/multistep nonlinear finite-element/volume analysis jobs.

Results: This project involves work in several topical areas. Work has been performed in the development of an integrated experiment and simulation methods to identify the high-strain-rate viscoelastic properties of soft gels that are used for impact and blast experiments of traumatic brain injuries. Shown in Fig.1, a computational model that corresponds to the impact experiment of a gel block at different impact conditions was used to simulate the gel dynamics. Parametric simulations utilizing optimization and correlation analyses were used to calibrate multiple material parameters in the nonlinear viscoelastic model to the experimental data. The optimal parameters for gels including Sylgard 184, 3-6636, and 527 were found. We have verified the integrated approach by comparing the material properties of the gels with analytical results based on shear wave propagation. This study provides a new approach to calibrate the material behavior of soft gels under high-strain-rate loading conditions. This methodology of integrating computational and experimental analyses leads to further developments to understand, quantify, and interpret brain injuries and auditory damage, to refine injury criteria, and to predict injury risk.

DoD Impact/Significance: Insights gained from this project are necessary for the advancement from concept to application. Navy/DoD expected results are an improved understanding of traumatic brain injury for Navy/DoD applications. New insights will be gained through quantifying the effects of anatomical and material property differences on the mechanical response of quantities correlated with traumatic brain injury, which will affect warfighter health in terms of improved protective gear and improved understanding of the correlation between mechanical response thresholds and traumatic brain injury. The development of techniques to model population-wide anatomical variability will provide insight into the importance of the fit of protective gear.

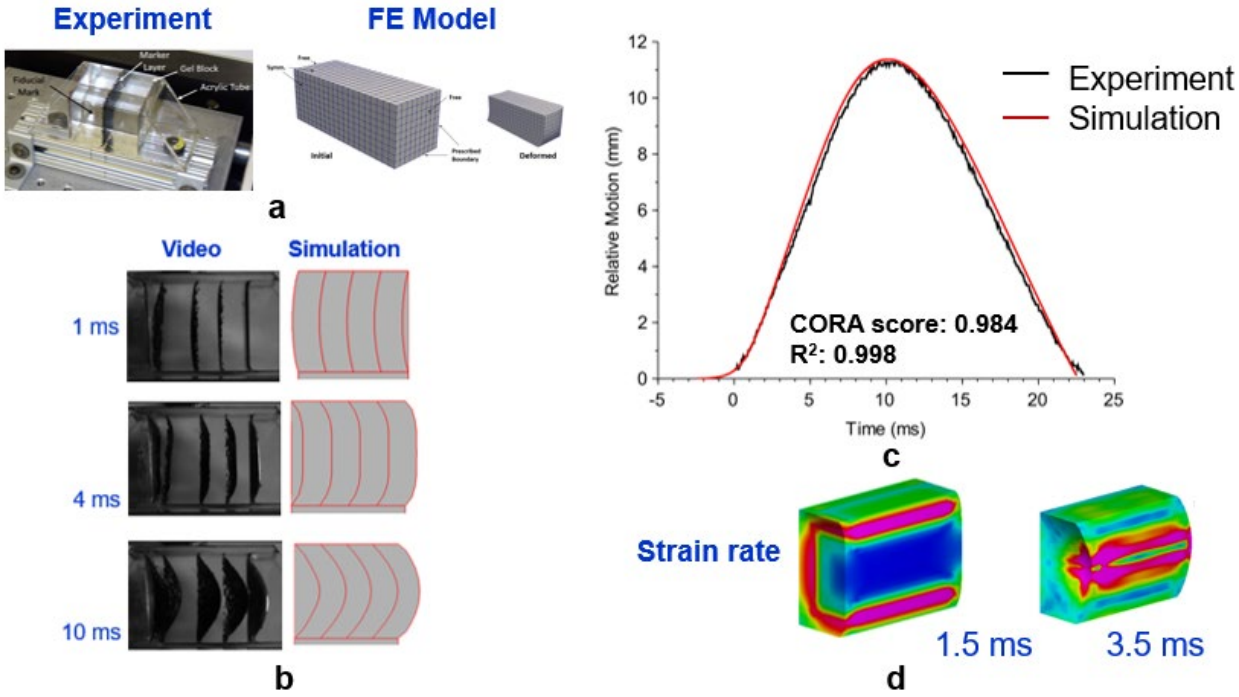


Figure 1. Simulation of a gel block during impact: a) experimental setup and corresponding FE model, b) comparison of bulging process during impact between video and simulation, c) comparison of experimental (in black) and simulated (in red) gel bulge time courses for impact velocity of 0.83 m/s for Sylgard 527 (1:1). CORA scores as well as R2 values are provided, d) rate of shear strain at 1.5 ms and 3.5 ms for half of the gel block.

Title: Stochastic Methods for Uncertainty Quantification in Computational Mechanics
Author(s): L.P. Kuna,[2] K. Teferra,[1] and R.N. Saunders[1]
Affiliation(s): [1]U.S. Naval Research Laboratory, Washington, DC; [2]National Research Council Postdoctoral Associate, U.S. Naval Research Laboratory, Washington, DC
CTA: CSM

Computer Resources: HPE Cray Shasta, HPE SGI 8600 [AFRL, OH]; Cray XC40/50 [ERDC, MS]; HPE SGI 8600 [NAVY, MS]

Research Objectives: The research objective for the work in FY22 is to be able to correlate and predict residual stresses and strains in additively manufactured (AM) 316L stainless steel parts to processing parameters and build conditions. While processing parameters have a large influence on microstructural features, their variations also have direct influence on residual stresses and strains. As AM is a relatively new processing technique, the impact of thermal history on material microstructure and part mechanical properties are not established at the level of reliability required for design standards. Thus, developing an understanding of the effect of heat source-processing parameters on part properties falls within microscale characterization, which is a necessary and essential component of material accreditation. Our goal is to be able to model and simulate this process in order to establish validated, predictive modeling capability so that rapid assessment of build strategies can be made.

Methodology: This work primarily utilizes a crystal plasticity finite-element method (CPFEM) application built on the Multiphysics Object Oriented Simulation Environment (MOOSE) developed and maintained by Idaho National Lab. First, solidification simulations of AM thin-wall parts are carried out using a cellular automata finite-element (CAFE) model to properly capture the polycrystalline microstructure associated with varying processing parameters. These thin-wall parts, with their processing parameter-specific microstructures, are then imported into the CPFEM application to fully characterize the AM process and the resulting mechanical properties of the part. With a voxel size of 4 mm and a part length of almost 1 mm, such large-scale simulations allow a full investigation of the correlations between processing parameters and the mechanical properties at both the local intragranular scale and the global part scale.

Results: Processing simulations of 316L AM thin-wall parts manufactured through laser powder bed fusion were performed. They included processing-specific polycrystalline microstructures and residual stresses and strains. The results illustrate why the inclusion of microstructure is an integral part of properly assessing the influence of processing parameters of AM parts. As shown in both Fig. 1 and Fig. 2, residual stresses and strains in the part congregate close to the center of the structure. Specifically, Fig. 2 shows the influence of raster pattern on the resulting equivalent plastic strains in the structure. Residual plastic strains are noticeably higher for the continuous pattern, and hence an alternating pattern presents more favorable final mechanical properties. Also examined, but not shown, was the influence of how changing the volumetric energy density (laser power and velocity), influences the resulting mechanical properties of AM parts as well.

DoD Impact/Significance: The enhanced structural material performance in terms of durability, strength-to-weight ratio, and manufacturability are essential ingredients toward transforming fleet capabilities. Understanding the nuances of processing parameters is increasingly more important as additive manufacturing becomes a more commonplace manufacturing technique for not only military applications, but also civilian applications. Understanding the influence of additive manufacturing processing parameters on resulting parts is integral to providing guidance to material designers to achieve manufacturing of materials with not only desired properties, but also maximally optimized properties.

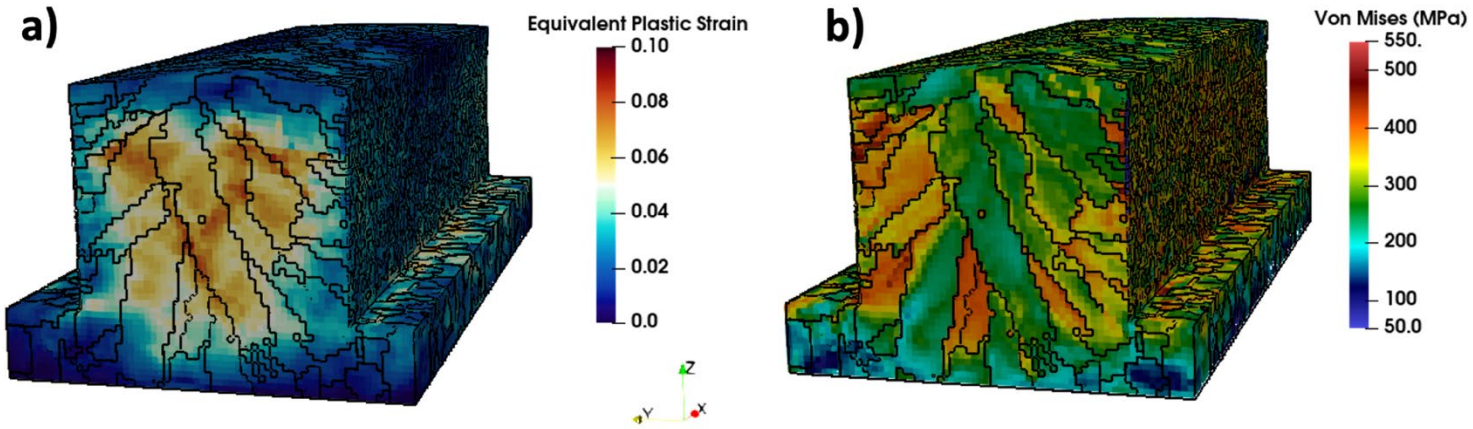


Figure 1. Results of crystal plasticity finite-element simulations carried out utilizing MOOSE. Isometric views of the resulting residual equivalent plastic strains (a) and Von Mises stresses (b) for a 7-layer simulation.

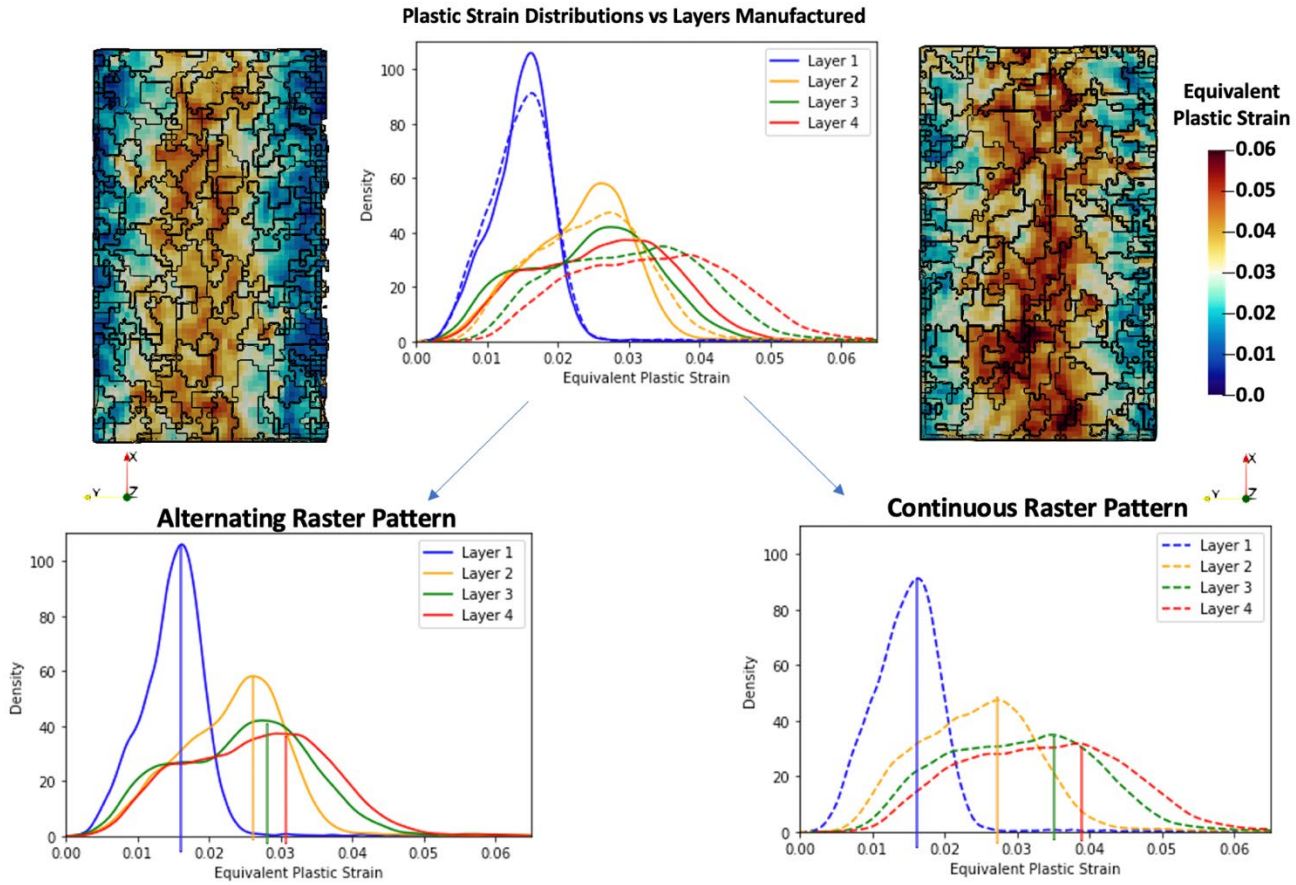


Figure 2. A direct comparison of how the residual plastic strains evolve for a continuous (always x+ direction) raster pattern as opposed to an alternating pattern. Residual plastic strains are noticeably higher for the continuous pattern, so an alternating pattern is more favorable.

Title: Geometric, Constitutive and Loading Complexities in Structural Materials
Author(s): S.A. Wimmer,[1] R.N. Saunders,[1] A. Arcari,[1] L.P. Kuna,[2] and J.G. Michopoulos[1]
Affiliation(s): [1]U.S. Naval Research Laboratory, Washington, DC; [2]National Research Council Postdoctoral Associate, U.S. Naval Research Laboratory, Washington, DC
CTA: CSM

Computer Resources: HPE Cray Shasta, HPE SGI 8600 [AFRL, OH]; HPE SGI 8600 [NAVY, MS]

Research Objectives: The research strives to develop rational bases and mathematical descriptions of complex material responses for structural and novel evolving materials. Structural integrity and life cycle evaluations require an understanding of material responses. Analytical models and techniques cannot describe complex materials and often do not account for interactions, complex geometries, or multiphysics loading. Finite-element methods are used to develop models involving multifunctional materials, novel evolving materials, and multiphysics. In order to accurately model the nonlinear response of conventional structural materials, rate dependence, large deformation, and damage-accumulation mechanisms must be understood and accurately represented. The performance of the overall structure or system is also examined via parameters such as kinematics, geometric complexities, loading path dependencies, and interaction between loading types.

Methodology: The project uses finite-element methods extensively. Nonlinear material constitutive response features are highlighted in much of the work. Implicit and explicit solutions methods are used as appropriate. The primary finite-element code used is ABAQUS. Coupled material responses, such as electric-thermal or electrical-mechanical-thermal, are exercised for evaluation of these effects. Model development is done with CUBIT, ABAQUS/CAE, ScanIP, or in-house software. Large run times and large model sizes are often required for the multistep nonlinear finite-element analysis jobs.

Results: This project involves work in several topical areas. Work has been performed on creating image-based microstructural models, modeling multilayer ceramic structures, modeling stress corrosion cracking, modeling biofoulants, and modeling transparent armor delamination. Representative results for modeling additive manufacturing are discussed. This work utilized an in-house cellular automata finite-element code optimized to run with MPI and Cuda. The simulations carried out in this work consisted of 900,000+ voxel domains. Crystallographic microstructure influences the resulting mechanical properties (on a macroscale) of additively manufactured parts. In particular, the recent focus on creating high-strength, low-weight parts requires understanding how process parameters influence microstructures, which can illuminate the root cause of failure. Grain shape, grain boundary characteristics, and texture, among other features, have all been identified as factors in mechanical failure. Figure 1 shows how the melt pool shape can vary even if the volumetric energy density used to manufacture a part stays the same. These variations in the melt pool morphology are directly linked to variations in the resulting microstructure, which can be seen in Fig. 2. As the velocity and power are increased, the grains in the thin wall part become larger, longer, and more columnar, with a higher propensity to be sources of mechanical failure (as determined by the maximum Schmid factor). Understanding such correlations is of great importance to manufacturing high-quality parts for various applications.

DoD Impact/Significance: The role of additive manufacturing is rapidly increasing not only in military applications, but also in civilian applications. The greater the understanding of the various processes involved in this advanced technology, the more efficiently it can be utilized and deployed for various applications such as rapid prototyping and optimized part production. By providing a better understanding of the influence of processing parameter on microstructure, the results of this study will enable a better understanding of how process parameters can be optimized to mitigate undesirable microstructural features.

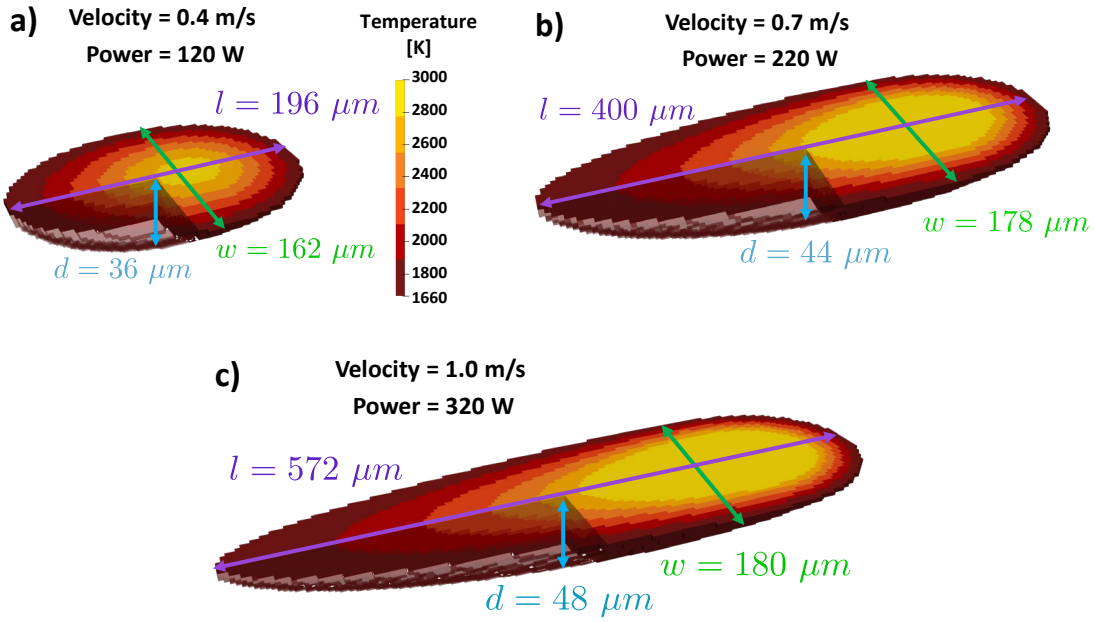


Figure 1. Three different melt pool morphologies are presented for the same volumetric energy density, but varying velocity and power. The processing parameters are scaled so that the volumetric energy density does not change, but as can be seen here, the morphology of the melt varies significantly and therefore influences the resulting microstructure.

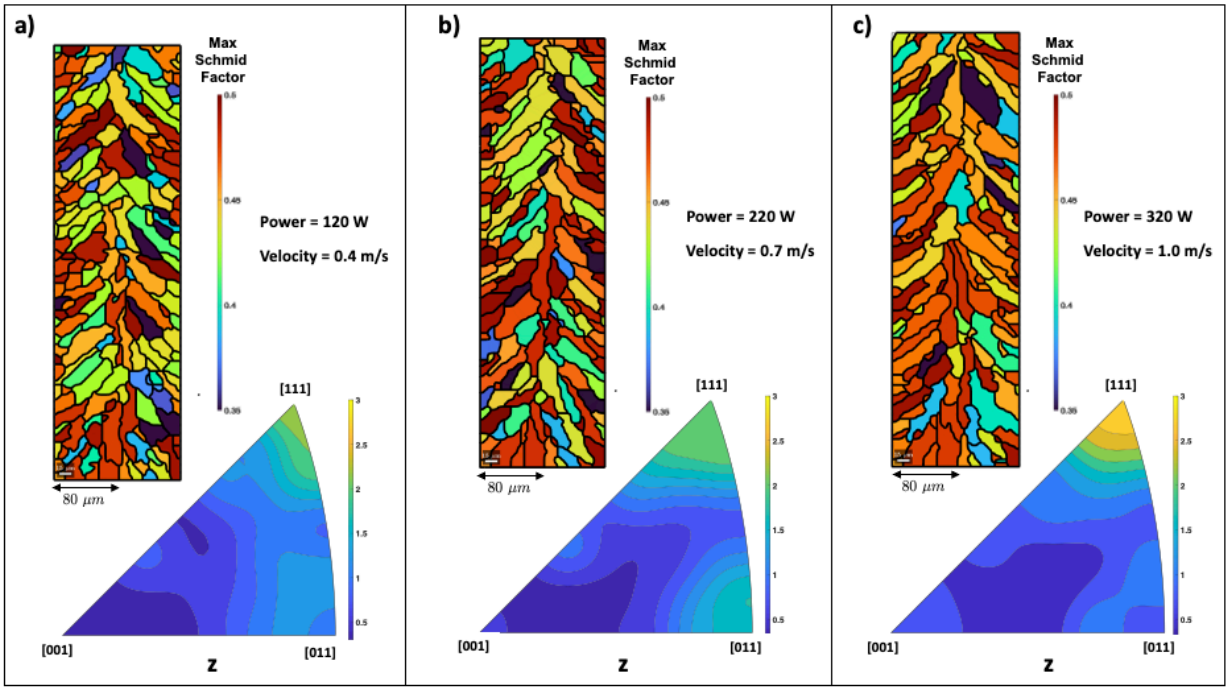


Figure 2. Analysis of the resulting crystallographic texture as a function of different processing parameters for the same volumetric energy density used to manufacture the thin-wall part. Included are a cross sectional cut of the wall colored by Schmid factor and an inverse pole figure projected along the build direction (z).

THIS PAGE INTENTIONALLY LEFT BLANK

CFD

Computational Fluid Dynamics

CFD covers high-performance computations whose goal is the accurate numerical solution of the equations describing fluid motion and the related use of digital computers in fluid dynamics research. CFD is used for basic studies of fluid dynamics for engineering design of complex flow configurations and for predicting the interactions of chemistry with fluid flow for combustion and propulsion. It is also used to interpret and analyze experimental data and to extrapolate into regimes that are inaccessible or too costly to study. Work in the CFD CTA encompasses all Reynolds number flow regimes and scales of interest to the DoD. Incompressible flows are generally slow (e.g., governing the dynamics of submarines, slow airplanes, pipe flows, and air circulation) while compressible flows are important at higher speeds (e.g., controlling the behavior of transonic and supersonic planes, missiles, and projectiles). Fluid dynamics itself involves some very complex physics, such as boundary layer flows, transition to turbulence, and turbulence dynamics, that require continued scientific research. CFD also must incorporate complex additional physics to deal with many real-world problems. These effects include additional force fields, coupling to surface atomic physics and microphysics, changes of phase, changes of chemical composition, and interactions among multiple phases in heterogeneous flows. Examples of these physical complexities include direct simulation Monte Carlo and plasma simulation for atmospheric reentry, microelectromechanical systems (MEMS), materials processing, and magnetohydrodynamics (MHD) for advanced power systems and weapons effects. CFD has no restrictions on the geometry and includes motion and deformation of solid boundaries defining the flow.

Title: Simulations of Laser-plasma Interactions and the Radiation Hydrodynamics of High-velocity Laser-accelerated Matter
Author(s): J.W. Bates and K. Obenschain

Affiliation(s): U.S. Naval Research Laboratory, Washington, DC
CTA: CFD

Computer Resources: HPE Cray Shasta, HPE SGI 8600 [AFRL, OH]

Research Objectives: The two principal obstacles to thermonuclear fusion with laser-driven implosions are hydrodynamic and laser-plasma instabilities. The objectives of this research are to gain a better understanding of the physics underlying these phenomena and also to develop practical strategies for their mitigation using the numerical codes LPSE, FastRad3D and ASTER.

Methodology: LPSE is a fluid-based, massively parallel computer code designed to model laser-plasma instabilities (LPIs) in the context of inertial confinement fusion (ICF) and high energy-density physics. Such instabilities can spatially redistribute significant fractions of the incident laser energy in an ICF implosion and thereby can reduce the ablation pressure, compression, and finely tuned symmetry of the target illumination. Moreover, some classes of LPIs also generate suprathermal electrons that can preheat the thermonuclear fuel and further degrade high-fusion yields. The most deleterious varieties of LPIs for direct-drive ICF are two-plasmon decay (TPD), stimulated Raman scattering (SRS), and cross-beam energy transfer (CBET) — all of which can be modeled with the LPSE code. The level of physical detail in LPSE is intended to lie between more fundamental particle-in-cell codes and full-scale radiation-hydrodynamic codes such as FastRad3D and ASTER, which are used to simulate full ICF implosions. Like LPSE, FastRad3D and ASTER are massively parallel codes, and while they do not account for LPIs, they do model a variety of other complex physical processes important for ICF such as laser absorption, radiation transport, thermonuclear burn, and hydrodynamic instabilities. We are using all three of these codes in an effort to improve our understanding of the physics of ICF implosions and to develop target designs that are less susceptible to the deleterious effects of both hydrodynamic and laser-plasma instabilities.

Results: Our principal results for FY2022 address the efficacy of a short laser wavelength and a broad laser bandwidth for suppressing the absolute forms of the TPD and SRS instabilities and CBET. Using the LPSE code, numerous two and three-dimensional simulations were performed this year to quantify the effect of short-wavelength, broadband laser light on these instabilities under conditions relevant to direct-drive ICF implosions. Our simulations demonstrate, for example, that using a frequency-tripled Nd:glass laser with a wavelength of 351 nm and a laser bandwidth of about 13 THz is sufficient to mitigate absolute TPD and SRS on an ignition-scale platform (see Fig 1(a)). Although such a value lies well beyond the capabilities of any contemporary Nd:glass lasers used for ICF research, it may be possible to achieve such bandwidth levels in the future by exploiting certain nonlinear processes such as optical parametric amplification [C. Dorrer et al., Optics Express **29**, 16135 (2021)] or stimulated rotational Raman scattering [J. Weaver et al., Applied Optics **56**, 8618 (2017)] at the output of the laser. An alternative and arguably superior approach to LPI suppression would be the use of an argon fluoride (ArF) laser driver, which has a shorter wavelength of 193 nm and a broad native bandwidth of approximately 10 THz. Two-dimensional LPSE simulations of ArF laser light irradiating an ICF coronal plasma indicate that the losses in laser absorption caused by CBET scattering, for example, are nearly eliminated using an ArF driver (see Fig 1(b)). Results of this work are highly encouraging and have helped to advance efforts by researchers in the Laser Plasma Branch at NRL who are advocating for the development of broadband laser sources for ICF.

DoD Impact/Significance: Suppression of hydrodynamic and laser-plasma instabilities will expand the design space available for viable ICF target designs, which will benefit the National ICF program and auxiliary research efforts related to stockpile stewardship.

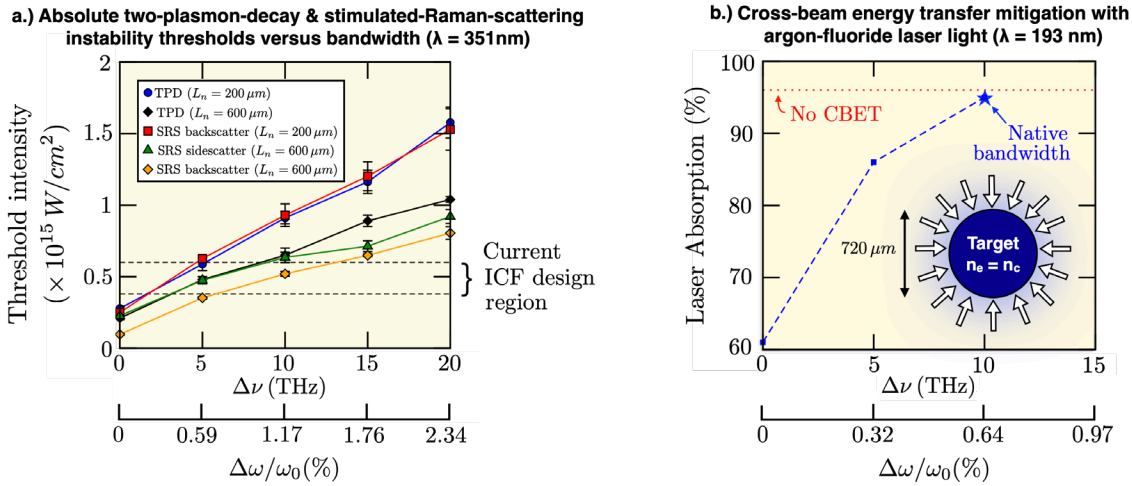


Figure 1. Numerical results from LPSE simulations showing: a) the multibeam intensity thresholds for the absolute forms of the TPD and SRS instabilities as a function of laser bandwidth (and different values of the density-gradient scale length, L_n, in the plasma) for 351-nm laser light, and b) laser absorption in a full-scale ICF coronal plasma driven by multiple beams from an ArF laser. The results in a) indicate that a bandwidth of approximately 13 THz is required for a frequency-tripled Nd:glass laser to mitigate absolute TPD and SRS on an ignition-scale platform. The results in b) show that the native properties of an ArF laser driver are nearly sufficient to fully counteract the losses in laser absorption caused by CBET scattering.

Title: Modeling of Detonations in Jet Fuel Sprays
Author(s): V.N. Gamezo[1] and A.Y. Poludnenko[2]
Affiliation(s): [1]U.S. Naval Research Laboratory, Washington, DC; [2]Univeristy of Connecticut, Storrs, CT
CTA: CFD

Computer Resources: HPE Cray Shasta, HPE SGI 8600 [AFRL, OH]; Cray XC40/50 [ERDC, MS]; Cray Shasta [NAVY, MS]

Research Objectives: Detonations in liquid fuel sprays play a central role in a wide range of contexts of direct DoD and Navy relevance. These include novel detonation-based propulsion and energy-conversion systems, such as rotating detonation engines (RDEs), as well as safe storage and handling of liquid fuels both aboard and on shore. Detonations in liquid fuels are also used in various munition applications. In the past, primary emphasis has been placed on studying gas-phase detonations. Obtained insights, however, may not be fully applicable to liquid-fuel detonations, which introduce qualitatively different effects associated with flow-droplet interactions, droplet secondary atomization, evaporation, and mixing. All such processes affect both the spray and the ambient flow, resulting in a complex mass, momentum, and energy exchange and ultimately in fuel mixing with the oxidizer, which are critical for the sustained detonation propagation. Such complexities can significantly alter the detonation structure and can directly impact its stability and propagation limits in liquid sprays, thus critically affecting the performance of the host system.

Methodology: We carry out two-dimensional (2D) simulations of a spray detonation in n-dodecane/air using detailed droplet drag and evaporation models. For the first time, these simulations use complex, multistep chemistry of a heavy hydrocarbon fuel that includes 24 species and 193 reactions based on the HyChem mechanisms, and realistic transport models in multicomponent mixtures. The physical model represents a coupled gas-particle system that is solved via an Eulerian-Lagrangian approach, in which the gas phase is simulated on an Eulerian grid while the liquid phase is treated as Lagrangian point particles. Simulations are performed on a uniform grid using a fully compressible, reactive flow solver *Athena-RFX*. The particle-gas interaction includes quasisteady drag and forced convective heat transfer, with the drag coefficient evaluated using the correlation of Loth (2008) for high-speed regimes. For droplet evaporation, the Nusselt and Sherwood numbers are given by the Ranz-Marshall correlation. Secondary droplet atomization is not considered due to the 2D nature of the simulations. Liquid spray consists initially of monodisperse 10 μm droplets. Grid resolution is 42 μm, and we consider 10-cm- and 50-cm-wide channels to minimize the effect of the channel size on the detonation.

Results: Figure 1 shows a comparison of the resulting structure of the spray and gaseous detonations, while Fig. 2 compares the corresponding numerical soot foils obtained by recording the maximum pressure in each computational cell in the domain. For both channel sizes investigated, spray detonations produce a regular cellular structure similar to that of stable gaseous mixtures, while the purely gaseous detonations produce highly irregular cells. The former produced cells that are much larger than the expected cell size, while the latter produced characteristic cell sizes much smaller than the expected cell size. In terms of stability, both single- and multiphase cases result in a healthy detonation, though the former exhibits highly unstable dynamics with quasi-failures and reignitions through transverse detonations, while the latter shows no evidence of such dynamics. These calculations also allowed us to investigate in detail the thermo- and hydrodynamic conditions experienced by the droplets in the detonation front, which is critical for the assessment of the accuracy of the existing physical models of droplet drag, evaporation, and atomization.

DoD Impact/Significance: Numerical models of the liquid-fuel detonations obtained in this work represent the state of the art in the field. They constitute a key step toward the development of the realistic 3D models of spray detonations, which do not exist yet and which are the focus of the ongoing work in FY23. Such models will provide understanding of the physics of liquid-fuel detonations, which is crucial for the development of advanced propulsion systems by the U.S. Navy. Work carried out in this project is tightly connected with the ongoing efforts at the U.S. Naval Research Laboratory under the 6.1 base program, and more broadly at the Office of Naval Research under the MURI program and at other DoD agencies, such as AFOSR, to study detonations in liquid jet fuel sprays.

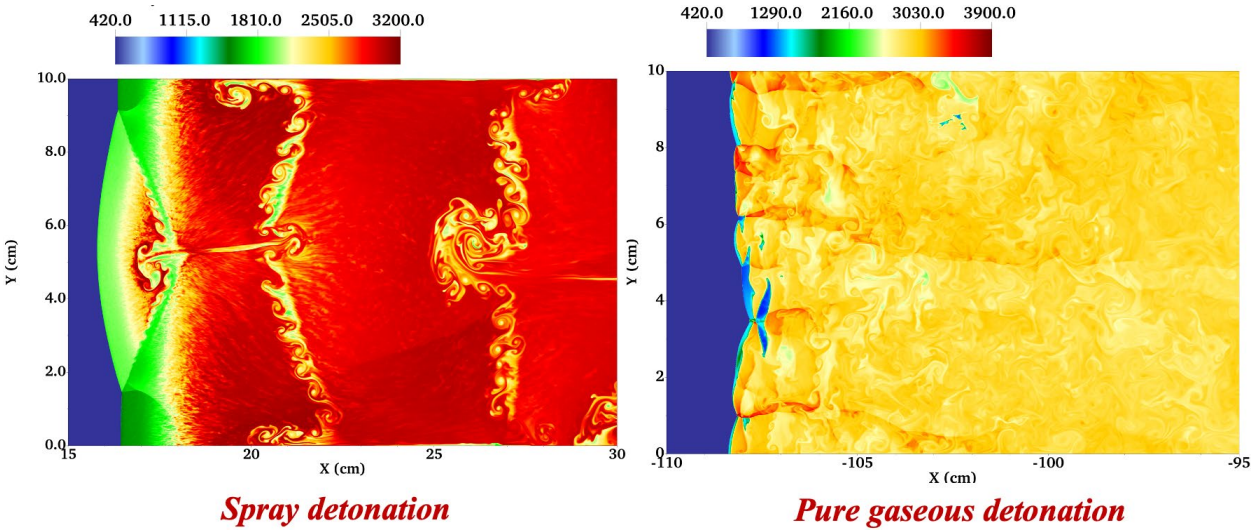


Figure 1. Comparison of the structure of a two-dimensional detonation propagating in a 10 cm channel in a liquid spray of n-dodecane (left) and in prevaporized n-dodecane (right). Initial pressure is 1 bar, and initial air temperature is 420 K. Equivalence ratio is 1.0 in both cases. Shown are the temperature distributions.

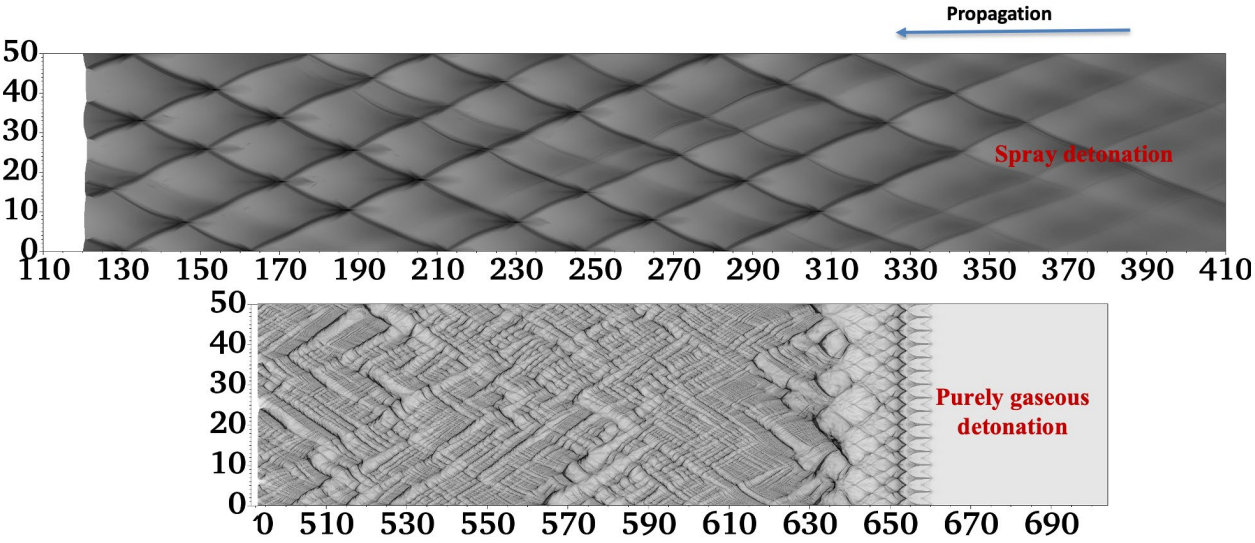


Figure 2. Numerical soot foils obtained by recording the maximum pressure in each computational cell from the simulations of detonations in a 50 cm channel in liquid-spray (top) and prevaporized gaseous (bottom) n-dodecane/air mixture (cf. Fig. 1 above).

Title: Airbreathing Combustion for Hypersonics
Author(s): G. Goodwin
Affiliation(s): U.S. Naval Research Laboratory, Washington, DC
CTA: CFD

Computer Resources: Cray Shasta [NAVY, MS]

Research Objectives: The objective of this research is to characterize the effect of fuel equivalence ratio on flame stability, thermal choking, and unstart in a supersonic cavity combustor. The ACT-II supersonic cavity combustor at the University of Illinois was used as the facility studied under this work. Simulations of combustion in the facility were performed using the JENRE® multiphysics framework.

Methodology: One of the predominant challenges in using air-breathing engines for hypersonic flight (typically, greater than five times the speed of sound) is that the extremely fast flow speeds through the engine present a challenging environment for reliable ignition of the fuel and stable combustion. The methodology for this research is to use high-fidelity computational fluid dynamics (CFD) to simulate the high-speed reactive flow in the combustors of air-breathing hypersonic vehicles. Boundary conditions, fuel chemistry and equivalence ratio, combustor geometry, and turbulence levels are varied to catalog the effect of these phenomena on achieving stable ignition and complete combustion. For the results described in this report, a supersonic cavity combustor with an inflow of Mach 4.5 air at 436 K and 500 Pa was used as the computational domain. Ethylene fuel was injected upstream of a cavity-ramp flameholder at equivalence ratios ranging from 0.5 to 20 in order to characterize the effect of increasing fuel equivalence ratio on thermal choking and unstart. These computations solve the fully conservative formulation of the multicomponent, chemically reacting Navier-Stokes equations. Combustion is modeled using a global three-step, seven-species ethylene-air combustion mechanism.

Results: Figure 1 shows temperature and Mach contours for seven time steps; steps i to iv are shortly after the fuel equivalence ratio was increased from 2 to 10 and steps v to vii are after the equivalence ratio was further increased to 20. In step i, a strong shock forms as the isolator crossflow impacts the fuel jet. The temperature increase across the shock is sufficient to cause the fuel jet to autoignite immediately upon penetration into the isolator crossflow. The flame remains relatively stable as the fuel jet shock propagates upstream, as seen in steps ii and iii. When the shock reaches the position shown in step iv, the flow stabilizes and the shock remains stationary. Although the flow through the combustor is choked at this time, as indicated by the subsonic flow behind the shock (labeled in step iv), because the flame remains stable, this was not considered a full unstart scenario. When the global equivalence ratio was increased to 20, the increased fuel mass flow into the isolator results in greater backpressure, forcing the strong shock in step iv to move upstream and to transition to a normal shock. The normal shock continues to propagate upstream before settling temporarily at the location shown in step v. Here, the normal shock moves upstream very slowly. When it intersects the oblique shock reflecting against the top boundary, visible in step v, it is accelerated further upstream as shown in steps vi and vii. The shock continues upstream until impact with the inflow boundary. The flow between the normal shock and the end of the cavity ramp is entirely subsonic and the flame becomes unstable as the shock continues to propagate upstream. Here, it is evident that unstart is occurring.

DoD Impact/Significance: The impact of this research is an improved understanding of the fine-scale combustion and unstart physics in scramjet engines. Using high-fidelity computational fluid dynamics to simulate scramjet combustion is a critical step in the engine research-and-development process. The simulations are run in tandem with accompanying experiments for validation and comparison.

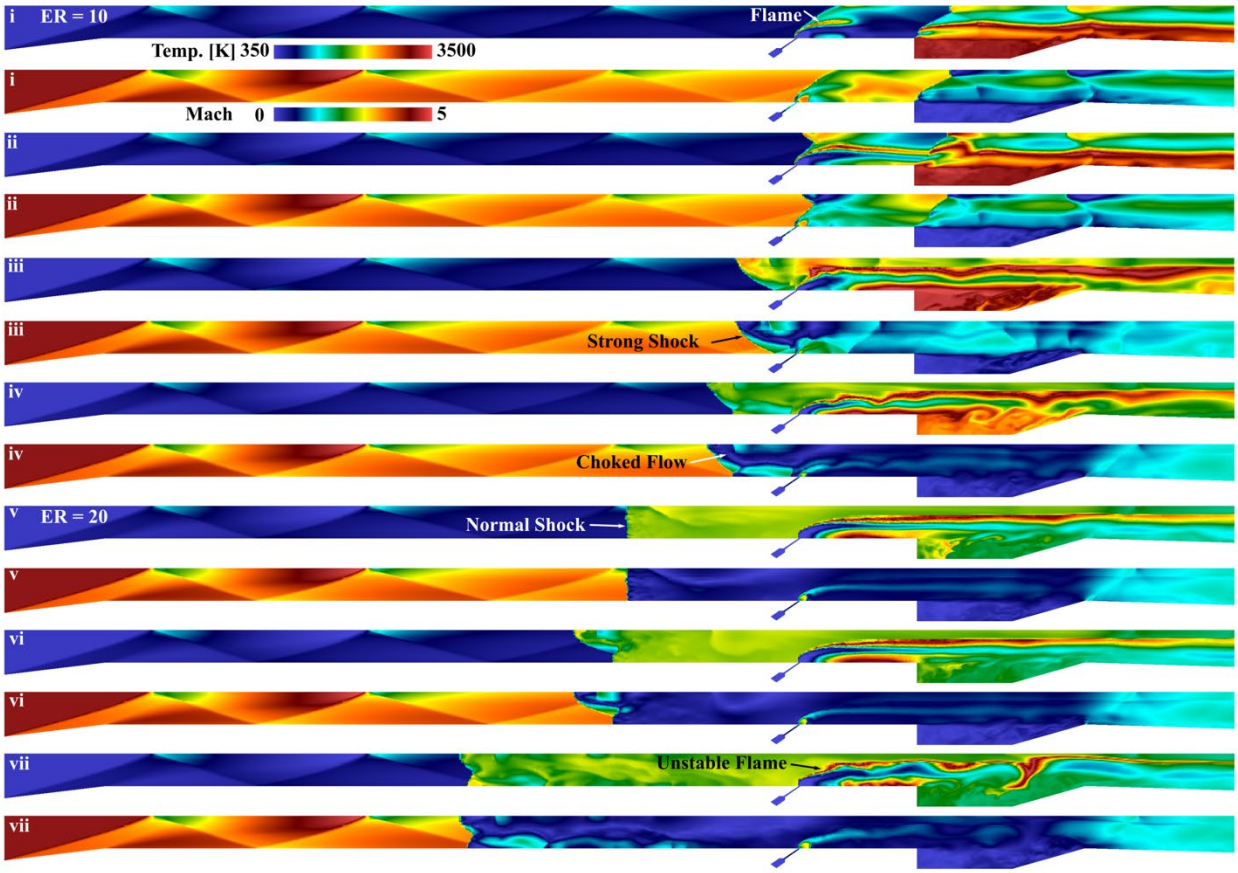


Figure 1. Computational fluid dynamics simulation of combustion in a supersonic cavity combustor with a Mach 4.5 inflow of air and injection of ethylene fuel upstream of the cavity-ramp flameholder. Temperature and Mach contours are shown for several time steps in the simulation. Time steps i to iv show combustion with a fuel equivalence ratio of 10 and the remaining time steps occur after the equivalence ratio is increased to 20. The combustor unstarts as the increase in fuel mass flow rate results in thermal choking and the formation of a normal shock that propagates upstream and leaves an unstable flame in its subsonic wake.

Title: Multidimensional Chemically Reacting Fluid Dynamics with Application to Flameless Combustors
Author(s): R.F. Johnson
Affiliation(s): U.S. Naval Research Laboratory, Washington, DC
CTA: CFD

Computer Resources: HPE SGI 8600 [AFRL, OH]

Research Objectives: Simulate computationally intensive chemically reacting fluid dynamics in various multidimensional configurations using HPC resources with the aim of gaining a deeper understanding of various complex, multiscale combustion phenomena.

Methodology: The codes utilized by The Laboratories for Computational Physics and Fluid Dynamics can predict flow fields in various configurations with precision. These codes use high-order methods, which are effective in simulating unsteady flows with strong shocks, chemical reactions, and other intricate features. The focus of this work is on the ongoing developments that will enable simulation of high- and low-speed chemically reacting flows using cutting-edge numerical methods. This year, we have achieved significant results that showcase the effectiveness of our methods in simulating chemically reacting flows.

Results: This year, we enhanced the previously developed methodology that can resolve the mixing of multicomponent chemically reacting flows without relying on traditional stabilization methods. In the past, simulating the simple mixing of two substances, such as hydrogen and oxygen, would have been unsuccessful without the use of costly stabilization methods. The Laboratories for Computational Physics and Fluid Dynamics have created a new method for simulating multicomponent flows that combines the features of the discontinuous Galerkin method (DG) and accurate thermodynamics to simulate propulsion problems. With this method, we can run these problems with detailed thermodynamics, transport, and chemical kinetics without any stability issues. This year, our goal was not only to increase stability, but also to produce results for larger-scale hydrocarbons in more practical applications.

A key advantage of the DG method is its ability to resolve structures with high-order accuracy without the need for mesh refinement. Instead, the DG method can arbitrarily increase cell accuracy to resolve flows within the computational cells. A significant challenge we encountered was that shock capturing still required some stabilization near discontinuities to fully utilize the power of DG. Without these methods, shock capturing would be too diffuse, and the resulting flow structures would not improve when increasing the order of accuracy for a given mesh. This year, we improved our new entropy-preserving limiters that prevent oscillations at high order, which previously had required additional artificial viscosity. We successfully generated three-dimensional detonation results, which are larger-scale simulations than the two-dimensional detonation we produced last year. Figure 1 illustrates one of these three-dimensional results for various z-locations. These simulations were conducted using HPCMP, the discontinuous Galerkin method (DG) with $p = 2$ tetrahedral cells, and the JENRE® multiphysics framework.

DoD Impact/Significance: Advancing numerical techniques for simulating propulsion devices will lead to a greater understanding and ability to predict the performance of Navy/DoD aircraft.

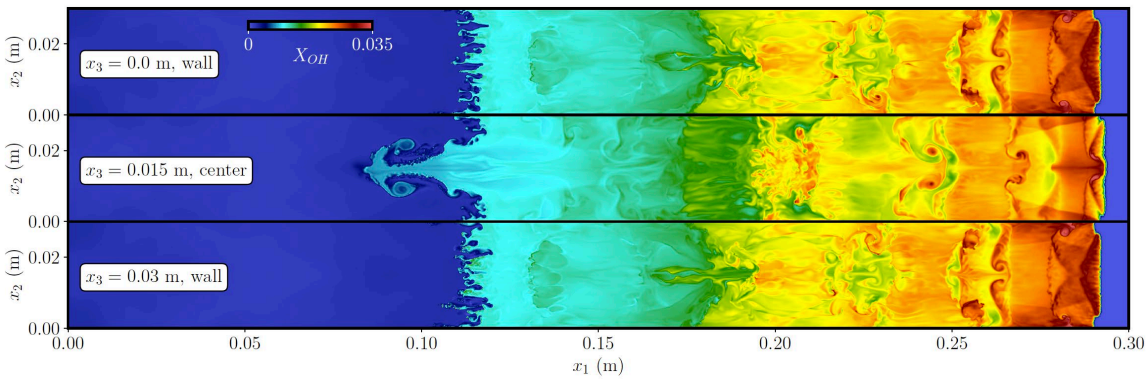


Figure 1. OH mole fraction distributions along various x_1x_2 -planes at t = 176 μs for a three-dimensional moving detonation wave in a rectangular channel computed with DG (p = 2) and 4.8h, where $h = 9\times10^{-5}$ m. Results were generated using the JENRE® multiphysics framework.

Title: High-Fidelity CFD Simulations of High-Speed Flows in Realistic Atmospheric Conditions
Author(s): D.A. Kessler, R.F. Johnson, A.M. Hess, and B.T. Bojko
Affiliation(s): U.S. Naval Research Laboratory, Washington, DC
CTA: CFD

Computer Resources: nvidia v100 [ERDC, MS]; HPE Cray Shasta, HPE SGI 8600 [AFRL, OH]; Power 9 [ARL, MD]; Cray Shasta [NAVY, MS]

Research Objectives: 1) Develop an improved physical understanding of how the aerodynamic performance of hypersonic vehicles changes when encountering multiphase flow environments. 2) Characterize the high-speed reacting-flow environment and flame-holding potential within a solid-fuel ramjet propulsion device.

Methodology: We are using the JENRE® multiphysics framework to perform high-fidelity and high-resolution simulations of the chemically reacting, two-phase flows associated with high-Mach-number hypersonic flight and thrust generation within an air-breathing engine.

Results: Solid-fuel air-breathing propulsion systems (e.g., solid-fuel ramjets and solid-fuel scramjets) represent an attractive option for achieving high-supersonic and hypersonic flight, a regime of critical importance for a variety of defense applications. Increasing technological readiness levels of these systems is hampered by a lack of fundamental knowledge regarding the combustion behavior in the complex multiphase flow environment under which they operate. Researchers at the U.S. Naval Research Laboratory are developing a multiphysics simulation methodology to address this technology gap that will be capable of describing the conversion of a solid fuel to a combustible gas, the transport and combustion of energetic metal additives, the gas-phase chemical kinetics, and the coupled convective and radiative heat transfer between the solid fuel and the gas, all on top of the background high-speed turbulent flow. Throughout FY22, significant progress has been made toward achieving this goal.

As a demonstration, snapshots of the temperature field computed within a model solid-fuel ramjet combustor during stable operation are shown in Fig. 1a. In this image, the light-blue bars represent a solid-fuel grain with properties that are analogous to a common fuel material: pure hydroxyl-terminated polybutadiene (no metal additives). Air flows through the system from left to right, and a turbulent flame forms that is anchored by flow recirculation formed by the sudden change in volume between the throat of the inlet nozzle and the combustion chamber (bounded by the solid-fuel grains). This effort was used to demonstrate the viability of our simulation approach for predicting conditions under which it is possible to anchor a flame and to achieve sustained combustion. For this particular design, we found anchoring to be possible. We next performed a companion simulation under similar flow conditions but with a different combustion chamber size, characterized by a smaller step change in volume between the throat and the combustor. This particular system showed complete extinction of the flame a short time after it was ignited. A snapshot of the temperature contours at an intermediate time (Fig. 1b) show a quenched flame along the bottom fuel surface and an unstable flame along the top. As noted, (but not shown here) the unstable flame does eventually quench at a later instant in time. This same anchoring-and-quenching behavior was observed in a series of laboratory tests, providing some measure of simulation validation.

DoD Impact/Significance: Achieving a global prompt-strike capability and countermeasures for similar technologies under development by our adversaries are critical for protecting our fleet and maintaining naval superiority. This work will provide an improved understanding of parameters critical to solid-fuel ramjet engine performance under a variety of operating conditions.

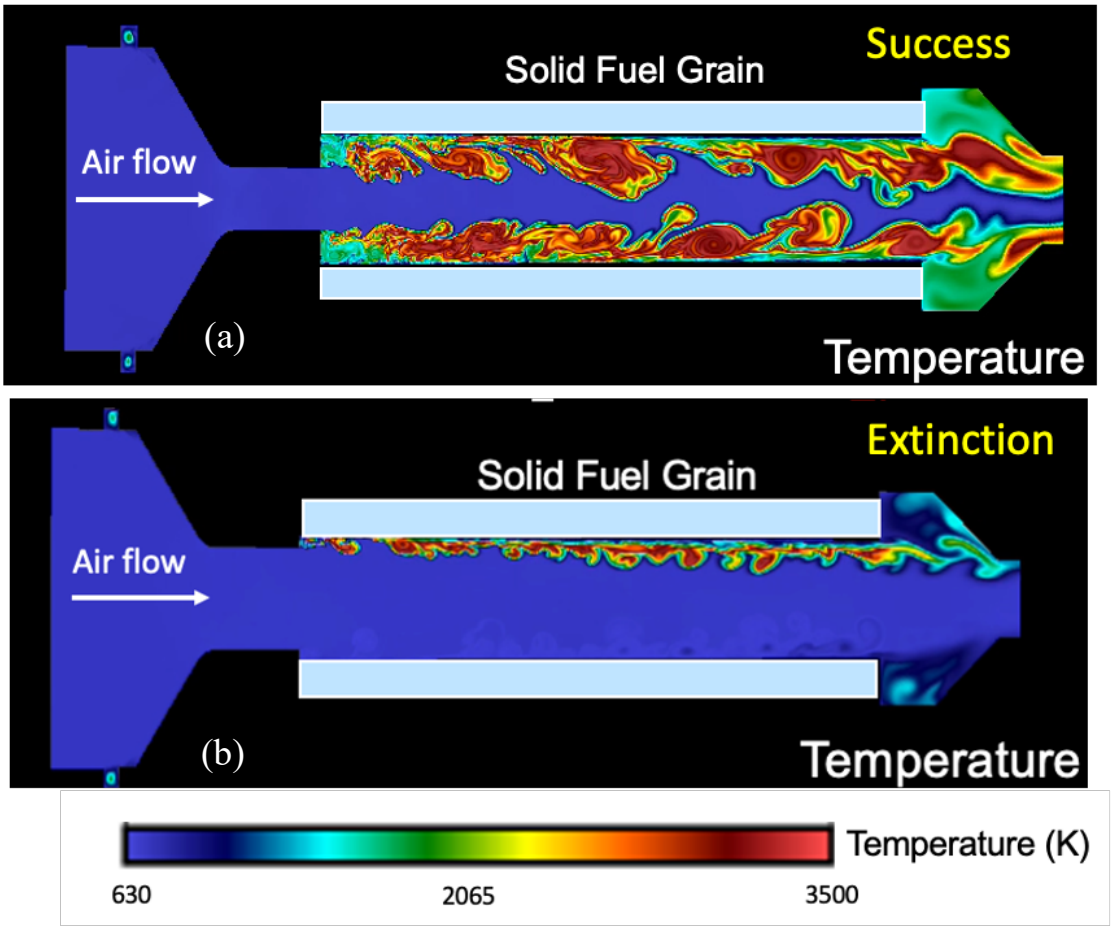


Figure 1. Instantaneous temperature contours extracted from a calculation of the operation of a model solid-fuel ramjet device showing (a) sustained combustion associated with a specified combustion chamber depth and (b) flame extinction for a system with a smaller combustion chamber.

Title: Jet Noise Reduction Studies
Author(s): Y. Khine
Affiliation(s): U.S. Naval Research Laboratory, Washington, DC
CTA: CFD

Computer Resources: HPE SGI 8600 [AFRL, OH]; Cray XC40/50 [ERDC, MS]; Cray Shasta [NAVY, MS]

Research Objectives: The goal of this project is to investigate and assess jet noise-reduction concepts for representative military aircraft jet engines such as microvortex generators (MVGs) and chevrons in order to address workplace health and safety issues and environmental concerns.

Methodology: Jet noise simulations require a very large computational domain to include both the near and far fields for long enough duration of physical time to study the effect of noise propagation. While the focus was on studying MVGs in FY21, the effects of various chevrons at the end of nozzles were studied in FY22. In this project, the JENRE® multiphysics framework is used to simulate turbulent flows in nozzles. The JENRE® multiphysics framework provides a large eddy simulation (LES) model that uses a nodal finite-element method and is implemented with multiple levels of parallelism. Different jet conditions are considered in the simulations. In this project, azimuthally varying chevrons are implemented on model-scale faceted nozzles that are representative of GE-F40 nozzles. Many parameters play important roles in producing desired effects from using the chevrons, and various cases of simulations are needed to understand the effects caused by the presence of chevrons. The results were compared with the jet noise reduction produced by the presence of MVGs in the nozzles.

Results: Figure 1(a) presents a sample faceted nozzle with chevrons attached at the nozzle exit and Fig. 1(b) presents a faceted nozzle with MVGs attached on alternate seal surfaces of the nozzle. The simulations are at the pressure ratio NPR = 2.7 and the temperature ratio NTR = 3.0 compared with ambient conditions. In each figure of Figs. 2 and 3, x is distance along the length of the nozzle and D is the equivalent nozzle exit diameter. In Fig. 2, the axial vorticity is displayed for the nozzle with chevrons shown in Fig. 1(a). The vortices generated by chevrons are stretched in the radial direction and the vorticity decreases very quickly downstream of the nozzle, as can be seen in Fig. 2(c) at x = 2.0D. In Fig. 3, the axial vorticity generated by the MVGs at x = 0.5D is less stretched in the radial direction and the vorticity is concentrated in a smaller area than those generated by chevrons. The vortices generated by MVGs are more rounded in shape and large vorticity magnitude can still be observed at x = 2.0D. In conclusion, chevron technology has been the most accepted noise-reduction concept for jet flows, but the noise reduction from using MVGs is very promising.

DoD Impact/Significance: Hearing disability caused by the noise generated by supersonic military aircrafts has been a very serious concern for DoD. These studies offer better insight of the physical phenomena for different jet conditions and allow us to optimize MVGs and chevrons that can provide significant reduction in noise level. This research also supports ongoing jet noise-reduction studies at other government agencies and academics.

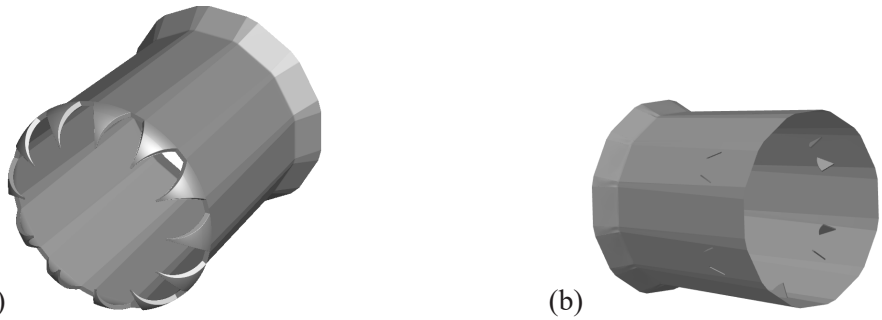


Figure 1. (a) Sample faceted nozzle with chevrons. (b) Sample faceted nozzle with MVGs on alternate seal faces.

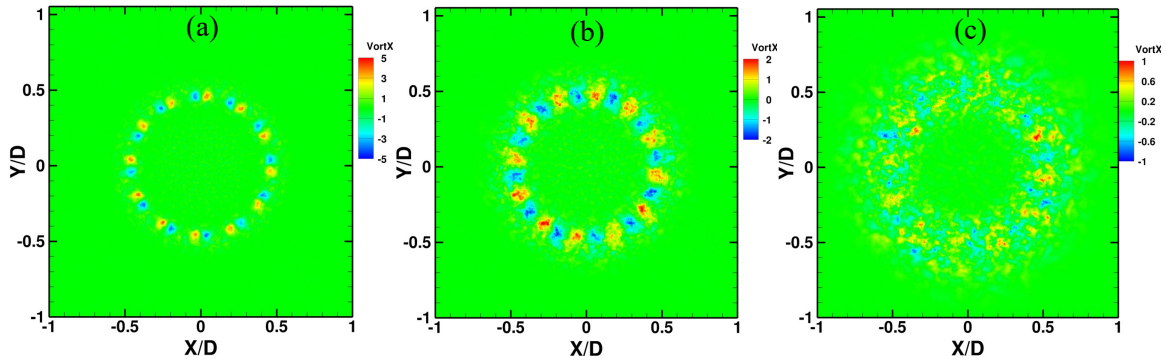


Figure 2. Axial vorticity of nozzle with chevrons as shown in Fig. 1(a) at NPR = 2.7 and NTR = 3.0. (a) x = 0.5D. (b) x = 1.0D. (c) x = 2.0D.

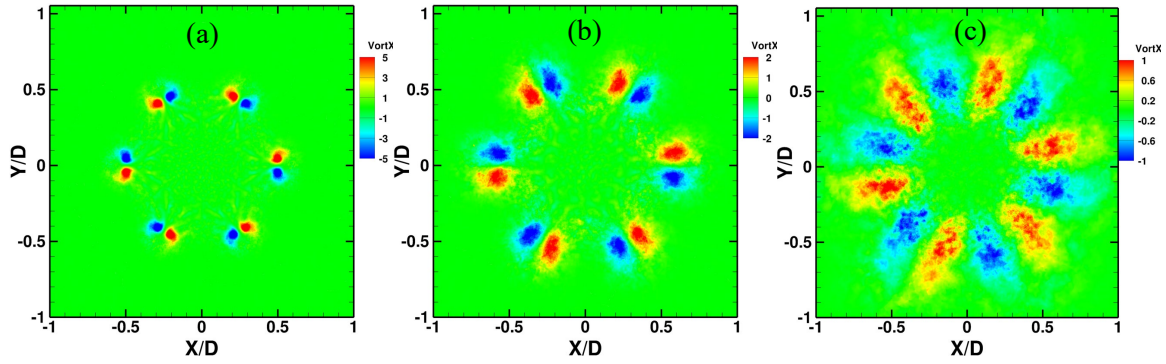


Figure 3. Axial vorticity of the nozzle with MVGs as shown in Fig. 1(b) at NPR = 2.7 and NTR = 3.0. (a) x = 0.5D. (b) x = 1.0D. (c) x = 2.0D.

Title: Numerical Investigation of Advanced Military Aircraft Noise Reduction Concepts
Author(s): J. Liu
Affiliation(s): U.S. Naval Research Laboratory, Washington, DC
CTA: CFD

Computer Resources: HPE Cray Shasta, HPE SGI 8600 [AFRL, OH]; Cray XC40/50 [ERDC, MS]; Cray Shasta [NAVY, MS]

Research Objectives: Use HPC computational resources to predict details of turbulent flow structures and noise generation in supersonic exhaust jets from representative military aircraft jet engine nozzles and use this information to investigate and assess promising jet noise-reduction concepts in support of ongoing jet noise-reduction programs.

Methodology: The flow solver is JENRE® multiphysics software, a Navy-based and NRL-developed nodal finite-element code. JENRE® multiphysics software can take structured meshes and unstructured meshes with arbitrary cell types and has multiple levels of parallelism: multicore CPUs or multicore GPUs, and MPI for interprocessor communication. JENRE® multiphysics software has achieved an exceptional computational performance and scalability. Since using large-eddy simulations (LES) to fully resolve wall-bounded flows at high Reynolds numbers is computationally prohibitive due to the limitations of the available numerical methods and computational resources, the wall-layer model approach is used to simulate the boundary-layer effect of the wall-bounded flows. The far-field noise prediction is based on the Ffowcs Williams and Hawkings (FW-H) surface integral method. To simulate the high-temperature effect observed in realistic jet engine exhausts, a temperature-dependent function of the specific heat ratio is developed and implemented in JENRE® multiphysics software.

Results: LES has become an important tool in developing and optimizing the jet noise-reduction technologies. It has been observed that increasing the nozzle temperature can reduce the jet noise when the jet velocity is fixed. This phenomenon sometimes is referred to as the "heating effect" or the "jet Mach number effect." Since the full-scale tests are costly and can be susceptible to structure and design problems, it has been suggested to first use LES to assess this concept. A scaling analysis has been conducted to provide guidance to the design of the LES test matrices. Three test matrices have been made as shown in Tables 1–3. Jets in the same table have the same fixed mass flow rate and thrust. The noise predictions show that a higher jet velocity does not necessarily generate a higher noise intensity because the noise generation also depends on the jet Mach number. In addition, LES predictions confirm that at fixed thrust and mass flow rate, using a lower jet Mach number can reduce noise, as shown in Fig. 1. This noise reduction should be associated with the observation that a lower jet Mach number increases the shear-layer growth rate and reduces the convection velocity. This assessment involves a large number of large-eddy simulations, which require a significant amount of HPC resources, but is still cost-effective compared to the cost and time that would be needed if this assessment were conducted in full-scale tests.

DoD Impact/Significance: There is a growing need to reduce significantly the noise generated by high-performance, supersonic military aircraft. The noise generated during takeoff and landing on aircraft carriers has direct impact on shipboard health and safety issues. It is estimated that the U.S. Veterans Administration pays $4.2 billion or more for hearing-disability claims each year. The results of our work will provide better understanding of the noise production for both industrial and military aircraft and will aid the current effort of noise reduction, especially for supersonic aircraft.

Table 1. Jet operating conditions and nozzle geometry parameters in Test 1.

	M_j	U_j (m/s)	NPR	NTR	ΔT(K)	Area Ratio	Nozzle-Exit Diameter
Test 1a	1.47	717.8	3.5	2.9	0	1.295	5.05”
Test 1b	1.11	717.8	2.12	4.5	465.8	1.05	6.6”

Table 2. Jet operating conditions and nozzle geometry parameters in Test 2.

	M_j	U_j (m/s)	NPR	NTR	ΔT(K)	Area Ratio	Nozzle-Exit Diameter
Test 2a	1.47	846.3	3.5	4.0	0	1.295	5.05”
Test 2b	1.12	846.3	2.12	5.94	564.7	1.05	6.6”

Table 3. Jet operating conditions and nozzle geometry parameters in Test 3.

	M_j	U_j (m/s)	NPR	NTR	ΔT (K)	Area Ratio	Nozzle-Exit Diameter
Test 3a	1.65	774.5	3.5	2.9	0	1.295	5.05”
Test 3b	1.28	774.5	2.6	4.18	372.3	1.05	6.6”
Test 3c	1.15	774.5	2.2	5.14	654.0	1.05	7.6”

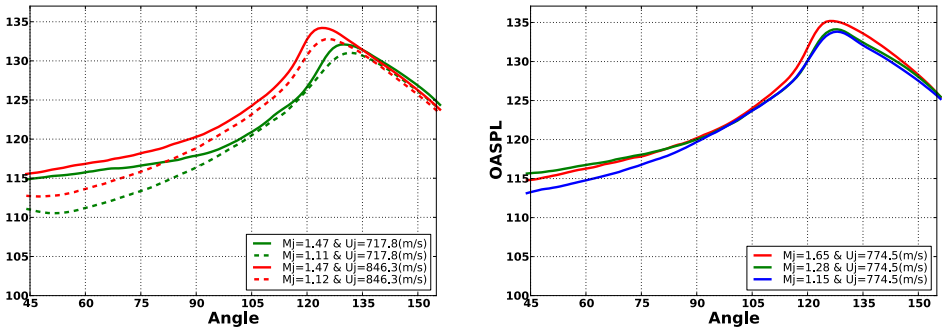


Figure 1. Figure on the left shows the far-field overall sound pressure levels of four jets shown in Table 1 and Table 2. Figure on the right is for jets shown in Table 3. The far-field distance is 42 feet away from the nozzle center.

Title: Aircraft Engine Noise Reduction Technology
Author(s): J. Liu
Affiliation(s): U.S. Naval Research Laboratory, Washington, DC
CTA: CFD

Computer Resources: HPE Cray Shasta [AFRL, OH]; Cray Shasta [NAVY, MS]

Research Objectives: Use HPC computational resources to predict details of turbulent flow structures and noise generation in supersonic exhaust jets from representative military aircraft jet engine nozzles and use this information to investigate and assess promising jet noise-reduction concepts in support of ongoing jet noise-reduction programs.

Methodology: The flow solver is JENRE® multiphysics software, a Navy-based and NRL-developed nodal finite-element code. JENRE® multiphysics software can take structured meshes and unstructured meshes with arbitrary cell types and has multiple levels of parallelism: multicore CPUs or multicore GPUs, and MPI for inter-processor communication. JENRE® multiphysics software has achieved an exceptional computational performance and scalability. Since using large-eddy simulations (LES) to fully resolve wall-bounded flows at high Reynolds numbers is computationally prohibitive due to the limitations of the available numerical methods and computational resources, the wall-layer model approach is used to simulate the boundary-layer effect of the wall-bounded flows. The far-field noise prediction is based on the Ffowcs Williams and Hawkings (FW-H) surface integral method. To simulate the high-temperature effect observed in realistic jet engine exhausts, a temperature-dependent function of the specific heat ratio is developed and implemented in JENRE® multiphysics software.

Results: LES has become an important tool in developing and optimizing jet noise-reduction technologies. LES has been used to develop and optimize the noise-reduction technology implemented on a model-scale F404 nozzle, which is a faceted biconic convergent and divergent nozzle made of 12 seals and flaps. This year we have continued the further development of the microvortex generator technology and also looked into another technology, namely sweeping jet actuators (SJA). SJAs are viable flow-control devices for improving the aerodynamic performance of high lift configurations by mitigating separated flow regions. In this work, we apply SJA technology to a simple, faceted nozzle and assess its noise-reduction potential. Figure 1 shows an SJA geometry and the flow field inside the SJA chamber. It can be seen that SJA emits spatially and temporally oscillating jets without any moving parts and relies primarily on the feedback mechanism inside the actuator chamber. Extensive large-eddy simulations and laboratory tests have been conducted to examine the dependence of the sweeping jet frequency on the geometry and the injection parameters. As shown in Fig. 2, the sweeping frequency is a strong function of the ratio L/d_1, which is the ratio between the SJA length and the SJA entrance width. Around 2 dB–3 dB, noise reduction is observed as shown in Fig. 3. The thrust loss is negligible, and in some cases, this technology can even increase thrust. However, the current simulations indicate that the noise reduction is not sensitive to the sweeping frequency.

DoD Impact/Significance: There is a growing need to significantly reduce the noise generated by high-performance, supersonic military aircraft. The noise generated during takeoffs and landings on aircraft carriers has direct impact on shipboard health and safety issues. It is estimated that the U.S. Veterans Administration pays $4.2 billion or more for hearing disability claims each year. The results of our work will provide a better understanding of noise production for both industrial and military aircraft and will aid the current effort of noise reduction, especially for supersonic aircraft.

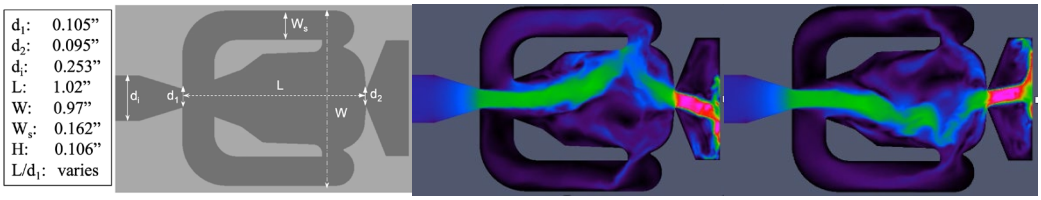


Figure 1. The geometry and flow field inside a sweeping jet actuator (SJA).

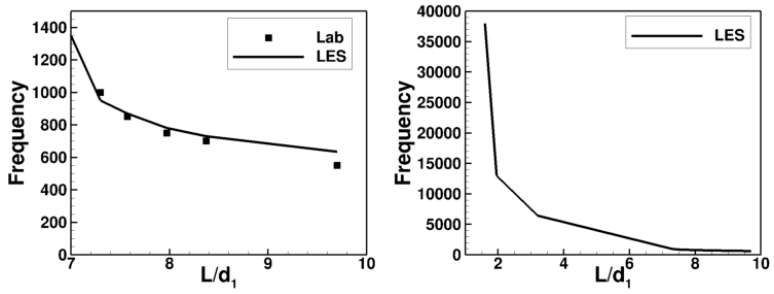


Figure 2. The dependence of the sweeping jet frequency on the ratio between the SJA length and the entrance width. The lab results were obtained by the Gas Dynamics and Propulsion Laboratory at the University of Cincinnati.

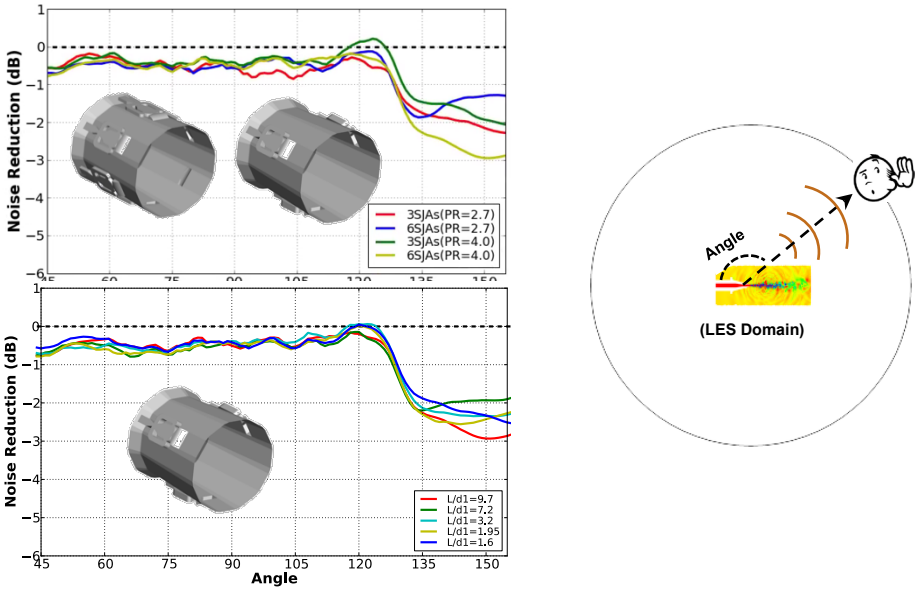


Figure 3. Noise reduction predicted by large-eddy simulations of nozzles implemented with SJAs. The nozzle pressure ratio is 2.7, which is a takeoff condition. The temperature ratio is 3.0, which is comparable to the maximum non-afterburning power level. PR is the SJA injection pressure ratio.

Title: Numerical Simulations of Turbulence Impact on Optical Signal Transmission and Near-Surface Turbulence
Author(s): S. Matt
Affiliation(s): U.S. Naval Research Laboratory, Stennis Space Center, MS
CTA: CFD

Computer Resources: SGI ICE X [ARL, MD]

Research Objectives: The objective is to refine work on the computational fluid dynamics (CFD) representation of numerical tanks to support and augment companion laboratory experiments. The laboratory tanks emulated are the Simulated Turbulence and Turbidity Environment (SiTTE) laboratory at NRL Stennis, and similar Rayleigh-Bénard (RB) tanks designed to generate convective, optically active turbulence, and the laminar-to-turbulent-flow tank flow SiTTE for boundary-layer dynamics and drag reduction, as well as the large state-of-the-art SUrge-STructure-Atmosphere INteraction (SUSTAIN) facility at the University of Miami. This work supported development of a new underwater communications system based on orbital angular momentum (OAM), novel fiber-sensor technologies, a new system for active boundary-layer control and drag reduction, and insight into the dynamics underlying near-surface turbulence and air-sea interaction processes to improve air-sea flux parameterizations.

Methodology: To accurately reproduce the turbulence dynamics, the representation of the numerical tanks is accomplished using large-eddy simulation (LES) and the full physical domain size of the respective tanks. The numerical experiments build on our previous work with OpenFOAM. We expanded our simulations of RB convection for simulation in air and for a wider range of boundary conditions and geometries, including a new physical RB tank recently completed at NRL DC (UWOC project, PI Judd).

Results: We performed simulations to provide a physics-based input for models of underwater optical propagation through turbulence with the goal of increasing propagation distance, which is of particular interest for optical communications using orbital angular momentum (OAM). We emulated the NRL DC RB laboratory tank, obtained fields of index of refraction variations for modeling of optical propagation, and assessed model performance through comparison to a high-order spectral model. Air-sea fluxes over waves and impact on upper ocean turbulence were studied to provide a scientific basis for physics-based air-sea flux parameterization for wave and coupled models. We used a multiphase model (with a volume-of-fluid approach to interface tracking) to emulate a comprehensive set of laboratory wind-wave experiments at the large SUSTAIN wind-wave facility (Fig. 1). We implemented temperature in the wind-wave multiphase model (Fig. 2) and tested the turbulence response with the goal of reproducing phase-dependent dynamics and determining the relationship between near-surface turbulent kinetic energy and wind speed depending on waves and heat flux conditions.

DoD Impact/Significance: CFD simulations emulating the convective SiTTE tank, the flow SiTTE tank, and the SUSTAIN wind-wave tank are critical for the success of research on a novel optical communication system based on OAM, novel methodologies for active boundary-layer control and drag reduction, new fiber-optics sensor development (temperature, flow), and parameterization of air-sea-interface dynamics.

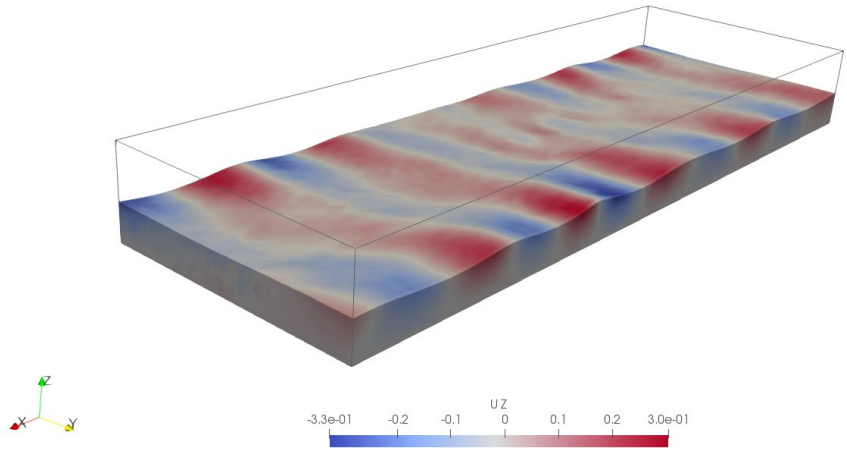


Figure 1. Numerical wind-wave tank in multiphase VOF model emulating the SUSTAIN laboratory. The domain simulates the full size of the lab tank: x = 18 m, y = 6 m, z = 2 m. Here, the water depth is 0.8 m. Vertical velocity (in m/s) in the water is shown at model time t = 680 s for wind-driven waves.

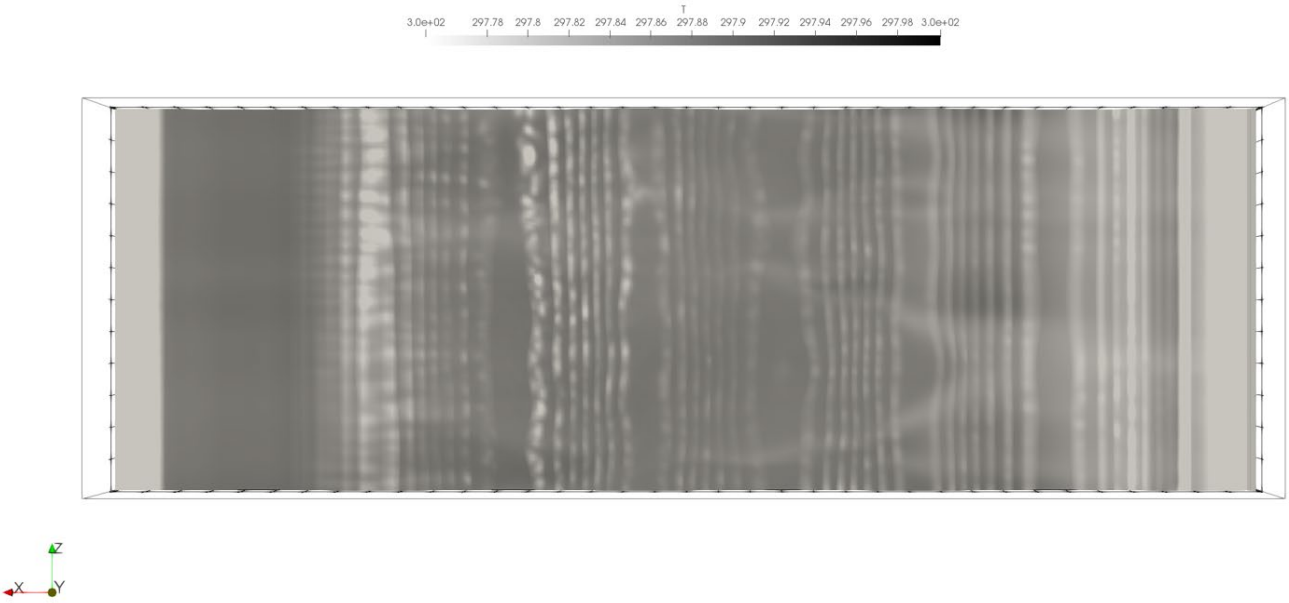


Figure 2. Top view of the temperature field in the water for the SUSTAIN wind-wave simulations with mechanically generated waves and added wind field (at time t = 450 s). Note the small-scale structures and streaks in the sea surface temperature field, indicative of near-surface shear. Temperature in K.

Title: Predicting Fluid-Structure Interaction for Military Applications
Author(s): D.R. Mott and Y. Khine
Affiliation(s): U.S. Naval Research Laboratory, Washington, DC
CTA: CFD

Computer Resources: HPE Cray Shasta, HPE SGI 8600 [AFRL, OH]; SGI ICE X [ARL, MD]; Cray XC40/50 [ERDC, MS]; Cray Shasta [NAVY, MS]

Research Objectives: Create the computational capability to predict the interaction of fluids with complex structures, and apply these capabilities to solve emerging problems critical to DON and the broader defense community. In the current context, simulations were used to assess various design criteria for helmets including blunt, ballistic, and blast performance, as well as thermal performance (highlighted below), and new methodologies for combining these performance parameters into a unified design approach were developed and explored.

Methodology: FY22's focus continued to be the transport phenomena around a warfighter in different ambient wind conditions in order to assess the impact of helmet configuration on passive cooling potential through perspiration and to inform the unified design approach cited above. Final reporting and documentation on these simulations were concluded in FY22. A baseline model was considered, including a bare head of the warfighter, and two configurations of helmet were investigated in no-wind and cross-wind conditions to compare the effects of natural and forced convection for the three configurations. A developmental version of CFD++ software that could address the physics of the simulations was received from Metacomp Technologies and it was installed on an ARL system with the support of HPC Helpdesk. The model employed a new boundary condition that simulated the sweating of the head by introducing water vapor at the head surface. Transport of this saturated air away from the head surface through natural and forced convection enabled the prediction of a maximum cooling effect through this evaporation.

Results: Figure 1 shows the plume rising from the head due to natural convection for the case with no helmet and no cross wind. Figure 2 shows how the helmets reduced transport of water vapor away from the head under these same conditions. Ambient relative humidity (RH) is 50%, and the head surfaces are assumed to be sweating sufficiently to fully saturate (100% RH) the air adjacent to the head. The helmets trap the saturated air between the head and the helmet shell, with only modest transport of this moisture-laden air away from the head apparent near the front and back brim in this cross section. With saturated air under the shell, the evaporation of additional perspiration is impeded and the cooling provided is reduced.

Table 1 gathers the average rate of transport for each geometry configuration and flow condition and quantifies the advantage of forced convection (a factor of 3 to 5) over natural convection for delivering effective cooling. The results also highlight that the 5-pad configuration with less blockage of the space between head and helmet shell delivers no advantage over the 7-pad case for natural convection but does improve cooling slightly for the studied forced convection case.

DoD Impact/Significance: Thermal loading in the field not only undermines concentration and performance of cognitive tasks, it also can result in heat-related injury. A design approach that accurately emphasizes the relative importance of a variety of design factors and threats, and that can be weighted differently for different scenarios, can produce optimal configuration options for targeted theaters and operations.

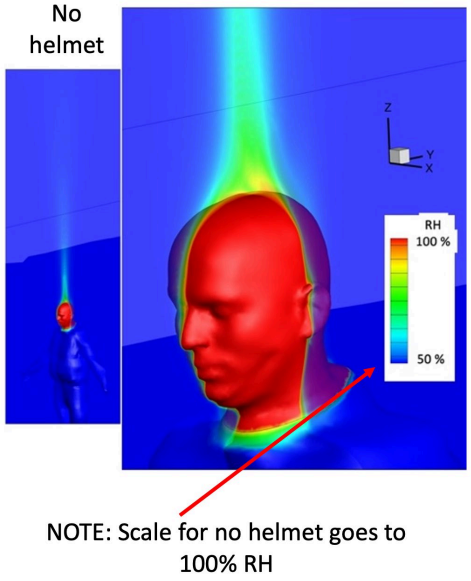
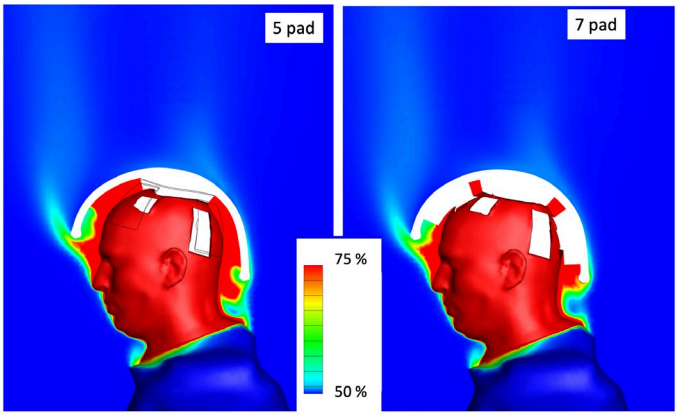


Figure 1. Relative humidity (RH) entrained by thermal plume for no helmet, no cross wind. RH scale goes to 100% (red).



Snapshots taken approximately 30 seconds after the simulation starts.
Planer cut through centerline with helmet shell and pads removed from image.

Figure 2. Relative humidity (RH) along head midsagittal plane for 5-pad (left) and 7-pad (right) helmet with no cross wind. RH scale is limited to 75% max, but boundary condition on head surface is 100% humidity.

	Natural Convection		Forced Convection	
Pad Configuration	**H_2O Vapor Transport [kg/s]**	**Watts**	**H_2O Vapor Transport [kg/s]**	**Watts**
no helmet	**7.57E-06**	**18.37**	**2.13E-05**	**51.70**
5 pad	**4.88E-06**	**11.84**	**2.12E-05**	**51.45**
7 pad	**4.72E-06**	**11.46**	**1.93E-05**	**46.84**

Table 1. Collected Vapor Transport and Cooling Capacity Results

Title: Developing a Shallow Water Environmental Database for Nearshore Operations
Author(s): A.M. Penko, K. Edwards, S. Harrison, R. Phillip, S. Schoenauer, and J. Veeramony
Affiliation(s): U.S. Naval Research Laboratory, Stennis Space Center, MS
CTA: CFD

Computer Resources: HPE SGI 8600 [NAVY, MS]

Research Objectives: A region's climatology is produced by averaging many years of environmental observations (e.g., wave heights, current and wind velocities) occurring over a specific length of time (e.g., seasons, months, days, etc.). Climatologies are often provided as an estimate of the typical environmental conditions a warfighter will encounter at a given time and location of an operational mission. Depending on the urgency of the mission, a climatology is sometimes the only information provided for operational mission planning. The Navy's existing environmental climatological database has a maximum resolution of 25 km and does not resolve the hydrodynamic features that are important at regional and near-shore scales (on the order of 100 m to1 km). The objective is to provide the Navy with a new capability to estimate the seasonal (monthly) and storm event (3 days) meteorological and oceanographic environmental conditions (ocean waves and currents, wind speeds and directions, and seafloor change) at high spatial resolution (on the order of 100 m) in near-shore coastal regions.

Methodology: The initial setup of the regional near-shore coupled wave-circulation model, Delft3D-FM, was completed and driven by two storm events in the Gulf of Mexico. The high-resolution simulations resolve local oceanographic features important to supported warfare areas (e.g., coastal water levels, wave height, and current magnitude). The output from this grid forced with time series of historical storms will be used to build the storm-event-driven climatological database. We also set up a sediment transport model (Seabed Mobility Regime Estimator - SeaMoRE) to build a database of sediment mobilization forced with regional model hydrodynamics. SeaMoRE calculates the bottom shear stress generated from predicted waves and currents and estimates the temporal and spatial variability of sediment mobilization and ripple formation. The output will be used to build the climatological database of seabed mobility critical for seabed infrastructure and mine countermeasure mission planning.

Results: Here, we show the storm-event-driven hydrodynamic (water level) output from one simulated hurricane and the duration of sediment mobilization over three days in the northern Gulf of Mexico. Figure 1(a-b) is the Delft3D-FM grid for the Gulf of Mexico (a), and a zoomed-in inset of the region around our demo site of Panama City, FL (b). Model-data comparisons of water level are plotted in (c). The observations are plotted in black and the final model is denoted with the red, solid line. This model is being used to simulate the data needed for the building of the storm-event-based climatology using the historical hurricanes to make landfall in this area (results currently in progress). Figure 2 is a plot of the predicted duration of sediment mobilization over three days in May of 2013. This model is being forced with a time series generated using an input reduction method over 20 years of hindcast reanalyses to build the sediment mobilization climatological database (results currently in progress). Additionally, this project supported the application of a method to optimize initial model parameter values by running ensembles and comparing to observations (see HPC Project report NRLSS06632054).

DoD Impact/Significance: The near-shore climatological database will be the first of its kind due to the recently available reanalysis datasets that can provide accurate forcing and boundary conditions as well as advances in the gridding and computational efficiency of high-resolution near-shore models. The new database will provide seasonal and storm-event time-scale estimates of environmental conditions in water depths of less than 100 m to support mine warfare (MIW) mission planning, naval special warfare (NSW), and subsea and seabed warfare (SSW) operations.

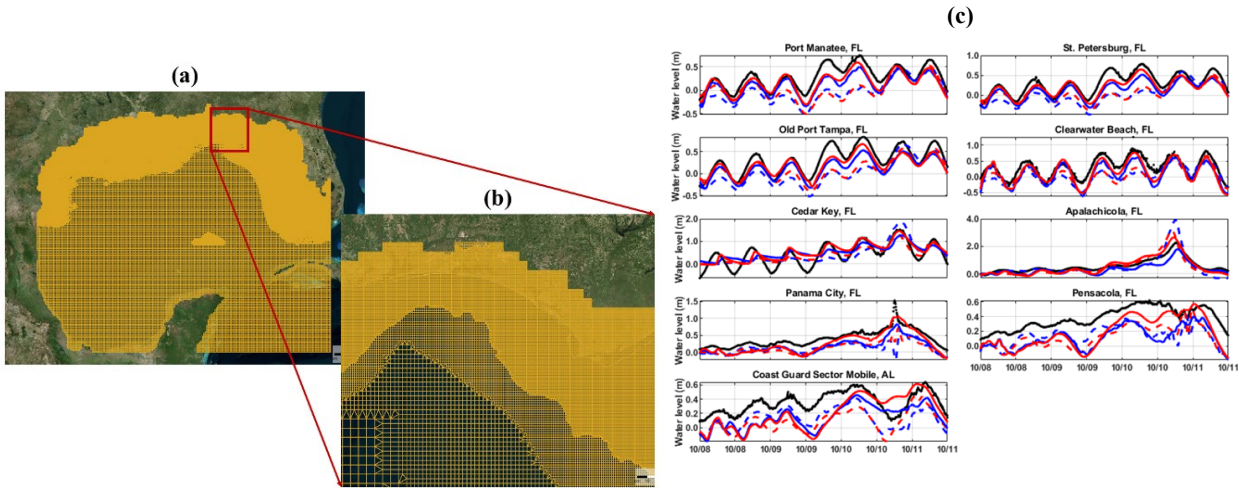


Figure 1. (a) Gulf of Mexico domain grid for the Delft3D-FM model. (b) A zoomed inset of the demonstration area around Panama City, FL. (c) Comparison plots of water levels at 9 NOAA 8729108, Panama City, FL leading up to and during Hurricane Michael in 2018. Observations are plotted in black and the final model to be used for building the climatology database is in solid red. The other lines on the plots are previous models to compare skill.

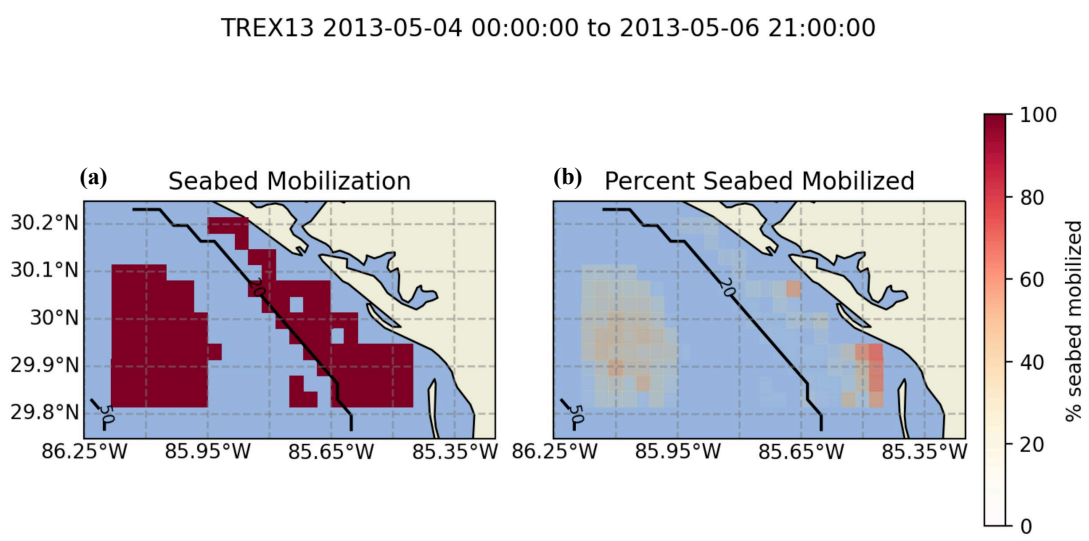


Figure 2. The Seabed Mobility Regime Estimator (SeaMoRE) predicts the occurrence and duration of sediment mobilization over a given time period in a requested location. It is forced with predicted hydrodynamic conditions (e.g., a Delft3D-FM model as shown in Fig. 1) and sediment information to determine the bottom shear stress due to waves and currents. (a) Denotes in red the locations where sediment was mobilized at least one time step over the three-day simulation. (b) Plots the percentage of time the bottom sediment was mobilized over the three-day simulation. This output can be used to determine hot spots of sediment erosion and ripple formation.

Title: Detonations with Multi-Phase Flows for Propulsion
Author(s): D.A. Schwer
Affiliation(s): U.S. Naval Research Laboratory, Washington, DC
CTA: CFD

Computer Resources: Cray Shasta [NAVY, MS]

Research Objectives: The main research goal of the present HPC project is to study high- and low-speed multiphase reacting flows for further understanding of advanced engine concepts, with the specific application for detonation engines.

Methodology: We have used two modeling codes for our research into blast and detonation engine simulations. Simulations are primarily done using the JENRE® multiphysics framework. Due to our extensive experience with using the DET3D codes for detonation propulsion, we continue to use them as a benchmark for comparison with the JENRE® framework. The framework utilizes unstructured meshes and both continuous- and discontinuous-Galerkin-FEM techniques to solve a wide variety of complex fluid dynamical phenomena. It has been built from the ground up at NRL in collaboration with other institutions to make efficient use of CUDA, HIP, Thread-Building-Blocks, OpenMP, and MPI through the use of the template libraries. By utilizing unstructured meshes, the solver can easily handle complex flow-paths from rig assemblies and engine concepts while remaining relatively efficient. Extensive work has gone into improving the JENRE® framework for both reacting and multiphase flows over the past several years.

Results: We did a series of calculations targeting experiments that use two different types of nozzles and high-pressure gas to investigate droplet-shock wave and droplet-detonation wave interactions. Simulations performed this year examined an atomizer at high pressure exhausting into a room, creating an underexpanded nozzle with a shock train in the high-speed jet. A series of simulations was conducted using the JENRE® code with different stagnation pressures, attempting to match the mass flow rate and pressure near the exit of the atomizer. The best match resulted from modeling the entire length of the atomizer and the mass flow rate, allowing boundary layers to develop and change the velocity profile of the gas as it travels through the atomizer. Preliminary comparisons were done with the location of the Mach disk that develops downstream of the nozzle exit. The simulation results replicated the shape and location of the Mach disk cases fairly accurately compared with experimental Schlieren. In addition, a Mach 5 overexpanded nozzle was modeled using the JENRE® code. The simulations included an exhaust plenum and, for some of the simulations, a fuel injector. A series of simulations was run examining the effect of backpressure and boundary layers on the jet flow field aft of the nozzle. Both nonreacting cases and one reacting case were computed. The simulations will help guide the experiments and determine the correct nozzle shaping and pressures for the experiment.

DoD Impact/Significance: The physics involved in RDCs and other detonation engines is substantially different than for gas-turbine engines. RDCs for propulsion concepts will require liquid fuels because of the high energy density of liquid fuels and the existing infrastructure. Simulations can play a significant role in helping to understand the interplay of the detonation wave and the liquid fuel droplets, which will determine the operability of RDCs for liquid fuels.

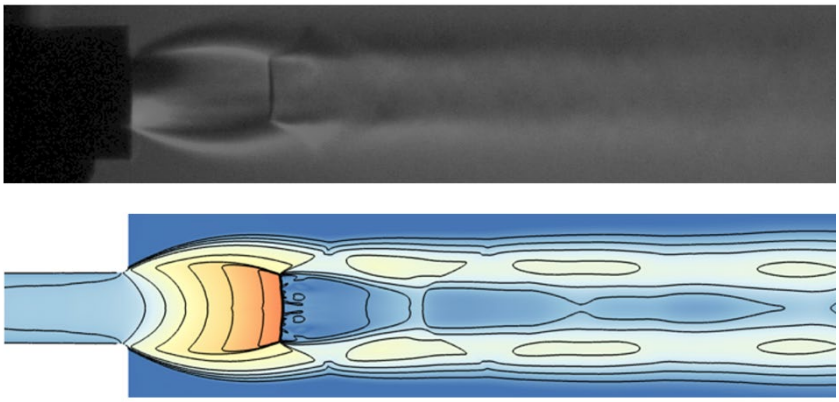


Figure 1. Comparison of experimental and simulation results for a strongly underexpanded jet. Contours of Mach number for simulation.

Title: Direct Numerical Simulation of Fluid-Sediment Wave Bottom Boundary Layer
Author(s): S. Schoenauer,[1] A.M. Penko,[1] J.A. Simeonov,[1] I. Adams,[2] S.P. Bateman,[1] J. Calantoni,[1] K. Edwards,[1] W.S. Kearney,[3] R. Phillip,[1] and J. Veeramony[1]
Affiliation(s): [1]U.S. Naval Research Laboratory, Stennis Space Center, MS; [2]National Research Council Postdoctoral Fellow, Stennis Space Center, MS; [3]American Society for Engineering Education Postdoctoral Fellow, Stennis Space Center, MS
CTA: CFD

Computer Resources: HPE SGI 8600 [AFRL, OH]; Cray XC40/50 [ERDC, MS]; Cray Shasta, HPE SGI 8600 [NAVY, MS]

Research Objectives: Predictive models for near-shore bathymetric evolution require a complete understanding of the physics of fluid-sediment interactions in the wave bottom boundary layer (WBBL). Since such processes are difficult, if not impossible, to measure in situ, we performed coupled fluid-sediment numerical simulations to increase our understanding of the sediment and hydrodynamics in the WBBL. Fundamental concepts used in describing the phenomena of sediment transport such as particle size and shape, mixture viscosity and diffusivity, hindered settling, bed failure criterion, bedform evolution, and the concept of acceleration-induced transport are addressed with our models. The models produce high-resolution results necessary to gain insight into the small-scale boundary-layer processes and clarify new directions for measurement techniques needed to improve predictive capabilities.

Methodology: Utilization and development of a suite of discrete and continuum WBBL multiphase models for simulating sediment transport in the near-shore environment from the microscale (cm to m) to the mesoscale (km) is ongoing with HPC resources. At the microscale (<10 cm), the three-dimensional sediment phase is simulated with discrete-element method (DEM) that allows individual grains and their interactions to be uniquely specified. The multiphase models vary in complexity from a simple one-dimensional eddy viscosity with one-way fluid-particle coupling to fully coupled fluid-particle models in three-dimensional direct numerical simulation (DNS). At the mesoscale (250 m to 8 km), ensemble simulations of coupled currents and waves with Delft3D Flexible Mesh were performed applying a range of parameters. Both wave and current parameters were varied in the ensembles for three time periods with a range of environmental conditions for a total of 260 simulations. The Generalized Likelihood and Uncertainty Estimation (GLUE) framework was employed to perform a model parameter sensitivity and optimization analysis for the study times.

Results: The two most sensitive parameters were bottom friction and horizontal eddy viscosity. Bottom friction has a pronounced effect on water levels (Fig.1), whereas eddy viscosity affects currents. The effect of the parameters on model results can be interdependent (i.e., the effect of eddy viscosity on currents is greater for lower values of bottom friction). We determined the optimal bottom friction coefficient values for both energetic (Fig. 2) and quiescent conditions in the northern Gulf of Mexico. Using this ensemble analysis and optimization method can efficiently show parameter sensitivity and can ultimately reduce uncertainty arising from model parameterizations.

DoD Impact/Significance: Ultimately, all process-based models for near-shore bathymetric evolution are limited by shortcomings in fundamental knowledge of multiphase boundary-layer physics. The microscale simulations provide an unprecedented level of detail for the study of fluid-sediment interactions that is impossible to obtain with available measuring technologies in the field or laboratory. These results are utilized to improve parameterizations of small-scale processes in larger-scale models. At the mesoscale, our models are highly efficient and well suited for coupling to regional operational hydrodynamic models. The computational resources consumed were in direct support of NRL base programs “Observations and modeling of biological cohesion on seafloor evolution time scales,” “Modeling sediment sorting in sand-shell environments,” “Predicting wind driven topographic change in sandy, coastal battlespace environments,” and “Developing a shallow water environmental database for nearshore operations.”

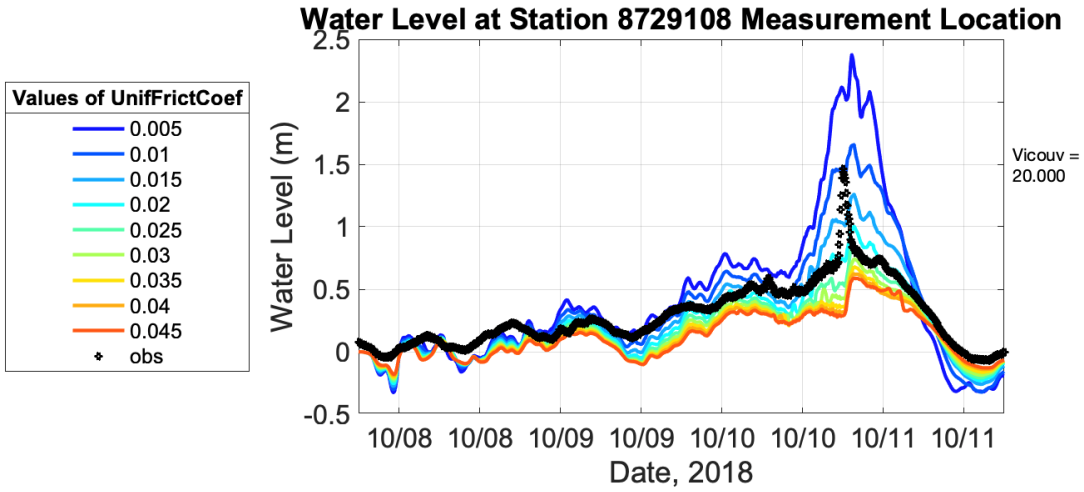


Figure 1. Model predictions applying varying bottom friction coefficient (UnifFrictCoeff) values (colored lines) and observations (black dots) of water levels at NOAA 8729108, Panama City, FL leading up to and during Hurricane Michael in 2018.

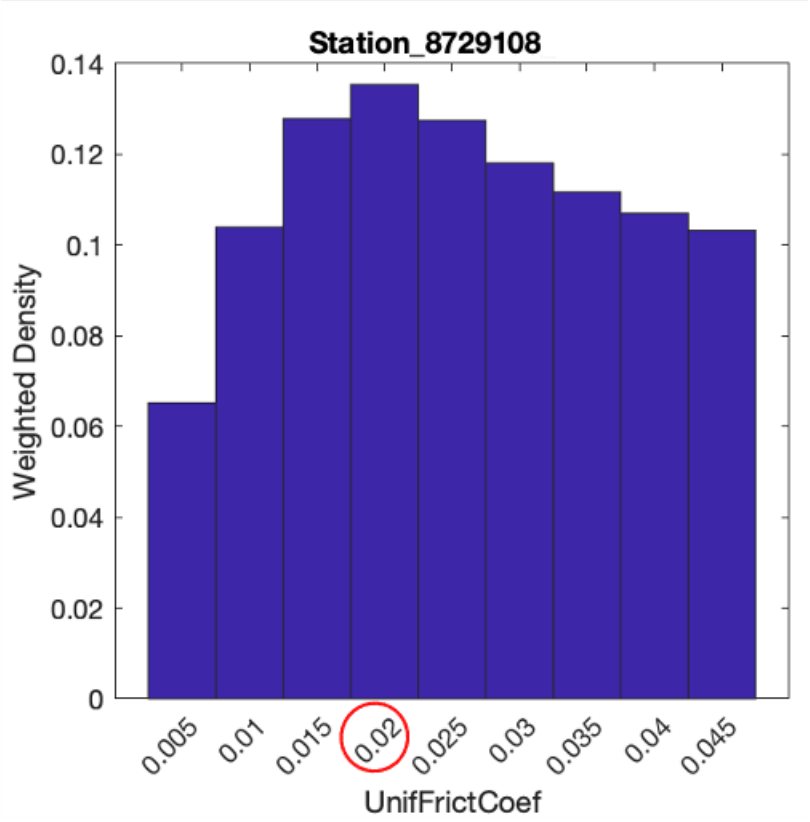


Figure 2. The relative performance of bottom friction coefficient values as determined by the Generalized Likelihood and Uncertainty Estimation (GLUE) method. The plot is a measure of the correlation between the ensemble model output with varying bottom friction coefficient values to water level observations at the NOAA 8729108 station near Panama City, FL, during Hurricane Michael in 2018. For these energetic conditions, the most optimal bottom friction coefficient value is 0.02.

Title: Numerical Simulations of Noise Generated by Non-Circular Advanced Military Aircraft Nozzles
Author(s): K. Viswanath and R. Ramamurti
Affiliation(s): U.S. Naval Research Laboratory, Washington, DC
CTA: CFD

Computer Resources: HPE Cray Shasta [AFRL, OH]; SGI ICE X [ARL, MD]; Cray XC40/50 [ERDC, MS]; Cray Shasta [NAVY, MS]

Research Objectives: Use HPC computational resources to predict details of turbulent flow structures and noise generation in supersonic noncircular asymmetric exhaust jets from representative military aircraft jet engine nozzles. This information will be used to investigate and assess promising jet noise-reduction concepts in support of the ongoing testing program.

Methodology: Simulations are performed using the JENRE® multiphysics framework, developed by the U.S. Naval Research Laboratory (NRL) with collaborating institutions. This U.S. Government-owned code provides unsteady compressible flow-solver capabilities that support various numerics, cell-centered finite-volume or nodal finite-element methods, while delivering high throughput on calculations. It was developed with an emphasis on raw performance and the ability to exploit emerging massively parallel, high-performance computing (HPC) architectures. It supports different HPC parallel programming paradigms for message passing such as MPI, OpenMP, CUDA, HIP, and hybrid models depending on the HPC cluster architecture. A key bottleneck of HPC throughput is data input-output (IO). The code supports parallel IO via MPI/IO to further complement the multiple levels of parallelism. Taylor-Galerkin finite-element method with second-order spatial accuracy for tetrahedral cells is used with the Finite-Element Flux Corrected Transport (FEM-FCT) method. The multidimensional FCT flux limiter provides an implicit subgrid stress model, which ensures monotonicity at shocks and sharp gradients with minimal artificial dissipation. We use an extended version of the code that features a wall model that supports high-speed flows and surface roughness effects while significantly reducing grid resolution requirements.

Results: Simulation of a supersonic twin jet at a highly overexpanded baseline operating condition and nozzle configuration was investigated with further simulations differing nozzle separation distance by increments of 2.7D and 3D (equivalent diameter D = 0.018 m). Nozzle pressure ratio is fixed at 2.5. The nozzle geometry, aspect ratio 2 nozzles and baseline separation distance of 2.3D as shown in Fig. 1, was imported and modified using CAD features of the Capstone software for each case. Changing the nozzle separation distance informed the impact of twin jet interaction and shielding effects on far-field noise. These simulations analyze potential nozzle configurations where there might be a noise-reduction effect due to the geometrically imposed constraints on jet interaction. The baseline case was validated with excellent agreement on noise production and flow features with experimental data from the University of Cincinnati (UC). The simulations showed far-field noise reduction in the upstream and sideline directions while increasing noise in the peak direction in both cases compared to the baseline case, shown in Fig. 2. Figure 3 is the normalized time averaged contours of the streamwise jet plume velocity, showing the shock cell structures and the jet core interaction for the 3.0D case with extracted line data highlighting differences with the baseline case. With increased nozzle separation distance, the jet interaction is delayed by almost 2.5D in the symmetry plane and complete mixing is not reached even at 20D downstream. However, this change in the interaction does not affect each jet core. This points to jet interaction effects on far-field noise.

DoD Impact/Significance: The results of our work will provide better understanding of the noise production for both industrial and military aircraft, and will aid the current effort of noise reduction, especially for supersonic aircraft, to reduce the impact of the jet noise on shipboard health and safety issues.

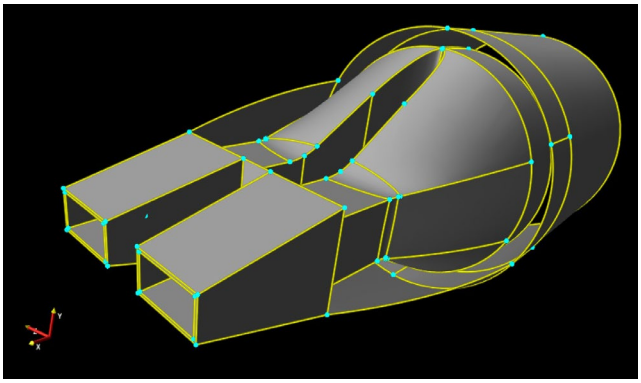


Figure 1. Twin jet nozzle geometry, aspect ratio 2 nozzles with separation distance of 2.3D.

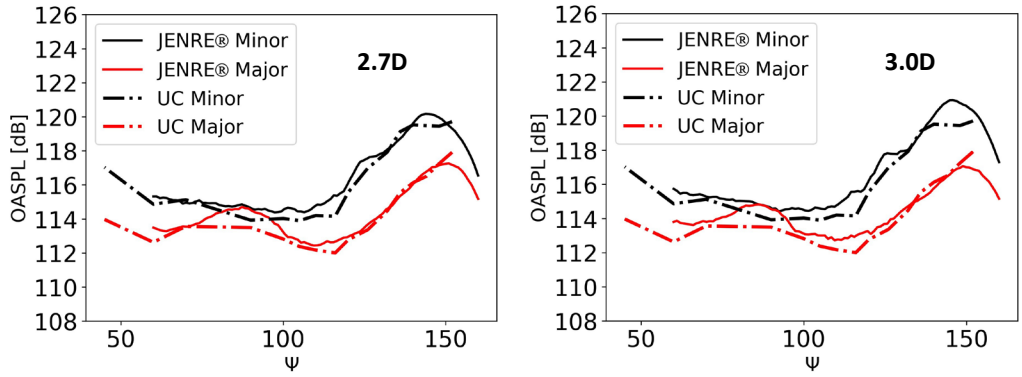


Figure 2. Far-field noise comparison at 60D for the NPR 2.5 case twin jet plume at different nozzle separations. Left shows 2.7D distance and right shows 3.0D case with UC data showing baseline noise.

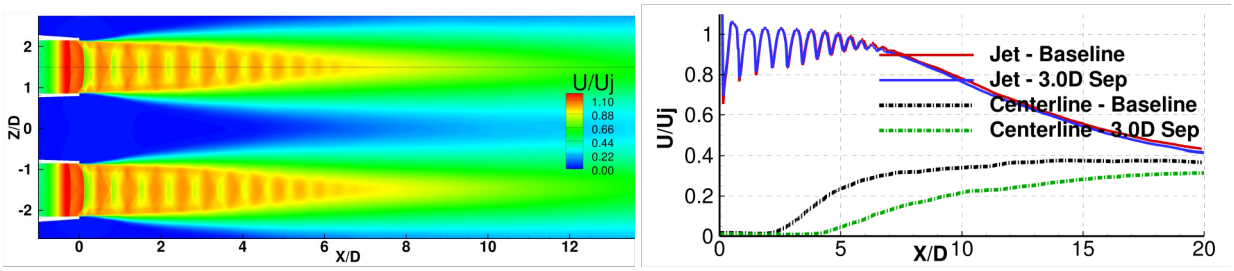


Figure 3. Twin jet interaction for the 3.0D nozzle separation distance case. Left shows the time-averaged flow field from simulation in the XZ plane passing through jet centerlines. Right shows the extracted line cuts from each jet centerline and the symmetry plane between the jets compared to the baseline case.

Title: Towards Simulation of Solid Fuel Combustion using Detailed and Reduced Order Modeling Approaches
Author(s): B.T. Bojko
Affiliation(s): U.S. Naval Research Laboratory, Washington, DC
CTA: CFD

Computer Resources: Cray Shasta [NAVY, MS]

Research Objectives: Develop and test solid-fuel combustion models for use in large-scale solid-fuel ramjet and scramjet combustor simulations. We will develop models to compare to experimental data. Models will be created starting from the fundamental processes of solid-fuel combustion in small-scale scenarios using high-fidelity fluid-dynamics solvers and finite-rate chemistry. Reduced-order models will be developed and created from the detailed simulations in order to employ them in large-scale combustion simulations of solid-fuel air-breathing propulsion combustors. Creating reduced models from fundamental physical processes will enable efficient calculations of large-scale systems that will ideally be capable of answering critical design questions.

Methodology: We conducted small-scale one- and two-dimensional combustion simulations of an opposed flow burner and a slab burner to better understand the coupling of the combustion zone on the fuel pyrolysis rate and gasified species. These simulations are then compared to experimental pyro-probe, counterflow, and slab burner data currently being collected at NRL, NAWCWD, NSWCIH, and Purdue University. For this project, we will be utilizing the NRL-developed multiphysics flow solver JENRE® multiphysics and will develop reduced-order models, such as the flamelet progress variable (FPV) approach. These models are used to incorporate the combustion details of the small-scale simulations efficiently into large-scale simulations of solid-fuel air-breathing propulsion systems. The FPV approach relies on tabulated chemistry models to define the reaction progression as a function of equivalence ratio and the flame strain rate. Mapping combustion species to flamelet variables is a nontrivial process that requires a careful mathematical definition such that species information can be accurately determined during large-scale simulations.

Results: We developed a FPV approach with the use of flamelet generated manifolds to model the detailed combustion of the compressible, fully conservative reacting Navier-Stokes equations using a discontinuous Galerkin (DG) flow solver. We developed a systematic process of creating and tabulating individual flame solutions using the definitions of mixture fraction (Z) and progress variable (C_{pv}) needed for translating flame solutions to a flamelet variable space. The fully conservative forms of the Navier-Stokes equations are expressed in terms of the mass, mixture fraction, progress variable, momentum, and total-energy-conservation equations. Where using the FPV approach reduces the overall species partial differential equations to be solved from $N - 1$, where N is the number of species, down to two, all the while, the numerical stiffness is significantly reduced by utilizing the reaction progress variable to define the extent of reactions. In this work, we studied the combustion of methane gas in a diffusion flame configuration behind a backward-facing step and within the expansion region. Three different configurations were investigated in order to understand the effects of reaction on the flow-field and vice versa. Firstly, an inert flow of air was studied as it traversed the backward-facing step, followed by a nonreacting case of fuel mixing from the bottom of the domain with the incoming air. This scenario is observed in Fig. 1, where the fuel (red) is being injected from the bottom surface and mixing with the vortices generated from the flow expanding over the step. Upon igniting the fuel and allowing it to combust for approximately 5 flow-through times, the recirculation zone and, subsequently, the mixing layer become dulled due to the heat release and decrease in viscosity as demonstrated in Fig. 2. This study will help illuminate the characteristics of diffusion flame combustion occurring in an expanding flow and will help in the design of combustors that share a similar geometry.

DoD Impact/Significance: This research is aimed at increasing the understanding and design capabilities of air-breathing hypersonic propulsion systems intended to increase the range and speed of current weapons systems within the fleet. Hypersonic technology is an identified primary focus area as defined by the under secretary of defense for R&E.

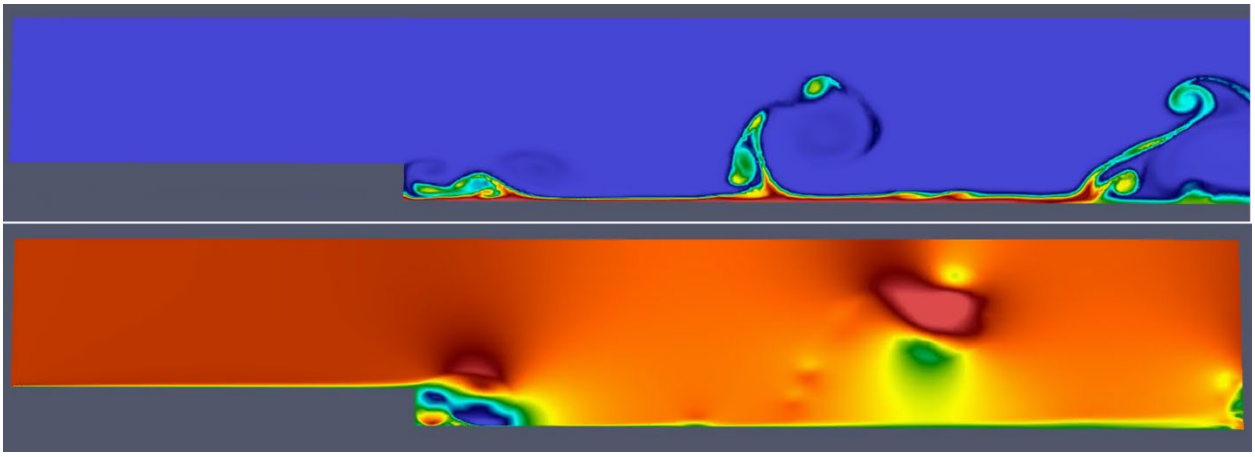


Figure 1. The top image shows the mixture fraction ranging from $Z = 0$ (blue) to $Z = 1$ (red) for a nonreacting fuel emanating from the bottom of the domain behind the backward-facing step. The bottom image shows the velocity profile ranging between $-5 \leq Vx \leq 14$ m/s from blue to red. A recirculation zone is shown behind the step with a shedding frequency on the order of $50Hz$.

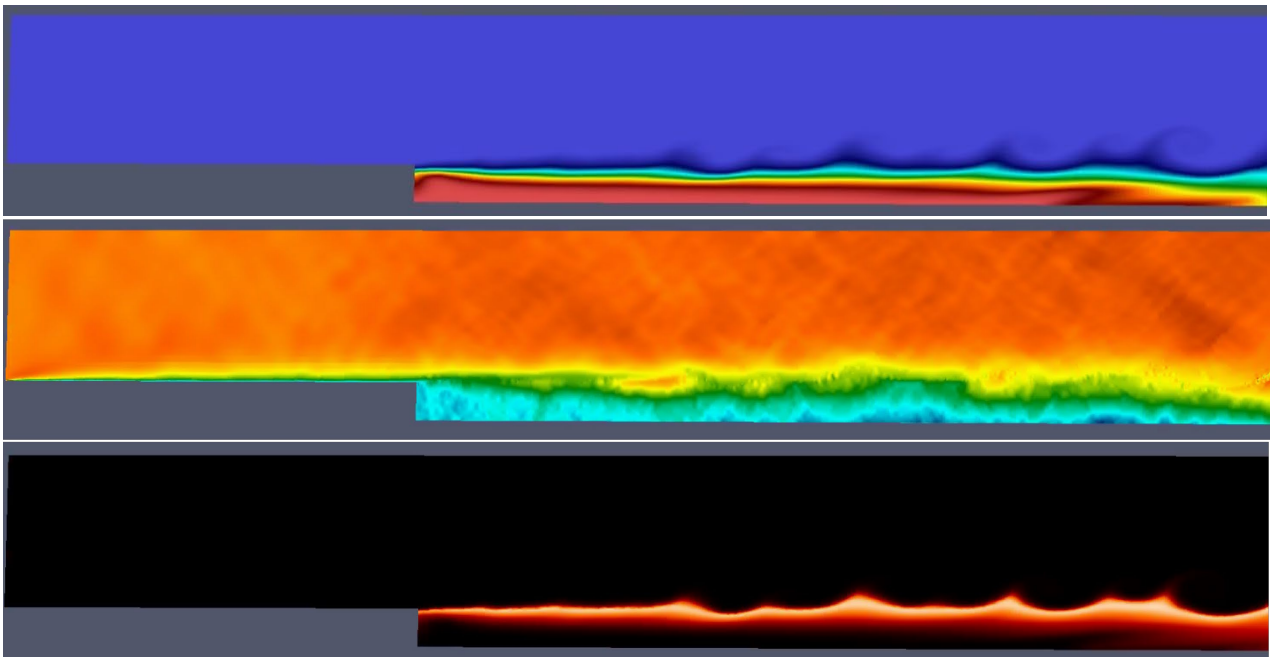


Figure 2. For the case with combustion, mixture fraction (top) — $0 \leq Z \leq 1$ [blue to red] — is shown to have a more distinct mixing boundary, with mixing occurring mostly in the shear layer. The velocity (middle) — $-5 \leq Vx \leq 14$ m/s [blue to red] — no longer has a clearly defined recirculation zone and shows the presence of acoustic waves. The temperature profile (bottom) — $300 \leq T \leq 1{,}800$K [black to orange] — demonstrates a clearly defined flame zone along the shear layer near the value of stoichiometric mixture fraction.

Title: Simulations of the Ionosphere/Plasmasphere/Thermosphere System
Author(s): J. Krall[1] and J.D. Huba[2]
Affiliation(s): [1]U.S. Naval Research Laboratory, Washington DC, [2]Syntek Technologies, Fairfax VA
CTA: CFD

Computer Resources: HPE SGI 8600 [AFRL, OH]; Cray XC40/50 [ERDC, MS]

Research Objectives: Predict the dynamics of the ionosphere/magnetosphere environment as it relates to operational communications and navigation systems used by the warfighter. Develop a first-principles physics-based model of near-Earth space based on the NRL code SAMI3, including understanding and predicting equatorial spread F disturbances and the dynamics of the plasmasphere.

Methodology: The research uses the NRL SAMI3 code, a comprehensive 3D simulation model of Earth's ionosphere/plasmasphere system, coupled to a model of the thermosphere (e.g., TIE-GCM, GITM, WACCM-X, HIAMCM) and the inner magnetosphere (e.g., RCM, CIMI) to self-consistently describe the geospace system.

Results: High-resolution simulation studies of the response of the ionosphere/plasmasphere system to the Tonga volcanic eruption were performed using the coupled SAMI3 ionosphere/plasmasphere model and the HIAMCM whole-atmosphere model with added primary gravity waves (GWs) from the MESORAC model. The Tonga eruption occurred on January 15, 2022.

An example of the results is shown in Figs. 1 and 2. In Fig. 1, we show isosurfaces of the vertical neutral wind velocity (left) and the disturbed electron density (right) at time 6.00 UT (6:00 UT), roughly 2 hours after the eruption. The disturbed electron density is a "smoothed" electron density subtracted from the actual electron density. At this time, concentric-like wave structures are evident in the vertical wind velocity emanating from the epicenter of the eruption. The vertical velocity is ± 15 m/s, which is significantly larger than nominal vertical wind velocities (± few m/s). Similar concentric-wave structures are also evident in the disturbed electron density. This is caused by ion-neutral collisional coupling in which the neutral wind "pushes" the ions up and down the magnetic field.

In Fig. 2, we show isosurfaces of the vertical wind velocity (left) and the disturbed electron density (right) at time 10.50 UT (10:30 UT), roughly 6 hours after the eruption. At this time, the atmospheric disturbance of the neutral wind has propagated across the southern polar cap and into the Northern Hemisphere. Interestingly, at this time, a series of EPBs has developed west of the epicenter; this is consistent with the observations reported by Aa et al. (2022).[1] These EPBs are generated in part because of large variations in the zonal neutral wind (not shown) that affect the electrodynamics of the ionosphere.

DoD Impact/Significance: Potential protection of communication satellites and the power grid. Support of ongoing experiments in remote sensing of the space environment. Provide input to ionospheric and thermospheric models.

[1] Aa, E., et al., *Space Weather, 20*, e2022SW003101. https://doi. org/10.1029/2022SW003101, 2022.

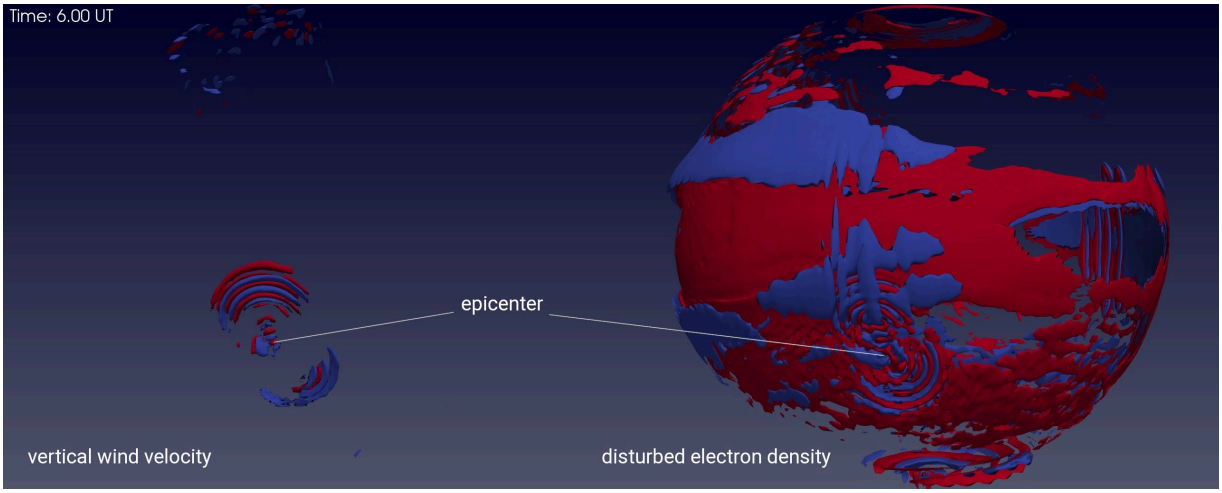


Figure 1. Isosurfaces of the vertical wind velocity (left) and the perturbed electron density (right) at time 6.00 (UT).

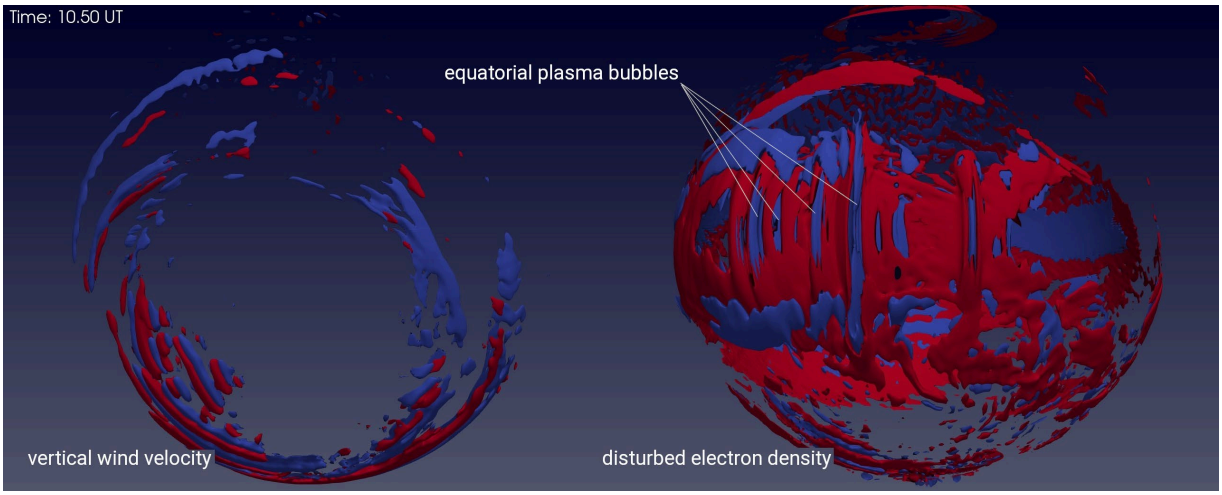


Figure 2. Isosurfaces of the vertical wind velocity (left) and the perturbed electron density (right) at time 10.50 (UT).

Title: Applications of FEFLO Incompressible Flow Solver
Authors: R. Ramamurti
Affiliations: U.S. Naval Research Laboratory, Washington, DC
CTA: CFD

Computer Resources: HPE Cray Shasta [AFRL, OH]

Research Objective: Perform three-dimensional (3D) numerical simulations of flow past complex configurations. The proposed studies will investigate the use of bioinspired skins for drag reduction for unmanned underwater vehicles.

Methodology: A finite-element solver, called FEFLO, for 3D incompressible flows based on unstructured grids is used. The flow solver is combined with adaptive remeshing techniques for transient problems with moving grids and is also integrated with the rigid body motion in a self-consistent manner, which allows the simulation of fully coupled fluid-rigid body interaction problems of arbitrary geometric complexity in three dimensions. NRL has developed a coupled fluid structure interaction solver for simulating flapping-fin propulsion for operations. In addition to three-dimensional unsteady flow simulations past passively deforming flapping pectoral fins in tandem configurations, simulations are performed over airfoils with bioinspired sharkskin denticles for drag reduction. Limited parametric studies are conducted varying configuration of the denticles and the angle of attack of the airfoil.

Results: The configuration used for simulations is the NACA0012 airfoil. The initial critical and time-consuming step for flow simulations is the generation of a 3D computational model. This is achieved by converting the stereolithographic (STL) representation of the denticle. Next, the denticles are positioned from 0.5 C to 0.83 C in both aligned and staggered configurations as shown in Fig. 1. A computational mesh consisting of approximately 80 million points and 460 million tetrahedral elements was used for simulating the viscous flow over these configurations. Simulations were performed with an inflow velocity of 1 m/s at various angles of attack in the range of ±15°. Figure 2 shows the variation of coefficients of lift and drag at various angles of attack. The lift produced by the two denticled airfoils at +ve angles of attack (α) remained similar to the baseline configuration and showed considerable improvement at $\alpha = -15°$, while the staggered configuration showed a slight improvement, shown in Fig. 2a. Expanding these parametric studies for passively deforming denticles will lead to the development bioinspired skins for UUVs.

DoD Impact/Significance: Simulations have enabled characterization drag prediction for bioinspired skins for use with unmanned underwater vehicles. This will provide the next steps toward development of a comprehensive analytical tool for drag reduction and vehicle design.

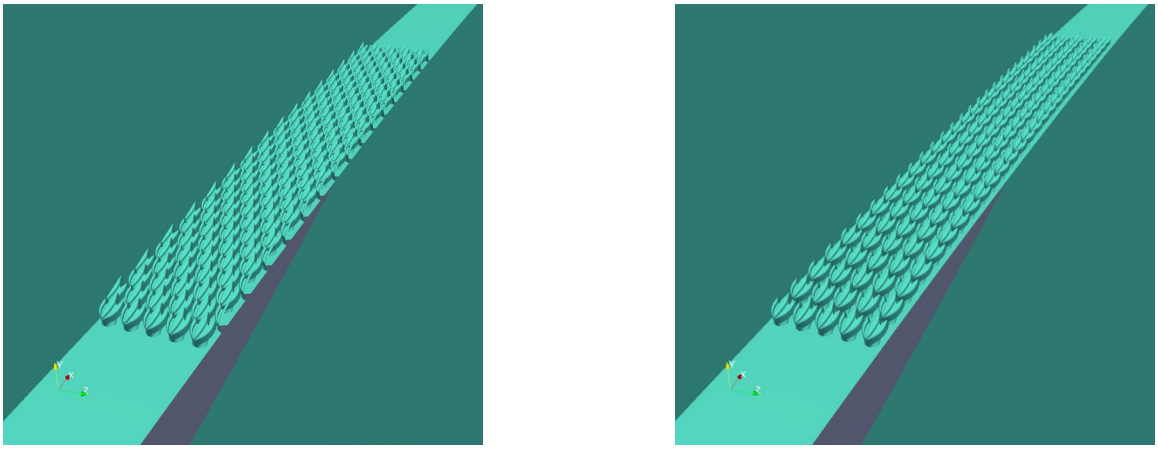


Figure 1. (a) Staggered and (b) aligned configurations of denticles on the NACA0012 airfoil.

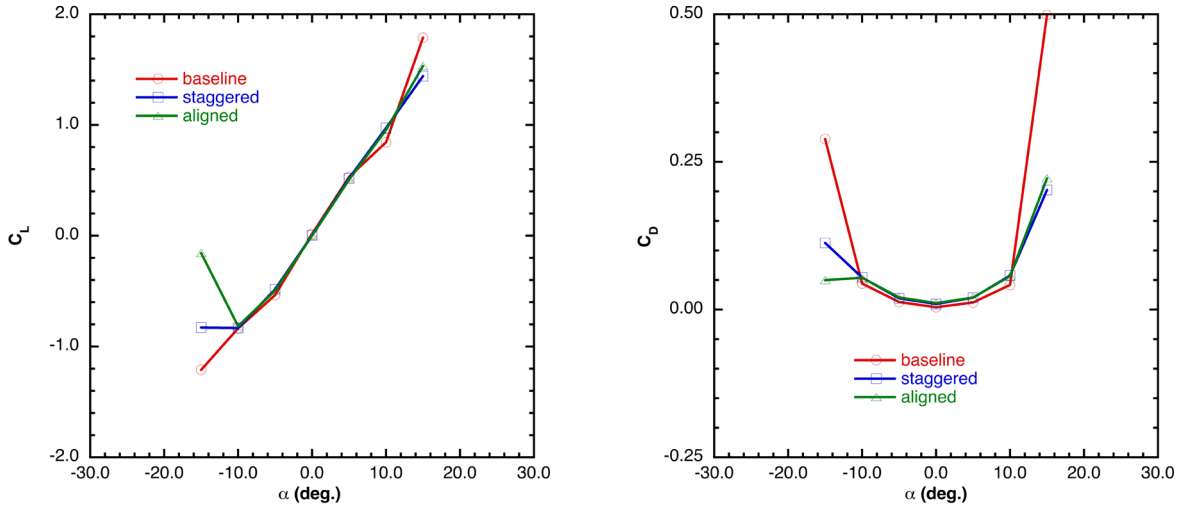


Figure 2. Effect of denticles on the lift and drag characteristics.

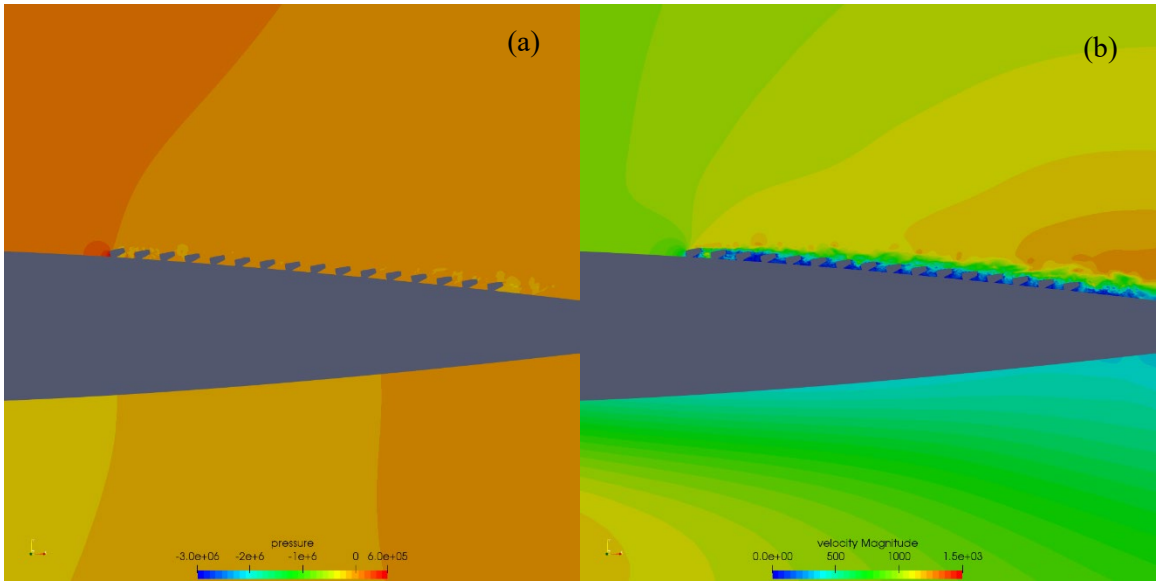


Figure 3. Instantaneous contours of (a) pressure and (b) magnitude of velocity on the spanwise symmetry plane for the staggered denticle configuration, $\alpha = -15°$.

Title: Mitigation of Blasts in Enclosures
Author(s): D.A. Schwer
Affiliation(s): U.S. Naval Research Laboratory, Washington, DC
CTA: CFD

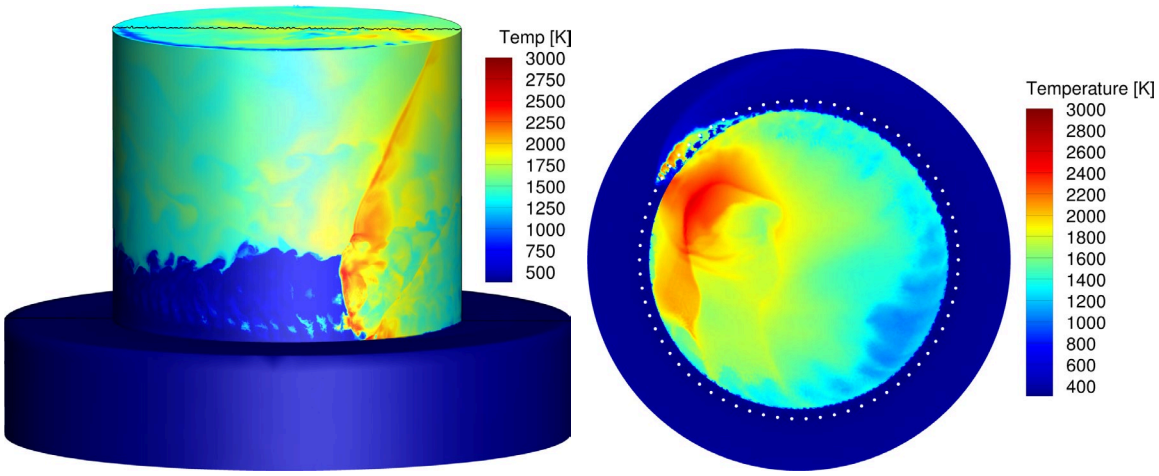
Computer Resources: Cray Shasta [NAVY, MS]

Research Objectives: The main research goal of the present HPC project is to study high- and low-speed multiphase reacting flows for further understanding of advanced engine concepts, with the specific application for detonation engines.

Methodology: We have used two modeling codes for our research into blast and detonation engine simulations. Simulations are primarily done using the JENRE® multiphysics framework. Due to our extensive experience with using the DET3D codes for detonation propulsion, we continue to use them as a benchmark for comparison with the JENRE® framework. The framework utilizes unstructured meshes and both continuous- and discontinuous-Galerkin-FEM techniques to solve a wide variety of complex fluid dynamical phenomena. It has been built from the ground up at NRL in collaboration with other institutions to make efficient use of CUDA, HIP, Thread-Building-Blocks, OpenMP, and MPI through the use of standard template libraries. By utilizing unstructured meshes, the solver can easily handle complex flow paths from rig assemblies and engine concepts while remaining relatively efficient.

Results: Research into simulating rotating detonation combustors (RDCs), and in particular, using rotating detonation combustion as a pilot to an augmentor, has been conducted. Two rig configurations were simulated. These simulations are extremely difficult to get working due to the usual complexities of an RDC simulation, and added to that, the large dump region in the central region that has to be simulated. The first was a hollow-RDC rig operated at University of Cincinnati with ethylene-air. Hollow-RDCs are an important first step toward getting an RDC piloted augmentor to work. The second rig considered is an augmentor concept from the Naval Postgraduate School (NPS). This concept relies on channels between an annular RDC and a core to allow high-pressure, hot gases into the core to serve as a pilot. The initial configuration considered by NPS showed only a small amount of penetration of hot gases into the core flow (ignition of the core flow was not considered at this time). A second iteration was done that considerably simplified the rig and looked at channel placement at two different axial locations. This iteration showed better penetration of the detonated gases into the core flow. Continued work with NPS will refine this concept in an attempt to determine what is needed for this concept to work. Simulations were also performed with the quasi-two-dimensional DET3D code examining axial instabilities in RDCs. This type of instability will become more important as the air inlet is opened and performance is pushed. The behavior of this instability and performance metrics with respect to a new, nondimensional parameter was shown to effectively collapse data from air inlet and exhaust nozzle area ratios.

DoD Impact/Significance: The physics involved in RDCs and other detonation engines is substantially different than for gas-turbine engines. Integrating rotating detonation combustion into an augmentor presents its own unique challenges, and our very limited experience with this type of engine requires investigation both experimentally and computationally. Simulations can play a significant role in helping to understand the interplay of the detonated gases with the core flow in an augmentor and to determine which types of engine configurations work well. Through this research, the potential of significant sizing and efficiency gains for augmentors can be realized.



(a) (b)

Figure 1. Temperature plot of University of Cincinnati hollow rotating detonation combustor (RDC) rig operating with non-premixed ethylene and air. (a) Outer wall of rig and (b) head end and injection plane of rig. A detonation wave formed along the outer wall of the combustion chamber and propagates azimuthally.

THIS PAGE INTENTIONALLY LEFT BLANK

CCM

Computational Biology, Chemistry, and Materials Science

CCM covers computational tools used to predict basic properties of chemicals and materials, including nano- and biomaterials. Properties such as molecular geometries and energies, spectroscopic parameters, intermolecular forces, reaction potential energy surfaces, and mechanical properties are being addressed. Within the DoD, quantum chemistry, molecular dynamics, statistical mechanics, and multiscale methods are used to design new chemical, polymer, nanomolecular, and biomolecular systems for fuel, lubrication, laser protection, explosives, rocket propulsion, catalysis, structural applications, fuel cells, and chemical defense. Solid-state modeling techniques are employed in the development of new high-performance materials for electronics, optical computing, advanced sensors, aircraft engines and structures, semiconductor lasers, advanced rocket engine components, and biomedical applications. Of recent emerging interest in the Computational Biology, Chemistry, and Materials Science (CCM) CTA are methodologies that cover bioinformatics tools, computational biology, and related areas, such as cellular modeling.

Title: Multiple Length and Time Scale Simulations of Material Properties
Author(s): N. Bernstein
Affiliation(s): U.S. Naval Research Laboratory, Washington, DC
CTA: CCM

Computer Resources: HPE Cray Shasta, HPE SGI 8600 [AFRL, OH]; Cray XC40/50 [ERDC, MS]

Research Objectives: To understand and predict mechanical, structural, and energetic material properties

Methodology: Molecular dynamics (MD) and Monte Carlo (MC) for the time evolution and sampling of atomic configurations. Trajectories use energies and forces from density functional theory (DFT) and interatomic potentials. Gaussian approximation potential (GAP), atomic cluster expansion (ACE), and message-passing neural network ACE (MACE) methods for single- and multispecies interatomic potentials. The software implementing these methods includes VASP and SPHInX for DFT simulations, LAMMPS for interatomic potential MD, ASE, libAtoms/QUIP, ACESuite and MACE for machine-learning potential development and interfacing between various programs. The MACE potentials fitting used GPGPUs via the pytorch library.

Results: A series of first-principles DFT calculations of the mechanical and structural properties of paramagnetic steels was completed and was published in the journal Physical Review Materials. The calculations were then extended to a more accurate approximation to the paramagnetic state using the SPHInX DFT software. DFT was also used to calculate the elastic properties of the flash-sintered ceramic TiO_{2-x}. These properties are challenging to calculate because the imperfect stoichiometry requires large unit cells to describe, but they are essential for understanding the different ordered phases that occur at the oxygen vacancy concentrations that arise in flash sintering.

A number of machine-learning interatomic potentials were also developed using HPC resources. The first is for the $CsPbBr_3$ perovskite, whose optical and electronic properties are determined by the subtle distortions that distinguish its cubic, tetragonal, and orthorhombic phase (in order of decreasing temperature). The second is CuAl, a model for Ni-Al bronzes, where very high DFT convergence parameters were required for an accurate description. Finally, a MACE model, which uses message-passing neural networks (MPNNs), was developed for GeTe to compare this new form of machine-learning interatomic potential to more established approaches such as GAP and ACE. Since these MPNNs are very efficiently implemented on GPUs, the NVIDIA V100-based visualization and machine-learning nodes on warhawk were used. Finally, an existing force-constant potential for the low-thermal-conductivity filled and unfilled skutterudite crystals was used to simulate their behavior for different compositions and filling atoms.

DoD Impact/Significance: Nonmagnetic steels and Ni-Al bronzes are structural materials with good strength and toughness, corrosion resistance, and low magnetic signature. First-principles simulations of their properties can help design compositions and processing that lead to improved technological performance. Ceramics are used for their mechanical properties and corrosion resistance, and flash sintering of ceramics greatly reduces the time and energy cost for their fabrication and leads to greatly enhanced toughness, which is facilitated by the defects simulated here. Functional materials are used for sensors, light emitters, and thermoelectric power generation. Inorganic halide perovskites have unprecedented brightness and light emission efficiency, as well as photovoltaic performance, and skutterudites have very low thermal conductivity, which gives them a high thermoelectric figure of merit. Atomistic simulations can reveal experimentally inaccessible microscopic details of their structure, which controls their performance, and can lead to material designs with better technologically relevant properties.

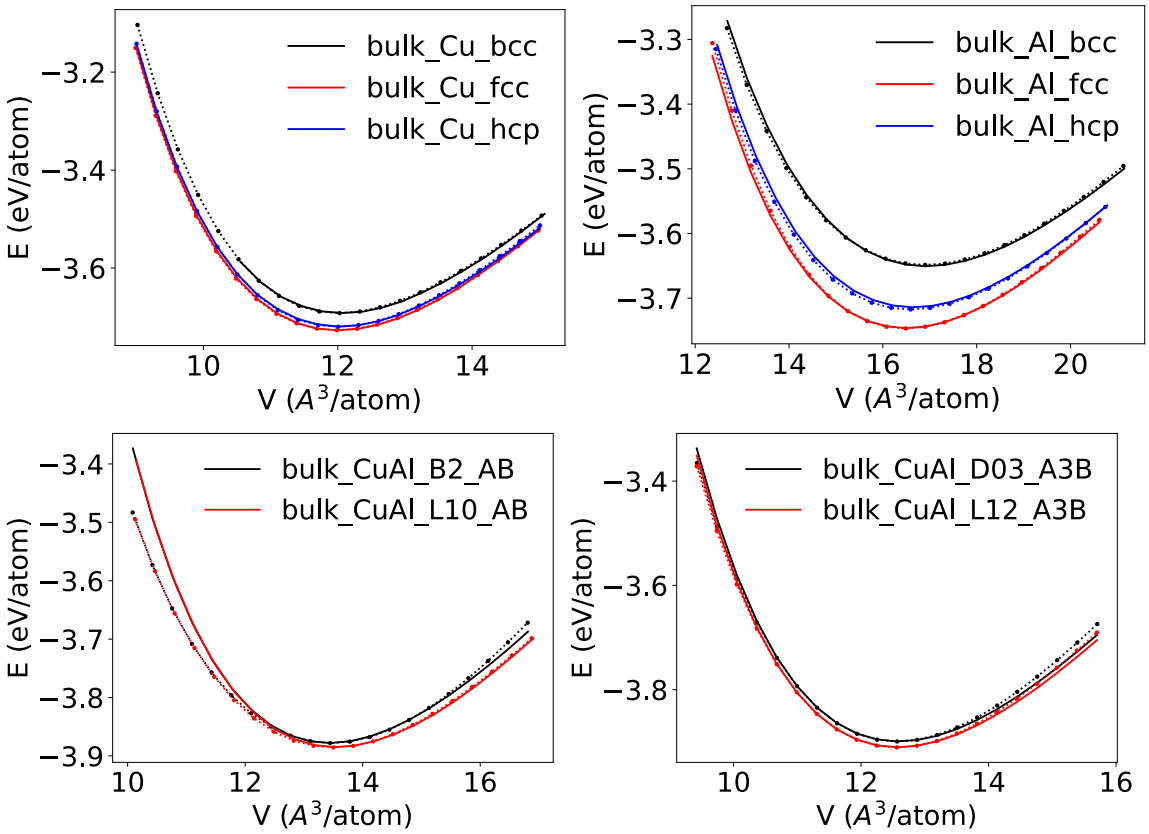


Figure 1. Comparison of bulk structure energy vs. volume data showing excellent agreement between GAP machine-learning interatomic potential (dashed lines) and DFT (solid lines) for various crystal structures (black, red, or blue) of pure Cu (top left), pure Al (top right), CuAl (bottom left), and Cu_3Al (bottom right).

Title: Surfaces and Interfaces in Oxides and Semiconductors
Author(s): C.S. Hellberg
Affiliation(s): U.S. Naval Research Laboratory, Washington, DC
CTA: CCM

Computer Resources: HPE SGI 8600 [AFRL, OH]; SGI ICE X [ARL, MD]; Cray XC40/50 [ERDC, MS]; Cray Shasta, HPE SGI 8600 [NAVY, MS]

Research Objectives: Determine the atomic and electronic structure of twisted van der Waals heterostructures.

Methodology: We performed highly converged first-principles density functional calculations of very large supercells containing up to 2,382 atoms of a monolayer of $MoSe_2$, WSe_2, MoS_2, or WS_2 on a monolayer of $MoSe_2$, WSe_2, MoS_2, or WS_2 to determine the electronic structure of the system as a function of twist angle. Larger supercells allow for smaller twist angles, and we are able to compute twist angles as small as 2.88 degrees. The layers are bound to each other via the van der Waals interaction. We used the VASP density functional theory (DFT) code at the AFRL, NAVY, ERDC, and ARL HPC centers. It is important to converge the atomic positions fully, as the structural relaxation provides the confining potential within the layers. Additionally, each monolayer is piezoelectric.

Results: We showed that flat electronic states shift into the electronic band gap at small twist angles. Flat valence band states emerge at twists below 4 degrees. Flat conduction band states emerge below 3.5 degrees, and a second higher-energy flat conduction state emerges at twist smaller than 3.2 degrees. In the sulfides, flat bands form in the valence band below 5-degree twists. There is significant strain in the moiré structures, both out-of-plane and lateral strain. The electronic band edges vary strongly with strain in dichalcogenides, and these strains provide the confining potential causing flat electronic states to form.

DoD Impact/Significance: Twisted dichalcogenide bilayers are candidates for hosting strongly correlated carriers (electrons or holes), where the dispersion of the carriers can be tuned by adjusting the angle of the twist. Our results show that at the band edges, electrons bind to the vertices of the moiré pattern, while holes bind to the "bulk" regions between the vertices and the domain walls. Thus, two types of confined carriers will form in the experimental structures: holes in the "bulk" regions and electrons away from the "bulk." Due to their tighter confinement, the Coulomb interaction will be stronger between electrons than between holes. However, the kinetic dispersions for both electrons and holes are small, potentially leading to Mott insulating and superconducting states for both types of carriers.

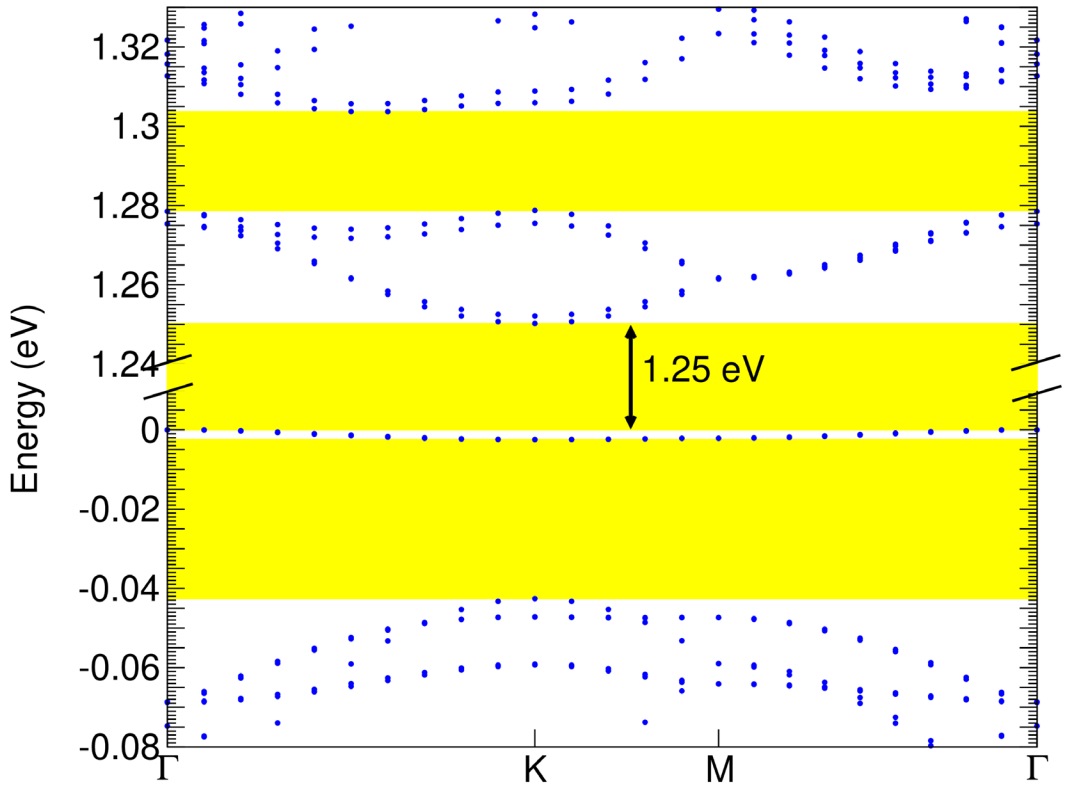


Figure 1. Electronic band structure of MoS_2/WS_2 twisted at 3.48 degrees. Energy ranges containing no states (energy gaps) are shown in yellow. There are two flat-band states potentially hosting strongly correlated electrons: One is at the bottom of the conduction band in the energy range 1.25–1.28 eV; the other is an extremely flat state at the top the valence band around energy 0.

Title: Marine Biofilm Metaproteomics
Author(s): W.J. Hervey and G.J. Vora
Affiliation(s): U.S. Naval Research Laboratory, Washington, DC
CTA: CCM

Computer Resources: HPE SGI 8600 [AFRL, OH]; Cray XC40/50 [ERDC, MS]

Research Objectives: To implement, adapt, and maintain a modular workflow of bioinformatics applications capable of leveraging distributed computing on HPC, such as the Message Passing Interface (MPI) or Shared Memory (SHMEM). This effort leverages a previous HPC Application Software Initiative (HASI) awarded for multi–*omics* data analytics of complex biological systems. An objective in FY22 was to test and evaluate the performance of emerging and updated software applications in our bioinformatics workflow. Selectively tailoring bioinformatics applications to specific Department of Defense use cases continues to enable –*omics* characterizations of microbiomes, biofilms, and complex marine eukaryotes.

Methodology: To test and evaluate emerging bioinformatics software tools for taxonomic profiling and *de novo* assembly of genome sequencing measurements (or "DNA reads") from complex microbiome samples. Microbiomes often include multiple disparate microbial species and resulting data are inherently complex. Taxonomic profiling (TP) applications allow inference of the identities of microbial species present in a sample. TP applications compare observed DNA sequences to large-scale reference sequences, frequently yielding strain-level resolution. Specific applications tested in FY22 include Centrifuge, Kraken2, GOTTCHA, and PanGIA. *De novo* metagenome assembly (MGA) tools reconstruct DNA reads into larger contiguous segments (or "contigs"), potentially joining these segments into chromosomes via graph theory. MGA provides biological insight into a microbiome, a microbial consortium, or a biofilm by enabling functional predictions of potential protein-coding open reading frames (or ORFs) by primary sequence similarity. MGA is essential for high-throughput proteome and metabolite profiling by mass spectrometry-based approaches. In FY22, three different MGA software tools were tested across multiple microbiome datasets.

Results: This subproject contributed to –*omics* data analyses among a range of biological systems that included single microbial isolates to complex environmental biofilms. FY22 allocations were leveraged to analyze model genome organisms in testing and evaluation, microbial isolate species (e.g., *Vibrio* sp.), emerging yeast strains for biomaterials production, and biomolecular measurements of the acorn barnacle, *Amphiblanus amphitrite*. Allocations enabled taxonomic profiling, genome and metagenome assembly, and proteome profiling from multiple experimental biological systems. Testing, evaluation, and examination of TP and MGA software applications ensured that select tools in our bioinformatics workflow ran efficiently on multiple disparate HPC systems. In FY22, HPC allocations on this subproject yielded contributions to two peer-reviewed publications, continued participation in an intralab study, and two invited presentations.

DoD Impact/Significance: This HPC subproject has broad DoD significance. It is directly applicable to "sense and sense-making" from large data, biotechnology, artificial intelligence, machine learning, biologically inspired materials design, biosensing, synthetic biology, systems biology, alternative energy sources, and platform sustainability.

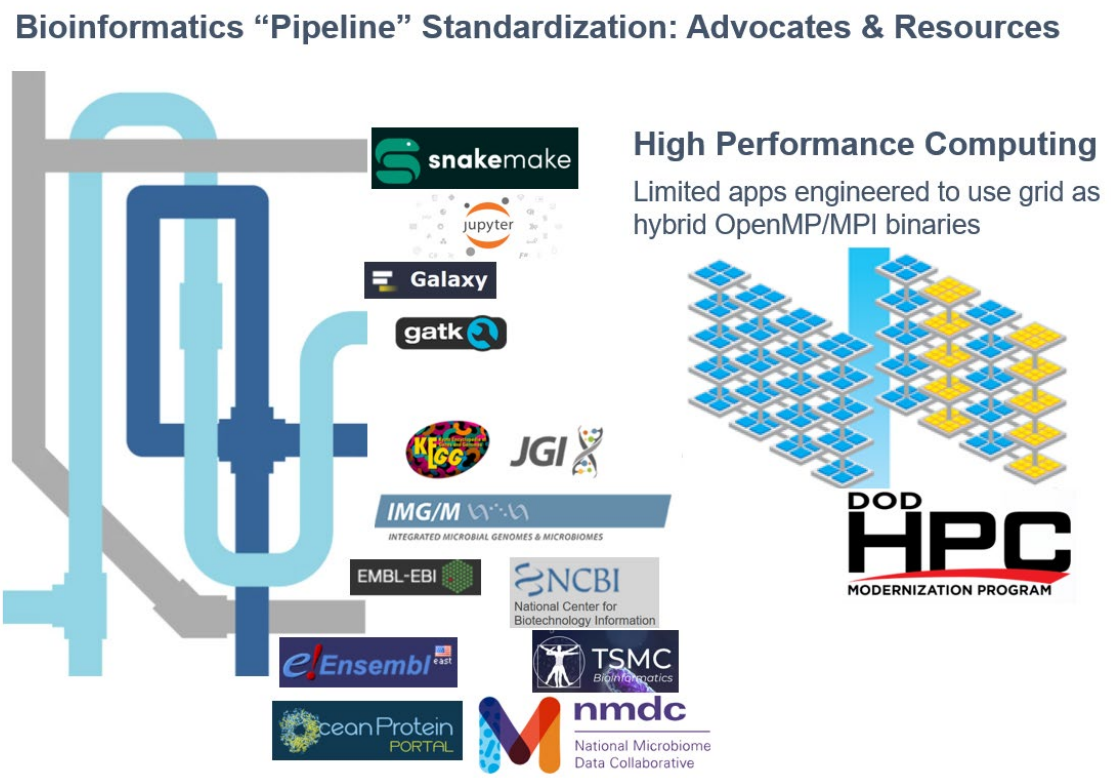


Figure 1. Bioinformatics "Pipeline" Standardization: Advocates & Resources. Resources for bioinformatics workflow standardization and software tool management include Snakemake,[1] Jupyter,[2] the Galaxy[3] genomics project, the GalaxyP[4] proteomics project, and the Broad Institute's Genome Analysis Toolkit (GATK).[5] Collectively, these projects enable reproducible research among *–omics* fields by replicating software tools, preprocessing steps, and experimental parameters for specific research use cases or "workflow management." Additional resources in the public domain are also shown above (KEGG, the Joint Genome Institute (JGI), EMBL, NCBI, and Ensemble). Advocates, working groups, and other researchers have formed communities to embrace *–omics* standardization, collaborative data sharing, and workflow management, such as the Tri-Service Microbiome Consortium (TSMC), the Ocean Protein Portal (led by Wood's Hole Oceanographic Institution), and the National Microbiome Data Collaborative (NMDC).

[1]Snakemake: https://snakemake.readthedocs.io/
[2]Jupyter: https://jupyter.org/
[3]Galaxy: https://usegalaxy.org/
[4]GalaxyP: http://galaxyp.org/
[5]GATK: https://gatk.broadinstitute.org/hc/en-us

Title: Synthetic Biology for Military Environments
Author(s): W.J. Hervey, S.M. Colston, J.R. Compton, D.H. Leary, Z. Wang, L.J. Bird, T. Tschirhart, and G.J. Vora
Affiliation(s): U.S. Naval Research Laboratory, Washington, DC
CTA: CCM

Computer Resources: HPE SGI 8600 [AFRL, OH]; Cray XC40/50 [ERDC, MS]

Research Objectives: To expand the suite of synthetic biology tools for materials production among microbial species of military relevance. Under optimal growth conditions, biotechnology harnesses genetically tractable model species, commercial expression systems, and molecular tools to overcome bottlenecks and limitations. Transitioning tool kits from model genomic species, such as *E. coli* and the yeast *Saccharomyces cerevisiae***,** to military-relevant species is an incredibly challenging endeavor. In recent years, NRL has deployed synthetic biology tools among novel biological chassis of relevance, including *Marinobacter atlanticus*, *Vibrio natriegens*, and multiple strains of the black yeast *Exophiala sp.* In FY22, HPC allocations were used to acquire and analyze large-scale proteome profiles of *Vibrio natriegens,* which assisted with development of a genome scale metabolic model (GSSM). Devising, implementing, and refining the GSSM in this microbial species could enable rapid, on-demand synthesis of designer materials, metabolites, and target intermediate analytes. In conjunction with multiple laboratory measurements, proteome profile measurements were used to assist with validation of the GSSM across a range of growth conditions. Among DoD triservice labs and the Reliance 21 Biotechnology Community of Interest (Biotech CoI), this HPCMP subproject serves an essential role for co-investigators to collaboratively analyze "*–omics*" data and to benchmark emerging bioinformatics software applications.

Methodology: An active area of synthetic biology research is engineering desirable, yet controllable, functions into cells. *In silico* metabolic models offer the potential to efficiently guide biological hypotheses and putative engineering targets at scale. At the genome scale, the metabolic model ingested disparate data inputs, such as the *V. natriegens* genome (DNA) sequence, central carbon metabolism, and gene essentiality. High-throughput proteome profiling of microbial systems yields "snapshots" of protein expression under specific growth conditions. To assist with model validation, these snapshots of *V. natriegens* protein expression were compared to *in silico* predictions of the genome scale metabolic model.

Results: The combination of *in silico* modeling, experimental measurements, and manual curation, yielded a genome-scale metabolic model (GSSM) for *V. natriegens*: iLC858. In FY22, HPC allocations contributed to one peer reviewed publication, two additional peer-reviewed publications in review, and multiple presentations and proceedings.

DoD Impact/Significance: This subproject is a collaborative triservice resource for synthetic biology and biotechnology research. Allocations are also used in exploratory tool development across the Reliance 21 Biotechnology Community of Interest. This subproject is directly applicable to "sense and sense-making" from large data, biotechnology, artificial intelligence, machine learning, biologically inspired materials design, biosensing, synthetic biology, systems biology, and alternative energy sources.

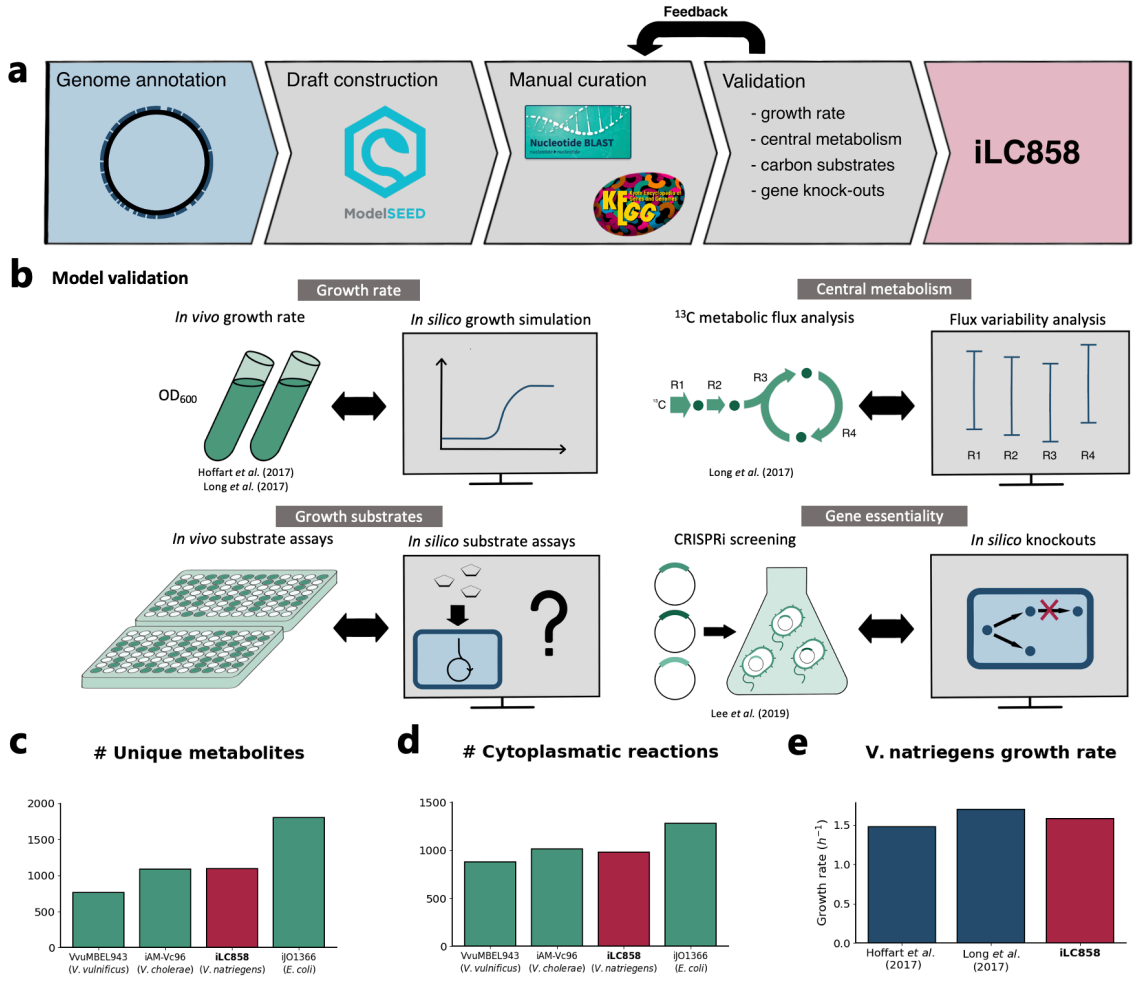


Figure 1. Construction and validation of the *Vibrio natriegens* Genome-Scale Metabolic Model (GSSM) iLC858: a) scheme representing construction steps of the GSSM iLC858, b) experimental measurements used for validation of the metabolic model, iLC858. C-d. Comparison of the *V. natriegens* GSSM iLC858 to other *Vibrio* metabolic models represented as c) unique metabolites and d) cytoplasmic reactions, and e) *in silico* vs. *in vivo* growth rates.

Image above is Figure 1, Coppens *et al*., *Molecular Systems Biology*, 2022. (in peer review).

Title: New Method for Calculation of Solid-Phase Heat of Formation Using Intermolecular Interactions in Crystal Structures
Author(s): I.D. Giles and G.H. Imler
Affiliation(s): U.S. Naval Research Laboratory, Washington, DC
CTA: CCM

Computer Resources: SGI ICE X [ARL, MD]; Cray XC40/50 [ERDC, MS]

Research Objectives: Energetic material properties must be well understood prior to incorporation into munitions. Experimental testing is time-consuming and expensive and is not feasible for every potential molecule of interest. Predicting energetic material properties is a powerful way to quickly screen candidate molecules to find the best possible material to scale up for further testing. Properties such as detonation velocity and detonation pressure can be calculated accurately if provided a reliable solid-phase heat of formation. This work examines prediction of sublimation enthalpy in order to more accurately determine solid-phase heat of formation. Heat of formation must otherwise be experimentally measured via bomb calorimetry, which is time-consuming and requires several grams of material. This method has the potential to have low computational cost and higher accuracy than current methods and would circumvent the need to measure sublimation enthalpy experimentally. Crystal structure intermolecular interactions involved in calculating enthalpy of sublimation will be examined further for trends that would allow calculation of other material properties.

Methodology: Density function theory calculations in Gaussian will be used to calculate a geometry-optimized minimum energy structure starting from the geometry of the single-crystal X-ray structure using a suitable method and basis set (B3LYP and 6-311++g to start). Further energy and frequency optimization will ensure a global energy minimum as well as determine the electronic structure, heats of formation, and vibrational spectra. TDDFT methods will be used with solvation models (H_2O and acetone to start) to understand the electronic transitions seen in their electronic spectra in the corresponding solvents. Interaction energies will be used to calculate enthalpy of sublimation based on intermolecular distances and the type of interaction. Interactions that were considered are dispersion forces, hydrogen bonds, π-π and nitro-π interactions. Sublimation enthalpy is derived from the sum of these interactions. Gas-phase heat of formation will be calculated using the accurate atom and group-equivalent methods developed by Edward Byrd and Betsy Rice at ARL. Our method for calculating enthalpy of sublimation will be used with gas-phase heat of formation according to Hess's Law to calculate solid-phase heat of formation.

Results: Total intermolecular energy has been calculated for a series of more than 50 molecules. This set includes a wide range of molecular weights, functional groups, and molecule families. This method only examines neutral C-, H-, Cl-, N-, and O-containing molecules. The average error was 14.5 kJ mol^{-1} for sublimation enthalpy compared to experimentally determined values. This is comparable with methods currently in use in literature. At this point, our method is operational and ready to be applied to novel molecules. A larger set of molecules would allow further training of the equations used to calculate intermolecular interaction energies, which would provide greater accuracy. Application of our current library of interaction data to study impact sensitivity is ongoing.

DoD Impact/Significance: At the current iteration, this method approaches or matches the accuracy of popular methods used to calculate enthalpy of sublimation. Enthalpy of sublimation can be used to calculate solid-phase heat of formation. Additional improvements have the potential to surpass methods in use today. Accurate calculation of sublimation energy and solid-phase heat of formation are relevant to a wide range of fields and are important for the safe storage of a solid-phase material.

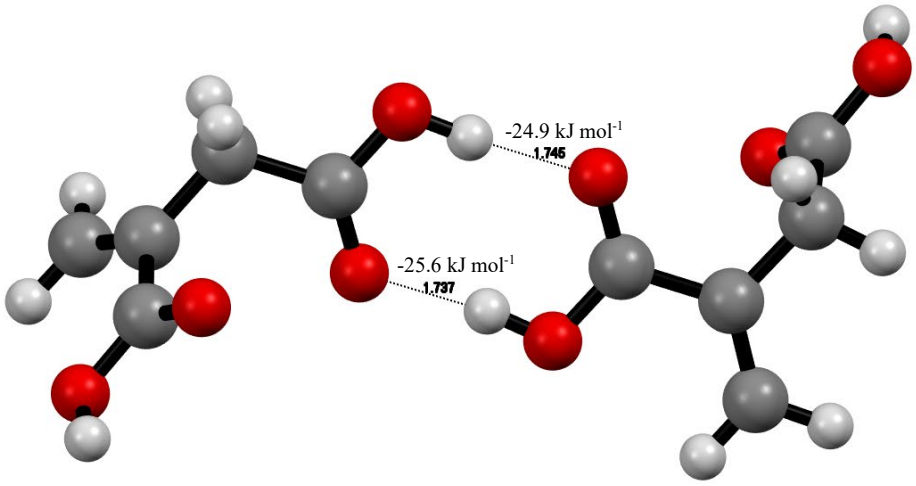


Figure 1. Structure plot demonstrating strong hydrogen bond in itaconic acid as identified in single-crystal X-ray structure. An equation has been developed that uses hydrogen bond lengths to calculate interaction energies.

Title: Materials for Energy Storage and Generation
Author(s): M. Johannes
Affiliation(s): U.S. Naval Research Laboratory, Washington, DC
CTA: CCM

Computer Resources: HPE SGI 8600 [AFRL, OH]; Cray XC40/50 [ERDC, MS]

Research Objectives: The objectives of this program are to use density functional theory (DFT) and its extensions including molecular dynamics to understand the materials properties that drive functionality in materials relevant to energy storage and generation, including new materials for low-power electronics and topological materials suitable for switching and spintronics.

Methodology: First-principles pseudopotential methods are employed to calculate the quantities of interest. The majority of the work was done using the Vienna Ab initio Software Program (VASP). Postprocessing is done using personal codes. Both standard (static) T = 0 DFT calculations and temperature-dependent molecular dynamics (MD) calculations were used.

Results: In FY22, the project's focus was mainly on energy materials, especially a new SAFC (solid acid fuel cell) electrolyte with superior proton transport at intermediate temperatures. The mechanism behind this extraordinary transport was revealed by calculation, showing that excess protons in the system, rather than dissociation of hydroxide units, were necessary for conduction. It was also discovered that although the compound itself has a one-dimensional "chain" structure along which conduction would be expected to proceed, actual conduction is substantially three-dimensional. This discovery, along with careful measurements, warranted the cover of *Advanced Energy and Sustainability Research* (see graphic). Calculations of $Ni(OH)_2$, which can serve as a fuel cell cathode or a positive electrode for Li ion batteries, showed that superior catalytic properties in comparison to NiO were due to increased poisoning of the surface of the latter (nearly a factor of 100) that dramatically suppresses surface reactivity.

We also continued our work in topological materials, investigating the In_2Se_3/Bi_2Se_3 interface and its spin-dependent topological aspects, including thickness dependence. We also did a careful calculation of the Fermi surface of CsV_3Sb_5 to determine whether an observed charge density wave has its origins in the electronic structure. We also looked at the YbB_{12} to understand why observed quantum oscillations in this ostensive insulator exist in an attempt to determine whether surface effects or topological effects underpin the phenomena.

DoD Impact/Significance: Topological materials have incredible potential for electronics usage, since the metallic surface states that characterize them are 100% spin polarized and impervious to the scattering effects of normal spintronics materials. Energy materials are also an obvious naval need and our investigation of the SAFC electrolyte has revealed a record-setting conductivity that could enable all-solid-state fuel cells without the necessity for large overpotentials or dangerously high temperatures.



Figure 1. Relaxed structure of ammonium borosulfate ($NH_4[B(SO_4)]_2$. Green polyhedra are boride units, while yellow are sulfate units. Red spheres are oxygen, light-blue spheres are hydrogen, and pink spheres are nitrogen. The black spheres represent excess protons (p^+) at various possible positions along the three-dimensional path of conduction uncovered by density functional theory calculations.

Title: DFT-Calculated IR Absorption Spectra for PFAS Molecules
Author(s): S. Lambrakos and A. Shabaev
Affiliation(s): U.S. Naval Research Laboratory, Washington, DC
CTA: CCM

Computer Resources: HPE SGI 8600 [AFRL, OH]; SGI ICE X [ARL, MD]; Cray XC40/50 [ERDC, MS]; Cray Shasta [NAVY, MS]

Research Objectives: Calculation of IR absorption spectra for PFAS molecules using density functional theory.

Methodology: The present study supports proof of concept for using density functional theory (DFT), based on quantum theory, to calculate IR spectra for target molecules, which provides complementary information to that obtained from spectroscopic measurements. Typically, determining spectral-signature features of target molecules using detection methodologies based on spectroscopy should be difficult because these molecules are within complex spectral-signature backgrounds. Accordingly, DFT provides an approach for estimating IR absorption spectra of isolated molecules. Identification of unknown molecules by comparison of measured spectra to reference spectra is accomplished using signal templets having spectral-signature patterns associated with known substances. The present study adopts the software GAUSSIAN16 (G16) (see reference) for the calculation of IR absorption spectra.

Results: The results of our study are DFT-calculated IR spectra and molecular geometries of stable structures for PFAS molecules. Shown in Figs. 1–3 are molecular geometries and DFT-calculated IR spectra for the PFAS molecules $C_{10}HF_{19}O_2$, $C_9HF_{17}O_2$, and $C_8HF_{15}O_2$, respectively. The DFT calculations described here, the geometry energy optimization, and the vibrational analysis were effected using the computer program G16. The chemical model used for these calculations and the procedure for IR analysis are given in the reference and references therein.[1]

DoD Impact/Significance: The DFT calculations presented in this study further demonstrate that computational experiments can provide an efficient methodology for estimating spectral features of target molecules. It should be assumed that in practice, it would be convenient to estimate spectral features, both computationally using DFT as well as experimentally using spectroscopies. This follows because computational capabilities with respect to DFT calculation of spectra are now sufficient for estimating spectral features of molecules efficiently for the purpose of database inclusion. Specifically, estimation of spectral features using DFT that is both sufficient and convenient for use as reference spectra, which is associated with practical detection, can now be achieved computationally. Significantly, with respect to highly toxic substances, it may be more convenient to estimate spectra using computational experiments rather than using laboratory measurements. This is certainly the case for PFAS molecules, which are chain-linked carbon/fluorine atoms widely distributed in the environment and are dangerously toxic biologically.[1] PFAS contamination of U.S. military installations poses a major problem, and thus PFAS detection is of significance to the DoD.

[1]S. Wallace, S.G. Lambrakos, A. Shabaev, L. Massa, "On Using DFT to Construct an IR-Spectrum Database for PFAS Molecules," Structural Chemistry, 2021, https://doi.org/10.1007/s11224-021-01844-5.

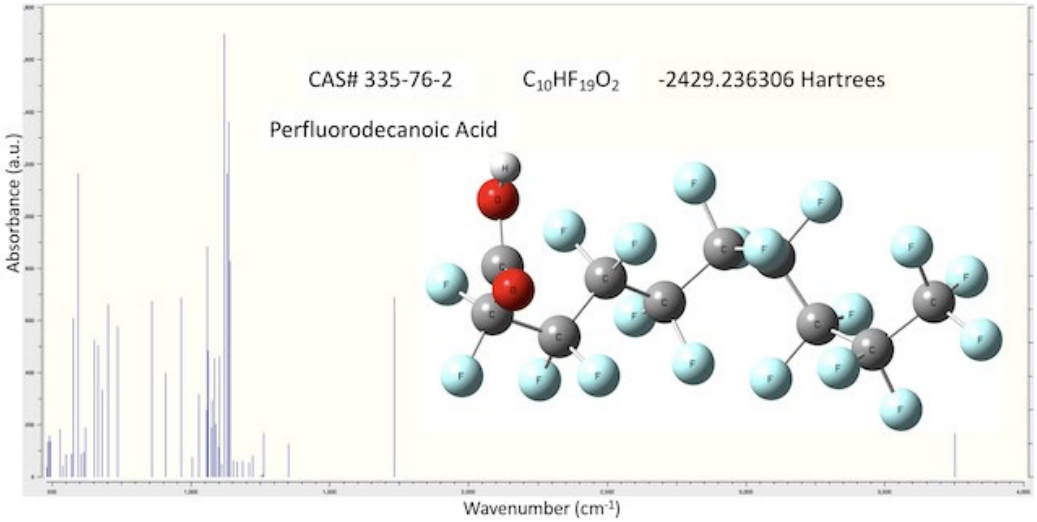


Figure 1. DFT-calculated IR spectra and molecular geometry for CAS# 335-76-2

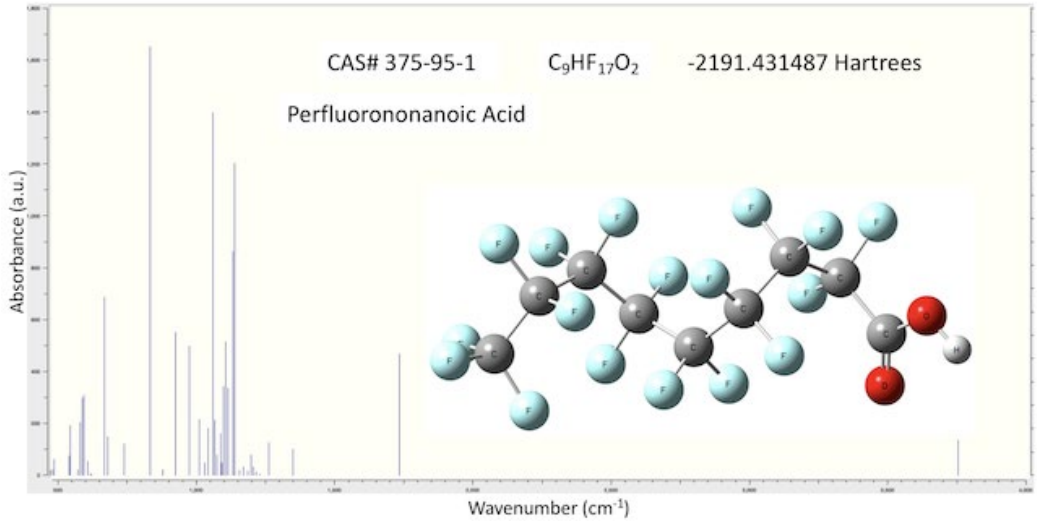


Figure 2. DFT-calculated IR spectra and molecular geometry for CAS# 375-95-1

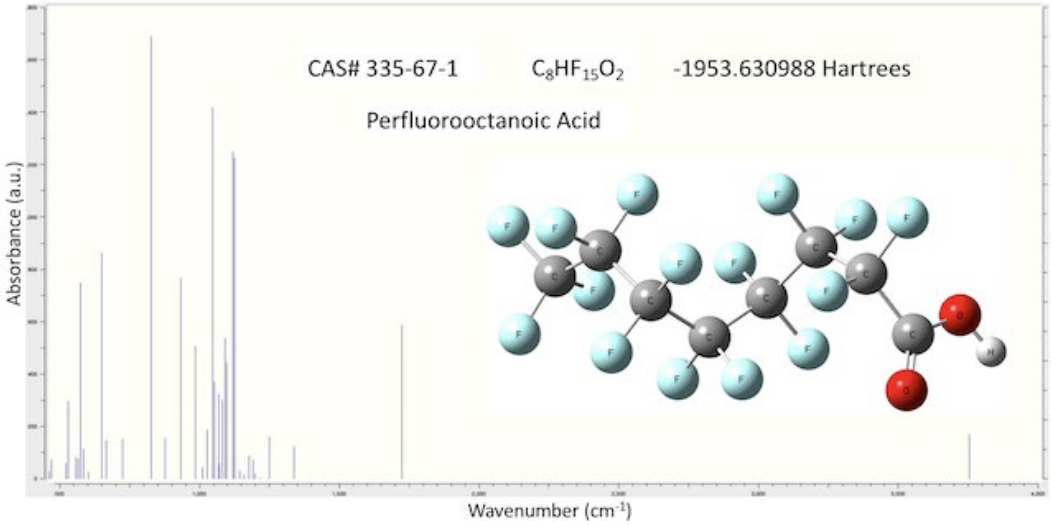


Figure 3. DFT-calculated IR spectra and molecular geometry for CAS# 335-67-1

Title: Calculation of Materials Properties Via Density Functional Theory and Its Extensions
Author(s): J.L. Lyons
Affiliation(s): U.S. Naval Research Laboratory, Washington, DC
CTA: CCM

Computer Resources: HPE Cray Shasta, HPE SGI 8600 [AFRL, OH]; SGI ICE X [ARL, MD]; Cray XC40/50 [ERDC, MS]; HPE SGI 8600 [NAVY, MS]

Research Objectives: The overall objective is to determine the electronic structure of ultrawide-bandgap semiconductors (UWBGS) such as gallium oxide (Ga_2O_3), and novel materials such as cesium lead bromide ($CsPbBr_3$), using accurate including hybrid density functional theory (DFT).

Methodology: DFT has long been the proven method for deducing semiconductor electronic structure. Although this method requires no experimental input, when applied to WBGS, the so-called "bandgap problem" makes difficult the quantitative prediction of defect properties. To overcome this issue, we employ hybrid DFT, which mixes in a fraction of screened Hartree-Fock exchange into the exchange-correlation functional. This approach provides accurate, quantitative prediction of bandgaps and defect transition levels, even in UWBGS. Using hybrid DFT, defect-related charge-state transition levels, formation energies, and optical transitions are calculated.

Results: In FY22, resources from this project were utilized to understand n-type doping of UWBGS including Ga_2O_3 and c-BN, to investigate self-trapped holes and polaronic acceptors in oxide UWBGS, to explore acceptor doping of lead halide perovskites, and to develop techniques for predicting nuclear magnetic resonance (NMR) parameters in metal-organic frameworks. One focus was on potential donor dopants in UWBGS such as c-BN and $AlGaO_x$ (AlGO) alloys, which are difficult to *n*-type dope. We found that in c-BN, Si is the most promising *n*-type dopant, followed by O. In AlGO alloys, most donors become deep at relatively low Al concentrations (~50%), with the exception of Si, which remains shallow up to ~80% Al content. We also focused on *p*-type doping of UWBG oxides, which is widely known to be limited by spontaneous hole trapping. We provided an explanation for Mg-related optical signals in Ga_2O_3, which we linked with holes that were highly localized at the Mg acceptors. Self-trapped holes were also found to cause a large increase in acceptor ionization energies in competing oxides. The exception was GeO_2, where hole polarons were slightly stable (0.01 eV), and which is potentially a *p*-type dopable UWBGO.

Also investigated in this FY were acceptor impurities in lead halide perovskites. Our calculations find that many acceptors have deep levels in $CsPbBr_3$, though Ag and Na are shallow acceptors. We explored how these dopants were limited by competing configurations and how native defects might compensate attempts at *p*-type doping. Our calculations provide a blueprint for experimentalists attempting to dope $CsPbBr_3$.

Finally, we also used DFT to predict resonance shifts, line shapes, and spin lattice relaxation rates with different species in a ZIF-67 metal-organic framework (MOF). Our results are in excellent agreement with NMR experiments and allowed us to have high confidence in assignment of observed peaks to specific sites in the MOFs. These results indicate that DFT is a powerful accompaniment to NMR experiments, and we plan to leverage this capability in future programs.

DoD Impact/Significance: UWBGS, including Ga_2O_3 and c-BN, could be utilized in power electronics that play a crucial role in many Navy-relevant applications and could afford significant SWaP-C when outperforming components based on traditional semiconductor materials. Optimizing impurity doping to control electrical conductivity, understanding contaminating species to minimize trapping centers, and characterizing unintentionally incorporated defects are crucial steps for improving such materials.

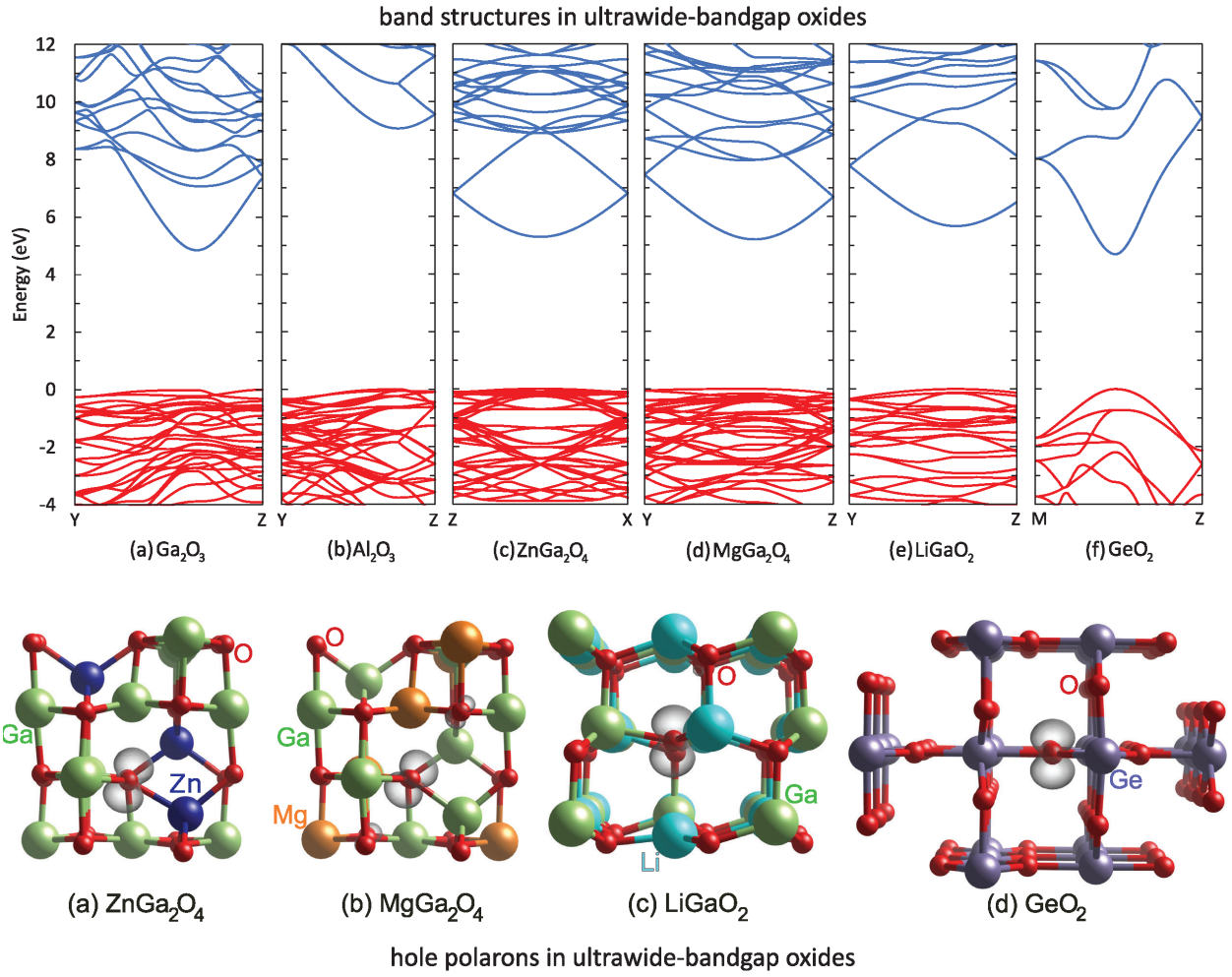


Figure 1. Band structures and hole polarons in ultrawide-bandgap oxides.

Title: Materials Properties of Surfaces and Two-dimensional Systems
Author(s): M. Phillips
Affiliation(s): U.S. Naval Research Laboratory, Washington, DC
CTA: CCM

Computer Resources: HPE SGI 8600 [AFRL, OH]; SGI ICE X [ARL, MD]; Cray XC40/50 [ERDC, MS]

Research Objectives: Characterize the electronic, optical, and structural properties of bilayer two-dimensional (2D) materials systems.

Methodology: The primary tool used to study the properties of 2D bilayers in this project is density functional theory (DFT) as implemented in the Vienna Ab initio Simulation Package (VASP). We compute electronic band structures using VASP and phonon band structures using a combination of VASP and the PHONOPY package. One of the most ambitious aspects of this project is the structural relaxation and band-structure calculation of twisted 2D materials systems with very long periodicities. These systems contain thousands of atoms in their fundamental computational units, and access to multiple large-memory nodes is required to converge the calculations. We use these large-scale DFT calculations in combination with small-scale DFT calculations and analytic models to build up an understanding of the properties of complex 2D materials heterostructures containing multiple length scales.

Results: We have used HPC resources to study three different systems comprising stacked transition metal dichalcogenide layers. First, we have gained an understanding of the differences in the photoluminescence spectra of WSe_2 bilayers stacked with a 0-degree twist vs a 60-degree twist. We have also shown that differences in the electronic structure of 0-degree vs 60-degree WSe_2 bilayers lead to different resonant Raman behavior in each of these systems. In addition, we have computed the band structure of a 0-degree stacked Bi_2Se_3/WSe_2 heterostructure for the first time and used it to understand the changing photoluminescence spectrum of the bilayer under laser exposure in an oxygen environment. To explore the role that oxygen plays in this process, we have also studied the stability of single quintuple layer Bi_2Se_3 with oxygen systematically replacing the selenium in the lattice. Finally, in large-scale DFT calculations of twisted $MoSe_2/WSe_2$ bilayers, we have shown that for twist angles smaller than about 3.5 degrees, flat bands emerge in both the conduction and valence electronic bands that are associated with state localization and local strain from atomic relaxation (Fig. 1).

DoD Impact/Significance: Due to the characteristically weak out-of-plane bonding of two-dimensional materials, a given 2D material layer can be stacked with virtually any other 2D layer without regard for the chemical makeup of the constituent layers, lattice matching, or interlayer twist angle. This flexibility raises the possibility of creating a nearly infinite array of stacked “designer” materials whose properties can be tailored by careful choices of constituent 2D material layers and twist angle. These carefully designed 2D materials systems are a promising platform for sensing applications (due to their high surface-to-volume ratio) and an attractive component of low-weight, low-power electronics, which are necessary for building reliable, autonomous systems for future naval applications.

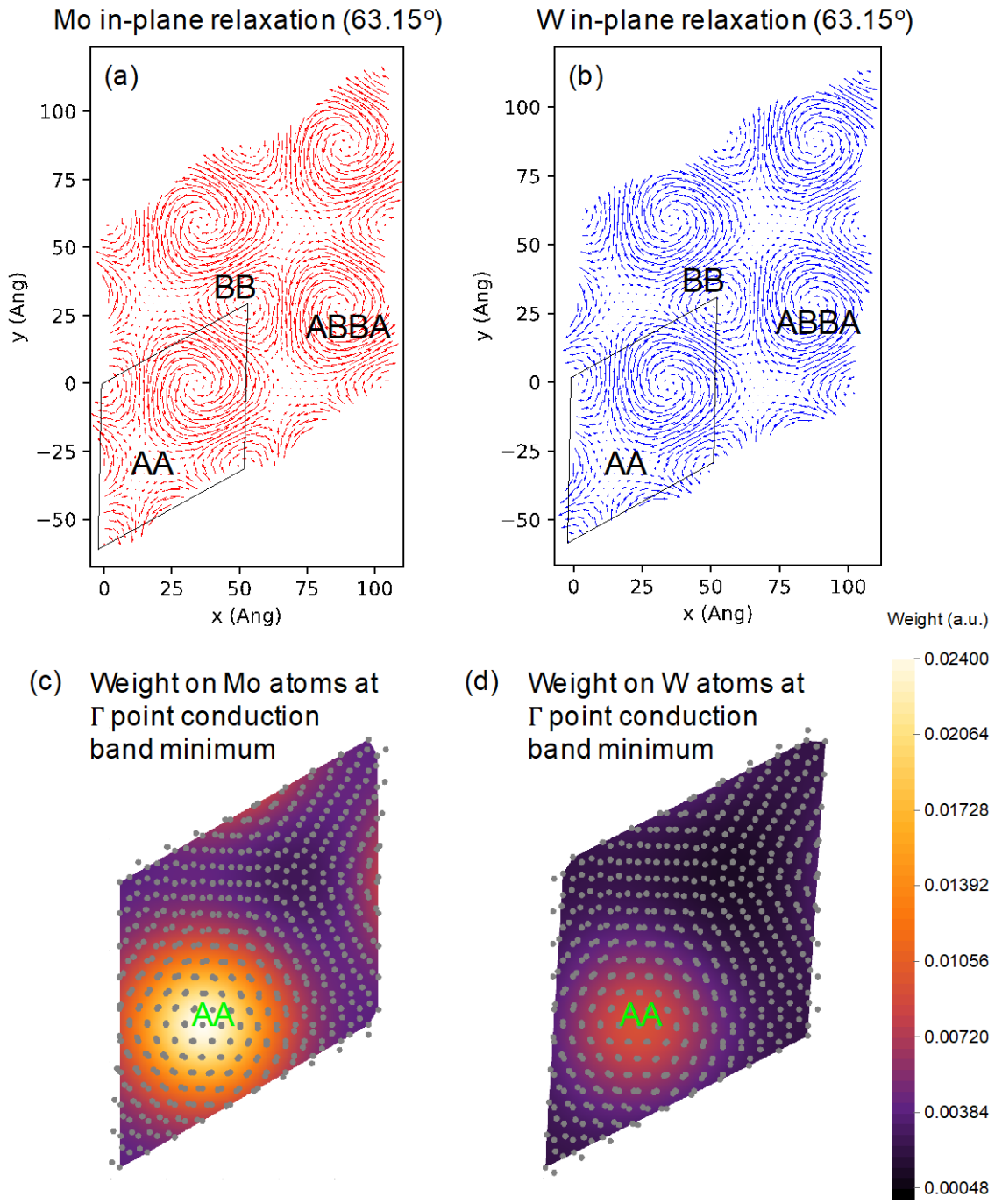


Figure 3. Relaxation of metal positions in a 63.15° twisted $MoSe_2/WSe_2$ bilayer for (a) molybdenum atoms and (b) tungsten atoms. Localization of states at the conduction band minimum at the Γ point on (c) the molybdenum atoms and (d) the tungsten atoms. Local strain induced by atomic relaxation and localization of states are associated with flat band formation.

Title: Numerical Studies of Semiconductor Nanostructures
Author(s): T.L. Reinecke[1] and I. Welland[2]
Affiliation(s): [1]U.S. Naval Research Laboratory, Washington DC; [2]National Research Council Postdoctoral Research Associate, U.S. Naval Research Laboratory, Washington, DC
CTA: CCM

Computer Resources: HPE SGI 8600 [AFRL, OH]; Cray XC40/50 [ERDC, MS]

Research Objectives: To accurately and efficiently simulate the time-varying behavior of waveguide quantum electrodynamics (QED) devices used in the generation of multiphoton states. To make first-principles calculations of the optical properties of the naturally hyperbolic material calcite to compare with experimental results and to obtain insight into potential imaging applications.

Methodology: A new particle method for numerically solving the phase space quantum Liouville equation was developed. This method was benchmarked on several models, including an InGaAs quantum dot in a cavity and a pair of InGaAs quantum dots coupled to a photon crystal cavity. *Ab initio* density functional methods using Quantum Espresso and VASP were used to calculate the electronic properties of the natural hyperbolic material calcite ($CaCO_3$). These results were used to describe the dielectric and optical properties of this material. Results for the optical properties were compared with NRL experiment.

Results: The need to accurately and efficiently simulate the detailed, non-Markovian dynamics of quantum devices has led to numerous new numerical methods for solving the quantum Liouville equation. We benchmarked our new approach against standard methods in the cases mentioned above. Our new method replicates existing results accurately, is stable for longer simulation times, and can effectively use parallel resources. This approach was demonstrated to provide greater accuracy and stability with the drawback of greater computational cost, as is typically expected for particle methods.

Naturally occurring materials with hyperbolic optical properties are attracting considerable interest due to their ability to confine light in small volumes and their resulting potential for applications in photonics and subwavelength imaging. This work uses a first-principles theoretical approach without adjustable parameters to calculate the hyperbolic optical properties of bulk calcite ($CaCO_3$). This material exhibits natural hyperbolic behavior within its Reststrahlen bands at 1403–1552 cm^{-1} and 864–887 cm^{-1}. The calculated results are shown to be in good agreement with NRL reflectance data. These results demonstrate that calcite is an attractive natural hyperbolic material for a range of applications.

DoD Impact/Significance: A new, fast, scalable approach to modeling quantum devices has been demonstrated that can outperform existing methods in stability and accuracy and provides a new method for simulation of quantum devices. It has been demonstrated that natural calcite is a highly attractive material for potential applications in advanced optics such as subwavelength imaging.

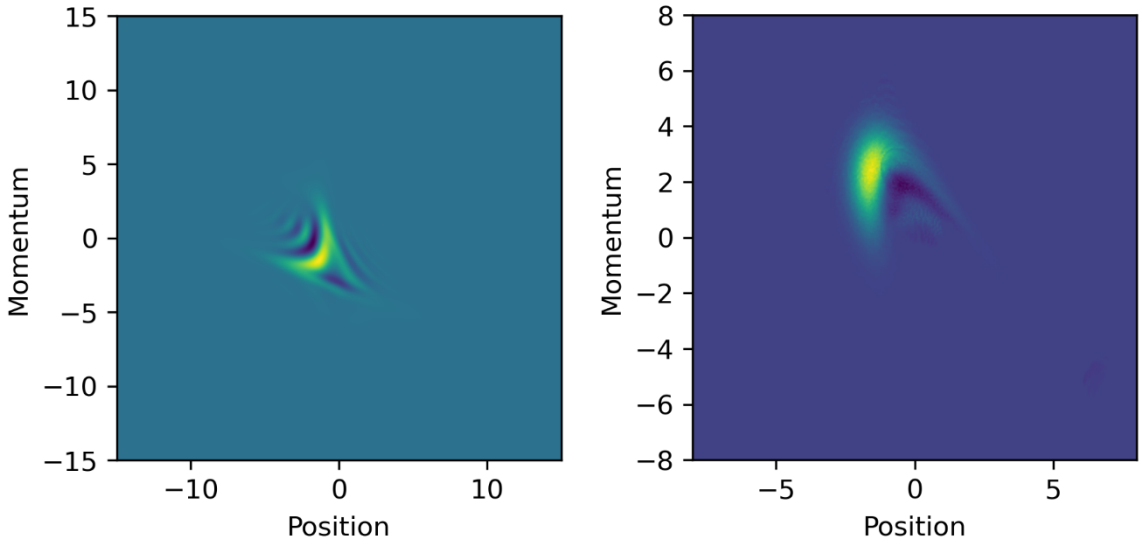


Figure 1. Left: Calculated Wigner function illustrating the formation of quantum interference between the transmitted and reflected wave packets of a two-photon wave packet scattering from two InGaAs quantum dots in a photonic crystal cavity, in units of position, $x_0 = \sqrt{\frac{2E_0}{m\omega^2}}$, momentum, $p_0 = \sqrt{2E_0\, m}$, where E_0 is the ground state energy, $m = 0.065m_0$ the effective mass of the electron in InGaAs, and $\omega = 0.042q/\hbar$. Right: Interference forming in the calculated Wigner function between the first excited state and the ground state of the electron in an InGaAs quantum dot as it is excited by an external electric field. The units and parameters are identical to the previous case.

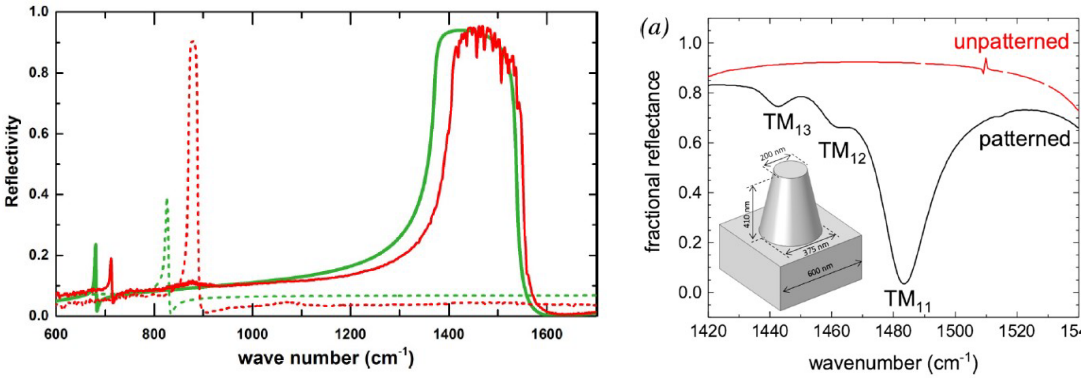


Figure 2. Left: calculated (green) and measured (red) normal-incidence reflectivity polarized along the ordinary (solid) and extraordinary (dashed) axes. Right: reflectance spectra of unpatterned (red) and patterned (black) calcite. Hyperbolic phonon polariton resonances are marked by the mode labels TM_{ml} and the dimensions of the nanocones used are given in the inset.

Title: First-principles Simulations of Condensed-phase Decomposition of Energetic Materials
Author(s): I.V. Schweigert
Affiliation(s): U.S. Naval Research Laboratory, Washington, DC
CTA: CCM

Computer Resources: SGI ICE X [ARL, MD]; Cray Shasta [NAVY, MS]; HPE SGI 8600 [AFRL, OH]

Research Objectives: To predict thermal, mechanical, and chemical properties of explosives subjected to elevated temperatures and pressures.

Methodology: We use crystal structure optimizations and quantum molecular dynamics (QMD) simulations to study physical and chemical changes in energetic materials subjected to elevated temperatures and pressures. Structure optimizations use variable-cell optimization algorithms to determine changes in atomic coordinates and lattice constants at elevated pressures. QMD simulations use constant-pressure, constant-temperature (NPT) integrators combined with multiple replicas to simulate changes in crystal structures at elevated temperatures. Atomic forces needed to perform these simulations are estimated using either density functional theory (DFT) or density-functional tight binding (DFTB) methods. Periodic-cell models are used to approximate bulk crystalline environments. Python and Perl scripts are being developed to facilitate the execution and analysis of these simulations.

Results: This year, we tested whether density-functional tight-binding (DFTB) methods can be used in place of density functional theory (DFT) in QMD simulations of crystal lattice parameters of high-energy-density molecular crystals. Specifically, we focused on testing the self-consistent-charge (SCC) variant of DFTB that uses a third-order expansion of the DFT Hamiltonian (DFTB3). The key advantage of SCC-DFTB3 is its computational cost, which is an order of magnitude smaller than that of full DFT. In our simulations, we used the so-called "mio" set of the Slater-Koster parameters for organic molecules to model bonding interactions and the Universal Forcefield (UFF) pair potentials for dispersion interactions. In a companion Pathfinder project, we determined the minimum model size, trajectory lengths, number of replicas, and other numerical parameters that are necessary to produce numerically convergent values. In this project, we applied DFTB-based QMD to simulate the lattice parameters of three nitramine crystals — dimethylnitramine (DMNA), 1,3,5-trinitro-1,3,5-triazinane (RDX), and 1,3,5,7-tetranitro-1,3,5,7-tetrazocane (HMX) — and their high-pressure polymorphs. Starting with the experimental crystal structures, atomic coordinates and lattice parameters were first optimized at 0 K using a variable-cell optimization algorithm. Based on the optimized structures, five replicas were generated for each crystal by assigning random atomic velocities sampled from a Boltzmann distribution at room temperature. Each replica was then simulated for 40 picoseconds using a Parrinello-Rahman NPT integrator that utilized two Nose-Hoover thermostats, one for momenta and another one for the lattice. After a 10-picosecond equilibration period, the instantaneous values of temperature, stress tensor, and lattice parameters were recorded every 0.1 picoseconds and were averaged over the remaining 10 picoseconds. The trajectory-average values were then averaged over the ensembles of five trajectories to provide the final estimates for the lattice parameters. The predicted lattice constants and tilt angles are compared to the experimental values in Table 1.

DoD Impact/Significance: Thermomechanical equations of state for high-energy-density nitramines are needed to support physics-based modeling of nitramine-based explosives and solid rocket propellants. The simulations completed this year ascertained the applicability of DFTB-based QMD simulations to crystal structures of nitramines under ambient and elevated pressures. Future simulations will focus on the equations of state under elevated temperatures and pressures, for which experimental data is currently unavailable.

	Pressure	a (Å)	b (Å)	c (Å)	β (deg)
DMNA, Z = 2, space group $P2_1/m$					
Experiment	1 atm	6.129(1)	6.501(1)	6.060(1)	114.66(2)
Simulations	1 atm	6.005(6)	6.651(20)	6.126(5)	113.48(6)
Difference		-2.0%	+2.3%	1.1%	-1.0%
α-RDX, Z = 8, space group $Pbca$					
Experiment	1 atm	13.201(1)	11.610(1)	10.729(1)	90.0
Simulations	1 atm	13.523(7)	11.403(9)	10.920(20)	90.0(1)
Difference		+2.4%	-1.8%	+1.8%	0.0
γ-RDX, Z = 8, space group $Pca2_1$					
Experiment	5.2 GPa	12.565(2)	10.930(1)	9.477(1)	90.0
Simulations	5.2 GPa	12.489(2)	10.660(2)	9.860(2)	90.0(1)
Difference		-0.6%	-2.5%	+4.0%	0.0
ε-RDX, Z = 4, space group $Pca2_1$					
Experiment	5.7 GPa	7.032(1)	10.530(3)	8.791(1)	90.0
Simulations	5.7 GPa	7.013(3)	10.465(7)	8.846(2)	90.0(1)
Difference		-0.3%	-0.6%	+0.6%	0.0
β-HMX, Z = 2, space group $P2_1/n$					
Experiment	1 atm	6.525(1)	11.024(2)	7.362(1)	102.64(1)
Simulations	1 atm	6.437(2)	11.057(20)	7.608(4)	102.57(6)
Difference		-1.3%	0.3%	3.3%	-0.1%
δ-HMX, Z = 6, space group $P6_1$					
Experiment	1 atm	7.714	7.714	32.480	120.0
Simulations	1 atm	7.866(7)	7.874(12)	31.531(40)	120.1(1)
Difference		2.0%	2.1%	-2.9%	0.1%

Table 4. Comparison between experimental[1] and simulated[2] crystal lattice parameters for several nitramines.

[1] Experimental crystal structure of DMNA was taken from Krebs et al., 1979, α-RDX from Zhurov et al., 2011, γ-RDX from Davidson et al., 2008, ϵ-RDX from Millar et al., 2010, β-HMX from Deschamps et al., 2011, and δ-HMX from Xue et al., 2008. Where applicable, the reported experimental values were rounded to three significant digits after the period. The associated uncertainties were rounded correspondingly. The uncertainties on the measurement temperatures are often not reported, but typically are assumed to be within 2 K. The uncertainties on the measured pressures are typically within 0.05 GPa.

[2] Theoretical crystal structures were obtained with QMD simulations using the SCC-DFTB3 method augmented with the UFF-based dispersion corrections.

Title: Crystal Properties of Explosives from Quantum Molecular Dynamics
Author(s): I.V. Schweigert
Affiliation(s): U.S. Naval Research Laboratory, Washington, DC
CTA: CCM

Computer Resources: HPE SGI 8600 [AFRL, OH]; Cray Shasta [NAVY, MS]

Research Objectives: To determine suitable numerical settings for density functional tight binding (DFTB) based quantum molecular dynamics (QMD) simulations of explosives.

Methodology: A judicious choice of numerical parameters controlling molecular dynamics (MD) simulations can drastically reduce the use of computational resources while ensuring an acceptable numerical accuracy and statistical validity of the results. However, the typical settings used in classical MD may not be applicable to QMD because the computational cost of QMD simulations is several orders of magnitude higher than that of classical MD. In this Pathfinder project, we performed density-functional tight binding (DFTB) based QMD simulations of a high-energy-density molecular crystal, 1,3,5,7-tetranitro-1,3,5,7-tetrazocane (HMX), to test the convergence of the predicted lattice parameters with respect to the model size, time step, trajectory lengths, number of replicas, and several other settings.

Results: Regarding the model size, previous QMD simulations of molecular crystals used periodic models containing no more than 4 primitive cells, while classical MD simulations of the same crystals used much larger models containing 30 or more primitive cells. With the DFTB method, we were able to simulate up to 32 primitive cells of β-HMX. As shown in the top left panel of Fig. 1, the observed lattice parameters quickly converged with the number of primitive cells included in the model. With the 2*2*2 supercell (8 primitive cells), the lattice parameters were within 0.5% of the values obtained with the much larger 3*3*3 and 4*2*4 supercells. Regarding the time step, previous MD simulations used time steps ranging from 0.1 to 2 femtoseconds. As shown in the bottom left panel of Fig. 1, using a time step of 2 femtoseconds in QMD resulted in a numerical instability (divergence of the constant of motion) during the integration of the Parrinello-Rahman equations. For smaller time steps, we observed no discernable differences between the results obtained with a time step of 1 femtosecond and a much smaller time step of 0.1 femtosecond. Regarding the trajectory length, previous classical MD simulations of HMX used very long trajectories, ranging from hundreds of picoseconds to several nanoseconds. However, in our QMD simulations, we found that the lattice parameters averaged over 10 picoseconds were already within 0.5% of the values averaged over longer periods. Regarding the necessary number of replicas, we found that if only one replica was used, the resulting trajectory averages deviated by as much as 1% from the reference value (the latter was obtained by averaging over all 50 trajectories). However, when five replicas were used, the resulting ensemble averages were within 0.4% of the reference value. We also tested variations in the observed lattice parameters with respect to the values of the coupling parameters in the Parrinello-Rahman solver, the scaling factor in Ewald summation, and self-consistent field settings (not discussed here). The resulting settings were used in the QMD simulations of several nitramine crystals, as described in the companion report.

DoD Impact/Significance: Unlike classical MD methods, QMD does not require reparameterization of interatomic potentials for new compounds and thus is applicable to various energetic materials of interest to DoD. In this Pathfinder project, we tested DFTB-based QMD simulations on a representative molecular crystal and established the optimal values for various numerical parameters.

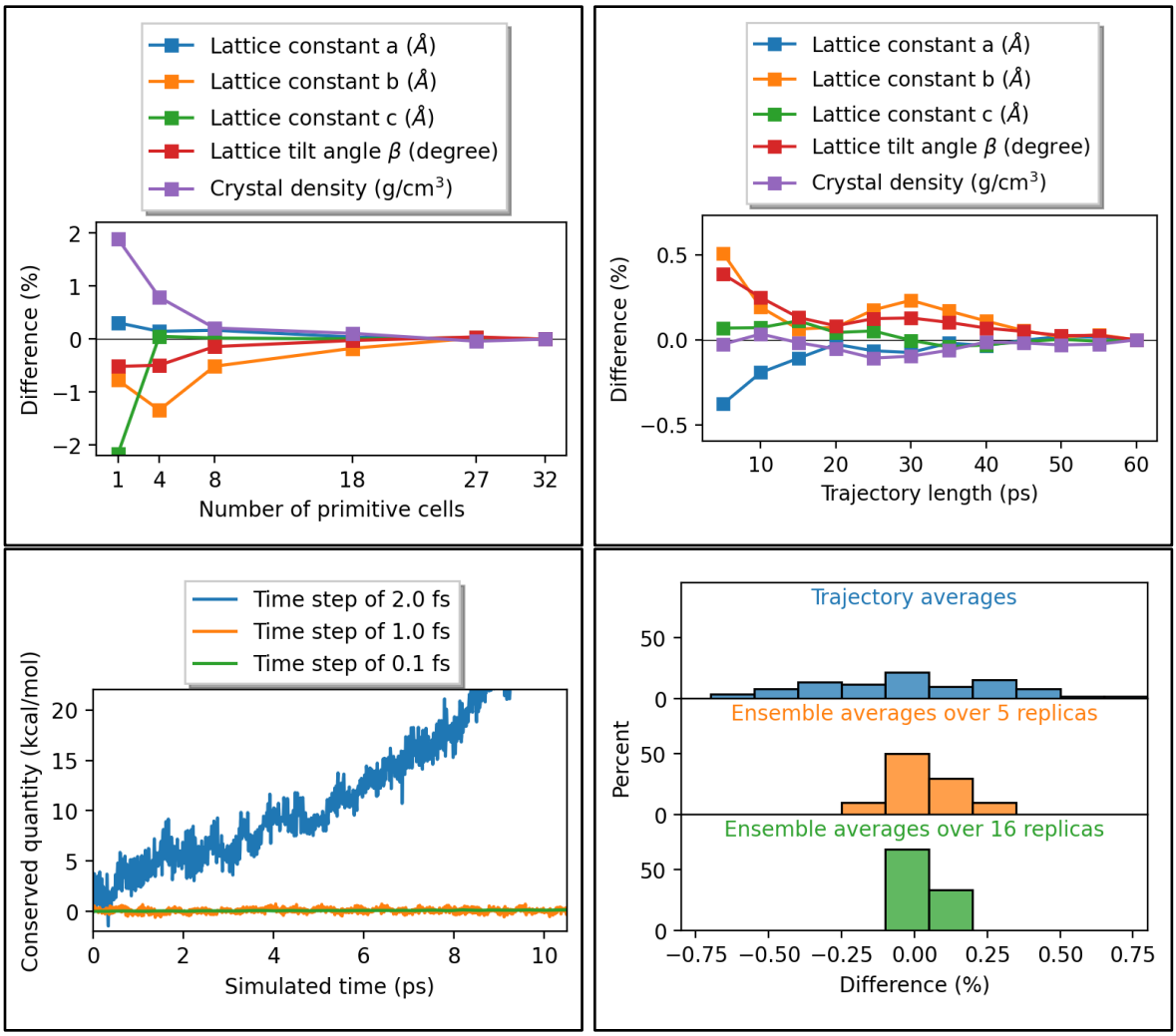


Figure 5. Top left: Crystal lattices parameters of $\boldsymbol{\beta}$-HMX computed with DFTB-based QMD simulations and periodic models containing various numbers of the primitive unit cell. Top right: Relative differences in the trajectory-averaged lattice parameters derived from trajectories of different lengths. Bottom left: Variations in the trajectory-averaged and ensemble-averaged values derived from different subsets of 50 trajectories. Here, the x values show percent differences with respect to the ensemble average over all 50 trajectories. Bottom right: Numerical deviations in the Parrinello-Raman constant of motion as the function of the time step.

Title: Molecular and Quantum Dynamics of Biomolecule-nanostructure Interaction
Author(s): K. Whitener
Affiliation(s): U.S. Naval Research Laboratory, Washington, DC
CTA: CCM

Computer Resources: HPE Cray Shasta [AFRL, OH]

Research Objectives: The objective of this research is to evaluate the molecular interactions between two-dimensional (2D) materials such as graphene and biologically relevant materials such as gelatin. Experimental observations of changing hydrophilicity and interaction strength between gelatin and graphene derivatives necessitate computational modeling to determine the root cause of the systems' changing surface properties.

Methodology: We used density functional theory (DFT) and *ab initio* quantum chemistry to evaluate the presence of large polycyclic aromatic hydrocarbons (PAHs) on tripeptides. The PAHs represent a computationally tractable graphene fragment that can be evaluated at various levels of theory without having to set up a periodic DFT calculation. Likewise, the tripeptides we used were chosen to model a common tripeptide motif present in gelatin and collagen without having to model a large peptide, which would be computational and memory intensive without a clear advantage over the smaller model system. In addition to these methods, we employed Grimme's DFT-D3 van der Waals correction scheme to account for nonlocal interactions between non-covalently bonded peptide and graphene fragments. We also accounted for solvent effects using a COSMO continuum electrodynamic model with the dielectric constant set to that of water.

Results: We found that the isolated tripeptide motif of proline-hydroxyproline-glycine that is repeated in gelatin and collagen binds strongly and noncovalently to the graphene fragment. The binding energy per tripeptide unit was found to be roughly 75 kJ/mol, which is comparable to roughly 3 hydrogen bonds in water. Indeed, the geometry of the interaction shows a strong heteroatom (hydrogen-bond like) association between the amine, carbonyl, and carboxyl groups of the peptide and the graphene surface, along with a flattening of the bent shape of the tripeptide, which likely leads to a larger effective van der Waals attractive interaction. Contributions from both the van der Waals and COSMO solvation interactions were sizable and likely played a role in the interactions. In native collagen and gelatin (which is an acid-hydrolyzed collagen), the peptide chains form a trihelical fibrillar structure with strong hydrogen bonds in the interior core of the fibril and relatively few hydrophilic moieties facing outward. This effect should be enhanced in air and diminished in water. Our results suggest that the presence of graphene can disrupt this structure and the individual strands of collagen or gelatin can strongly bind to the graphene. This would account for the experimentally observed behavior of air-exposed gelatin adhering strongly to hydrophobic graphene oxide even under water, while water-exposed gelatin does not adhere to graphene at all.

DoD Impact/Significance: Interactions between biomolecules and nanomaterials are important for a number of reasons. The DoD operates in a number of different environments where biomolecules come into contact with advanced structural materials, some of which may have nanomaterial aspects. These include biofilms on ships, nanomaterials in advanced wound dressings, and other bio-nano interactions. Controlling these environmental interactions favorably could lead to development of materials that inhibit biofilm growth on military-relevant structures as well as more effective treatment of wounds. The latter of these has dual use both within the DoD and in the civilian sphere.

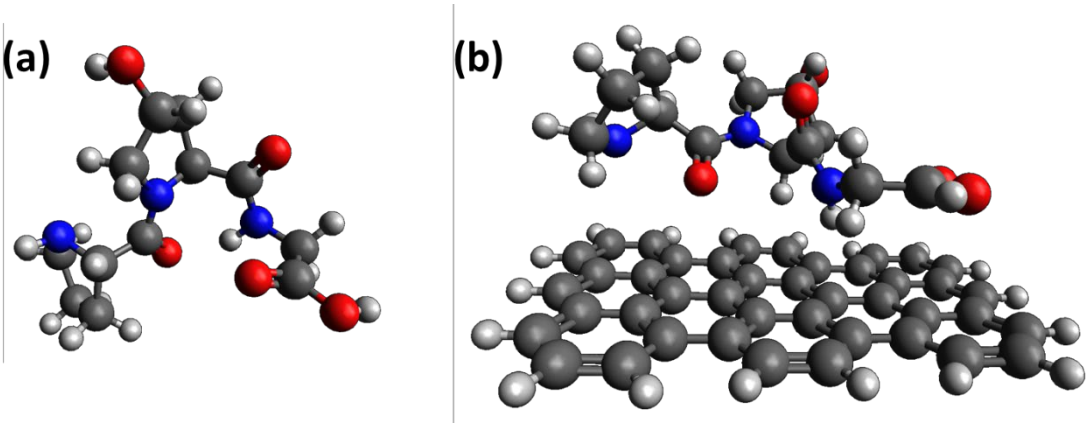


Figure 1. (a) DFT-optimized geometry (B3LYP//6-31G*) of Pro-Hyp-Gly tripeptide gelatin/collagen model in the presence of dispersion (DFT-D3) and water solvent (COSMO) effects. (b) DFT-optimized geometry (B3LYP//6-31G*) of Pro-Hyp-Gly tripeptide interacting with a graphene fragment in the presence of dispersion (DFT-D3) and water solvent (COSMO) effects. Note the flattening of the helical structure and strong heteroatom-graphene interactions.

Title: Point Defects and Interfaces in Two-Dimensional Materials
Author(s): D. Wickramaratne
Affiliation(s): U.S. Naval Research Laboratory, Washington, DC
CTA: CCM

Computer Resources: SGI ICE X, Cray XC40 [ARL, MD]

Research Objective: To understand and predict the electronic, structural and optical properties of point defects, dopants, and interfaces in bulk and low-dimensional semiconductors.

Methodology: We use density functional theory (DFT) and the projector augmented wave (PAW) method as implemented in the Vienna Ab Initio Simulation (VASP) code for our calculations. To accurately describe the bandgap of semiconductors, we use screened hybrid functional calculations. Accurate forces and total energy calculations are required to identify the most stable configurations of point defects in their various charge states. We use this information to determine the formation energies, charge-state transition levels, and optical transitions of various defects.

Results: We systematically explore the properties of H, Si, Ge, Sn, Hf, Zr, and Ta as candidate *n*-type dopants substituting on the cation site in corundum aluminum gallium oxide (AlGO) alloys using first-principles calculations. In Ga_2O_3, each of these dopants is a shallow donor. In Al_2O_3, they are deep defects leading to either negative-*U* (+/-) or positive-*U* (+/0) levels deep within the bandgap. We combine our calculations of these dopant charge-state transition levels across the alloy composition space with information on the alloy band structure to estimate the critical Al composition where each dopant transitions from being shallow to deep. We also assess the detrimental impact that cation vacancies may have on efforts to achieve n-type doping by acting as compensating acceptors. Based on this, we identify Si to be the most efficient dopant to achieve *n*-type conductivity in high Al-content corundum AlGO alloys. A paper on these results was published in Applied Physics Letters.

DoD Impact/Significance: There are growing experimental efforts to alloy Ga2O3 with Al, which would enable power electronic devices that operate at higher electric fields and UV devices that operate at shorter wavelengths. Such devices are of interest for DoD applications. The successful operation of these devices is predicated in part upon the ability to identify donor dopants that would give rise to *n*-type conductivity.

This work has helped identify potential donor dopants in wide-bandgap alloys of Al_2O_3 and Ga_2O_3 and the critical alloy composition at which the different donors transition from being shallow to being deep defects, at which point they no longer give rise to *n*-type conductivity.

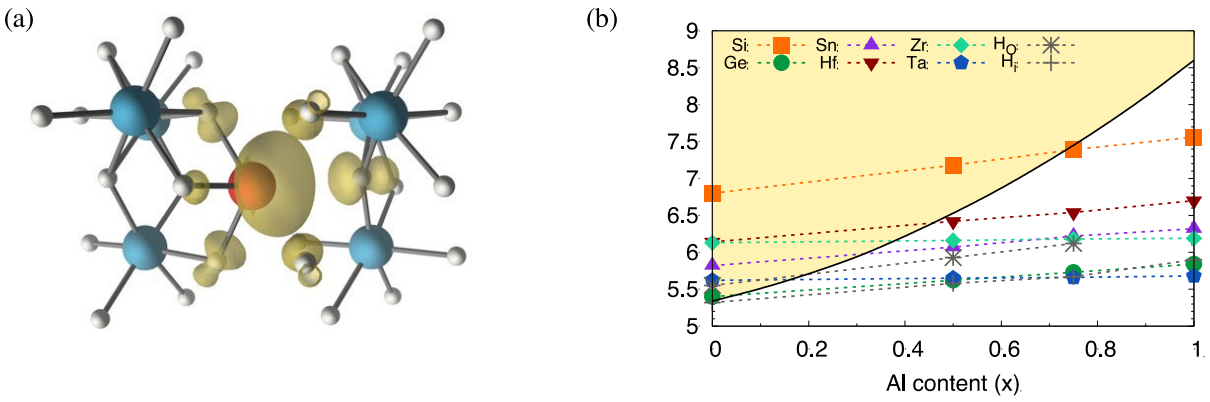


Figure 1. (a) Atomic structure and charge density of the negative charge state of Si substituting on the Al site in Al_2O_3 (b) Thermodynamic transition levels of the different dopants obtained from calculations at different alloy compositions. The CBM energy (shaded yellow) across the range of Al content is plotted with respect to the VBM energy of Ga_2O_3.

Title: Computation of Refractive Indices and Birefringence in Novel Polyimide Optical Polymers
Author(s): G. Kushto and A. Rosenberg
Affiliation(s): U.S. Naval Research Laboratory, Washington, DC
CTA: CCM

Computer Resources: HPE Cray Shasta [AFRL, OH]

Research Objectives: Utilize density functional methods to help explain polymer optical birefringence and to help guide future synthetic efforts.

Methodology: Hybrid density functional theory calculations on moderately sized organic materials systems.

Results: Polymeric optical components are generally desirable for both military and commercial applications because of their light weight, high impact resistance, and ability to incorporate sophisticated shapes or gradient index (GRIN) profiles. One class of polymeric materials that have shown great promise is aromatic polyimides, which show excellent optical properties over a wide temperature range but tend to suffer varying degrees of optical birefringence (Δn) even as nominally amorphous films. We investigated the origin of this birefringence using the static polarizability tensors of the polymer repeat units as calculated using density functional theory (microscopic), and compared these results with experimentally derived birefringence data (bulk) through the Lorentz-Lorenz equation as modified by Vuks.[1]

All quantum chemical calculations were conducted using the Gaussian suite of programs[2] with the functional and basis sets as defined therein. The equilibrium ground state molecular geometries of the polyimide repeat units were determined using the B3LYP hybrid functional and Pople's 6-31G double-ζ basis set augmented with a single polarization function (6-31G*). The calculation of the static polarizability tensors was effected using the long-range corrected density functional LC-ωhPBE at the above equilibrium geometry. For the polarizability calculations, we used the 6-31+G* basis, which includes an additional diffuse function. This has been shown to be necessary to achieve accurate polarizability tensor values. Termination of the repeat units was achieved by including the next functional group expected from the chemical structure of the polymer.

Results show that although there is a qualitative agreement between the calculated birefringence data and that derived through quantum mechanical analysis (see Fig. 1) there can be significant deviation between the two dependent upon several factors associated with the chemical structure of the repeat unit. As the complexity and nonlinearity of the polymer backbone increase through programmed isomerization, we observe larger deviations between theory and experiment. The most likely explanation for this observation is that the deviations between theory and experiment increase with increasing long-range disorder in the film, which can be associated with the complexity of the repeat unit but cannot be quantified using the approach taken here.

By comparing the measured birefringence to the intrinsic birefringence obtained from DFT calculations of the polarizability anisotropy, we showed that the observed Δn is only weakly associated with the polarizability of the repeat units. Instead, we identified the dominant effect on birefringence as the degree of polymer chain disorder, which is mainly determined by the structure of the repeat unit. This is consistent with the description of disorder introduced by de Gennes[3] for liquid crystals. Interestingly, we found that increased chain disorder, which acts to reduce or eliminate the observed birefringence, does not significantly modify the thermal properties of these amorphous polymers. Finally, we also found that copolymerization enables fine-tuning of the polyimide properties, but only to an extent limited by nonideal copolymer formation at certain compositions.

DoD Impact/Significance: Lightweight, durable, high-performance polymeric optical materials.

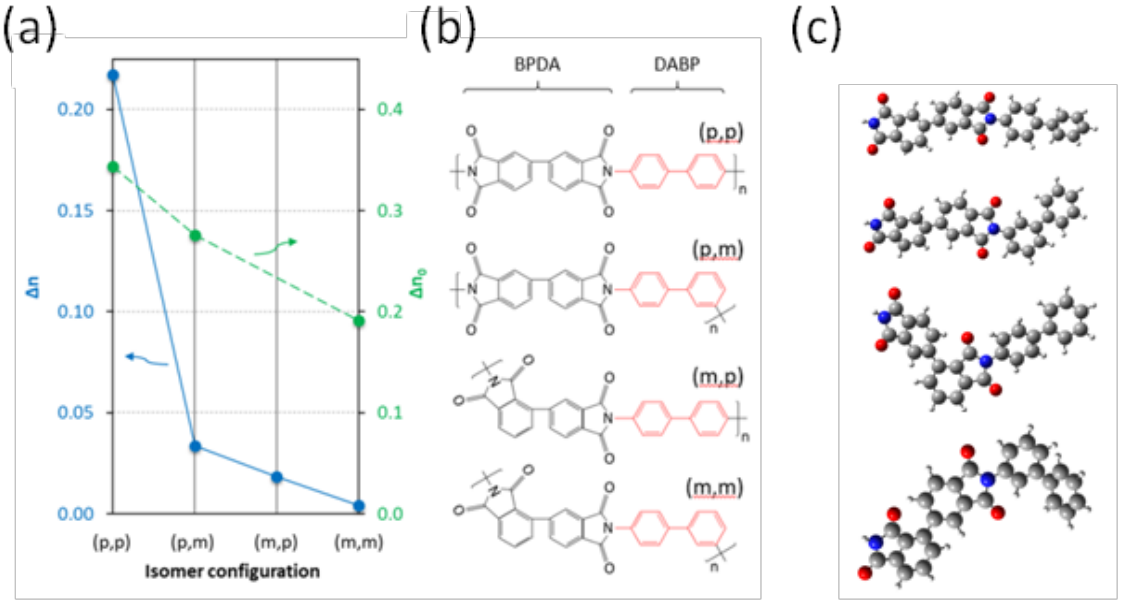


Figure 1. Effects of structural isomer substitution in the BPDA-DADP system: (a) observed birefringence (Δn, experimental) and intrinsic birefringence (Δn_0, theory), (b) generalized chemical structures of the polyimide repeat units, and (c) B3LYP/6-31G* optimized geometries pertaining to the chemical structures. Note the differences in scale in (a) suggesting overall qualitative agreement between theory and experiment (trend is decreasing going left to right), but poor quantitative prediction from the theory.

[1]Vuks, M.F. "*Determination of the optical anisotropy of aromatic molecules from the double refraction of crystals*" Opt. Spectrosc. **20**, 361-364 (1966).

[2] Gaussian 16, Revision C.01, Frisch, M. J.; Trucks, G. W.; Schlegel, H. B.; Scuseria, G. E.; Robb, M. A.; Cheeseman, J. R.; Scalmani, G.; Barone, V.; Petersson, G. A.; Nakatsuji, H.; Li, X.; Caricato, M.; Marenich, A. V.; Bloino, J.; Janesko, B. G.; Gomperts, R.; Mennucci, B.; Hratchian, H. P.; Ortiz, J. V.; Izmaylov, A. F.; Sonnenberg, J. L.; Williams-Young, D.; Ding, F.; Lipparini, F.; Egidi, F.; Goings, J.; Peng, B.; Petrone, A.; Henderson, T.; Ranasinghe, D.; Zakrzewski, V. G.; Gao, J.; Rega, N.; Zheng, G.; Liang, W.; Hada, M.; Ehara, M.; Toyota, K.; Fukuda, R.; Hasegawa, J.; Ishida, M.; Nakajima, T.; Honda, Y.; Kitao, O.; Nakai, H.; Vreven, T.; Throssell, K.; Montgomery, J. A., Jr.; Peralta, J. E.; Ogliaro, F.; Bearpark, M. J.; Heyd, J. J.; Brothers, E. N.; Kudin, K. N.; Staroverov, V. N.; Keith, T. A.; Kobayashi, R.; Normand, J.; Raghavachari, K.; Rendell, A. P.; Burant, J. C.; Iyengar, S. S.; Tomasi, J.; Cossi, M.; Millam, J. M.; Klene, M.; Adamo, C.; Cammi, R.; Ochterski, J. W.; Martin, R. L.; Morokuma, K.; Farkas, O.; Foresman, J. B.; Fox, D. J. Gaussian, Inc., Wallingford CT, 2016.

[3] de Gennes, P. G., "The Physics of Liquid Crystals," Clarendon Press: London, p. 31 (1974).

Title: Atomistic Simulations of Navy-relevant Materials
Author(s): D. Fragiadakis
Affiliation(s): U.S. Naval Research Laboratory, Washington, DC
CTA: CCM

Computer Resources: HPE Cray Shasta, HPE SGI 8600 [NAVY, MS]; HPE SGI 8600 [AFRL, OH]; SGI ICE X [ARL, MD]

Research Objectives: The objective of the work conducted was to determine the effect of chain length and branching on the unimolecular decomposition pathways of perfluoroalkyl substances (PFAS) under thermal incineration conditions.

Methodology: Structures of the relevant chemical species and transition states were optimized using density functional theory calculations at the M06-2XD3/def2-TZVPP level of theory. Reactants and products connected by each transition state were verified using intrinsic reaction coordinate computations. The Gaussian 16 software package was used to conduct the calculations on HPCMP resources, with in-house software for data analysis.

Results: The unimolecular decomposition of perfluoroalkyl sulfonic acids takes place via several mechanisms with energetic barriers low enough to make them relevant under incineration conditions; this is in addition to C-S bond fission, which was considered separately in a parallel study. These pathways were investigated for perfluoro n-alkyl sulfonic acid with n = 1 to 8, and all structural isomers of the perfluoropropyl- and -butyl- sulfonic acids.

For the linear sulfonic acids, the favored decomposition pathway is HF elimination forming a cyclic intermediate, which subsequently yields a perfluoro carbonyl species. Pathways beginning with (a) simultaneous HF and SO_3 elimination, (b) isomerization to a structure with oxygen linking the sulfur atom to a carbon, (c) SO_3 elimination and (d) SO_2 elimination follow in order of increasing energetic barriers. This order holds for n = 1 to n = 8; the barrier for HF elimination increasing with increasing n, especially from n = 1 to n = 2, while the energetic barriers for the remaining pathways decrease with increasing n, leveling off around n = 4.

Moving to the branched propyl and butyl sulfonic acids, the decomposition of perfluoroisobutyl sulfonate occurs by equivalent pathways to those of the linear species. However, for the isomers with secondary sulfonic group, i.e., perfluoro-sec-butyl sulfonate and perfluoro isopropyl sulfonate, the barrier for $HF+SO_3$ elimination lowers and becomes significantly lower than that of HF elimination, which increases by approximately 20%. The barrier for $HF+SO_3$ elimination decreases even further for perfluoro-tert-butyl sulfonate, for which the HF elimination reaction cannot take place.

The decomposition pathways of PFMS and perfluoroethane sulfonic acid (PFES) at incineration temperatures of 600 and 1,200 °C show only minor temperature dependence in the barriers for individual decomposition steps, but large decreases in reaction free energy due to entropic effects. The preferred decomposition routes remain unchanged at these higher temperatures.

DoD Impact/Significance: Reaction rates, calculated from the results of the study, can be incorporated into existing kinetic models and enable accurate prediction of chemical reactions occurring in incinerators utilized for PFAS mitigation. This will enable optimization of incineration conditions to maximize destruction of PFAS and to avoid releasing persistent and/or harmful products of intermediate combustion.

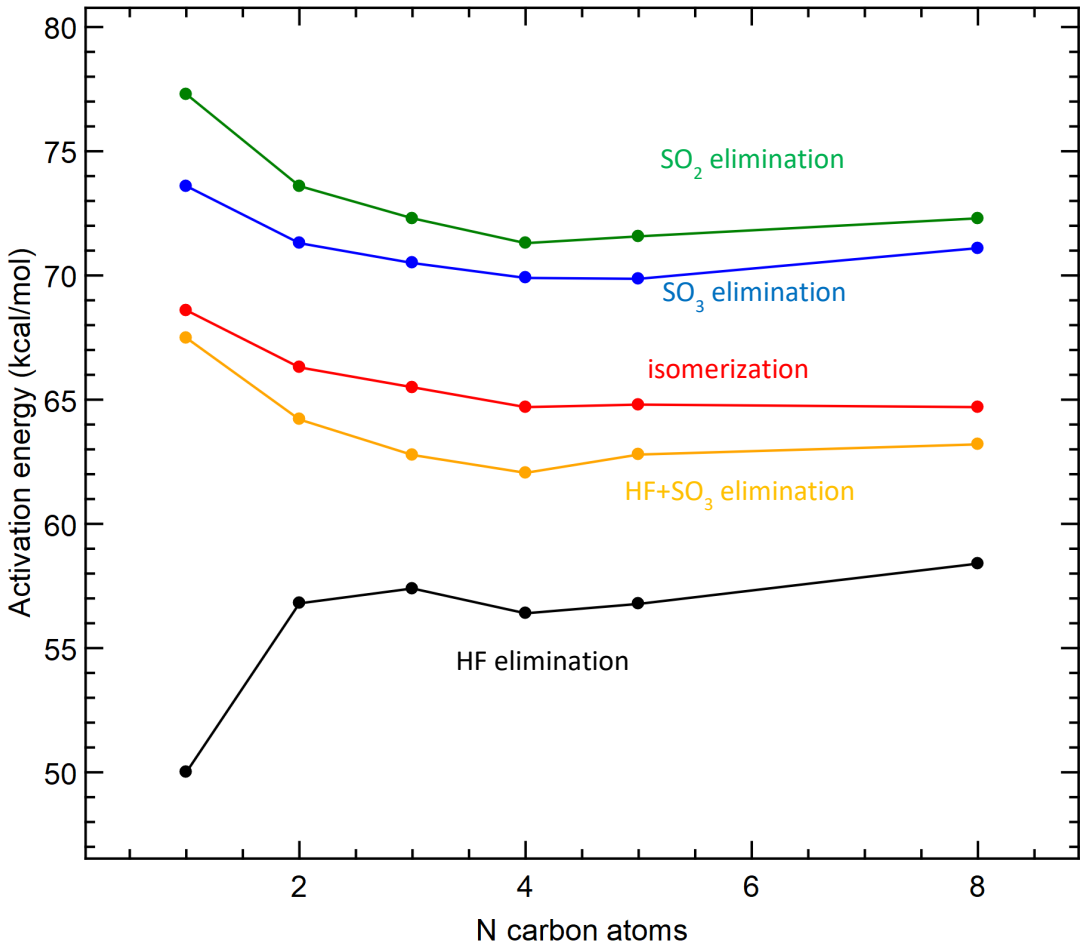


Figure 1. Activation energy of the initial step of indicated elimination pathways for the unimolecular decomposition of n-alkyl sulfonic acids as a function of alkyl chain length.

Title: Engineering Phase Change Materials for Neuromorphic Photonic Applications
Author(s): J.G. Champlain[1] and K.A. Cooley[2]
Affiliation(s): [1]U.S. Naval Research Laboratory, Washington, DC; [2]National Research Council Postdoctoral Research Associate, U.S. Naval Research Laboratory, Washington, DC
CTA: CCM

Computer Resources: HPE SGI 8600 [AFRL, OH]; Cray Shasta [NAVY, MS]

Research Objectives: This program seeks to demonstrate how alloying can be used to modify the structural, optical, and electronic properties of phase-change materials for neuromorphic photonic devices. The effect of alloying elements on these properties offers a straightforward way to tune materials to achieve optimum device performance and efficiency for neuromorphic applications, which are of great interest to the Navy and the Department of Defense.

Methodology: Density functional theory (DFT) atomic structure calculations using the Quantum ESPRESSO software suite are used to analyze changes to the crystalline and electronic structure caused by alloying GeTe with elements that include Cu, Bi, and Sn.

Results: Initial results indicate that Bi, Sn, and Cu alloying elements will have varied effects on the crystal structure of GeTe. Bi and Cu are predicted to increase and decrease the cell volume of GeTe, respectively, while Sn is expected to cause the smallest effect on GeTe cell volume and Ge-to-Te bond lengths. This information is important to understanding how alloying could affect the phase change process of GeTe in a future device, where density changes between crystalline and amorphous phases can induce problematic stresses.

In addition, new calculations on the optical properties of GeTe alloys suggest the alloying has a varied effect on the optical properties of the resulting materials. These changes are quite notable in the plot of absorption coefficient vs. wavelength provided in Fig. 1. For each considered alloy, the system with the lowest considered alloying concentration (6.25 at. % Bi, Cu, or Sn) behaved most similarly to pure GeTe, and yet each absorption curve was unique.

DoD Significance: This work synergistically combines materials computation with materials synthesis and characterization to identify and confirm metal and metalloid alloys that will widen the GeTe optical bandgap and will reduce free carrier concentration for increased PCM switching contrast and reduced signal losses for neuromorphic photonics and other optical applications. Engineering phase-change materials in this way will not only be significant for the development of neuromorphic photonics platforms that are valuable for Navy, DoD, and commercial computing applications, but also will have far-reaching impact in other PCM-based technologies, such as RF electronics, photonics, and metamaterials.

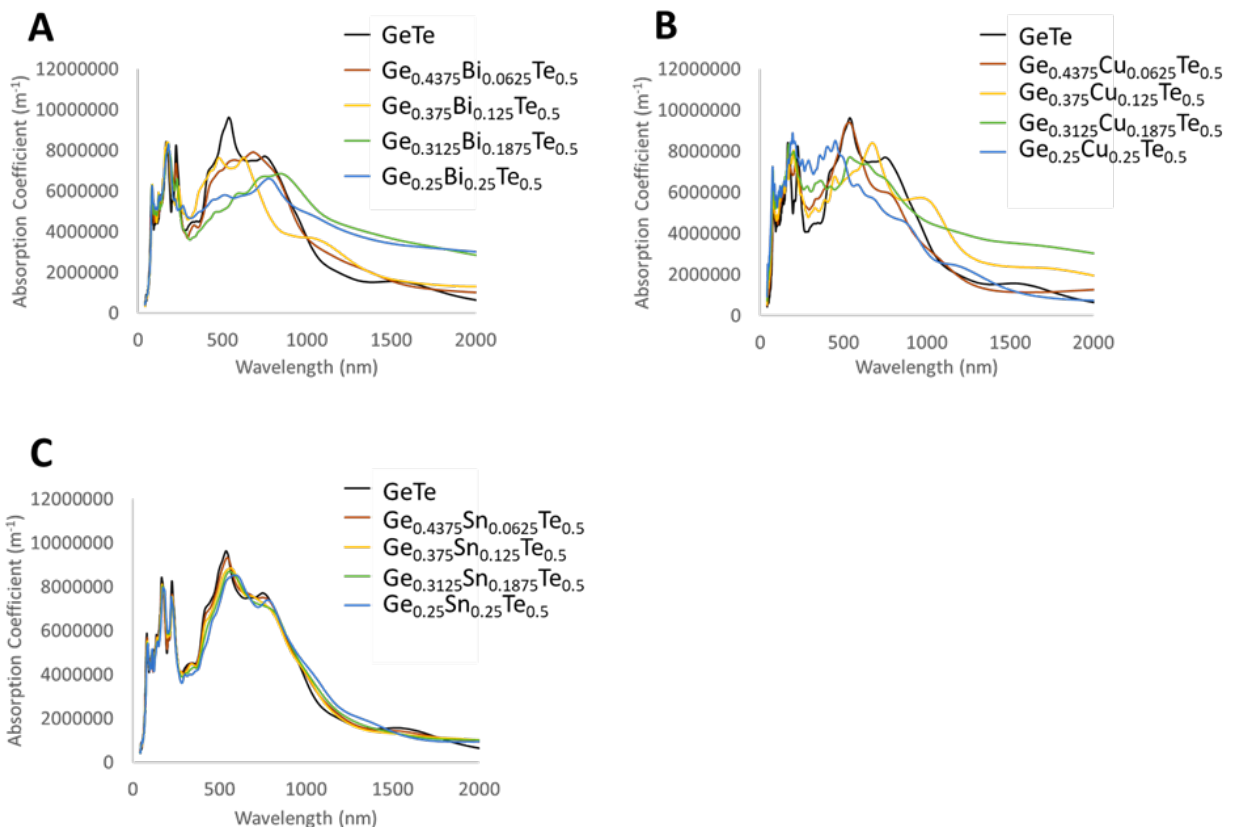


Figure 1. The absorption coefficient of $Ge_{0.5-x}M_xTe_{0.5}$ alloys, where M = Bi (A), Cu (B), or Sn (C) and x = 0.0625, 0.1250, 0.1875, and 0.2500.

Title: DFT Studies of Small Molecule Adsorption on Monolayer Transition Metal Dichalcogenide Films
Author(s): F.K. Perkins[1] and C.H. Sharp[2]
Affiliations(s): [1]U.S Naval Research Laboratory, Washington DC; [2]National Research Council Postdoctoral Research Associate, U.S. Naval Research Laboratory, Washington DC
CTA: CCM

Computer Resources: HPE SGI 8600 [AFRL, OH]

Research Objectives: Monolayer films of transition metal dichalcogenides, e.g., WS_2, WSe_2, and MoS_2, have shown empirical promise as chemical vapor sensors. Ambient concentrations of low-vapor-pressure amines as low as parts per billion have induced measurable changes in electrical conductivity and photoluminescence, while high concentrations of water vapor, alcohols, and other benign compounds induce no observable changes in the same properties. In the work carried out here, we attempted to perform electronic structure calculations to understand how adsorption of amines affect the films, and in particular, how the small electronic charge donation from Lewis acids (such as amines) might induce a structural phase change that could be observable in Raman spectroscopy, and a transition from a semiconducting 2H to a metallic 1T state. The results will aid in developing a mechanistic model for the response of TMD-based chemsensor devices, suggesting a path toward improved specificity.

Methodology: The methodology used as part of this research involved the use of the computational chemistry software packages Gaussian and Quantum Espresso.

Gaussian: Gaussian employs localized basis sets to construct molecular orbitals of small molecules. Gaussian was employed to perform structure optimizations of the small-molecule adsorbates as well as to provide calculated vibrational spectra that will serve as a reference for infrared spectroscopy studies performed in the laboratory at NRL. The graphical user interface Gaussview was used to design chemical structures and to set up calculations.

Quantum Espresso: Quantum Espresso utilizes plane wave basis sets and pseudopotentials to analyze periodic structures. Using literature-based crystallographic data, we constructed TMD supercells and used Quantum Espresso to perform structure and energy optimizations of small gas molecules adsorbed at different binding sites to quantify the adsorption energy.

Results: Results from FY21 and FY22 include single-point (fixed-ion) self-consistent field calculations of MoS_2 and WS_2 crystalline monolayers in the 2H, 1T, and 1T' phases calculated with Quantum Espresso on AFRL "Mustang" and ERDC "Onyx." These will provide the basis for the electronic band calculations and structure optimization in the presence of adsorbates. Attempts to perform structural relaxation calculations using the Gaussian software were attempted as well, but the calculations did not run successfully.

DoD Impact/Significance: Computational studies of interactions with monolayer TMD films will support laboratory experiments currently underway at NRL (work unit 6B28), ranging from fundamental ultrahigh vacuum-based investigations to *in situ* chemiresistive sensor testing. Calculated band diagrams of TMD surfaces before and after exposure to adsorbates will be used to validate ultraviolet photoelectron spectroscopy and low-energy electron diffraction data.

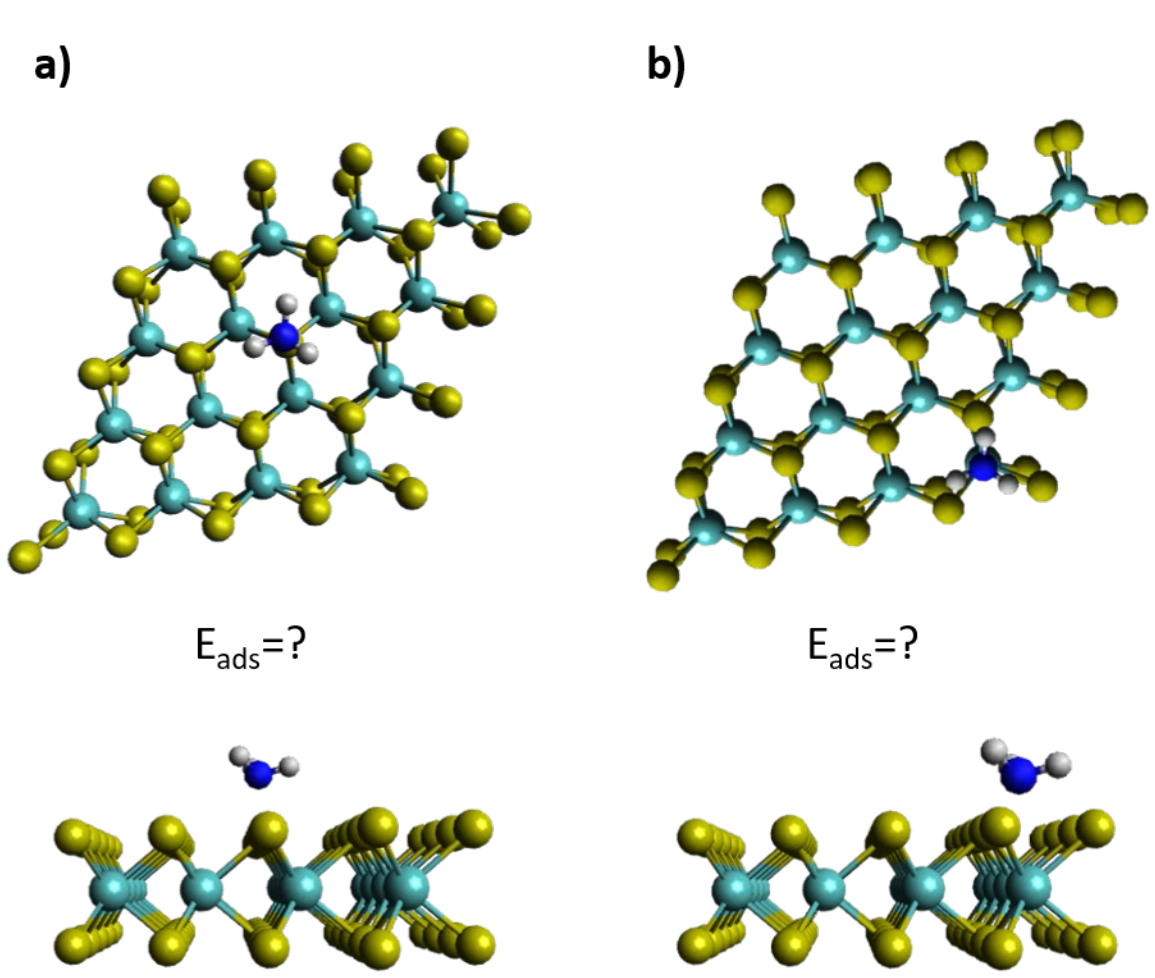


Figure 1. Ammonia adsorbed on 4x4x1 MoS_2 periodic slab (a) over top-layer S atom or (b) over middle-layer Mo atom. White, blue, cyan, and yellow colors refer to hydrogen, nitrogen, molybdenum, and sulfur, respectively.

THIS PAGE INTENTIONALLY LEFT BLANK

CEA

Computational Electromagnetics and Acoustics

CEA covers two primary computational disciplines. Computational electromagnetics covers the high-resolution multidimensional solutions of Maxwell's equations. DoD applications include calculating radiofrequency (RF) sensor performance, radar scattering of tactical ground, air, and sea vehicles, the electromagnetic signature of buried munitions, high-power microwave performance, and the interdisciplinary applications in magnetohydrodynamics and laser systems. The computational acoustics area covers the high-resolution multidimensional solutions of the acoustic wave equations in solids and fluids. DoD applications include the modeling of acoustic fields for surveillance and communication, seismic fields for mine detection, and the acoustic shock waves of explosions for antipersonnel weapons.

Title: Pinched-beam Diode Particle in Cell Simulations
Author(s): J.C. Foster,[1] S.B. Swanekamp,[2] and P.E. Adamson[2]
Affiliation(s): [1]Air Force Institute of Technology, Wright-Patterson AFB, OH; [2]U.S. Naval Research Laboratory, Washington, DC
CTA: CEA

Computer Resources: HPE SGI 8600 [AFRL, OH]; Cray Shasta [NAVY, MS]

Research Objectives: There is a renewed interest in intense ion beams produced by pinched-beam diodes (PBDs) for materials science applications that require uniform ion beam fluences over large areas. The focus of this research, the planar PBD, has advantages over the cylindrical PBD, including two experimental target object locations and improved ion fluence uniformity. However, these features come at the cost of lower ion fluence. Also, Cartesian geometries show instability and unexpected ion energy distributions with thinner anodes. In this research, we examined the ion beam properties produced from the Cartesian planar diode in more detail.

Methodology: Charged-particle flow is modeled in Chicago, a three-dimensional capable finite-difference time-domain code that utilizes particle-in-cell (PIC) methodology. The PIC methodology utilizes a spatial grid to provide weighting between particles and grid points, solves Maxwell's equations to obtain the electric and magnetic fields, and moves particles with novel use of the Lorentz equation. High-performance computing is required to simulate the dynamics of millions of particles.

Results: The simulations identified two potential sources of ion beam nonuniformity. The first possible source is the formation of electron hot spots. Both cylindrical and planar diode geometries have shown electron hot spots in the charged particle flow that can modulate the ion beam flow, and Fig. 1 provides a brief description of hot spots in the planar geometry. The second possible source of nonuniformity is spotty ion emission from a planar diode. Figure 2 shows spotty ion emission as the anode is made longer. This is a source of future work, as the exact cause for the spotty ion emission is not known but is suspected to be related to the relatively large specific heat of polyethylene. Figure 2 shows spotty ion emission from a 3,200-micron-thick anode of various lengths. Another significant result of this work has been the observation of improved ion beam fluence uniformity in planar diode geometries. We have found that an 8-cm-long, 400-micron-thick anode can provide a fluence of 10 cal/cm^2 over 100 cm^2 with a uniformity of +/- 25%. This result is encouraging because we observe ion fluence uniformities of +/- 50% with experiments using a cylindrical diode. Figure 3 illustrates the ion fluence from a planar geometry.

DoD Impact/Significance: The results of this research have illuminated promising avenues for future theoretical and experimental research to understand the spotty nature of ion emission. Once understood, it is hoped that methods can be developed to improve the uniformity of intense ion beams generated from PBDs. More uniform ion beams are needed to enable future material science applications.

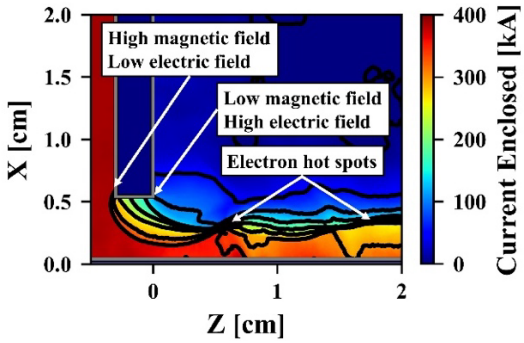


Figure 1. Current enclosed contour plot near the cathode plate of a planar pinched-beam diode with a 100-micron-thick anode at 45 ns. Current flows parallel to black contour lines, separated by 50 kA. Electron hot spots cause nonuniform ion flow where contours meet.

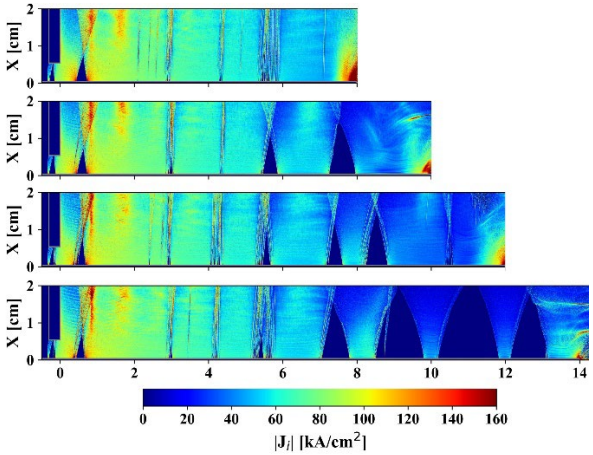


Figure 2. Ion current density for a 3,200-micron-thick anode with lengths of 8, 10, 12, and 14 cm at 50 ns illustrate spotty ion emission.

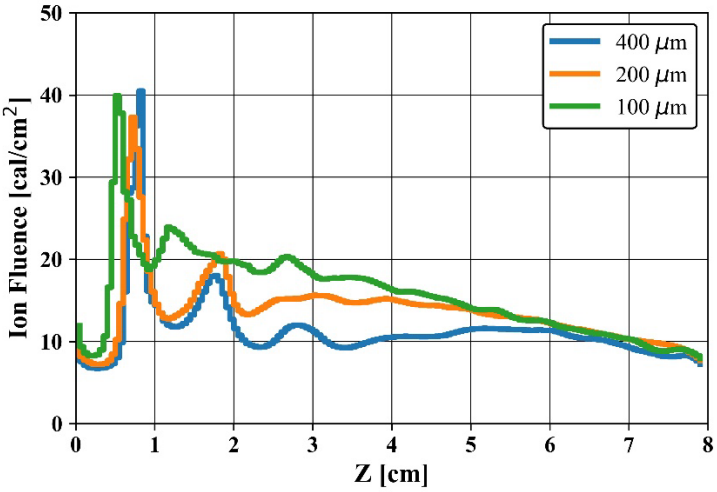


Figure 3. A comparison of ion fluences for an 8-cm-long anode with thicknesses of 400 (blue), 200 (orange), and 100 microns (green) shows that beyond Z = 2 cm, uniformity improves with thicker anodes, but fluence is lower than thinner anodes.

Title: Parallel Cylindrical Reflex Triode (CRT) Particle-in-Cell (PIC) Simulations
Author(s): I.M. Rittersdorf, B.V. Weber, S.B. Swanekamp and P.E. Adamson
Affiliation(s): U.S. Naval Research Laboratory, Washington, DC
CTA: CEA

Computer Resources: Cray XC40/50 [ERDC, MS]; Cray Shasta [NAVY, MS]

Research Objectives: The CRT is a bremsstrahlung diode that is notable for its ability to create low-endpoint X-ray spectra useful for radiation-matter interaction studies. The primary objective of this research is to perform PIC simulations that will inform designs that combine multiple CRTs in either series or parallel to increase X-ray output.

Methodology: PIC simulations of two CRTs in parallel were performed in a two-dimensional (2D) cylindrical geometry, as shown in Fig. 1, using the code Chicago. A stiff voltage source was used to drive all four ports of the diode at once. Sixteen PIC simulations were performed over a time scale of 50 ns, varying the drive voltage and the anode-cathode (AK) gap spacing. The total current flow through all four ports at 50 ns is used as a figure of merit for scaling as a function of drive voltage and AK gap.

Results: Figure 2 shows the electron density at t = 20 ns for a representative drive voltage of 400 kV and an AK gap of 5 mm. A contour plot of current flow (not shown due to space constraints) reveals the interesting feature in which the current contours on the two CRTs wrap around the tip of the anode foil and do so away from each other. As expected, there is a large population of electrons within the anode foil. There is also a high density of electrons in the gap between the two CRTs that is not contributing to the flow of diode current. Trajectories of electron tracer particles (also not shown due to space constraints), reveal electron motion from the cathode to the anode foil tip (downstream). The electrons then scatter in the foil as they travel in the negative-z direction (upstream). The simulations also indicate that electrons emitted from one CRT interact with the other CRT. The full extent of this coupling between the two CRTs is an active area of research. The results of a scaling study are shown in Fig. 3. In the study, drive voltage was varied from 100 kV to 400 kV in increments of 100 kV, and the AK gap was varied from 2 mm to 5 mm in increments of 1 mm. The total current flow scales up with increasing drive voltage and decreasing AK gap.

DoD Impact/Significance: The simulations described here are the first PIC simulations of two CRTs connected in parallel, and the results of the scaling study will be used to inform future simulations and experimental studies to increase X-ray output of the device.

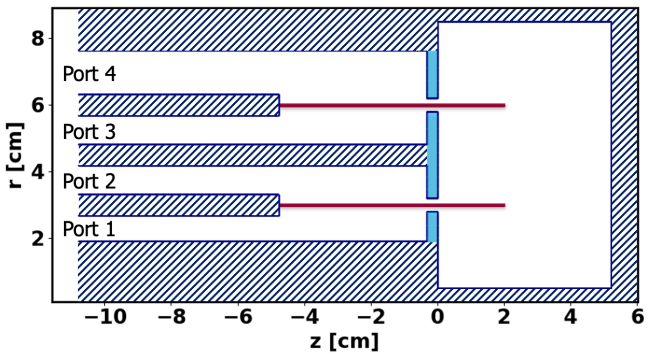


Figure 1. Two-dimensional cylindrical geometry of cylindrical reflex triode used in particle-in-cell simulations. The blue regions are the cathode plates where an electron emission threshold, $E_{th} = 300\ kV/cm$, is set. On the tantalum anode foils (shown in red), proton emission is controlled via a temperature threshold emission criterion.

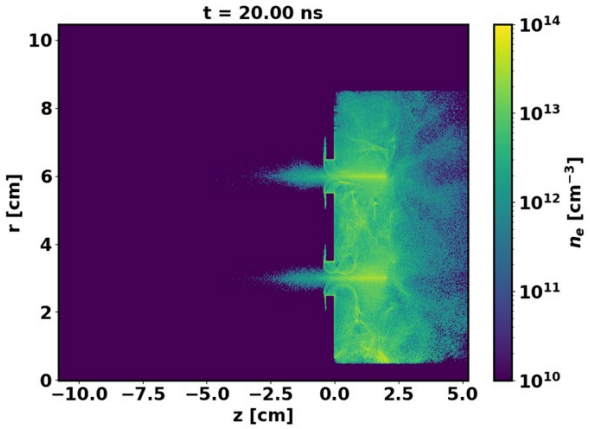


Figure 2. Electron density at t = 20 ns for a representative parallel CRT simulation with drive voltage of 400 kV and AK gap of 5 mm.

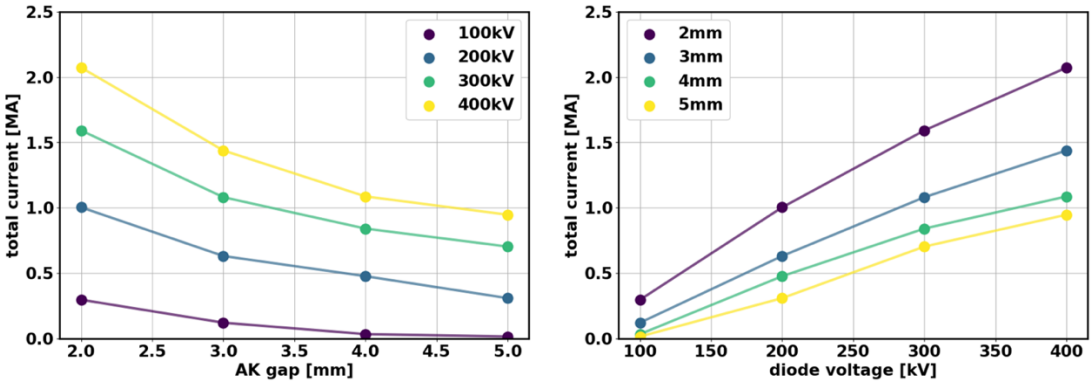


Figure 3. The results of a scaling study in which drive voltage was varied from 100 kV to 400 kV in increments of 200 kV, and the AK gap was varied from 2 mm to 5 mm in increments of 1 mm. The figure of merit, total current flow, scales up with increasing drive voltage and decreasing AK gap.

Title: Small-Slope Approximation (SSA) Rough-Surface Backscattering Analysis
Author(s): J. Alatishe
Affiliation(s): U.S. Naval Research Laboratory, Washington, DC
CTA: CEA

Computer Resources: HPE Cray Shasta [AFRL, OH]; Cray Shasta, HPE SGI 8600 [NAVY, MS]

Research Objectives: To determine and characterize the spatial coherence effects inherent in sea clutter by numerically analyzing the associated response at the antenna port of a monostatic radar. The sea-surface coherence effects are examined with respect to the associated antenna characteristics and the surface properties.

Methodology: The surface model used in the Time Evolving Backscatter Sea-Clutter Simulation (TEBSS) is based on the linear propagation model for deep-water ocean waves. Once the response from the surface has been computed, the properties of the simulated sea-clutter responses are characterized. The surface scattering amplitude (SA) characterizes the spatial coherence of the scattered electromagnetic field. The surface scattering approximation for small slopes (SSASS), which approximates the induced field distribution on the sea surface, is employed in the SA. Once the SA has been computed, the response at the antenna port is determined and the coherence effects due to the surface are examined. Numerical integration is used to determine the antenna response from the rough-surface profile. The sea surface is derived using the Elfouhaily ocean wave-number spectrum for wind speeds of 5 to 10 m/s for an upwind direction. With both the SA and the surface model calculated, the response at the antenna port was computed for each antenna aspect angle. The codes used to execute these steps were first written in MATLAB and then were converted into FORTRAN 90. The codes were then parallelized using the message passing interface (MPI) and were run on 1,024 processors (minimum) or up to 32 graphics processing units (GPUs) at the U.S. Naval Research Laboratory (NRL) High-Performance Computing (HPC) facility. Simulations were conducted at X-band (10 GHz).

Results: Data obtained from the Microwave Microscope sea-clutter experiment (a previous NRL base funded 6.2 effort, MWM) were used as a baseline for comparison. These sea-clutter values were measured at various wind speeds and wind directions for given antenna aspect angles (elevation and azimuth) and polarizations of the antennas. The corresponding simulated received sea-clutter responses were computed for an elevation angle of 85° for both vertical and horizontal polarizations. The simulation generated an 8,192-point frequency response of the sea surface for a given wind speed for an observed time increment. Fast Fourier transform (FFT) convolution was used to generate the complex time-dependent echo, which is the spectral product of the associated sea-surface frequency response and the transmitted waveform. As a result of the previous step, multiple coherent processing intervals (CPIs) were generated for analysis and were compared to experimental data as depicted in the range-time-intensity plots in Fig. 1. The number of spatial samples of the sea surface was set to 23,103 and 2,047 in the downrange and crossrange dimensions, respectively. The simulation results showed that the range-time properties are similar to real sea clutter in that the appearance of spiky clutter returns are prevalent. However, further investigation of the simulated data is still required.

DoD Impact/Significance: Understanding the spatial coherence effects in radar sea clutter provides further insight into the phenomenology of backscattering from the ocean. This will be useful in devising new algorithms for detecting threats over the sea.

Example results:

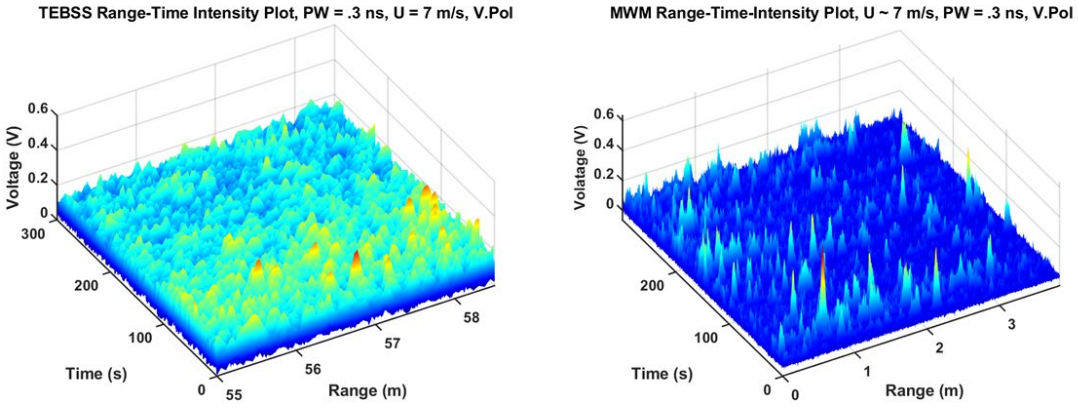


Figure 6. Range-time intensity plots of X-band simulated (TEBBS, left) and experimental (MWM, right) sea-clutter returns for VV polarization at 85° elevation. Pulsewidth is 0.3 ns, pulse repetition interval (PRI) is 300 ms, and wind speed is 7 m/s toward the radar.

Title: Acoustic Parameter Variability over an Ocean Reanalysis (AVORA)
Author(s): J.P. Fabre
Affiliation(s): U.S. Naval Research Laboratory, Stennis Space Center, MS
CTA: CEA

Computer Resources: HPE SGI 8600 [NAVY, MS]

Research Objectives: Long time reanalyses of the ocean are becoming available (e.g., NRL 7300) and are potentially extremely useful for understanding the variability of environmental parameters that impact acoustic sensor performance. Additionally, geoacoustic prediction of the seafloor is beginning to transition to the operational community. Finally, methods are being sought to compress ocean fields for easier transmission to forward platforms. The objectives of this effort are to investigate potential for improved understanding of the ocean acoustic environment, to provide recommendations for future Navy products to support operations, and to develop prototype products for test and evaluation.

Methodology: Investigate the NRL 30-year Ocean Reanalysis to quantify and understand the variability over various time frames. Parallelize and investigate geoacoustic predictions made with the Global Predictive Seabed Model (GPSM) estimates and compare to measurements. Investigate the sensitivity of acoustic propagation and proxy parameters to the environmental variability. Develop prototype products and make recommendations based on the results for products that could be derived from the described reanalyses and sediment characterizations. Such products will facilitate improved understanding of acoustic parameter variability in areas of propagation and ambient noise. Develop prototype products and compression techniques and test various ways of storing and accessing large data sets. NRL has been working extensively in the areas of big data and machine learning. We will include such technologies as part of our analysis, testing, and recommendations and incorporate lessons learned into existing products. If successful, these products could become Navy standard.

Results: We supported several fleet exercises by analyzing fields from the reanalysis compared to real-world acoustic data to assess ocean acoustics. We also provided some research-based analysis for premission support by analyzing current forecasts and past (reanalysis) trends. We used the transfer queue to cut out (from the global reanalysis) Navy areas of fleet interest and to transfer to our local and classified systems for a number of current and future efforts including, but not limited to, premission support, data assimilation, model evaluation, and reconstruction and analysis. In a similar way, we supported two NRL research experiments with timely ocean acoustic fields and prototype capabilities off the US East Coast. We automated evaluation of tau-tau differences in sound speed to inform operations. This year's technical focus was on sediment characterization and compression of ocean fields of various sizes and time spans. The figure shows application of a learned dictionary for use in compressing ocean fields; the compression ratio is approximately 2,000:1 with mean errors near 0.15°.

DoD Impact/Significance: "In Joint Vision 2020, the Department of Defense's strategic plan to ensure battlespace dominance in the 21st century, a key element is information superiority enabled by emerging technologies ..." "An important aspect of information superiority is situational awareness. This implies knowing where you are, where allied and coalition forces are and where enemy forces are. It means understanding the environment, from the sea floor to the top of the atmosphere." [Heart of ForceNet: Sensor Grid, Advanced Command and Control by RADM Steven J. Tomaszeski]. Our efforts directly inform environmental variability as it applies to acoustics.

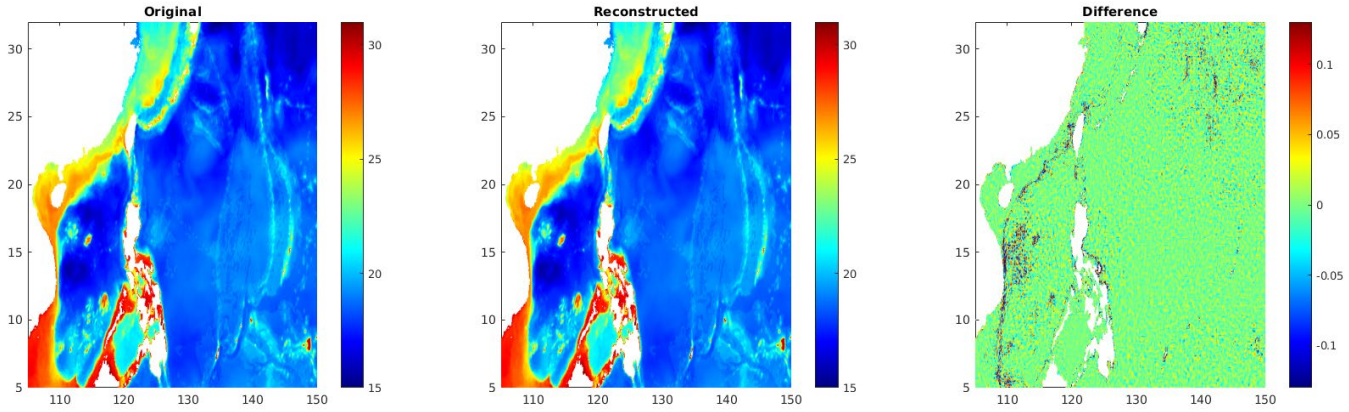


Figure 7. A dictionary is trained, or learned and preloaded, on a forward platform. A sparse set of coefficients is generated that can be compressed and sent forward, then applied to the dictionary to reconstruct full ocean fields for in-situ applications. The example shows water temperature at a single depth in the western Pacific Ocean; the uncompressed original field is on the left, the field reconstructed from the dictionary and coefficients is in the center, and the difference between the two is on the right.

Title: Simulation of Passively Model-Locked and Frequency-Modulated Interband Cascade Laser Frequency Combs
Author(s): M. Povolotskyi,[1] I. Vurgaftman,[2] and J.R. Meyer[2]
Affiliation(s): [1]Jacobs, Hanover MD; [2]U.S. Naval Research Laboratory, Washington DC
CTA: CEA

Computer Resources: HPE SGI 8600 [AFRL, OH], [NAVY, MS]

Research Objectives: 1) Use the HPC cluster research tool to develop the numerical modeling of Interband Cascade Laser (ICL) frequency combs. 2) Expand an existing approach that was developed previously for intersubband quantum cascade laser (QCLs) frequency combs to treat interband systems.

Methodology: The light propagation inside the cavity is modeled in the slowly varying envelope approximation with a single transverse mode cavity being considered. The group velocity dispersion of the mode without the active layer effect is obtained from an external simulator. A stable algorithm based on the fast Fourier transform for the pulse propagation has been developed and implemented. It was validated against analytical results for the Gaussian pulse propagation in a cavity without an active layer and showed no numerical error accumulation for the relevant propagation time.

The active layer effect is included into the light propagation equation via dipole polarization term. The polarization is computed by solving the semiconductor Bloch equations for the coupled electric field/electron/hole system. The major difference between the interband and intraband systems is that in the former, the transition energy is a function of the carrier momentum. Therefore, the laser performance depends on the distribution of electrons and holes over the Brillouin zone. Modelling of a nonequilibrium electron gas distribution over energy is a challenging task. In this research, it is assumed that the electron and hole energy relaxation time is small, so the electrons and holes have local Fermi distributions with different local Fermi levels. A set of equations has been developed in which the Fermi levels are obtained from the particle conservation law considering the injection current, stimulated radiative recombination, and Auger non-radiative recombination. Local charge neutrality is assumed and ambipolar diffusion of the carrier system is considered. The model uses as an input the electron and hole subband dispersion in the cascade heterostructure, which is computed in 8-band $k \cdot p$ approximation.

Results: The simulator has been validated for a structure without a saturable absorber against analytical model developed for a flat-band approximation. The code has been optimized for speed and parallelized for the DOD HPC cluster usage. The tests of the model show that it can describe a soliton formation in an ICL structure with a saturable absorber (SA) that corresponds to the broad spectrum in the frequency domain (see Fig. 1). The model has been checked for numerical convergence for both real space and momentum space grids. The convergence has been demonstrated (Fig. 3). The availability of the HPC resources enabled us to find the optimal grids for a given structure, which is important because the simulation time scales up quadratically with the real space grid size and linearly with the momentum space grid size (see Fig. 4). Several parameter studies have been performed to find how the output signal depends on the cavity and SA parameters. An example is shown in Fig. 2. A critical value of the SA length of ~100 μm is found, below which an ICL does not produce a stable short pulse. An increase in the SA length leads to regular pulses, but the output power is lower.

DoD Impact/Significance: The results show the importance of design parameter optimization for ICL combs. The developed tool is being used to guide the experimental fabrication of an ICL frequency comb generator that will be used for fast optical sensing.

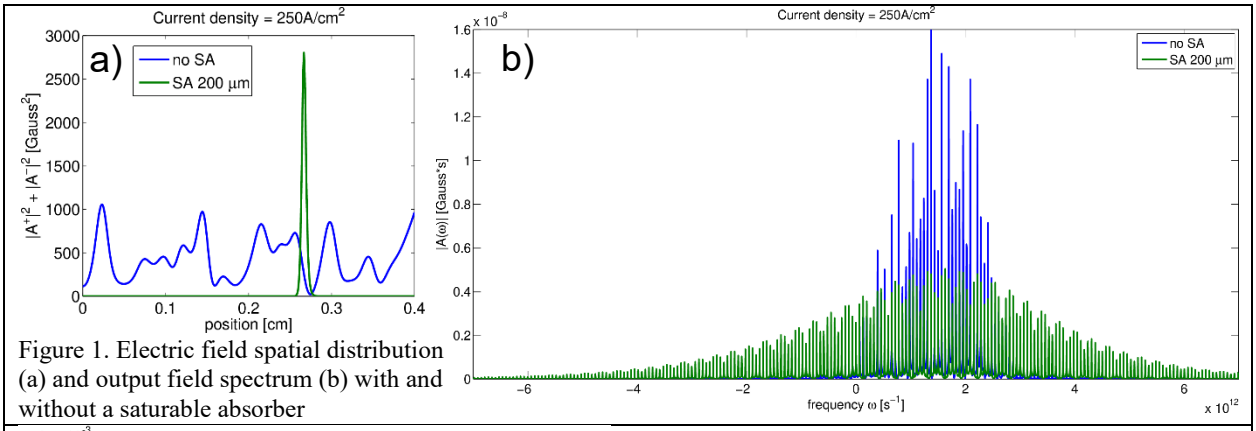


Figure 1. Electric field spatial distribution (a) and output field spectrum (b) with and without a saturable absorber

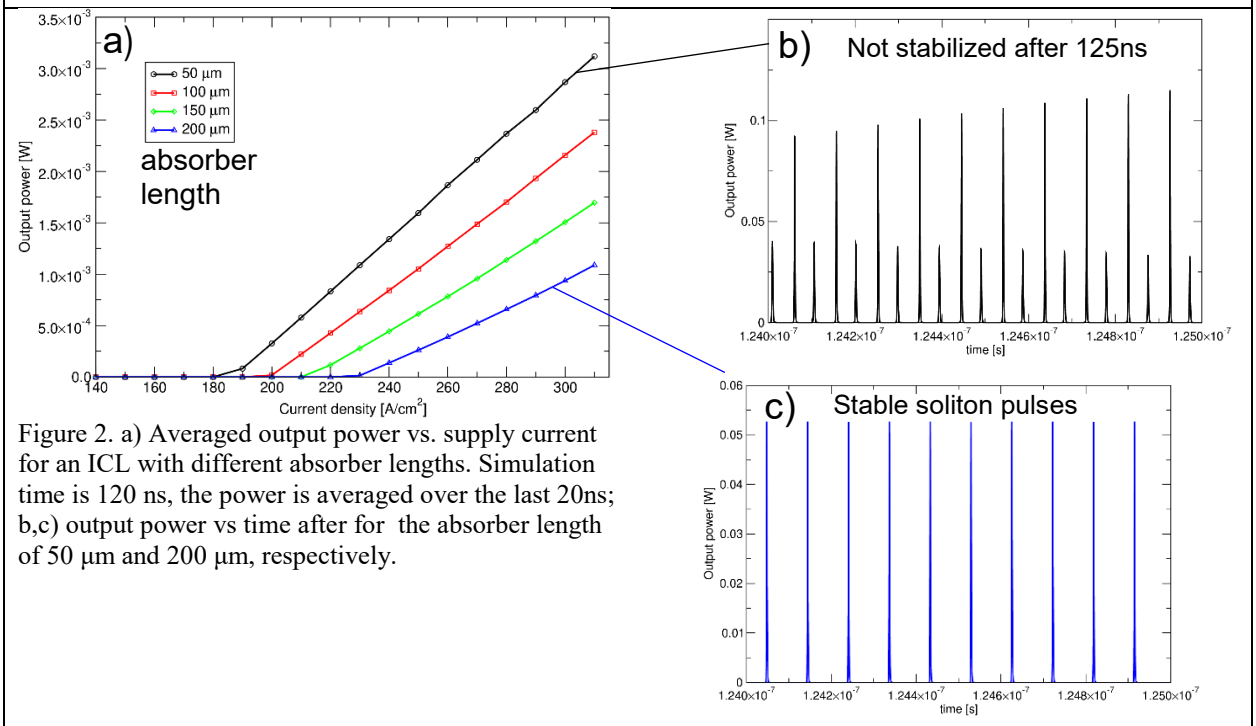


Figure 2. a) Averaged output power vs. supply current for an ICL with different absorber lengths. Simulation time is 120 ns, the power is averaged over the last 20ns; b,c) output power vs time after for the absorber length of 50 μm and 200 μm, respectively.

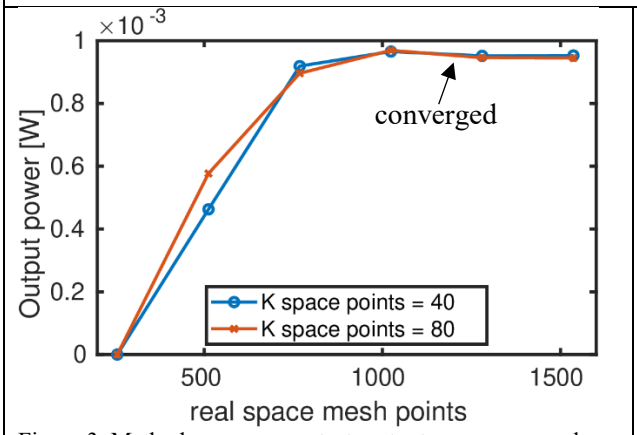


Figure 3. Method convergence test: output power vs. number of points in the real space mesh for different values of nodes in the momentum space points

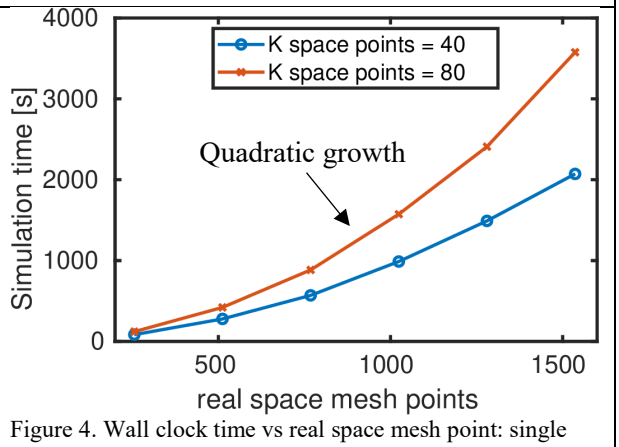


Figure 4. Wall clock time vs real space mesh point: single supply current value, 125 ns simulation, 48 CPU on single node of Mustang

Title: Molecular Dynamics Simulations and Electric Micro-field Distribution in Two-component Plasmas
Author(s): G.M. Petrov
Affiliation(s): U.S. Naval Research Laboratory, Washington, DC
CTA: CEA

Computer Resources: HPE SGI 8600 [NAVY, MS]

Research Objectives: Three-dimensional molecular dynamics simulations of electric microfield distribution relevant to plasma spectroscopy of dense plasma.

Methodology: Quasistatic electric microfield distributions can be obtained from molecular dynamics (MD) simulations by directly measuring the electric field at specific locations in the plasma, e.g., a test ion. A method specifically designed for MD simulations in a two-component plasma (electrons and ions are treated on an equal footing) makes use of a decomposition of local fields into a sum of fast and slow components in which the slow component is defined as a local average of the total field produced by electrons and ions: $\left\langle \vec{E}(t) \right\rangle = \frac{1}{\Delta t} \int_{-\Delta t/2}^{+\Delta t/2} \left(\vec{E}_e(t+t') + \vec{E}_i(t+t') \right) dt'$ [1]. The instantaneous local field at the location of a test particle α, $\vec{E}(t+t') = \vec{E}_e(t+t') + \vec{E}_i(t+t')$, is calculated by summing over the fields of all other particles β: $\vec{E}(\vec{r}_\alpha) = \sum_{\beta \neq \alpha} \vec{E}(\vec{r}_\beta)$. This field is then averaged over a period of time Δ*t*, yielding the slow field component, which is then used to build the probability distribution function *P*(*E*) by constructing a histogram of $\left|\vec{E}(\vec{r}_\alpha)\right|$. Finally, it is multiplied by a factor $4\pi E^2$ and normalized to unity. We use a three-dimensional molecular dynamics code that was developed in house at the Plasma Physics Division at NRL and has been parallelized using message passing interface (MPI).

Results: Sample simulation results are presented for Ar plasma at ion density 10^{27} m^{-3} and temperature 1 keV. The number of computational particles is ~10^4, the simulation cube size is 2.7 nm and the time step is ~0.5 as. The Holtsmark field is $E_H = 7.37\times10^{10}$ [V/m]. For low fields, the distribution is well reproduced, but for large fields (close encounters), a deviation from the Holtsmark distribution is observed, most likely due to the large coupling factor $\Gamma_{ii} \sim 0.7$, or because the MD uses screened Coulomb potentials, while Holtsmark assumes bare Coulomb potentials. The microfield distribution is relevant to atomic physics simulations. As an illustration, it is applied to the Stark splitting of the Ly$_\alpha$ line of Al^{12+} (1728.1 eV) in a fully ionized Al plasma at solid density and temperature 1 keV. The typical Stark splitting of the Ly$_\alpha$ line is $\Delta\omega = 3a_Z e_0 \left\langle E \right\rangle / \hbar$, where $a_Z = a_{Bohr} / Z$ is the reduced Bohr radius, $Z = 13$, and $\langle E \rangle = \int_0^\infty EP(E)dE$ is the averaged value of the microfield. [2] In the linear Stark effect, two of the four $n = 2$ levels remain unaffected, while the electric field shifts the other two levels by ±Δω. One therefore expects a strong central peak and wings, which reflect the distribution *P*(*E*) (Fig. 2). The position of the wings, shifted by ±ħΔω w.r.t. central peak, is proportional to the averaged microfield: $\hbar\Delta\omega = 3a_{Bohr} e_0 \left\langle E \right\rangle / Z$.

DoD Impact/Significance: This modeling and results are of significant interest to the Navy and the DoD, as it is related to problems such as generation of X-rays in dense plasmas and plasma diagnostics, which can be used for fundamental research. The research is of great interest to the scientific community dealing with high-energy density plasmas and laser-material interactions. The simulations have been used to support experiments related to Z-pinch and laser-material interactions. The payoff is that long, arduous, and expensive experiments have been modeled and guided using "virtual experiments" on computers, saving time and resources.

---

[1] A. Calisti, S. Ferri, C. Mossé, B. Talin, M. A. Gigosos, M. Á. González, "*Microfields in hot dense hydrogen plasmas*", High Energy Density Physics **7**, 197-202 (2011)
[2] J. Marten and C. Toepffer, "*Microfield fluctuations and radiative transitions in laser-generated strongly coupled plasmas*", Eur. Phys. J. D 29, 397-408 (2004)

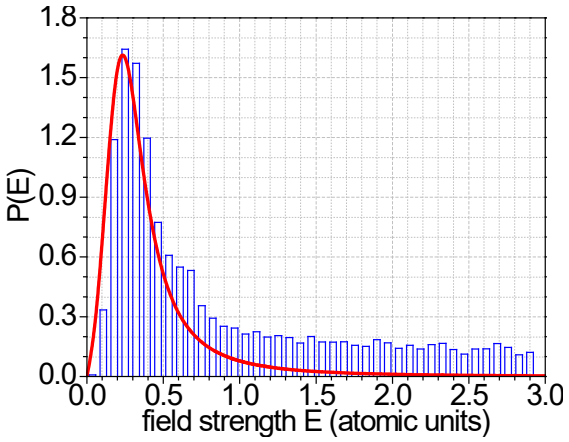


Figure 1. Calculated (bars) and Holtsmark distribution (solid line) in Ar at ion density 10^{27} m^{-3} and temperature 1 keV.

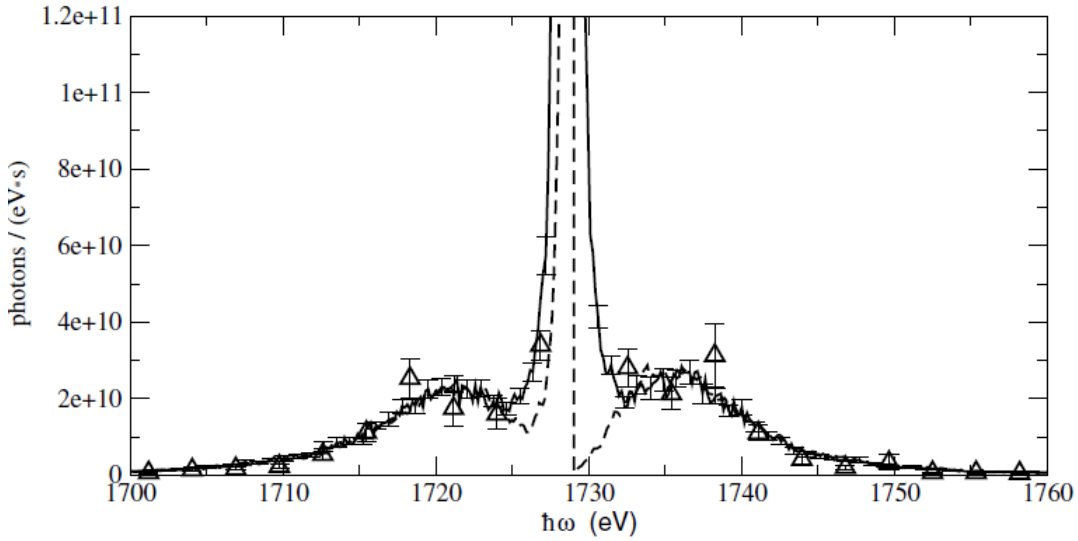


Figure 2. The Lyα–line in an Al^{13+} plasma at ion density 10^{27} m^{-3} and temperature 1 keV. [2]

Title: Low Grazing Angle Radar Backscatter
Authors: J.V. Toporkov, M.A. Sletten, and J.D. Ouellette
Affiliation: U.S. Naval Research Laboratory, Washington, DC
CTA: CEA

Computer Resources: HPE Cray Shasta [AFRL, OH]; Cray XC40/50 [ERDC, MS]; Cray Shasta [NAVY, MS]

Research Objectives: Reflections from the ocean surface are observed in many radar systems operating in the ocean environment. They are often regarded as clutter that masks a target return, but they also can carry information about local ocean conditions. Understanding the properties of sea scattering, their dependence on environmental parameters, and how they differ from those of man-made target echoes is key to improving or even enabling performance of such radar systems and applications. This project studies detailed characteristics of radar returns from the ocean surface under both monostatic and bistatic observation geometries. The task is accomplished through simulations that involve both direct numerical solution of the scattering problem and, where suitable, numerical implementations of approximate scattering models.

Methodology: The approach combines a physics-based model for an evolving ocean surface with computationally efficient evaluation of the scattered electromagnetic field. The most rigorous implementation is limited to the two-dimensional (2D) space but has direct relevance to commonly occurring three-dimensional (3D) geometries (e.g., oncoming or receding long-crested waves). A wind-driven surface is represented by realizations of a Gaussian random process defined by a certain wave spectrum. Hydrodynamic nonlinearities and associated wave-wave interactions are modeled by subsequent application of the Creamer transformation. This affects shape and motion of smaller ripples that have great impact on scattering of decimeter- and centimeter-scale electromagnetic waves. The field scattered by a "time-frozen" scene at a particular frequency is found by iteratively solving a boundary integral equation (BIE) for the induced surface current. This first-principles formulation automatically accounts for many phenomena (multiple scattering, shadowing) that could be problematic for analytical treatment. The calculations can be run at many frequencies covering a certain band to simulate pulse scattering. The procedure is repeated for every surface profile in the sequence representing temporal evolution. The 3D code implementation thus far relies on the small slope approximation (SSA) scattering model in lieu of the exact BIE-based solver.

Results: Part of the research effort supported assessing feasibility of sensing the long-wave part of the surface wave spectrum by utilizing illumination from an HF skywave radar in conjunction with a satellite-based receiver. Here, we used the newly implemented 3D technique to model bistatic scattering at HF frequencies. The simulations confirmed that a "single-realization" measurement is very fluctuating, and averaging over a number of resolution cells would be needed. It also was revealed that the small perturbation theory used for retrievals may not be adequate for higher HF frequencies, which would lead to an underestimated spectral magnitude. In another study, we investigated the accuracy of the coherent two-scale model (CTSM) for scattered field depending on the choice of the inherent but vaguely defined scale separation parameter. For that, we used comparisons with the exact numerical solution in the 2D space. Figure 1 illustrates discrepancies that the approximate model exhibits depending on the separation length when evaluating radar cross section and Doppler moments. The calculations were done at X band for both vertical (VV) and horizontal (HH) polarizations. We then computed detailed error maps shown in Fig. 2. The error "landscape" allows both constant and incidence angle-dependent choices for the optimal scale separation length. With the knowledge of the latter, the coherent two-scale model could potentially serve as an efficient core solver in the 3D scattering code.

DoD Impact/Significance: More comprehensive and detailed characterization of sea clutter will help in design and performance assessment of the Navy radar systems. This knowledge also supports obtaining more comprehensive and accurate information about environmental conditions in operating areas.

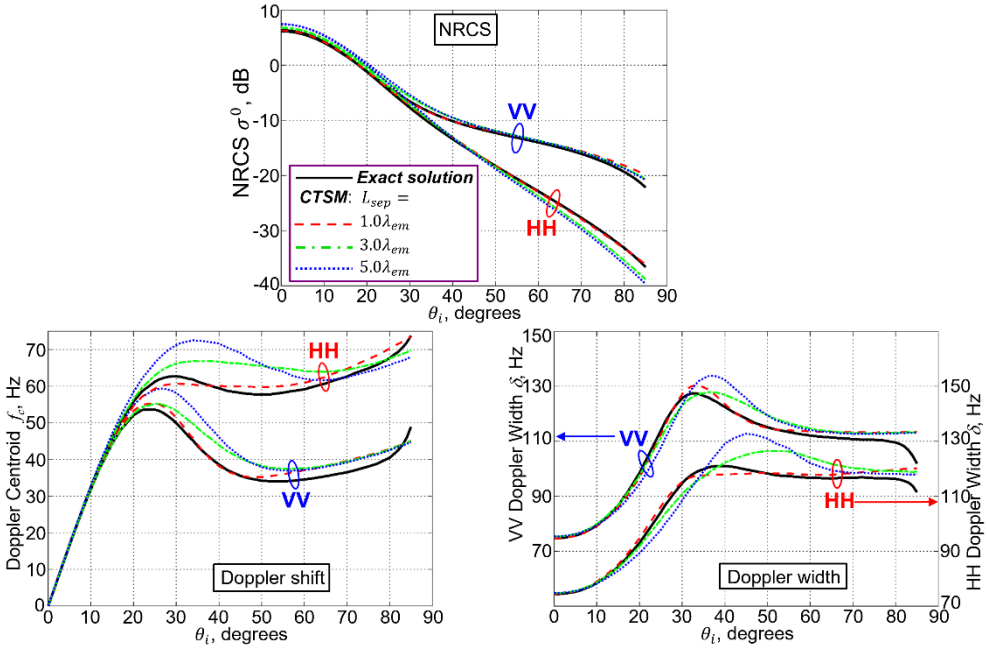


Figure 1. Normalized radar cross section (NRCS), Doppler shift, and Doppler width of the sea backscatter obtained using the exact numerical technique and the coherent two-scale model (CTSM). Various choices of the scale separation length are considered for the latter. The wind speed is 9 m/s and the electromagnetic wavelength is 3 cm (X band). The CTSM discrepancies with the exact solution are sensitive to the scale separation and become prominent at changing incidence angles.

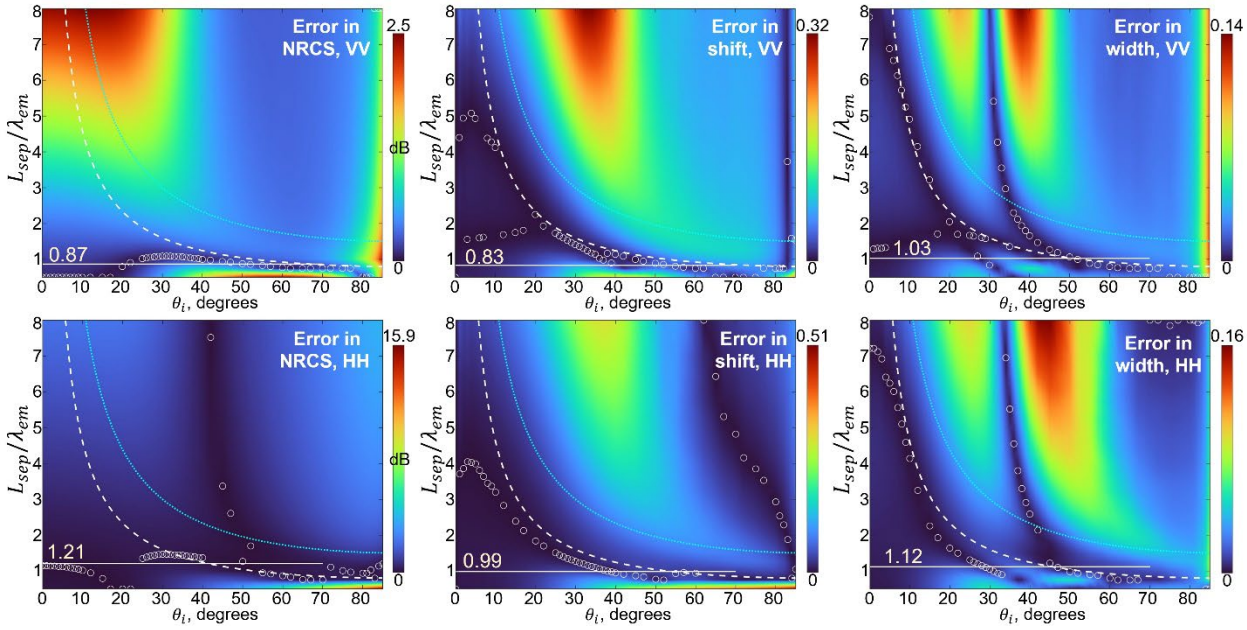


Figure 2, CTSM error maps as functions of incidence angle and separation length. Circles indicate actual minima locations for the θ_i values used in the simulations. The dotted curves correspond to the angle-dependent $L_{sep} \cong 1.5\lambda_{em}/\sin\theta_i$ mentioned in literature. The error landscapes suggest changing it to $L_{sep} \cong 0.8\lambda_{em}/\sin\theta_i$ (dashed curve). Horizontal lines represent the paths chosen by the minimax solution for optimal angle-independent separation lengths (whose values are shown next to the lines).

Title: Underwater Electrical Impedance Tomography
Author(s): G.R. Gatling and E.M. Tejero
Affiliation(s): U.S. Naval Research Laboratory, Washington, DC
CTA: CEA

Computer Resources: Cray Shasta [NAVY, MS]

Research Objectives: Use HPC computational resources to generate Jacobians and sensitivity matrices for electrical impedance tomography to facilitate imaging internal impedance structures from boundary measurements of voltage and current. Investigate image reconstruction methods for resolution and stability. Discover novel algorithms to improve inclusion detection, to improve signal-to-noise ratio, and to decrease computation costs.

Methodology: The forward solver is implemented using python and several open-source tools, including Gmsh for generating arbitrary meshes, scikit-fem, which is a finite-element assembler, NumPy, which is a library of fast numeric algorithms for python based on LAPACK, and SciPy, which includes a library of sparse matrix routines used to solve the system of equations generated by the FEM. These tools have been built up into an NRL-developed electrical resistance tomography code and have been used to explore the performance of arrays of electrodes placed onto the edges of polygons.

Results: The tools have been used to characterize arrays of up to 24 electrodes, determining the size of inclusions that are detectable and or resolvable. The results of simulations run on Narwhal have informed decisions in the design of an array of sensors intended to measure the spatial density structure in magnetically confined plasmas. Shown in Fig. 1 are the resolving powers for several different array designs. The “radius of resolution,” shown in the first column, is the marginal case. Inclusions of this size are almost, but not quite, unresolvable.

DoD Impact/Significance: There is a wide-ranging need for noninvasive remote sensing in a number of environments. Applications include biomedical imaging, characterizing fusion plasma, underwater imaging, undersea-floor mine detection, resource prospecting, and a variety of fluid process monitoring applications. Yet modern impedance tomography methods continue to present critical challenges in low signal-to-noise ratio, inherently limited resolution, intense computational costs, and slow reconstructions. Overcoming these challenges will keep the DoD on the frontier of imaging capability.

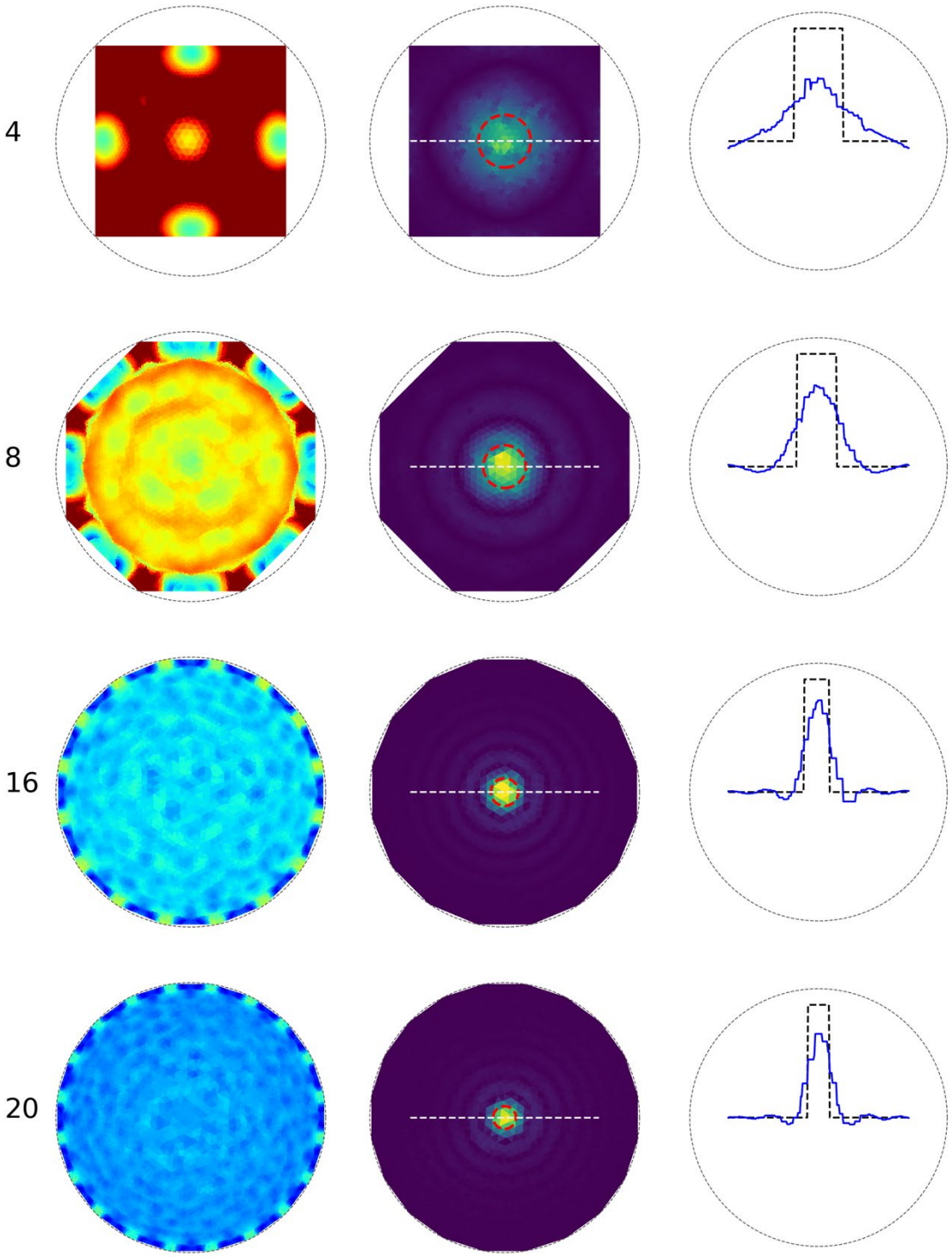


Figure 1. Increasing the number of electrodes improves the resolution of the array. The left column in this figure shows the radius of resolution maps for different arrays. The center column shows the reconstruction for a circular perturbation (marked with a dashed circle). The right column shows the data in the reconstruction under the white, dashed line.

THIS PAGE INTENTIONALLY LEFT BLANK

CWO

Climate Weather Ocean Modeling

CWO focuses on the accurate numerical simulation of the Earth's atmosphere and oceans on those space and time scales important for both scientific understanding and DoD operational use. This CTA includes the simulation and forecast of atmospheric variability (e.g., temperature, winds, pressure, relative humidity, cloud cover, precipitation, storms, aerosols and trace chemicals, surface fluxes, etc.) and oceanic variability (e.g., temperature, salinity, currents, tides, waves, ice motion and concentration, sediment transport, optical clarity, etc.). Numerical simulations and real-time forecasts are performed from the very top of the atmosphere to the very bottom of the ocean. CWO also includes the development of numerical algorithms and techniques for the assimilation of in situ and remotely sensed observations into numerical prediction systems. CWO has DoD applications on a daily basis for specific warfare areas, mission planning, and execution (air, ground, sea, and space), as well as for flight and sea safety, search and rescue, optimal aircraft and ship routing, and weapon system design. This CTA provides DoD with: (1) real-time, high-resolution weather and oceanographic forecasts leading to incisive decision making and enhanced operational capability in adverse weather and ocean conditions, and (2) realistic simulations of the dynamic oceanic and atmospheric environment to permit effective mission planning, rehearsal and training, and materiel acquisition.

Title: Coupled Ocean-Wave-Air-Ice Prediction System
Author(s): R. Allard, [1] T. Campbell, [1] E. Douglass, [1] K. Edwards, [1] D. Hebert, [1] T. Jensen, [1] A. Rydbeck, [1] T. Smith, [1] J. Veeramony [1] and M. Phelps[2]
Affiliation(s): [1]U.S. Naval Research Laboratory, Stennis Space Center, MS; [2]Peraton, Inc., Stennis Space Center, MS
CTA: CWO

Computer Resources: HPE SGI 8600, Cray Shasta [NAVY, MS]

Research Objectives: Perform research studies with the Coupled Ocean Atmosphere Mesoscale Prediction System (COAMPS®) meteorological forecast model, which is six-way coupled with the Navy Coastal Ocean Model (NCOM), the WAVEWATCH III® (WW3) and SWAN wave models, and the COAMPS atmospheric model. Perform modeling studies with the Community Ice Code (CICE v6), which includes a landfast ice parameterization. Perform storm surge and inundation modeling studies with the Delft3D Flexible Mesh modeling system.

Methodology: For accurate simulation and prediction on regional scales in the tropics, we have used various configurations of NRL's state-of-the-art fully coupled atmosphere-ocean-wave model system COAMPS with very high spatial and temporal resolution. One component under development for the COAMPS model is the generation of spatially varying coefficients for grounding and tensile strength for landfast ice in Arctic regions. These spatially varying parameters will be used in regional COAMPS-CICE and Navy Earth System Prediction Capability (ESPC) V2 ensemble and deterministic forecast systems.

Results: We used a series of cylc scripts to optimize the grounding coefficients (k_1) for landfast ice using a conjugate gradient technique. Studies were performed for regions in the Beaufort, Chukchi, East Siberian, and Laptev seas using a standalone CICE6 configuration on a 2 km Navy ESPC deterministic grid. Boundary conditions from the GOFS3.1 reanalysis were used with atmospheric forcing from NAVGEM for the periods of 2015–2016 and 2017–2018. All hindcast runs began on October 1 (when landfast ice first begins to form) and extended into July of the following year. Typically, 15 to 20 iterations were needed to optimize the k_1 values for a given region and time period. Results were compared against ice chart data from the National Ice Center. Figure 1 depicts preliminary results for three domains in which optimization was performed. The white and cyan lines show the modeled (white) versus observed (cyan) poleward landfast ice extent on April 19, 2018. Also evident is the formation of polynyas, or flaw leads where winds flowing poleward cause the pack ice to be displaced, resulting in openings in the ice (white ovals in Fig. 1) which is important for air-sea heat exchange. This does not occur in the proper location when landfast ice is not included. We also performed numerous studies using Delft3D FM that resulted in the submission of two validation test reports (VTR). The first VTR detailed the performance of the Delft3D FM model for surge predictions during hurricanes Katrina, Ike, and Michael. The report illustrated the improved performance of the Delft3D FM model. The second VTR detailed the performance of the probabilistic surge predictions using ensemble winds generated accounting for the significant errors in the forecast track (cross-track error, along-track error and wind intensity). The surge and inundation modeling system is scheduled for operational transition in FY23.

DoD Impact/Significance: The development of a coupled air-ocean-wave prediction system can have a pronounced effect on Navy forecasting by improving ASW performance, tropical cyclone prediction, and search-and-rescue and mission planning. The relocatable COAMPS-CICE system will provide high-resolution Arctic forecasting of ice thickness, ice drift, and concentration to support navigation. Inclusion of landfast ice in the Navy's global ice prediction systems will yield a more realistic representation of pan-Arctic sea ice.

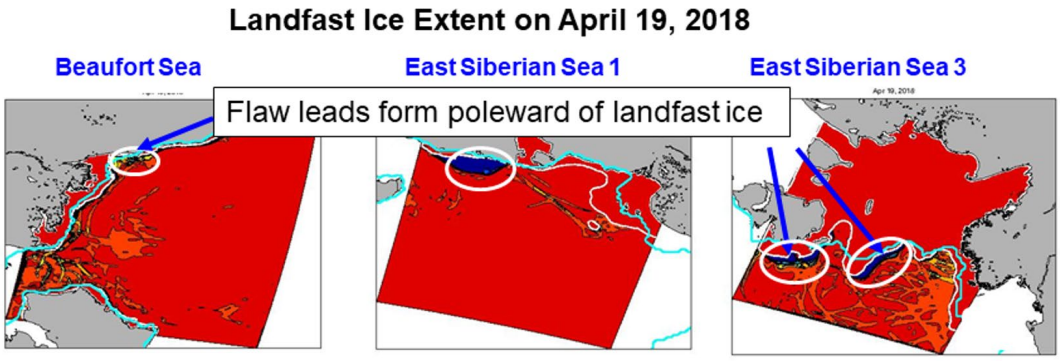


Figure 1. Studies performed with multiple regional CICE6 (2 km) domains. Figures above depict modeled landfast ice extent (white) versus NIC observed landfast ice extent (cyan). Good agreement with observations. Shaded regions denote ice concentration near 100%. Landfast ice identified if ice speed is <= 0.05 cm/sec over a 14-day period.

Title: Multi-scale Characterization and Prediction of the Global Atmosphere from Ground to the Edge of Space using Next-Generation Navy Modeling Systems
Author(s): C.A. Barton, S.D. Eckermann, J.F. Kelly, M.A. Herrera, K.W. Hoppel, D.D. Kuhl, D.R. Allen, J. Ma and T. Rhodes
Affiliation(s): U.S. Naval Research Laboratory, Washington, DC
CTA: CWO

Computer Resources: Cray XC40/50 [ERDC, MS], HPE SGI 8600, Cray Shasta [NAVY, MS]

Research Objectives: To develop and test new seamless atmospheric specification and prediction capabilities from 0 to 500 km altitude for future Navy Earth System Prediction Capability (ESPC) and Space Environment Prediction with High Resolution (SEPHIR) systems, linking prediction of the ocean, atmosphere, and space over time scales from hours to decades.

Methodology: This project develops and tests key components of state-of-the-art systems required for improved modeling, prediction, and analysis of the extended operational environment for Navy applications, focusing on the atmosphere, the near space, and the geospace. Several model prototypes and operational systems are under development, including: (a) two high-altitude versions of the Navy Global Environmental Model (NAVGEM-HA), based on upward extensions of the Navy's operational global numerical weather prediction (NWP) system into 1) the middle atmosphere for seasonal prediction and 2) the upper atmosphere for thermospheric data assimilation, (b) the next-generation Navy NWP model NEPTUNE (Navy Environmental Prediction system Utilizing a Nonhydrostatic Engine), and (c) the SEPHIR ground-to-space prediction prototype comprising an upward extension of NEPTUNE into the thermosphere initialized with atmospheric states provided by the NAVGEM-HA coupled thermospheric forecast/data assimilation system.

Results: Major results directly facilitated by HPC resources during FY22 include: (a) testing and transition of NAVGEM-HA code to operations at Fleet Numerical Meteorology and Oceanography Center through the Navy ESPC program, (b) maintenance of long-term NAVGEM-HA meteorological analysis products covering 11 contiguous years with high vertical resolution and middle atmosphere physics tuning extending into the mesosphere (Fig. 1), (c) improved short-term forecast performance through a novel in-line algorithm for determining gravity wave drag parameterization settings minimizing analysis increments in the coupled NAVGEM-HA data-assimilation/forecast system, (d) development and implementation of a new ensemble-based high-altitude data assimilation capability incorporating new wind measurements of the mesosphere and the lower thermosphere from meteor radar and satellite observations into the NAVGEM-HA system to use as initial conditions for high-altitude NEPTUNE R&D (Fig. 2), and (e) continued development of a new NEPTUNE modeling capability extending from the surface to 400 km altitude using advanced numerical algorithms that enable the non-hydrostatic dynamical core to operate at high altitudes (e.g., upper boundary conditions, diffusive fixers for stability, physics porting from NAVGEM-HA).

DoD Impact/Significance: This research addresses Navy requirements to develop and test new high-altitude atmospheric specification and prediction capabilities leading to a planned Navy Earth System Prediction Capability (ESPC). This project performs the R&D needed to install high-altitude (both middle- and upper-atmosphere) specification and forecast capability in next-generation Navy NWP systems, ultimately providing improved near-space specification and prediction capabilities to the warfighter over both tactical and strategic time frames. HPC resources for this project provide critical support for the development of novel ground-to-thermosphere prediction capabilities fully coupled to ionospheric models and data assimilation to address key space-environment prediction goals of the Defense Advanced Research Projects Agency's Space Environment Exploitation (DARPA SEE) program.

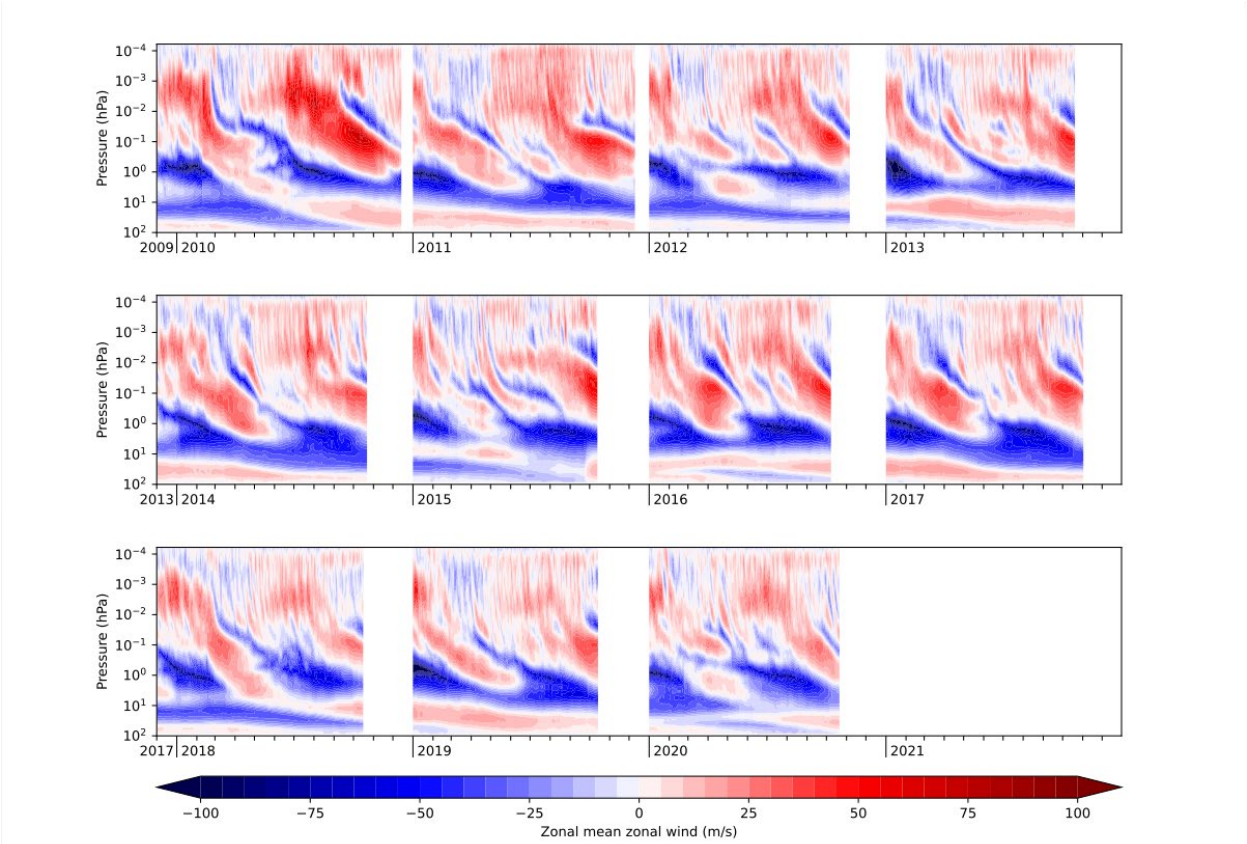


Figure 1. Time series of equatorial zonal-mean zonal wind from the 11-year-long streams comprising the reanalysis generated by the high-altitude version of NAVGEM tuned for middle atmosphere research.

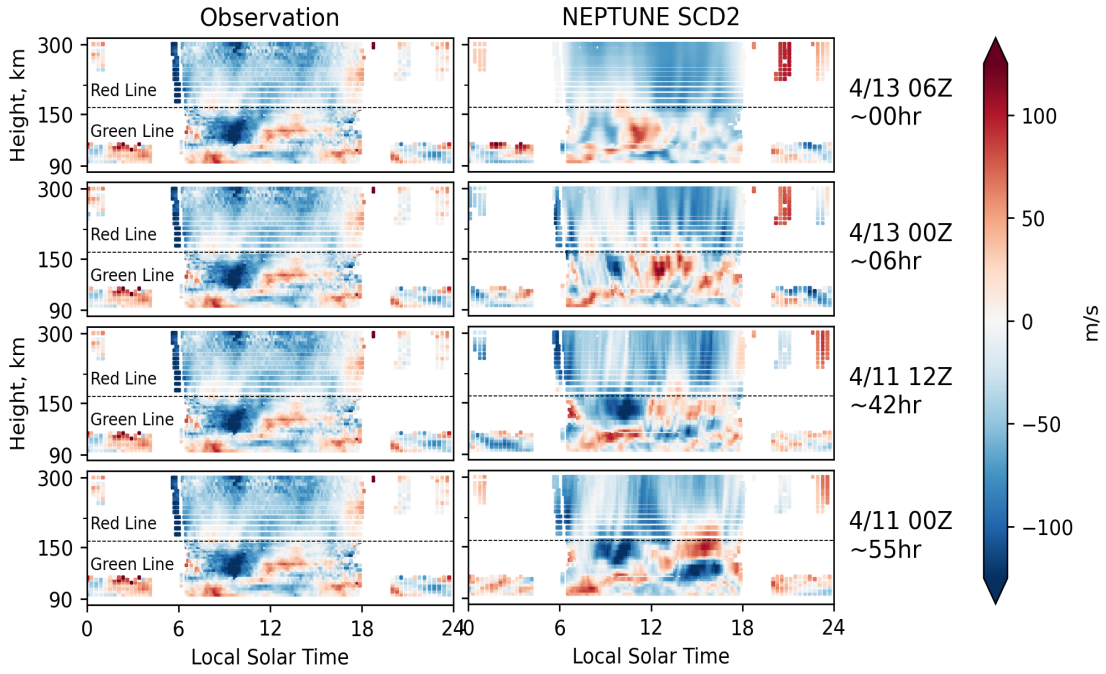


Figure 2. Validation of NEPTUNE zonal winds from a ground-to-thermosphere forecast configuration against ICON MIGHTI observations.

Title: COAMPS-TC® Tropical Cyclone Rapid Intensification Prediction
Author(s): J.D. Doyle
Affiliation(s): U.S. Naval Research Laboratory, Monterey, CA
CTA: CWO

Computer Resources: Cray XC40/50 [ERDC, MS]; Cray Shasta, HPE SGI 8600 [NAVY, MS]

Research Objectives: Tropical cyclone (TC) track forecasts have improved in a steady manner during the past several decades, but intensity forecasting has shown much slower increase in skill during the same time period. This is due, in part, to our limited ability to properly model physical process controlling TC structure and intensity, but also is related to the inherent sensitivity that TC forecasts exhibit to initial conditions. The objective of this project is to advance and test the COAMPS-TC® model, which is a state-of-the-science numerical weather prediction system designed for the prediction of TCs in support of Navy and DoD operations and for civilian applications. The COAMPS-TC® system is operational at Fleet Numerical Meteorology and Oceanography Center (FNMOC) and has undergone substantial upgrades recently for both the deterministic and ensemble systems. Our goal is to improve the COAMPS-TC® system's TC predictions through improved vortex initialization and physical processes.

Methodology: There are several types of COAMPS-TC® model deterministic and ensemble forecast experiments performed. The first type of application is used to facilitate rapid development and testing of the COAMPS-TC® system. The prototype testing for the COAMPS-TC® system needs to be rigorous and involves running hundreds of individual cases in order to assess the performance of the system in a statistically meaningful manner. Each incremental change in the development process, such as an increase in resolution or improved parameterizations, needs to be tested through this procedure. This rapid prototyping is required to develop and evaluate the new version of COAMPS-TC® software that will be run operationally at FNMOC. A second type of COAMPS-TC® application involves the near-real-time execution on the DSRC of an experimental version of COAMPS-TC® system that contains more advanced capabilities than the operational version. The testing of the experimental COAMPS-TC® system is performed for many TCs worldwide.

Results: In the past year, many configurations of the COAMPS-TC® model were rigorously tested over a suite of storms in the Atlantic Ocean and Pacific Ocean basins based on three previous TC seasons. A new version of the ensemble system with significant improvements was transitioned to operations at FNMOC in November 2021. Additional improvements have been made to the COAMPS-TC® deterministic system run in real time by NRL in support of the National Hurricane Center. Figure 1 shows a series of five-day forecast of the track and intensity for Hurricane Ian in late September and October 2022. Hurricane Ian was a destructive Category 4 hurricane that severely impacted Florida and South Carolina. As illustrated in Fig. 1, COAMPS-TC® model accurately captured Ian's track and landfall location even at longer lead times. COAMPS-TC® model also correctly and consistently forecasted the observed rapid intensification of Ian, which is a challenge for models to capture. The COAMPS-TC® model continues to be one of the top-performing TC prediction models worldwide for track, intensity, and storm structure (storm size). This new advanced version of COAMPS-TC® software developed on the DSRCs Cray XC40/50, the HPE SGI 8600, and the HPE Cray EX indicates even greater accuracy for improved research and operational TC applications.

DoD Impact/Significance: TCs remain one of the most disruptive and devastating environmental threats that impact U.S. Navy operations. We anticipate that an increase in accuracy of TC forecasts will result in significant cost benefit to the Navy through better sortie decisions and avoidance of hazardous winds and seas. Real-time testing and development of the system at HPC DSRCs have led to significant improvements in the predictive skill of COAMPS-TC® model and more rapid transitions to Navy operations at FNMOC. These improvements will inform future directions of TC model development, particularly as computational power increases allowing for higher-resolution capabilities and increased fidelity in the physical process representations, as tested in this project.

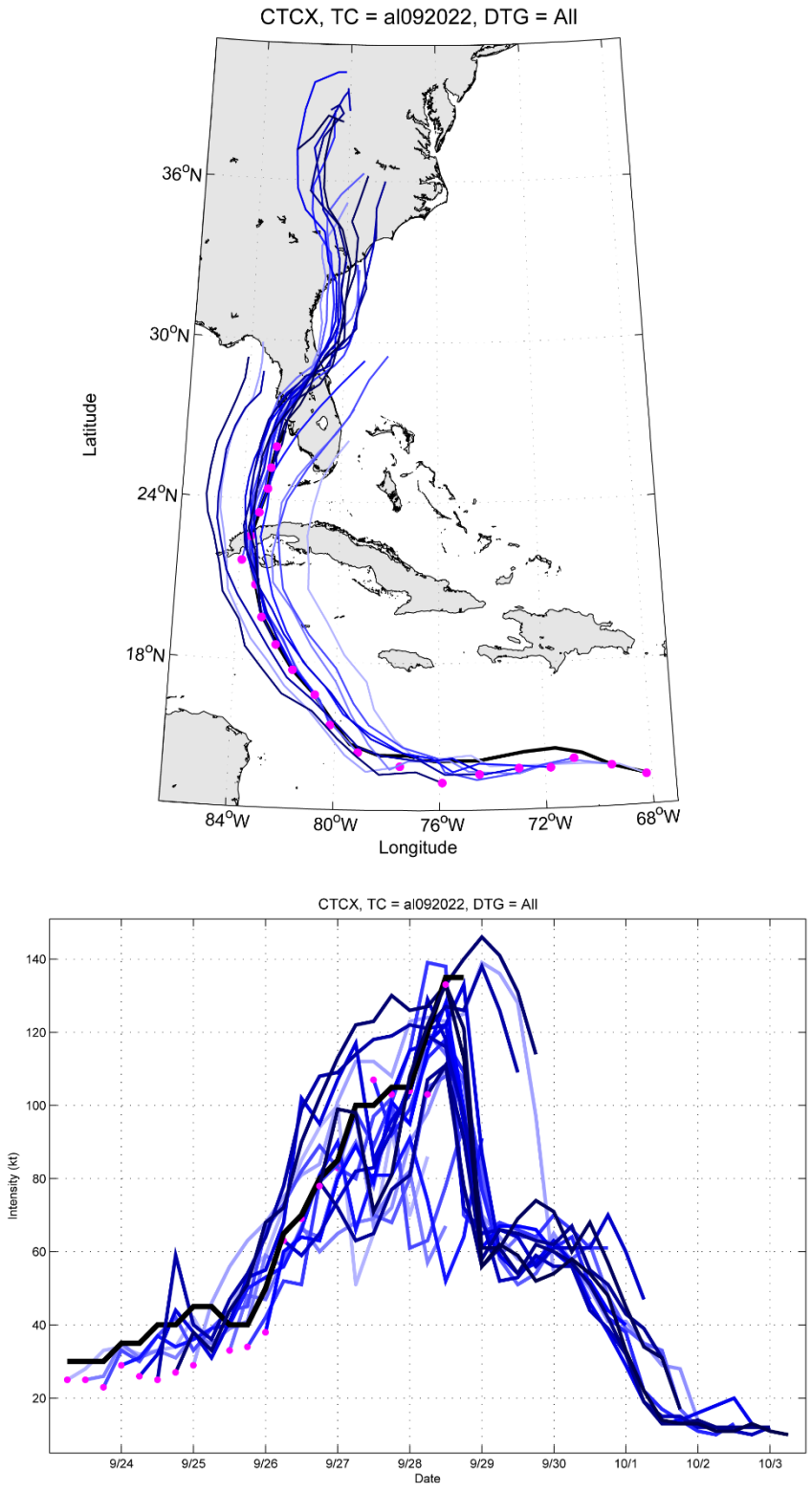


Figure 8. Five-day COAMPS-TC model forecast (blue) and observed (black) tracks for Hurricane Ian for September 23–October 3, 2022 (top). The magenta dot shows the initial position for each forecast every 6 hr. Five-day forecast (blue) and observed (black) intensity for Hurricane Ian (bottom). Progressively lighter blue color corresponds to earlier initialization times.

Title: Turbulent Mixing in NCOM and HYCOM
Author(s): Y. Fan
Affiliation(s): U.S. Naval Research Laboratory, Stennis Space Center, MS
CTA: CWO

Computer Resources: HPE SGI 8600 [NAVY, MS]

Research Objectives: The goal of this project is to provide guidance on the proper setup of ocean boundary layer (OBL) mixing schemes within NCOM and HYCOM, including optimized vertical coordinate systems and resolutions, and to demonstrate the interaction mechanisms between the boundary layer turbulence and submesoscale processes in the oceanic mixed layer.

Methodology: The project focused on two areas of research during FY22 using carefully designed idealized HYCOM, NCOM, and LES experiments. The first area of research focused on the interaction mechanisms between the boundary layer turbulence and submesoscale processes in the presence of moving submesoscale eddies and surface wind stress. The second area of research focused on the ability of hydrostatic models to simulate frontogenesis. The combined effects of the dynamical processes on different spatial scales in modulating the upper-ocean density structure were quantified.

Results: The effect of submesoscale eddies on oceanic boundary layer turbulence was investigated through controlled numerical experiments conducted using HYCOM and the NCAR LES model with a moving eddy and weak surface forcing. To represent the impact of the submesoscale eddy in the LES, we have incorporated the large-scale forcing in the model using the scale separation approach following Wang et al. (1998). LES experiments were conducted to explore the relative importance of each large-scale forcing term on the boundary layer response to the eddy. We found that the joint effect of buoyancy and momentum eddy forcing dominate the mixed layer responses. Momentum eddy forcing generates strong mean current in the water column that accelerates westward density advection generated by the temperature and salinity eddy forcing. The lighter/heavier fluid intrusion brought by the mean flow led to strong upwelling/downwelling, enhanced mixing, and deepening of the mixed layer. At the arrival of the eddy center, the density structure in the water column is dominated by the eddy and the mixed layer restratifies. So far, the only available submesoscale parameterization is Fox-Kemper et al. (2011), which is based on the overturning stream function and has an effect to slump isopycnals and to restratify the upper ocean. Thus, its main impact is a reduction of the mixed layer depth (MLD). All models using this parameterization have shown reduction in deep MLD biases and increase in shallow MLD biases. This is because the parameterization only considers the restratification effect at the eddy center and ignored the enhanced mixing and deepening of the mixed layer demonstrated in our study. Thus, a new parameterization is needed to correctly represent the submesoscale eddy effect in the boundary layer. The second part of our work focused on the ability of hydrostatic models to simulate frontogenesis. We followed the procedure in Sullivan & McWilliams (2018) to set up the front simulation in NCOM and compared our NCOM results with their LES results. We found that NCOM's ability to correctly represent the characteristics of frontal evolution depends on forcing scenarios. It was able to successfully represent the characteristics of the front evolution under cross front forcing scenarios, but totally missed the rapid intensification and frontal arrest under along-front forcing scenarios. The along-front winds can help to maintain the symmetry in the secondary circulation, and thus are more effective in creating a coherent downwelling jet, thus leading to a narrower front width and enhanced frontogenesis. The lack of nonhydrostatic physics and the coarse resolution (100 m) used for the NCOM simulations could be the reasons for it to fail to come to a frontal arrest stage.

DoD Impact/Significance: This study will improve the battlespace environment forecasting accuracy for ocean models with more accurate vertical thermal profiles and better prediction of acoustic and optic properties in the upper ocean. Strong scientific foundation and guidelines will be achieved for intelligent ocean forecasts for regional and global tactical planning.

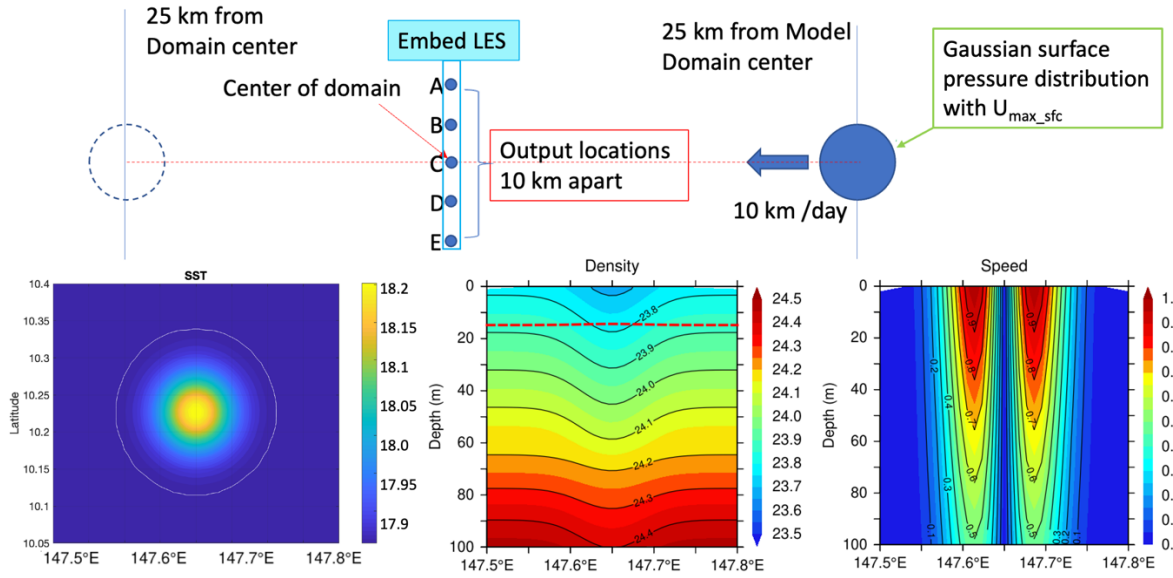


Figure 1. Experiment design for research area 1, the interaction of submesoscale eddy and boundary layer turbulence. The HYCOM domain is set to 540 by 540 km in the horizontal and 450 m in the vertical. An idealized eddy created using Gaussian surface pressure distribution is imposed to the model domain with the eddy center 25 km from the center of the model domain. The bottom-colored contour plots are the initial sea surface temperature of the eddy and the cross section of initial potential density and current velocity of the eddy. We let the eddy freely evolve afterwards. Steady background current is used to advect the eddy westward at 10 km/day. Weak constant westward wind forcing is applied to the entire model domain. Five locations 10 km apart from each other along the center cross section of the model domain are selected for our analysis. The LES experiments are conducted at these five locations using the large-scale forcing calculated from the HYCOM experiment.

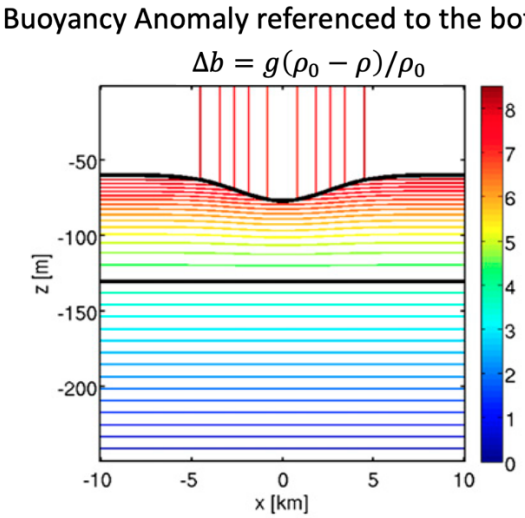


Figure 2. Experiment design for research area 2, the ability of hydrostatic models to simulate frontogenesis. The figure on the left shows the cross section of the dense front at initial state with a width of 2km. The table on the bottom compares the domain size, vertical and horizontal resolution, and turbulence specifications for the model. The vertical extent of both the LES and NCOM domain is 450m.

	NCOM	LES (Sullivan & McWilliams 2018)
Domain size	90km x 10km x 250m	12km x 4.5km x 250m
Vertical levels	101	256
Horizontal resolution	100 m	1.46 m
Turbulence	Parameterized	Solved

Title: Coupled Ocean-Wave-Air-Ice Prediction System
Author(s): T. Jensen,[1] A. Rydbeck,[1] H. Wijesekera,[1] C. Luecke,[1] D. Wang,[1] M. Flatau,[2] and T. Campbell[1]
Affiliation(s): [1]U.S. Naval Research Laboratory, Stennis Space Center, MS; [2]U.S. Naval Research Laboratory, Monterey, CA
CTA: CWO

Computer Resources: HPE SGI 8600 [NAVY, MS]

Research Objectives: Perform air-sea interaction research studies using models developed at NRL. The Coupled Ocean Atmosphere Mesoscale Prediction System (COAMPS®), which is six-way coupled with the Navy Coastal Ocean Model (NCOM), the WAVEWATCH III® (WW3) and SWAN wave models, and the COAMPS atmospheric model, is an important tool for regional studies and the Hybrid Coordinate Ocean Model (HYCOM) has been used for large-scale and global simulations.

Methodology: For accurate simulation and prediction on regional scales in the tropics, we have used various configurations of NRL's state-of-the-art fully coupled atmosphere-ocean-wave model system COAMPS with very high spatial and temporal resolution. For the Bay of Bengal (BoB) and simulation of cyclone Fani, the atmospheric model has 60 vertical levels and 9 km area cells. Coupling interval for data exchange between the three models is 6 min. The composite equatorial Rossby (ER) wave analysis in Rydbeck et al. (2021) is based on an index derived from satellite observations of sea surface height. A state-of-the-art HYCOM reanalysis run on the DSRC is also used to examine subsurface characteristic of ER waves. The reanalysis covers the years 1994 to 2015 and uses surface forcing fields from the National Centers for Environmental Prediction Climate Forecast System Reanalysis.

Results: Tropical cyclone Fani formed west of Sumatra on 25 April 2019 as a depression, moved northwestward, and intensified into an extremely severe Category 4 storm before landfall in Odisha, India, on 3 May. The oceanic structure under Fani's track was captured by NRL moorings, while the atmospheric and oceanic variability was studied using satellite observations and a coupled COAMPS® model run (Wijesekera et al., 2021a). The cold wake generated by Fani extended from 4°N to 21°N, persisted nearly two weeks, and suppressed local atmospheric convection above the wake. After the passage of Fani, the heat content in the upper 50 m increased steadily at a rate of ~200 W/m^2 for three weeks while the ocean surface was heating at a rate of 110–130 W/m^2. This large heat imbalance shows that vertical and lateral heat transport can be as large as net surface heating. COAMPS® model simulations support this view and further illustrate transports of warm, salty water from the east coast of India to the northwest-central Bay of Bengal through eddies. A large collection of precipitating clouds and strong winds in the tropical atmosphere, known as the intraseasonal oscillation (ISO), generates ER waves in the ocean (Rydbeck et al., 2021). The surface expression of ER waves are only several centimeters but are capable of transporting large amounts of heat. The ER waves (Fig. 2) take several months to cross the Indian Ocean from east to west. We observe that these ocean waves are generated by the eastward winds within the ISO and subsequently are intensified by westward winds that are in front of the next ISO. The waves increase the amount of warm water in the upper ocean so that when the next ISO arrives, the waves support the development and intensification of clouds and precipitation within the ISO. In short, a portion of the energy from the ISO is stored in the ocean in the form of ocean Rossby waves, which then warm the upper ocean and strengthen the following ISO.

DoD Impact/Significance: The development of the relocatable coupled air-ocean-wave prediction system can have a pronounced effect on Navy forecasting by improving ASW performance, tropical cyclone prediction, search and rescue, and mission planning.

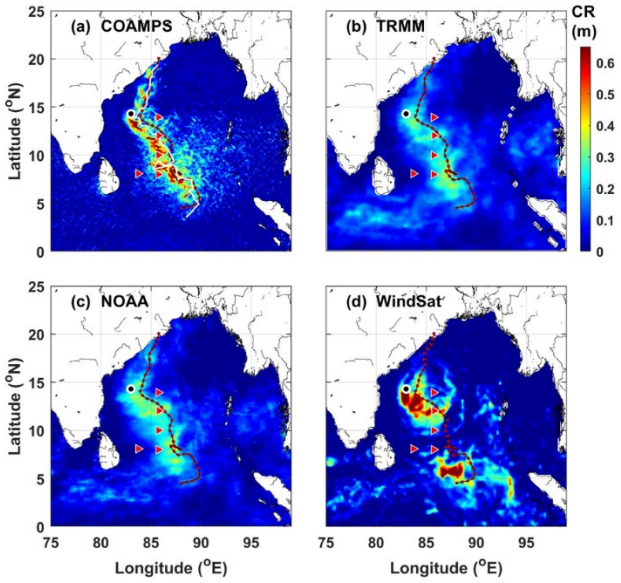


Figure 1. Cumulative rainfall (CR) estimated 27 April to 4 May. COAMPS® model (a), TRMM (b), NOAA (c), and WindSat (d). Note that each product has different spatial and temporal averages. The black line with red dots is the track of Fani, and the thin, white line in (a) is the COAMPS® model track. The magenta triangles are the locations of NRL moorings. (From Wijesekera et al., 2021a)

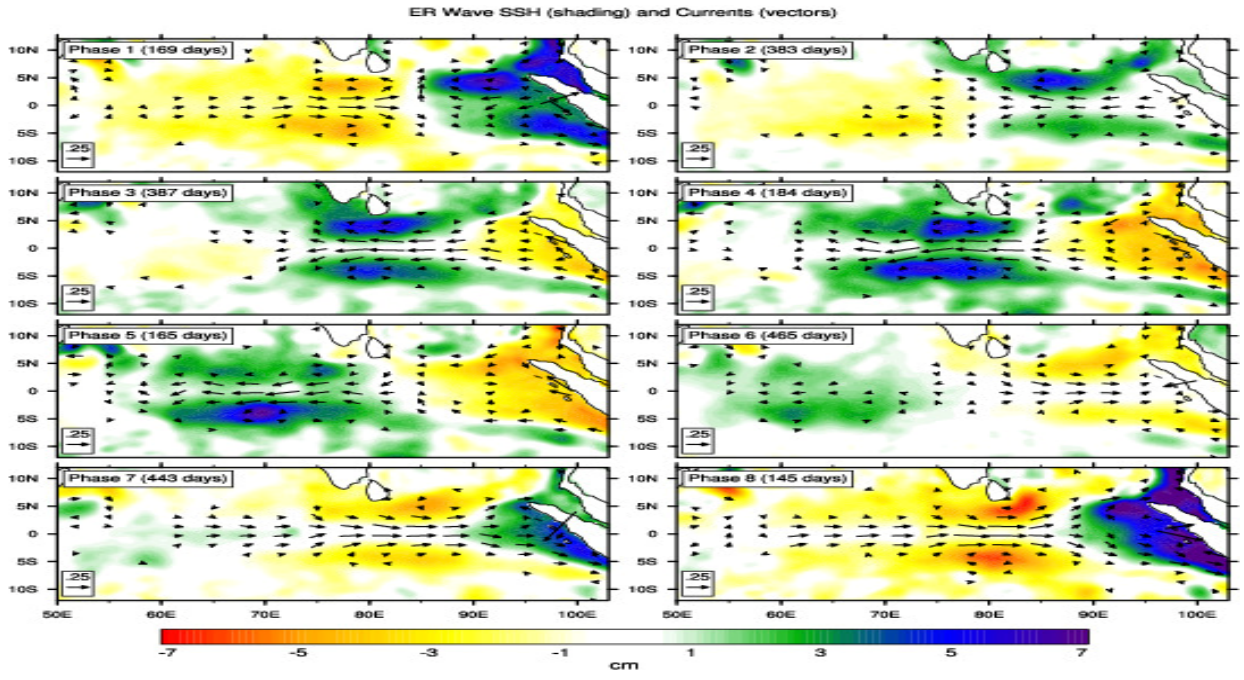


Figure 2. Magnitude composite maps of the 30- to150-day band-pass-filtered AVISO SSH (shading, cm) and ocean surface current analysis real-time surface currents (vector, m/s) anomalies based on the ER wave index for phases 1 to 8. The number of days in each phase composite is shown in the upper left, and the reference current vector is shown in the bottom left of each panel. (From Rydbeck et al., 2021).

Title: Bio-Optical Modeling and Forecasting
Author(s): J.K. Jolliff, S. Ladner, and T. Smith
Affiliation(s): U.S. Naval Research Laboratory, Stennis Space Center, MS
CTA: CWO

Computer Resources: HPE SGI 8600 [NAVY, MS]

Research Objectives: The research objective for FY22 was to resume final testing and transition of an optics code branch addition to the Navy Coupled Ocean Data Assimilation system (NCODA). This system uses satellite-based measurements of surface ocean clarity to determine solar heating rates in numerical ocean models and coupled ocean-atmosphere models in support of the 6.4 "Visible Band Satellite Data to Improve Ocean Model Radiative Transfer" (VISOR) program. Additional hours were used for execution of the Coupled Ocean Atmosphere Mesoscale Prediction System (COAMPS®) meteorological forecast model in support of the 6.1 program "Integrated Radiometric Indices of Surface Ocean Features," wherein we compare numerical model results with satellite image sequences.

Methodology: All numerical ocean models must represent solar heating in the upper ocean through some representation of surface ocean radiative transfer. Solar energy is the principal source of heat for the surface ocean and the rate of solar heating, particularly in the gyres and subtropical regions, determines changes in ocean temperature and cascades to other ocean variables impacted by density. The 6.4 VISOR program is improving ocean model representation of this process by ingesting satellite-based determinations of ocean turbidity into the models. A constellation of polar-orbiting ocean-viewing radiometers is now available to provide this information every 24 hours. These data are now directed to the NCODA system, where a variational analysis is performed to provide the ocean models with a continuous two-dimensional field of surface optical properties. The correct scaling for solar energy penetration is then applied. We are in the final testing phase of the end-to-end flow of information from satellite processing to ocean model. NAVO presently provides real-time ocean optical data products for mission support; these data are obtained from the polar-orbiting satellite radiometer constellation. Simultaneously, NAVO and Fleet Numerical Meteorology and Oceanography Center (FNMOC) rely on ocean circulation models that presume fixed optical water types that are erroneous. Directing the satellite optical data streams toward the ocean models is a prudent and justified course of action that will efficiently use existing resources to improve ocean model fidelity to observations.

Results: The final testing experiments consist of running the present operational model (control) versus the new model that uses the VISOR system to improve model radiative transfer. Experimental results show gross errors in the control run with respect to both the diurnal SST patterns and the upper ocean temperature structure when compared to the VISOR results. For example, the control model, COAMPS®, run permits too much solar energy to penetrate below the halocline in the northern Gulf of Mexico. Due to the overwhelming salinity stratification secondary to effluent from the Mississippi/Atchafalaya River systems, the penetrating radiation manifests as simulated temperature inversions: warm water accumulates on the ocean bottom (Fig. 1). Temperature inversions are not observed in this region, and it is important to note that the control run is the present operational model.

DoD Impact/Significance: The immediate impact of this project is to improve operational model performance via increased fidelity to the three-dimensional temperature field as well as other planetary boundary variables in both the atmospheric and ocean models that are impacted by thermal perturbations. As the demands for model performance at higher scales of time/space increase, improved model accuracy of the density field rendering is required.

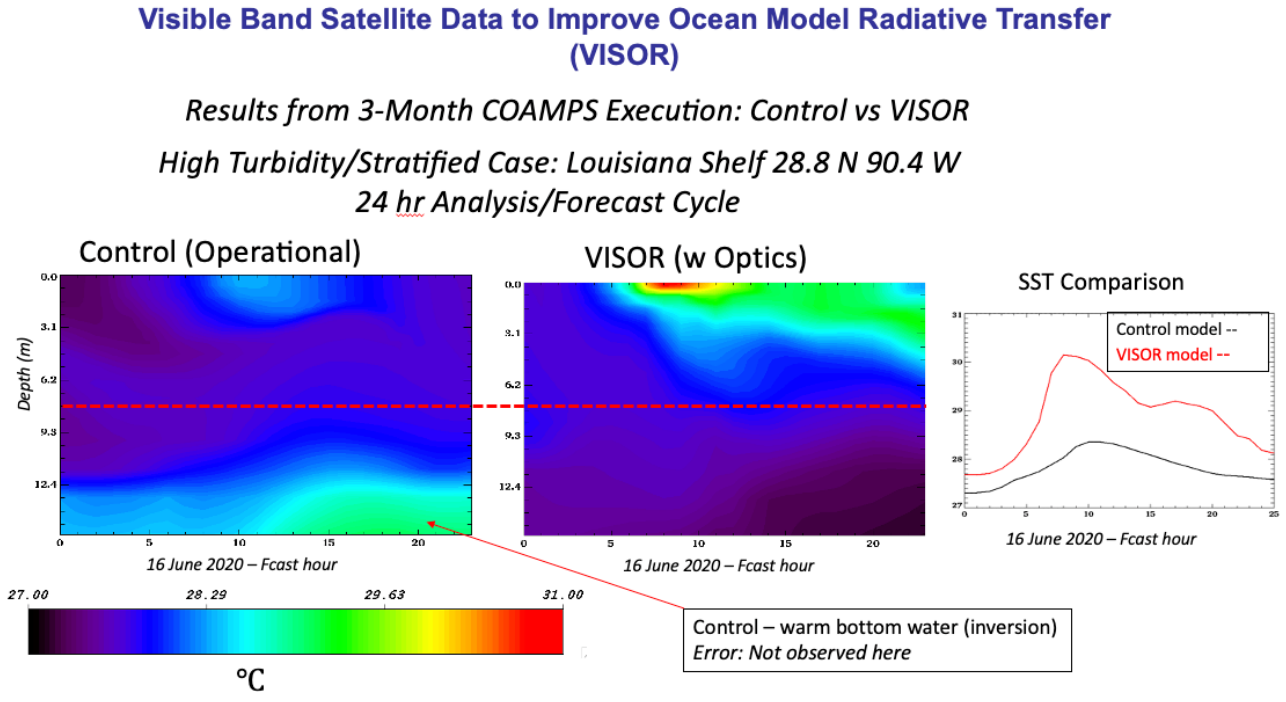


Figure 1. Comparison of water column temperature for a 24-hour forecast/analysis cycle: control (operational) is on the left and the VISOR version is on the right, SSTs are compared on the far-right panel.

Title: Investigation and Implementation of GPU Capability to Next Generation Weather Prediction Code, NEPTUNE
Author(s): Y. Khine
Affiliation(s): U.S. Naval Research Laboratory, Washington, DC
CTA: CWO

Computer Resources: HPE SGI 8600 [AFRL, OH]; Cray XC40/50 [ERDC, MS]; Cray Shasta [NAVY, MS]

Research Objectives: The goal of this project is to investigate and implement GPU capability to Navy Environmental Prediction sysTem Utilizing the NUMA corE (NEPTUNE) code in order to enhance its performance, and to utilize DoD GPU accelerator-based architectures efficiently for high-resolution three-dimensional (3D) simulations.

Methodology: In FY22, we investigated the possibility of using OpenMP to offload the NEPTUNE code to the Nvidia V100 GPUs on the Navy DSRC system (Narwhal). Due to the issues with available compilers on Narwhal, it was determined that translating the code to OpenMP would not be possible for this current project, although it remains a long-term goal for the NEPTUNE code. We also examined the CUDA stalls in the diffusion kernel and the implicit solver of the code. We found that the biggest performance limitations for NEPTUNE-ADSII code on the GPUs arise from its underlying linear algebra subroutines. NEPTUNE-ADSII code uses Compact LAPACK library or linear algebra and it was targeted for optimizations to improve the performance on GPUs. One option we investigated was to possibly replace Compact LAPACK libraries with NVIDIA libraries (cuBLAS/cuSOLVER) but unfortunately, they were not compatible with Compact LAPACK. Thus, the focus was on optimizing the Compact LAPACK by multiple rewrites.

Results: As no existing GPU libraries support the Compact LAPACK data layout, it is difficult to achieve good GPU performance with the Compact LAPACK library due to low data reuse causing frequent CUDA stalls and bottlenecking the code. The rewrites were performed for OpenACC, cuBLAS and CUDA Fortran versions. Figure 1 presents the timings of LU decomposition for the original OpenACC version compared with the optimized register OpenACC version, the OpenACC rewrite version, and the CUDA Fortran rewrite version. In the optimized register OpenACC version, limiting the number of registers available to each thread could improve occupancy and we found a speedup of 1.3x from the original OpenACC version for the test case of interest. In the OpenACC rewrite version, the code is rewritten so that the loop over threads came outside of the loop over array elements. This version results in 2.3x speedup from the original OpenACC version and 1.75x speedup from the optimized register OpenACC version. In the CUDA Fortran rewrite version, the LU decomposition is implemented without using shared memory. The CUDA version performance falls between the original OpenACC and OpenACC rewrite versions. However, the cuBLAS rewrite version turns out several orders of magnitude slower than the OpenACC versions and the results are not presented here. This work serves as a model for future work with the Compact LAPACK library to improve the performance of NEPTUNE code on GPUs.

DoD Impact/Significance: Since weather modeling requires a large computational domain on the scale of kilometers and a long physical time in simulations, it is important to achieve results in desired time frame. The GPU implementation to NEPTUNE code will allow users to generate realistic simulations within a reasonable turnaround time while utilizing less HPC resources. Accurate weather forecasting is very important to the DoD to achieve successful missions and it is also vital in preventing potential natural disasters.

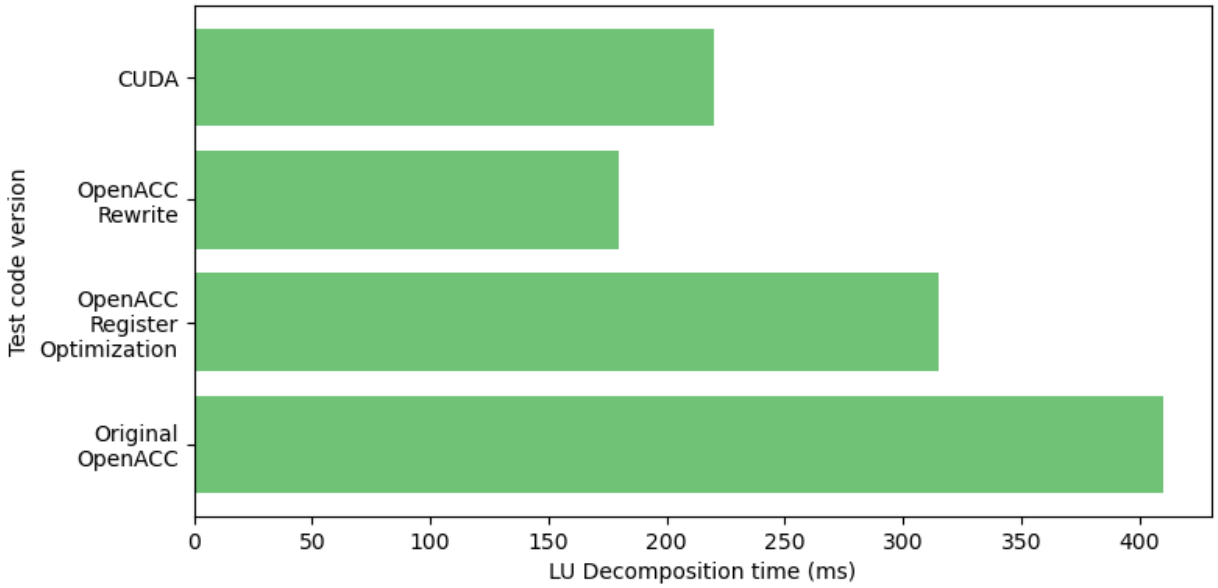


Figure 1. Comparison of original OpenACC, optimized register OpenACC, OpenACC rewrite, and CUDA Fortran rewrite versions of a LU decomposition of a test case of interest on a GPU. Lower time is better.

Title: Coastal Mesoscale Modeling
Author(s): W.A. Komaromi and P.A. Reinecke
Affiliation(s): U.S. Naval Research Laboratory, Monterey, CA
CTA: CWO

Computer Resources: SGI ICE X [ARL, MD]; Cray XC40/50 [ERDC, MS]; Cray Shasta, HPE SGI 8600 [NAVY, MS]

Research Objectives: Our objective is to develop and validate a fully coupled coastal/littoral prediction system that can be used to provide high-resolution (<5 km) data assimilation (DA) and short-term (0 to 48 h) forecast guidance for tactical-sized areas of the world. This system can also be used for basic and applied research leading to an improvement in our understanding of atmospheric and oceanic processes. Improvements to our mesoscale prediction systems and DA systems will result from this research.

Methodology: The Coupled Ocean/Atmosphere Mesoscale Prediction System (COAMPS®) meteorological forecast model is being developed further for independent and coupled simulations of the atmosphere and the ocean for the mesoscale. The atmospheric component of COAMPS® model is made up of a DA system, an initialization procedure, and a multinested, nonhydrostatic numerical model. This model includes parameterizations for moist processes, surface and boundary-layer effects, and radiation processes. The NRL Coastal Ocean Model (NCOM) is currently being used for the simulation of the mesoscale ocean circulation response to the COAMPS® model forcing in one-way and two-way interactive modes. COAMPS® code has also been recently modified to predict electro-optical quantities of interest for directed-energy applications.

Results: In FY22, HPC resources were used to run COAMPS® model simulations for a validation test report (VTR) to transition COAMPS® code update v2022 to FNMOC, as well as validation of the recently transitioned v2021 and comparison against earlier versions of the model. COAMPS® model v2022 features upgrades to the air, ocean, wave, ice, and coupling layer. In FY22, a new Cylc layer was developed to include the atmosphere and ocean validation software in the COAMPS® model workflow, an atmospheric refractive structure function forecast for EO was transitioned, the team completed the development of cloud type verification software using GOES16 and Himawari satellites, and forecast verification for low-level coastal stratus cloud cover was performed utilizing the World Wide Merge Cloud Analysis (WWMCA). Validation test data comparing COAMPS® model v2020.5 to v2021 for the Southern California mesoscale subdomain during the summer months reveals reduced RMS error and bias for both temperature (Fig. 1a) and dew point (Fig. 1b) in v2021, although an overall warm bias remains a challenge (Fig. 1c). Some reduction in warm bias can be attributed to an improved model representation of the marine coastal stratus layer, which is a better match to observations (WWMCA) in v2021 than in v2020.5 (Fig. 1d). Increased coastal marine stratus reflects incoming solar radiation, keeping the boundary layer cooler and closer to observations.

DoD Impact/Significance: The COAMPS® model continues to play a significant role in providing atmospheric forecasts in support of Navy missions involving the deployment of weapons systems, strike warfare, radar propagation, and search and rescue. Research and development performed at HPC DSRCs have led to significant improvements in the predictive skill of the COAMPS® model that will greatly benefit its operational performance. The HPC DSRCs will be the primary computing resources in FY23 and beyond for the development of the fully coupled COAMPS® system, including the emerging electromagnetic and electro-optical (EM/EO) and ensemble capabilities for the COAMPS® system.

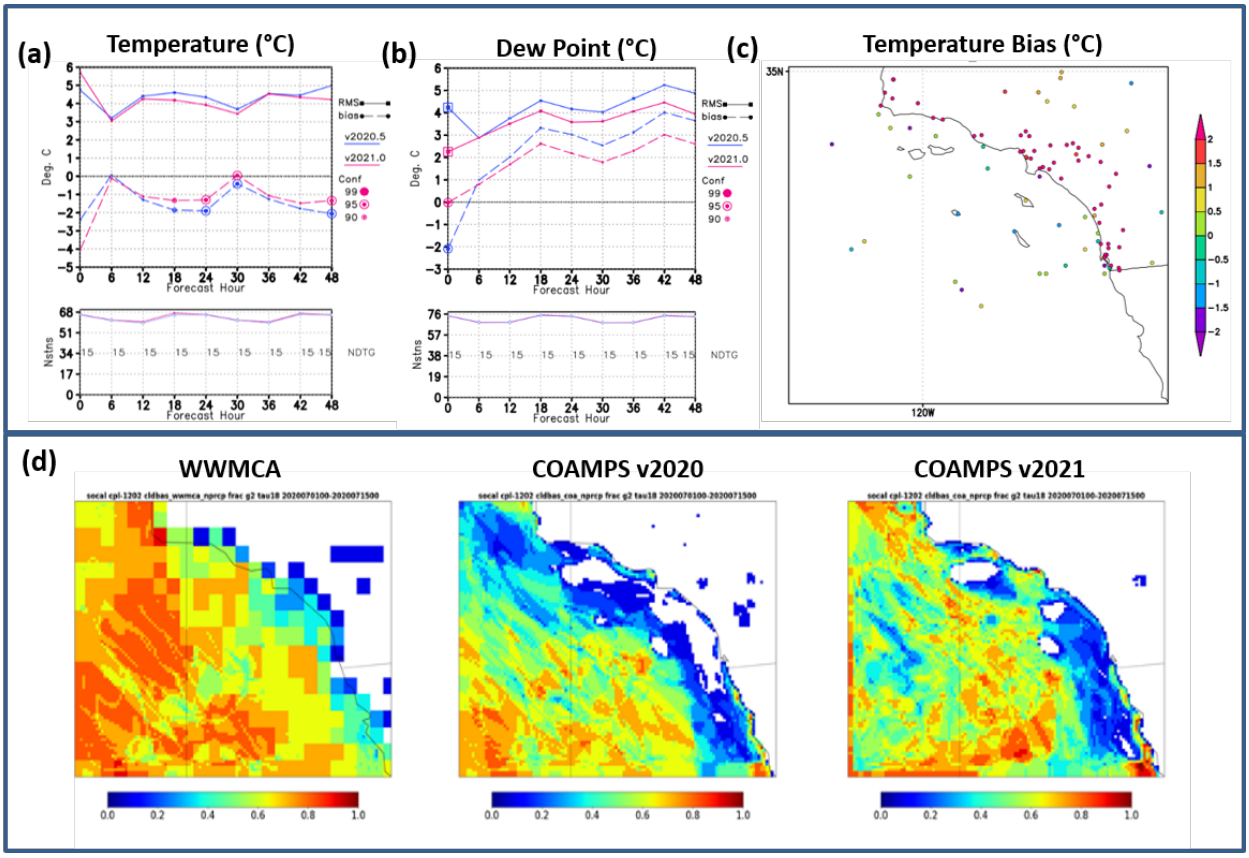


Figure 1. Validation test data comparing the existing COAMPS® model v2020 to the new COAMPS® model v2021 for the Southern California mesoscale domain during the summer months. (a) Temperature RMS error (solid) and bias (dashed), for v2020 (blue) and v2021 (magenta), (b) dew point RMS error (solid) and bias (dashed), for v2020 (blue) and v2021, (c) temperature bias in v2021 for individual stations along Southern California coast, (d) non-precipitating cloud cover comparing World Wide Merge Cloud Analysis (WWMCA), COAMPS® model v2020, and COAMPS® model v2021. (S. Chen, J. Nachamkin 2022).

Title: Eddy-Resolving Global/Basin-Scale Ocean Modeling - Arctic OSSE
Author(s): E. Douglass
Affiliation(s): U.S. Naval Research Laboratory, Stennis Space Center, MS
CTA: CWO

Computer Resources: Cray Shasta [NAVY, MS]

Research Objectives: *Arctic OSSE:* Simulation of the Arctic Observing system with intent of making better use of observations being made and determining which additional observations would be the most cost-effective way to improve our forecasts and prediction of Arctic/sub-Arctic dynamics. The emphasis is on ensuring that our assimilative systems are adapting appropriately to a fast-changing Arctic environment.

Methodology: This project used the Observing System Simulation Experiment (OSSE) framework, which is as follows: A high-resolution global model run is created, spanning several years, forced with real atmospheric forcing and run with no assimilation. This model output is then sampled as our observing system would sample it, and results are assimilated into a separate model. The output from this "OSSE model" is then compared back to the "nature run" to determine how well the model simulates reality given the particular dataset input. This allows for the evaluation of different observing system setups to determine which is most effective and the most useful way to improve our system going forward. It also allows an evaluation of how well our model and assimilation system do at replicating "nature" given the observing system in place.

Results: In FY22, four OSSEs were integrated through a full year and their results were compared with each other and with the nature run. An important note is that sea surface height is not assimilated directly; sea surface height anomalies are associated with "synthetic" temperature and salinity profiles, which are then assimilated. When comparing a run that assimilated temperature and salinity directly from the model with a run that assimilated synthetic temperature and salinity, it was found in some regions that the synthetic profiles are not representative of the observed temperature (T) and salinity (S) structure (Fig. 1). This may be due to changes in the Arctic environment. A new, more recent climatology that accounts for rapid climate-based changes in the Arctic is necessary. A second comparison was made between a run that only used synthetic profiles when stratification was above a predefined threshold and one that applied synthetic profiles everywhere. In some regions, using more of the data already being corrected was useful. The proxy used for stratification is the difference between surface temperature and temperature at 1,000 m; if the climatology is accurate, subsurface structure affects sea surface height in a predictable way, and assimilating T and S representing the subsurface changes associated with surface SSH anomalies gives an improved representation. However, there are also regions in which truly unstratified conditions mean that synthetic T and S profiles do not accurately represent conditions. This indicates that a more nuanced approach is necessary to avoid discarding data from which useful, useable information can be readily extracted.

DoD Impact/Significance: Accurate nowcasts and forecasts of the Arctic region and sub-Arctic oceans are of increasing importance in a warming world. Ensuring that our operational models are evolving as the environment in which they operate evolves is essential to remaining at the technological forefront. Using available observations to their maximum potential (including using data currently being discarded) is a cost-effective way to improve our operational modeling system.

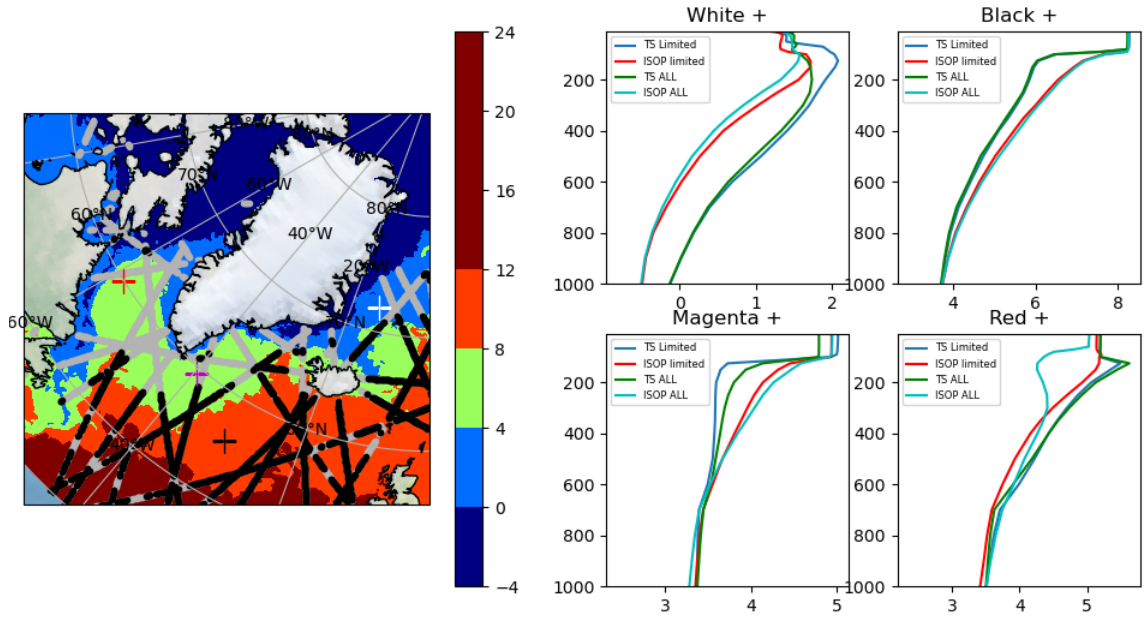


Figure 9. On the left is a map of sea surface temperature around Greenland on Nov 15, 2017. Black dots represent locations where data are assimilated by all OSSEs, while gray dots are locations where data are assimilated only by OSSEs that assimilate regardless of stratification. On the right are profiles at locations marked by crosses in the map figure. The profiles are from four different OSSEs; two assimilate temperature directly ("TS ALL and TS Limited") and are differentiated by whether they limit assimilation based on stratification. The others use synthetic profiles (ISOP), and either assimilate ALL or only stratified (Limited) profiles. Results show that at the black and magenta "+" symbols, the synthetic profiles are close to accurate but the thermocline is not sharp enough. At the white "+" symbol, the synthetic profiles are far too cool, indicating an inaccurate underlying climatology. At the red "+", it is demonstrated that using ISOP in a location where stratification implies it shouldn't be used is negatively impacting the result.

Title: Eddy-Resolving Global/Basin-Scale Ocean Modeling - Global Ocean Reanalysis
Author(s): E.J. Metzger and L. Zamudio
Affiliation(s): U.S. Naval Research Laboratory, Stennis Space Center, MS
CTA: CWO

Computer Resources: Cray Shasta, HPE SGI 8600 [NAVY, MS]; Cray XC40/50 [ERDC, MS]

Research Objectives: *6.4 Global Ocean Reanalysis:* Generate a multiyear Global Ocean Forecast System (GOFS) 3.1 reanalysis and assess the veracity through validation and verification using standard ocean and sea ice error metrics. Climatologies of ocean state variables will be built from the reanalysis and used by the Naval Oceanographic Office (NAVOCEANO), the Fleet Numerical Meteorology and Oceanography Center (FNMOC), and others. Additionally, exploit the GOFS 3.1 reanalysis by creating climatologies of acoustic variables.

Methodology: The multiyear GOFS 3.1 reanalysis provides a rich source of output from the existing Navy operational global ocean nowcast/forecast system. Because it assimilated all available observations over a centered assimilation data window, it provides the best ocean analysis available. And unlike observational databases, it has the advantage of having temporally continuous, fully spatial global fields at all depths of the water column. The reanalysis (currently 27 years in length) will eventually be expanded to 30 years, the standard length of environmental climatologies. Efforts in this project will be expanded to exploit this dataset and to provide climatological products of value to Navy customers. Discussions with NAVOCEANO and FNMOC have guided product development, and this fiscal year will focus on an acoustic parameter climatology. Because of its length, the reanalysis also provides a good measure of interannual variability.

Results: The GOFS 3.1 reanalysis has been extended through calendar year 2021 using HPC resources, making its total length 28 years: 1994–2021. Model-derived acoustical parameters have been computed over all years of GOFS 3.1 reanalysis output. A total of 636 PB of temperature and salinity input was run through the APARMS software and generated acoustical parameter output totaling 21 TB/year (uncompressed) or 6.9 TB/year (compressed). This work was performed in the serial queues on the Navy DSRC SGIs (Gaffney and Koehr). NAVOCEANO communicated a need for a modal analysis of APC variables due to the fact that certain variables (e.g., sonic layer depth) may have modal distributions with high bin counts at both shallow and deep depths. In such scenarios, the arithmetic mean gives an answer between these two modes that rarely occurs. Software was developed to examine the 1st and 2nd dominant modes and the probability of occurrence of these bins similar to the example shown in Fig. 1.

DoD Impact/Significance: FNMOC and NAVOCEANO have requirements to maintain up-to-date ocean climatologies and databases to provide the fleet with impactful information globally. This ocean reanalysis provides consistently configured, long-term, model-based climatologies of prognostic variables (currents, temperature, and salinity) and diagnostic variables (mixed layer depth, acoustic parameters). It has an advantage over observational-based climatologies in that it includes output of the full water column and at 3-hourly temporal frequency. Other uses include provision of boundary conditions for regional models run in hindcast mode (i.e., covering previous time periods), initial conditions for global and regional reforecasting, for use as a verifying analysis for reforecasting, and for comparison against another national/international global ocean reanalyses.

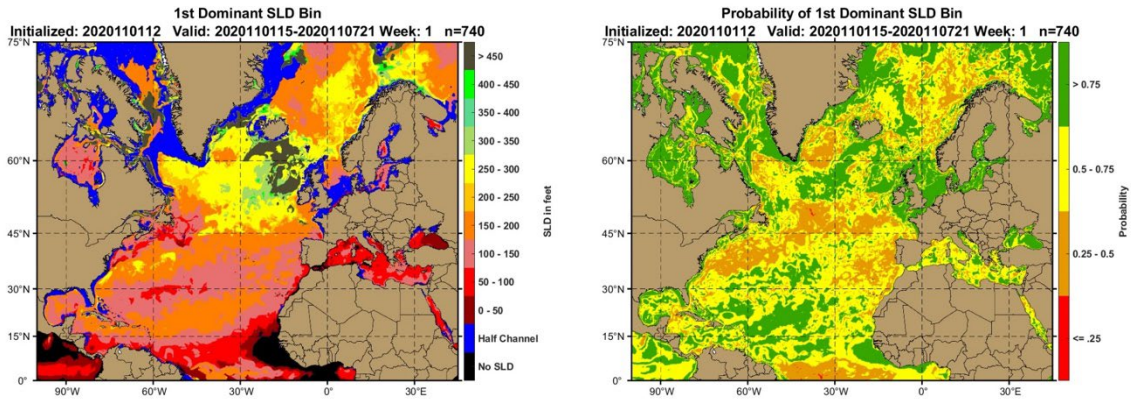


Figure 1. Sonic layer depth (feet) of the first dominant bin (left) and the probability of occurrence (%) of the first dominant bin (right). Sonic layer depth is the vertical distance from the surface to the depth of the sound speed maximum, often but not always at the base of the mixed layer.

Title: Eddy-Resolving Global/Basin-Scale Ocean Modeling - Internal Tides
Author(s): J.F. Shriver, R.W. Helber, and E.J. Metzger
Affiliation(s): U.S. Naval Research Laboratory, Stennis Space Center, MS
CTA: CWO

Computer Resources: HPE SGI 8600 [NAVY, MS]

Research Objectives: *Modeling, characterizing, and predicting effects of internal gravity waves on acoustic propagation on basin to global scales:* Assess the impact of internal gravity waves on basin- to global-scale propagation of acoustic waves using the HYbrid Coordinate Ocean Model (HYCOM). Assess the impact of the inclusion of tides on the realism of simulated acoustic properties using available contemporaneous observations.

Methodology: For about a decade, HYCOM simulations have been run with tidal as well as atmospheric forcing. The simulations develop a rich field of internal tides and near-inertial flows. Interactions between near-inertial waves and internal tides produce a partially resolved supertidal internal gravity wave continuum. With the advent of these new simulations that resolve internal wave motions on a global scale, we are well poised to examine the impact of internal waves on acoustic motions. Global simulations of HYCOM with/without tides provide the experimental setup to evaluate differences in acoustic properties. Acoustic parameters that characterize the ocean acoustic transmission properties resulting from the vertical structure of sound speed profiles provide a rough estimate of the acoustic impact of tides in the simulated ocean.

Results: Global simulations of HYCOM with/without tides provide the experimental setup to evaluate differences in acoustic properties. To examine the impact of internal tides, we focus on transects along which internal tides are known to propagate using Hovmöller diagrams to highlight internal tide impact/influence on acoustic parameters of interest. Focusing on the Amazon Delta, sonic layer depth is shown (Fig. 1). The impact of propagating features (slanting from lower left to upper right) are evident in Fig. 1b (HYCOM with tides). But are these features tidal in nature? They almost certainly are, since they do not occur in the cases without tides (Fig. 1c). There are two pieces of evidence to confirm their tidal nature: propagation speed and frequency. Mode 1 internal tides propagate at roughly 3 m/s, which is very similar to the propagation speeds we can infer from Fig. 1b. To examine the dominant frequencies in these figures, we computed simple spectra and note clear spectral peaks at the M_2 tidal frequency in the cases with tides. Tidal frequencies and mode 1 internal tide propagation speeds are as we'd expect if these variations were due to internal tides. A question of interest to the Navy is to further learn how these tidal impacts affect internal tides. We find that the inclusion of this tidal variability does indeed increase realism (Fig. 2), where comparisons of model results against contemporaneous glider lines off the coast of California show that the model with both data assimilation and tides produces the most realistic sound speed variability. This is a very encouraging result; getting good comparisons in an area away from major internal tide generation regions is a challenge because even small errors in stratification or the strength and/or location of fronts and eddies in the medium through which internal tides propagate (away from generation regions) could result is large amplitude or phase errors.

DoD Impact/Significance: Data assimilative eddy resolving models are important components of global ocean and sea ice prediction systems. Tactical decision aids (TDAs) and mission planning tools (MPTs) based on these systems provide vital enabling capabilities for the Navy at spatial scales ranging from operational areas to entire theaters and over time horizons ranging from a few hours to many months. The utility of these tools for enabling the Navy to exploit the environment and plan future operations is determined in large part by the realism of the oceanographic models that are employed.

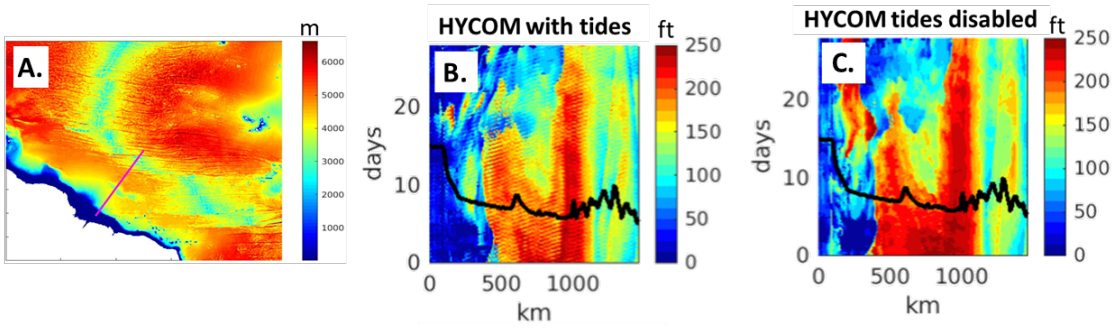


Figure 1. (A.) Amazon Delta transect location overlaid on bottom topography. Depth is in meters. Amazon Delta sonic layer depth for experiments with tides (B.) and without tides (C.). The x-axis is distance along the transect in km and the y-axis is time in days. Units are in feet. Relative depth of bottom topography is overlaid on B. and C.

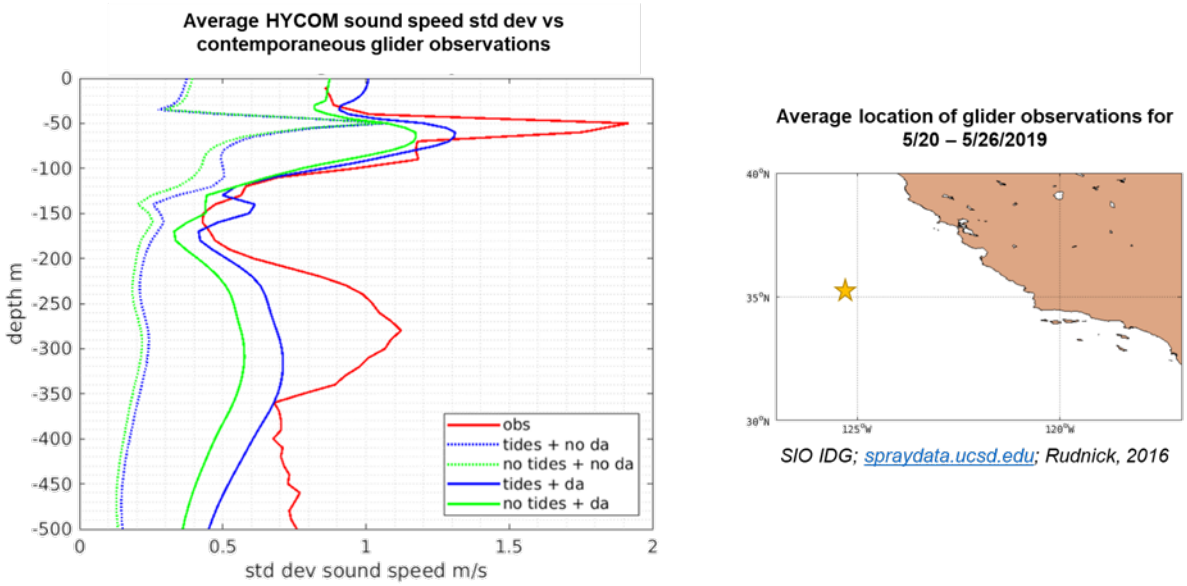


Figure 2. (Left panel) Average HYCOM sound speed standard deviation vs contemporaneous glider observations. Model solutions with tides enabled/disabled and data assimilation (DA) enabled/disabled are depicted by the colors in the legend to the lower right. (Right panel) The average location of the glider observations during this time are depicted by the star near 125˚W/35˚N.

Title: Eddy-Resolving Global/Basin-Scale Ocean Modeling - Large Scale Prediction
Author(s): E. Metzger and L. Zamudio
Affiliation(s): U.S. Naval Research Laboratory, Stennis Space Center, MS
CTA: CWO

Computer Resources: Cray Shasta, HPE SGI 8600 [NAVY, MS]; Cray XC40/50 [ERDC, MS]

Research Objectives: *6.4 Large Scale Ocean Prediction:* Development of a global naval ocean/ice nowcasting and forecasting capability based on the HYbrid Coordinate Ocean Model (HYCOM) two-way coupled to the Community Ice CodE (CICE) model and using the Navy Coupled Ocean Data Assimilation system (NCODA) that runs daily at CNMOC production centers. The system will 1) depict the location of mesoscale features such as oceanic eddies and fronts, i.e., the "ocean weather," 2) provide accurate three-dimensional (3D) ocean temperature, salinity, and current structure, 3) provide boundary conditions for regional and nested coastal models, 4) provide acoustical proxy measures (mixed layer depth, sonic layer depth, below layer gradient, and deep sound channel axis), and 5) provide sea ice concentration, thickness and drift.

Methodology: Incorporate new capabilities into the global ocean/sea ice forecast systems to more accurately predict the marine and cryosphere environments. This is being accomplished through updates to the model physics as well as implementing advances in the data assimilation. Initially, the implementation will be performed in the stand-alone Global Ocean Forecast System (GOFS) to allow a more stepwise approach and analysis of the impacts and because it is more efficient than using the fully coupled Earth System Prediction Capability (ESPC) model.

Results: One new capability implemented in GOFS is the inclusion of rivers and evaporation minus precipitation (E-P) as mass fluxes within HYCOM. More realistic river discharge will benefit regional Coupled Ocean Atmosphere Mesoscale Prediction System (COAMPS®) forecast systems that receive boundary conditions from GOFS. Improved E-P fluxes will lead to improved surface salinity in the system. A yearlong HYCOM simulation implementing rivers and E-P as a mass flux was integrated for comparison against a HYCOM simulation using the original formulation that treats river discharge as a precipitation flux, i.e., the fresh water in river deltas is parameterized by heavy rainfall. The impact was examined at the five largest river deltas (Amazon, Yangtze, Ganges, Mississippi, and Zaire) and compared against satellite salinity observations. The new formulation had a positive impact on the salinity distribution near the vicinity of river deltas. Figure 1 shows sea surface salinity (SSS) of the Amazon River outflow into the Atlantic Ocean for the old and new formulations in comparison against independent satellite-derived SSS. The new formulation clearly agrees better with the observations and extends down into the top 30 m of the water column.

DoD Impact/Significance: GOFS provides the U.S. Navy with a first look of the three-dimensional ocean environment "anywhere, anytime" across the global ocean. These environmental fields are also used to provide real-time predictions of derived acoustic parameters including sound speed and sonic layer depth. The inclusion of astronomical tides allows for the simulation of internal waves at tidal frequencies. In addition, GOFS provides boundary conditions for higher-resolution regional/coastal models. Ocean forecasts are also valuable for tactical planning, optimum track ship routing, search-and-rescue operations, long-range weather prediction, and the location of high current shear zones.

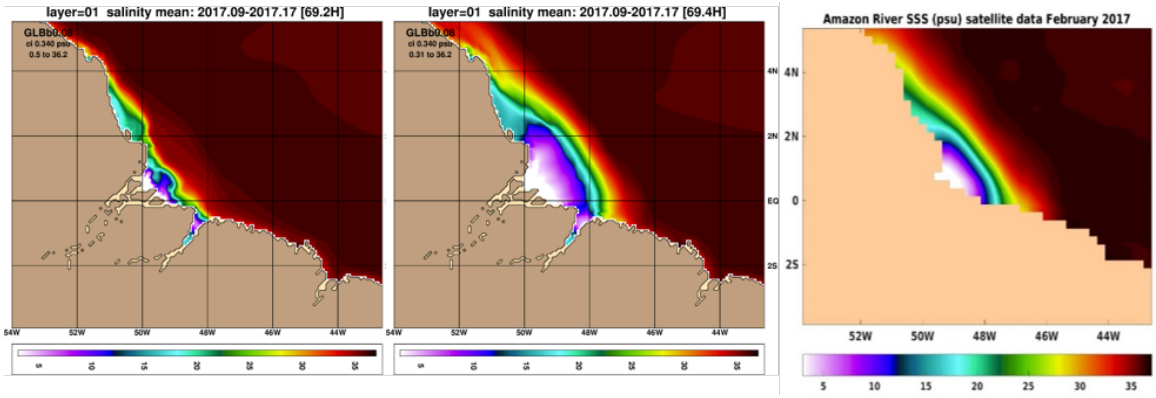


Figure 10. Monthly sea surface salinity (psu) near the Amazon River Delta in global HYCOM using the original river formulation (left) and the new formulation (middle), and from Soil Moisture Active Passive (SMAP) satellite observations (right) averaged over February 2017.

Title: Eddy-Resolving Global/Basin-Scale Ocean Modeling - Sea Ice Assimilation
Author(s): D. Hebert,[1] J. May,[1] T. Townsend,[1] M. Phelps[2]
Affiliation(s): [1]U.S. Naval Research Laboratory, Stennis Space Center, MS; [2]Peraton, Inc., Stennis Space Center, MS
CTA: CWO

Computer Resources: HPE Cray EX, HPE SGI 8600 [NAVY, MS]

Research Objectives: *Operationally implementing satellite-derived ice products within the Navy's ice forecast systems:* The goal is to improve short-term (5- to 7-day) and long-term (up to 45-day) forecast skill of sea ice predictions by assimilating current and future satellite-derived ice products into the Navy's operational sea ice forecast systems.

Methodology: This project updates Navy Coupled Ocean Data Assimilation system (NCODA) to ingest satellite-derived sea ice products for use with Navy Operational forecast systems (CICE). In FY22, this project 1) added the ability to assimilate U.S. National Ice Center (USNIC) analyzed sea ice edge in the Arctic and the Antarctic, 2) tested assimilation of SMOS sea ice thickness, and 3) tested assimilation of high-resolution (375 m) VIIRS observed ice concentration using an updated cloud detection algorithm developed by Dr. Li at NRL-DC. Each NCODA system update is tested in an uncoupled, nonoperational version of the Community Ice CodE (CICE).

Results: *Assimilate USNIC Ice Edge:* Assimilating the USINC ice edge reduced the initial ice edge error by 12 km (51%) in the Arctic and 35 km (89%) in the Antarctic. Through a 72-hour forecast, the ice edge error was 5 km (14%) in the Arctic and 22 km (47%) in the Antarctic (Fig. 1). *Assimilate SMOS Ice Thickness:* The NCODA system was successfully able to assimilate SMOS ice thickness with CryoSat-2 ice thickness. They are complementary: SMOS detects thin ice (< 0.5m) while CryoSat-2 detects ice > 0.5 m (Fig. 2). *Assimilating High Resolution VIIRS Ice Concentration with Updated Cloud Detection Algorithm:* This test is 6 months into a one-year test. Preliminary results show improved ice edge compared to the Global Ocean Forecast System (GOFS) without VIIRS, especially in the Canadian Archipelago (Fig. 3).

DoD Impact/Significance: The sea ice environment has become increasingly important for strategic and economic reasons, given the diminishing trend in sea ice extent and thickness and the potential summertime opening of the Northwest Passage and Siberian Sea routes. Fractures, leads, and polynya forecasts are also valuable to the naval submarine community. The location of sea ice is important for both safety of navigation and within coupled sea ice/ocean/atmosphere models.

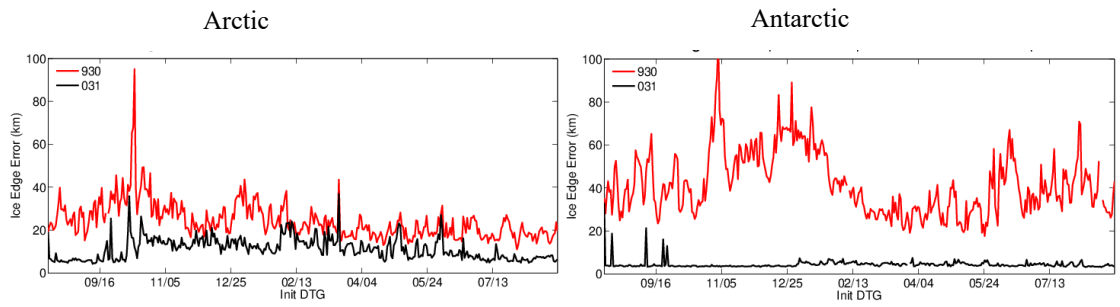


Figure 1. Initial ice edge error of GOFS without assimilating USNIC ice edge (red line) and CICE test with assimilating ice edge (black line). Overall, the ice edge is reduced by 51% in the Arctic, 89% in the Antarctic.

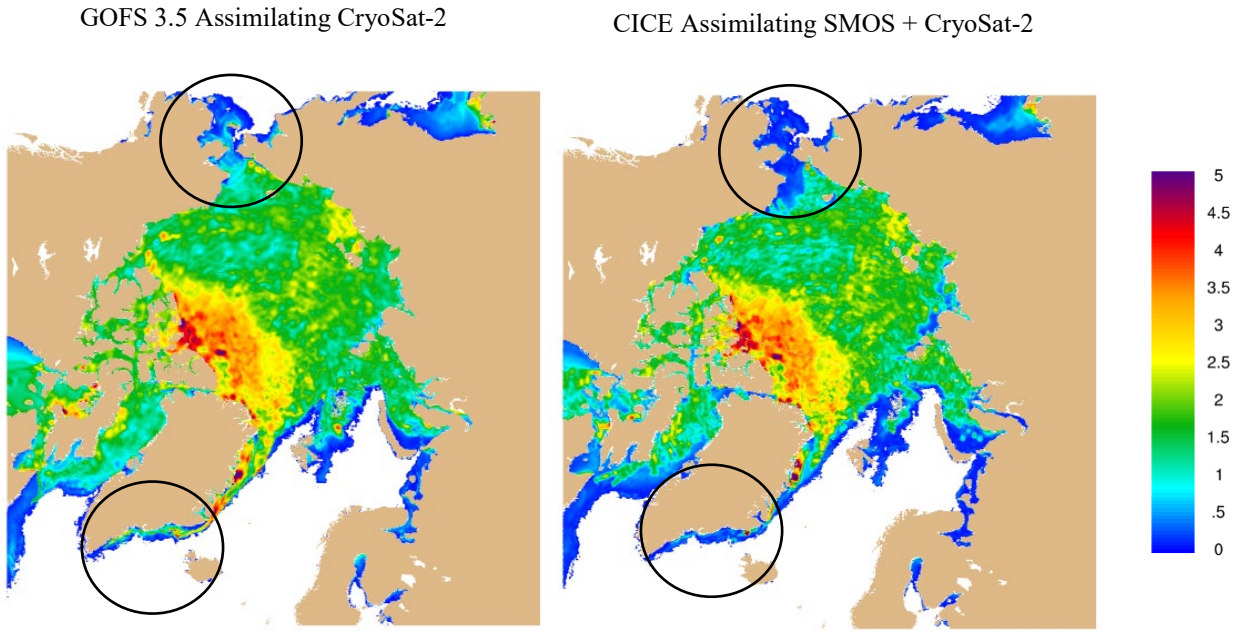


Figure 2. Modeled ice thickness on Feb. 15, 2018, for (left) GOFS 3.5 assimilating CryoSat-2 and (right) CICE assimilating SMOS and CryoSat-2 ice thickness. Circled areas highlight areas ice thickness was reduced by addition of SMOS "thin" (< 0.5 m) ice observations.

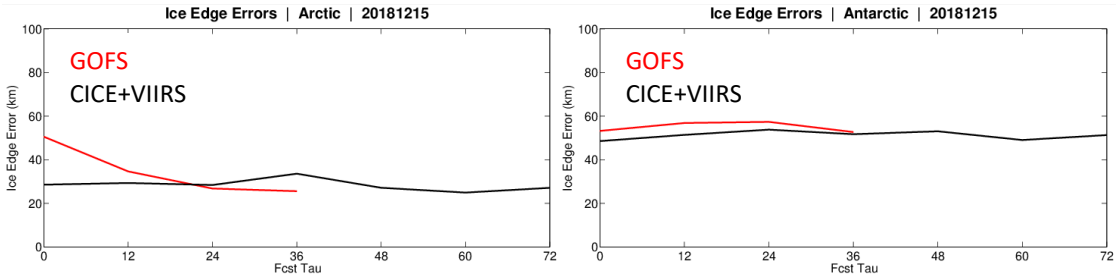


Figure 3. Ice edge error on model day Dec. 15, 2018, for the Arctic (left) and the Antarctic (right). Red line is GOFS without VIIRS, black line is CICE test assimilating VIIRS. The addition of VIIRS reduced the initial ice edge error in the Arctic by 15 km and 5 km in the Antarctic. Note in this test, CICE was only run for a 36-hour forecast to conserve computational resources.

Title: Eddy-Resolving Global/Basin-Scale Ocean Modeling - South China Sea
Author(s): E.J. Metzger and Z. Yu
Affiliation(s): U.S. Naval Research Laboratory, Stennis Space Center, MS
CTA: CWO

Computer Resources: Cray Shasta, HPE SGI 8600 [NAVY, MS]; Cray XC40/50 [ERDC, MS]

Research Objectives: *6.1 South China Sea (SCS) circulation dynamics:* Unravel the dynamics behind the seasonal variability of the coastal currents along the China and Vietnam coasts (i.e., the SCS Warm Current and the South Vietnam Offshore Current) and study the impact of Kuroshio penetration and eddy shedding into the northern SCS using a combination of the Navy's ocean circulation models and observations. This is leading to a better understanding of the physical processes that control the time-varying flow and the interaction of the deep offshore currents with the coastal currents.

Methodology: Employ 1/12° and higher horizontal resolution versions of the HYbrid Coordinate Ocean Model (HYCOM) to study the dynamics of the SCS coastal and throughflow currents and their interactions. New simulations of global and nested SCS domains using both climatological and interannual forcing will be utilized. Data assimilative hindcasts, which have a realistic representation of the mesoscale features, provide a means of assessing how nondeterministic Kuroshio eddy shedding affects the northern SCS circulation. Simulations that employ tidal forcing will also be analyzed where appropriate to study the impact of internal tide generation at Luzon Strait. Observational data sources will be used to determine simulation skill. HYCOM's ability to accurately transition from the deep ocean onto the shelf makes it ideal for studying how the coastal currents interact with deeper offshore currents.

Results: An empirical method is developed to predict the counter-wind South China Sea Warm Current (SCSWC) using wind stress at a specific location that is built on the most dominant empirical orthogonal function (EOF) mode of the sea surface height (SSH), i.e., the Ekman mode (Yu et al., 2021). Based on the most dominant EOF modes from a 22-year HYbrid Coordinate Ocean Model (HYCOM) reanalysis, a rectangular box and a specific location are carefully chosen for SSH and wind stress, respectively. In the rectangular box (specific location), more than 90% of the SSH (wind stress) variance is explained by the most dominant EOF mode. SSH in the rectangular box is predicted from the wind stress at the specific location. When the average cross-shore pressure gradient force in the rectangular box is negative, the SCSWC exists in the model solution. The critical alongshore (38° to the north of east) wind stress at the specific location is -0.117 N/m^2. The SCSWC occurs in the rectangular box when the wind further relaxes. The accuracy of this method varies from 74.9% to75.3% and the representativeness varies from 84.5% to 85.9% with time lags from 12 to 16 hours when applying the method to predict the SCSWC during the 21 winters in HYCOM reanalysis. Figure 1 provides an application of the empirical formula under various extreme wind conditions. A paper by Yu et al. (2022) was published on this topic.

DoD Impact/Significance: The SCS is a region of high strategic U.S. Navy interest, thus accurate simulation skill of the temperature, salinity, and current structure is essential for numerical ocean systems providing surface and subsurface forecasts to the fleet. A more accurate thermal structure will lead to improved knowledge of the acoustical environment and the propagation of internal waves that will be beneficial to Navy applications such as anti-submarine warfare/surveillance and tactical planning.

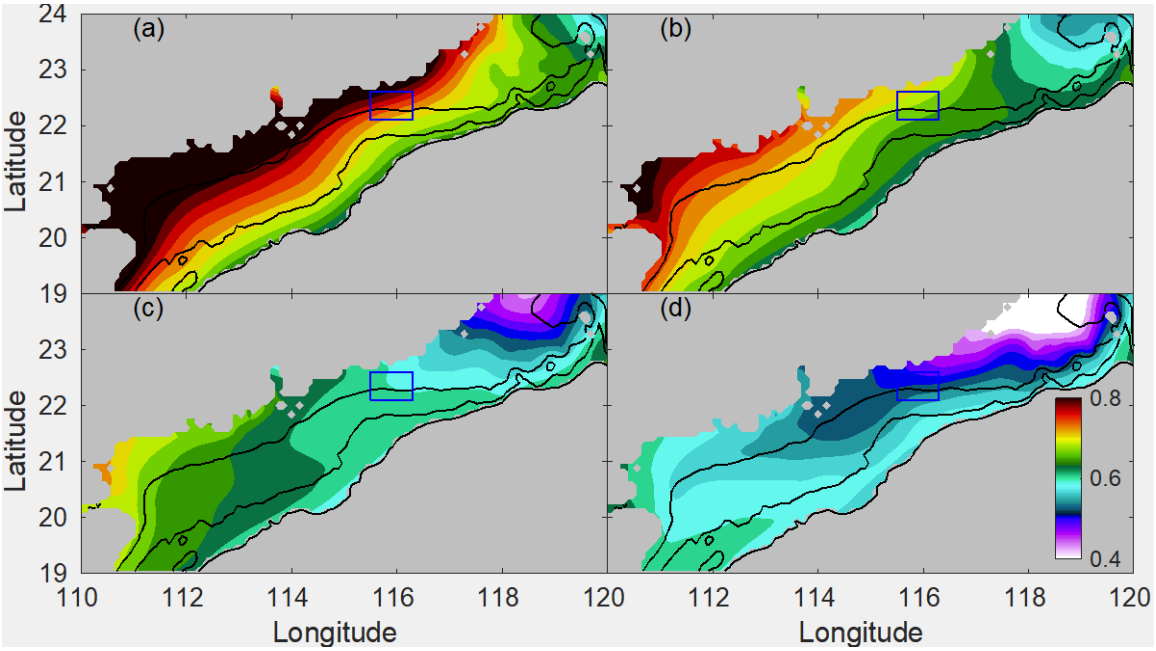


Figure 1. Sea surface height (m) derived from the empirical equation of Yu et al. (2022) to determine the predictability of the South China Sea Warm Current (SCSWC) in the northern South China Sea. (a) northeasterly wintertime wind burst case, (b) mean wintertime wind case, (c) critical SCSWC wind stress case, and (d) zero alongshore wind stress case. The gray area in the southeast corner of each panel is water depths deeper than 200 m and has been masked out.

Title: Eddy-Resolving Global/Basin-Scale Ocean Modeling - Winter Convective Mixing
Author(s): P. Thoppil
Affiliation(s): U.S. Naval Research Laboratory, Stennis Space Center, MS
CTA: CWO

Computer Resources: HPE SGI 8600 [NAVY, MS]

Research Objectives: *6.1 Winter Convective Mixing in the Northern Arabian Sea during Contrasting Monsoons:* The project aims to identify and isolate the role of mesoscale eddies on the convective formation of water masses and to quantify the physical processes associated with it. The long-term goal of this project is to understand the impact of mesoscale eddies and fronts on the air-sea interaction and how and why such interaction modifies the upper-ocean convection and water mass formation through turbulent heat fluxes.

Methodology: We employed a combination of idealized and realistic simulations using Hybrid Coordinate Ocean Model (HYCOM) and data analysis.

Results: Winter convective mixing in the northern Arabian Sea during the winters of 2017–2018 and 2018–2019 were studied using one-dimensional (1D) model experiments (Fig. 1). Although winter convective mixing is a response to the local surface buoyancy loss from the ocean, mainly due to the heat loss, we show the modulation of winter convective mixing resulting from the freshwater-induced salinity stratification from the summer conditions preceding winter. During 2017–2018, the excess precipitation over evaporation during the summer monsoon precedes a shallower and short-lived winter mixed layer. The freshwater-induced salinity stratification (0.7 psu) during the summer inhibited the convective mixing in the ensuing winter, resulting in a shallower winter mixed layer (103 m). This combined with weak buoyancy loss due to weaker-than-usual latent heat loss, explained by higher-than-usual specific humidity in the northeastern Arabian Sea, caused an early termination of the convective mixing (February 26, 2018). In contrast, during 2018–2019, the winter convective mixing was deeper and long-lived. The 2018 summer, by comparison, was characterized by normal or below precipitation and generated a weaker stratification preconditioned to winter mixing. As a result, convective mixing was more intense and deeper by mixing cooler and saltier waters down to 143 m. This combined with colder and drier air from the north and its lower specific humidity produced larger latent cooling and buoyancy loss in the northeastern Arabian Sea. This resulted in a prolonged winter convective mixing through March 25, 2019.

DoD Impact/Significance: Ocean convection occurs in regions of surface buoyancy loss in winter and plays an important role in the stratification of water columns. Convective mixing is highly inhomogeneous in regions of mesoscale eddy activity, where propagation of sound speed becomes complex and less predictable. Improved knowledge of the interaction between mesoscale eddies and convective mixing will lead to a better representation of acoustic parameters in ocean models.

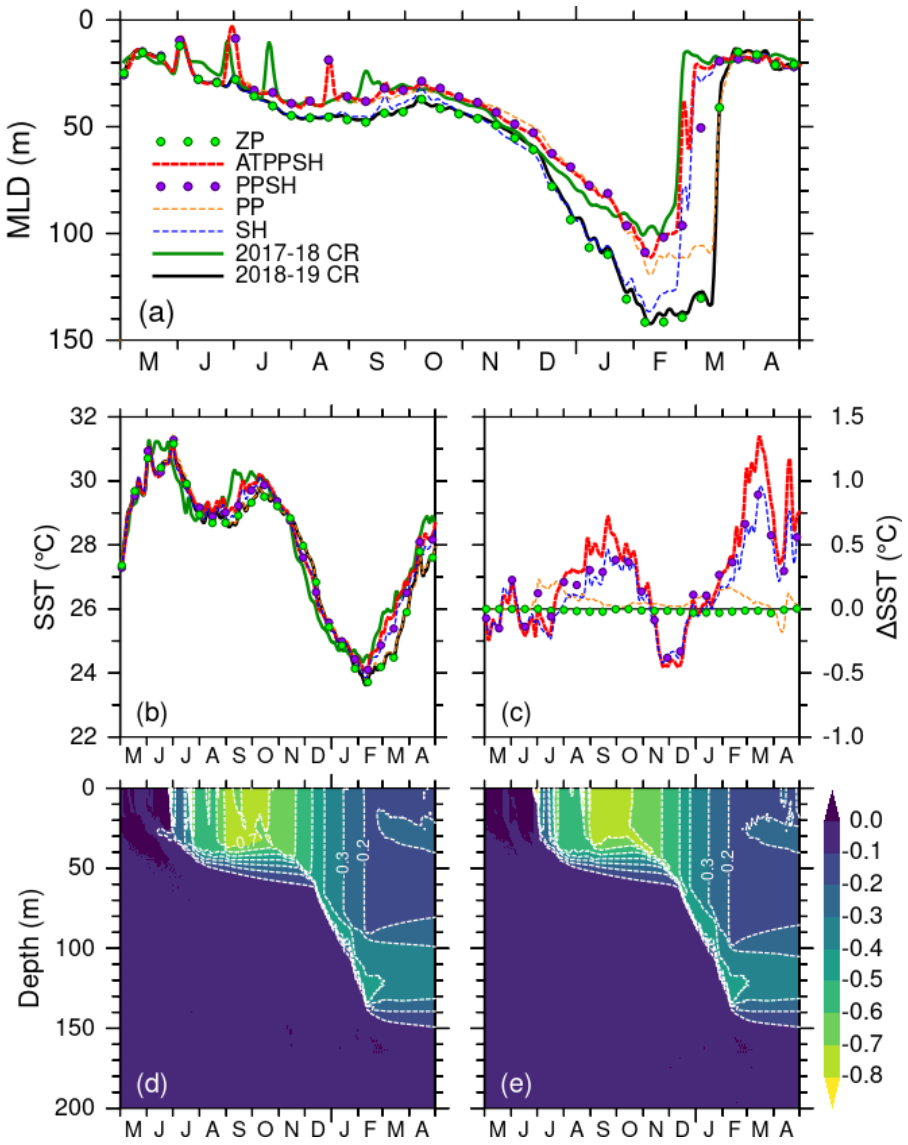


Figure 1. (a) Mixed layer depth (MLD, m) and (b) SST (°C) from control simulations 2017–2018 (solid, dark-green line) and 2018–2019 (solid, black line), perturbation experiments in dashed lines from SH (blue), PP (orange), PPSH (purple, filled circles), ATPPSSH (red), ZP (light-green, filled circles) at 67°E, 22°N. SST differences between the control simulation 2018–2019 and perturbation experiments are displayed in Figure 1c. The symbols are plotted every 10 (15) days for MLD (SST and SST differences). To distinguish each line, a 5-day Parzen smoothing is applied for MLD, SST and SST differences. Monthly mean salinity differences from 1D model between (d) 2017–2018 and 2018–2019 control runs (e) 2018–2019 control run and PPSH. All perturbation experiments are started from 2018–2019 control simulations by replacing each component of the atmospheric forcing with 2017–2018 specific humidity (SH), precipitation (PP), combined specific humidity and precipitation (PPSH), and air-temperature (ATPPSH), and zero precipitation in 2018–2019 (ZP).

Title: Rogue Wave Probability Estimator for WAVEWATCH III®
Author(s): M. Orzech
Affiliation(s): U.S. Naval Research Laboratory, Stennis Space Center, MS
CTA: CWO

Computer Resources: HPE SGI 8600 [NAVY, MS]

Research Objectives: Overall objective is to develop, validate, and transition software enabling WAVEWATCH III® (WW3) to estimate the relative threat of rogue waves throughout the global ocean. The system operates in a broad range of deep-water wave environments and computes a rogue threat index (RTI) to estimate rogue threat as the product of several scalar metrics representing the contributions of selected environmental causal factors. Computations are based on established theory and extensive analysis of representative sea states. The project was moved to 6.4 level in May 2020. During the 5-month FY20 period, we completed a 20-year WW3 reanalysis with wave-current interaction, implemented the rogue threat utility in WW3. In FY21, we completed the system calibration, modifying the determination of RTI to use a lookup table. Objectives accomplished in FY22 include complete validation of the system (with published VTR) and initiation of operational testing in preparation for transition of software to the Fleet Numerical Meteorology and Oceanography Center (FNMOC).

Methodology: The validation testing of the WW3 rogue threat estimator was completed in FY22Q2 and the VTR document was reviewed and approved in FY22Q3. In the validation, we completed an extensive analysis combining 10 years of model output with a 10-year rogue event dataset, with which we demonstrated that the magnitude of RTI is well correlated with the occurrence rate of measured rogue wave events. Additional analysis was performed to investigate the variations in RTI values with geographic location, water depth, and wave characteristics. A 6-month preoperational test was performed using a configuration very similar to the operational WW3 at FNMOC. A validation panel (VTP) was established to offer guidance and feedback on the validation procedures, including Roberto Padilla-Hernandez and James Dykes of FNMOC, Rodney Jacques of FWC-S, and Anton Kraft of FWC-N. Operational testing of the system by FNMOC has now been initiated.

Results: Higher values of RTI were found to consistently coincide with more frequent measurement of rogue waves by the analyzed buoys (Fig. 1). While the system cannot be used to predict an individual rogue wave at a specific location and time, it can identify and warn navigators about ocean conditions that are more conducive to rogue development. Larger rogue waves were found to occur more frequently at buoys in shallower water, suggesting that the operational system might be upgraded in the future to incorporate bathymetry as an additional causal factor. The preoperational test of the system verified that it functioned correctly under operational conditions (Fig. 2), increasing computation time by only 2% and producing no adverse effects on other model output. Occasional anomalously large RTI values were obtained in shallow regions, providing evidence in support of previously issued guidance that the system should only be used in deep-water, open-ocean locations (i.e., $h > 150$ m, at least 25 km from any shoreline). After extensive discussions with the VTP, the VTR was approved and published in May 2022 (Orzech, 2022).

DoD Impact/Significance: Accurate prediction of environmental hazards is important to tactical and strategic operations in the world's oceans. The results obtained from these simulations will form the core of the configurable WAVEWATCH III® rogue threat utility, which will enhance the safety of naval missions and will reduce the potential for damage or loss of Navy assets in rogue wave events.

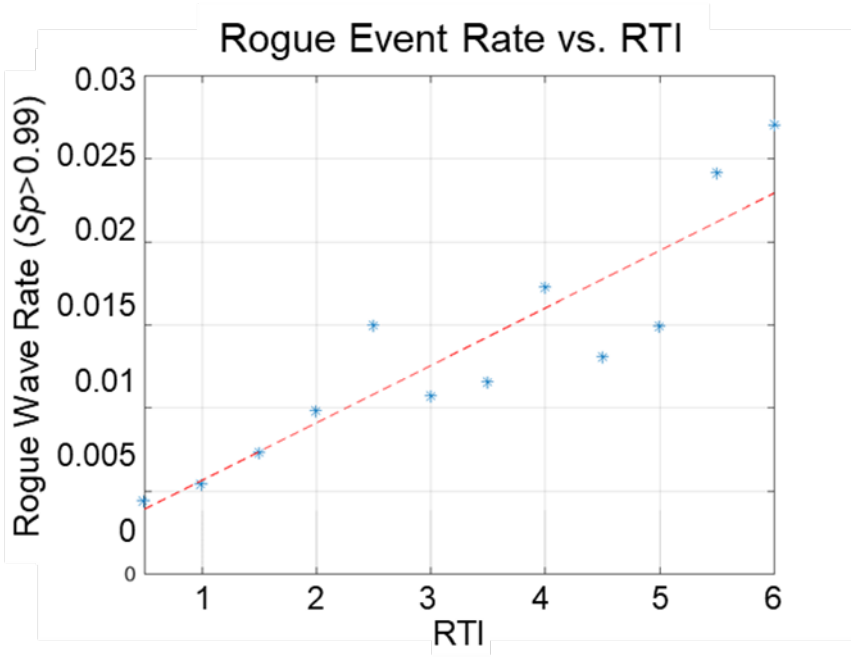


Figure 1. Rogue wave occurrence rate, or fraction of total model time steps that are rogue events (i.e., N_{Rogue}/N_{Tot}), averaged for bins of RTI (each of width 0.1 m). Averaged results from complete 10-year validation dataset, restricted to cases for which specificity Sp > 0.99.

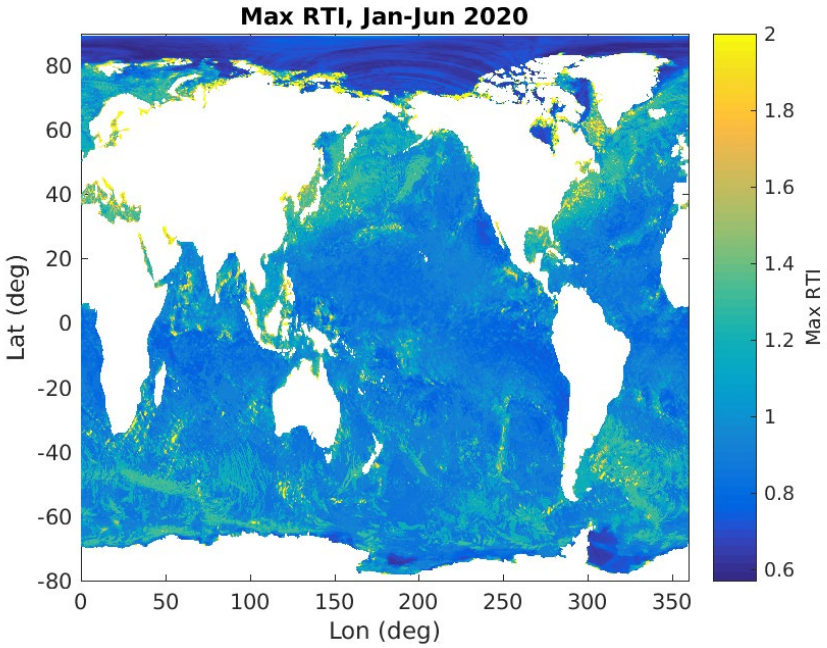


Figure 2. Maximum values of RTI returned for global output of the 0-hr nowcasts from preoperational simulations. While RTI did not exceed 2.0 for most of the domain, a value of RTI = 10 was attained at 15 locations and a value in the range 8 < RTI < 10 was reached at 32 additional locations. Nearly all of these locations were either in the lower Arctic, very close to a land boundary, or both. As noted earlier, it is not recommended that this system be relied upon in shallower and/or coastal regions.

Title: Dynamics of Coupled Models
Author(s): I. Shulman, B. Penta, and S. Cayula
Affiliation(s): U.S. Naval Research Laboratory, Stennis Space Center, MS
CTA: CWO

Computer Resources: HPE SGI 8600 [NAVY, MS]

Research Objective: Improve our understanding of coupled bio-optical and physical processes in the coastal zone and the variability and predictability of the coastal ocean's optical properties on time scales of 1–5 days. Investigate the coupled dynamics of ocean bio-optical, physical, and atmospheric models. Provide a foundation for the development of scientifically valid, dynamically coupled atmosphere-ocean models.

Methodology: The approach is based on using nested, coupled physical-bio-optical models of the coastal region together with bio-optical and physical in-situ and remotely sensed observations. Data assimilation techniques for both physical and bio-optical fields are being used to examine project research issues and objectives. Approach is also based on joint studies of the bioluminescence (BL) potential and inherent optical properties (IOPs) over relevant time and space scales. Dynamical, biochemical, physical, and BL potential models are combined into a methodology for estimating BL potential and nighttime water leaving radiance (BLw).

Results: We published a refereed paper "Modeling studies of the bioluminescence potential dynamics in a high Arctic fjord during polar night" and submitted a refereed paper "Bioluminescence potential during polar night: impact of behavioral light sensitivity and water mass pathways." We demonstrated that the highest bioluminescent emissions for offshore stations are located at depths below the reported irradiance thresholds for the behavioral light sensitivity of krill and copepods and that behavioral light sensitivity is one of the reasons for high values of BL potential observed below 100 m at offshore stations. In order to understand sources of bioluminescent taxa responsible for the observed high values of BL potential in offshore waters, we have investigated the origin and pathways of water masses circulating to the north, offshore of the fjord Rijpfjorden (Svalbard, Norway) by using a hydrodynamic model. The model water masses mostly originate from the west, where the Atlantic water is flowing northward, then along the shelf and the shelf slope of northern Svalbard, and offshore of the fjord (Fig. 1). This indicates that the advection of zooplankton by North Atlantic water is one possible source of bioluminescent organisms offshore of northern Svalbard.

DoD Impact/Significance: Emerging Navy electro-optical (EO) systems under development and special operations missions require an improved understanding of the ocean optical environment. This is critical for operations and weapon deployment, especially in the coastal and littoral zones. Improved basin-scale-to-mesoscale forecast skill is critical to both military and civilian use of the oceans, particularly on the continental margins.

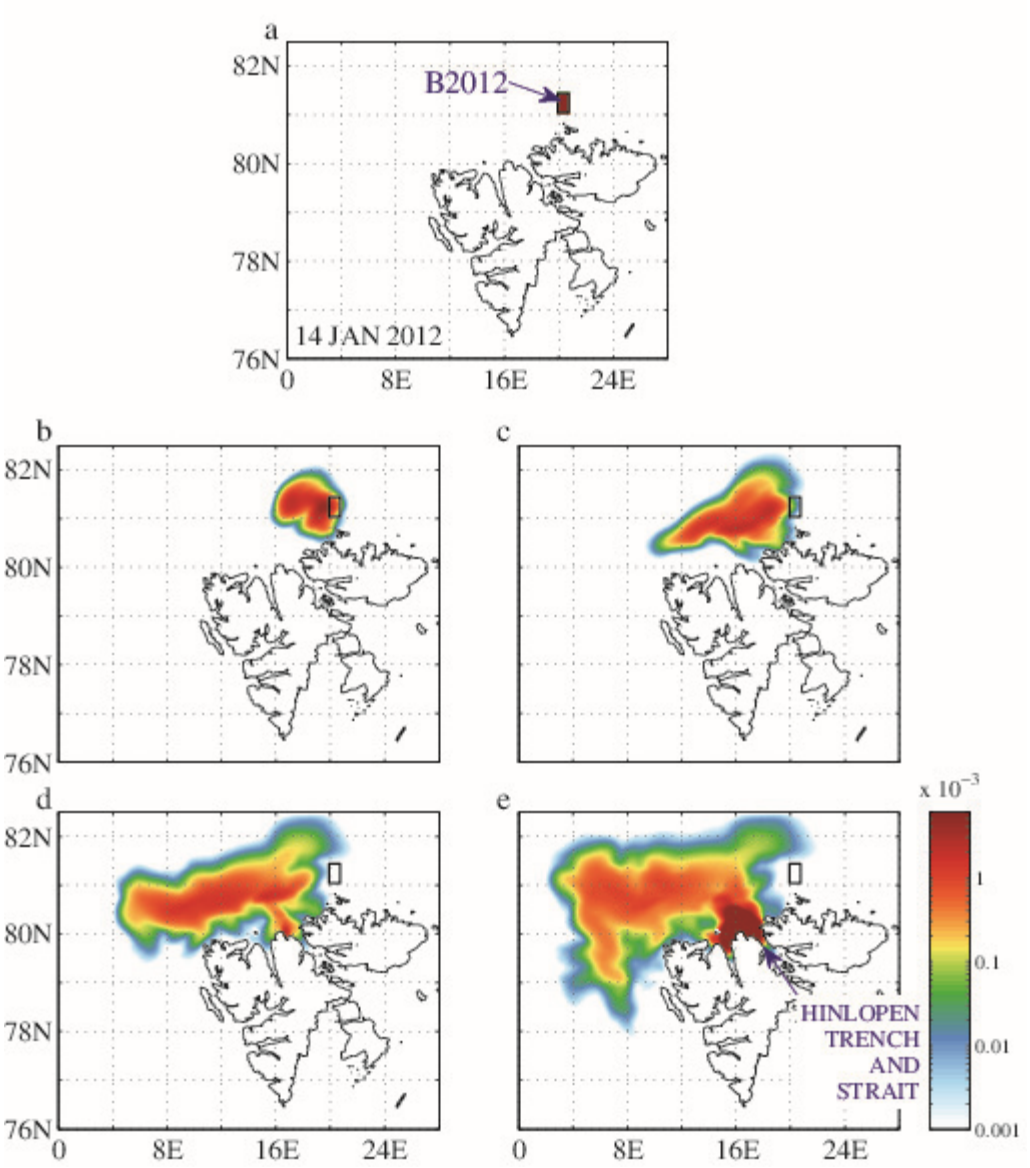


Figure 1. Adjoint distribution maps for the Polar night of 2012. (a) Initial distribution of the adjoint, (b) distribution of the adjoint after 4 days of integration (vertically integrated adjoint for each model grid normalized by the volume of the area of interest), (c) as in (b), but after 10 days of integration, (d) as in (b), but after 20 days, and (e) as in (b), but after 30 days of integration. Those adjoint maps show areas where the model tracer-tagged water masses were 30, 20, 10, and 4 days before circulating into the area of interest (red box around station B2012).

Title: Ocean Data Assimilation - Deterministic and Predictability of Mid-Frequency Acoustic Ducts
Author(s): J.J. Osborne,[1] C.M. Amos,[2] and G.A. Jacobs[1]
Affiliation(s): [1]U.S. Naval Research Laboratory, Stennis Space Center, MS; [2]American Society for Engineering Education, Stennis Space Center, MS
CTA: CWO

Computer Resources: Cray Shasta, HPE SGI 8600 [NAVY, MS]

Research Objectives: This project addresses several issues, with purposes of quantifying observed vertical gradients and inversions of temperature and salinity and then using this information to improve their representation in ocean models. Temperature inversions are parcels and layers of warm water that are warmer than water immediately above and below — in contrast to the canonical mode of temperature decreasing from the surface to the ocean floor. Inversions are associated with fronts and hence the interaction of different water masses. Using in-water observations, gradients and inversions are identified and characterized for location, spatial extent, water column position, seasonal variability, coincident ocean features, etc. Using computer models run on DoD HPC resources, model gradient characteristics are identified and compared against observations to understand deterministic and statistical predictability. Additional work will combine high-resolution observations and models via new data-assimilation approaches to better initially place and then temporally evolve ocean features that control vertical gradients and inversions.

Methodology: An iterative feedback approach is used to reach the science objectives, with analysis of observations leading to 1) identifying the deficiencies of standard ocean model configurations in the study area (US West Coast/northeastern Pacific Ocean) and 2) hypothesizing and testing new configurations to address these deficiencies. Further, a field experiment has been executed (July–August 2022) to specifically observe and characterize vertical gradients over the continental shelf and has been supported in real time with both standard configuration and high-resolution test configuration models. More specifically with the models, the standard configuration model had 3 km horizontal resolution and 50 vertical levels (with 30 levels in the upper 225 meters). In contrast, the high-resolution model has 1 km horizontal resolution and 100 vertical levels (with 47 levels in the upper 250 m). Most critically, the finer vertical resolution resolves vertical gradients of temperature and salinity at the depth range (50–150 m) where the largest gradients occur and temperature inversions are frequent.

Results: A major result to date is identifying that maximum gradients of temperature and salinity are observed to be typically offset in the vertical, with the maximum temperature gradients typically near 50 m depth in summer, while the maximum salinity gradient is deeper, at 125 m depth. This is shown in Fig. 1. This is significant because it indicates that a wide range of depths must be resolved to accurately resolve both temperature and salinity vertical gradients. Further, we have confirmed that ocean models that are assimilating observed gradients (through in-water temperature and salinity data) are able to capture the offset, but not necessarily at the correct depth level. Further, assimilating the observed gradients is critical for capturing the magnitude of the gradient.

DoD Impact/ Significance: These experiments will demonstrate a model configuration for accurately forecasting temperature and salinity vertical gradients at tactically relevant scales. If successful, NRL will propose new standards for ocean model configuration, providing warfighters and reach-back units with accurate ocean vertical structure that is fundamental for understanding underwater acoustics.

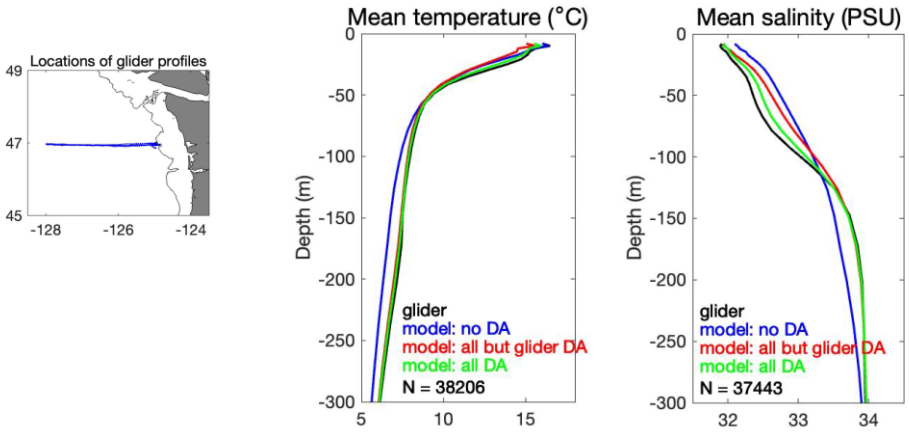


Figure 1. (Left) Location of in-water glider observations, summer 2020. (Center) mean temperature profile from observations (black), free-running non-assimilative model (blue), model assimilating all data except glider data (red), and model assimilating all data including glider data (green). (Right) mean salinity profiles. The experiment assimilating glider data (green) best matches the depth of maximum observed gradients and the magnitude of the observed gradients.

Title: Ocean Data Assimilation – GHOST and Multi-Scale/Multi-Physics
Author(s): J. D'Addezio,[1] G. Jacobs,[1] C. Barron,[1] L. Smedstad,[1] S. Smith,[1] J. Crout,[3] R. Linzell,[3] I. Souopgui,[2] M. Carrier,[1] C. Dehaan,[3] and H. Ngodock[1]
Affiliation(s): [1]U.S. Naval Research Laboratory, Stennis Space Center, MS; [2]University of New Orleans, Stennis Space Center, MS; [3]Peraton Inc., Stennis Space Center, MS
CTA: CWO

Computer Resources: Cray Shasta, HPE SGI 8600 [NAVY, MS]

Research Objectives: Currently, the Navy ocean multiscale 3DVAR capability (NCODA v5.0) is being transitioned to Navy operations. In this configuration, two analysis steps are performed for two different horizontal scales. However, the same vertical physics are used in both analysis steps despite the knowledge that vertical physics differ in each horizontal regime. The goal of this project is to derive observation- and model-based vertical physics in these two different horizontal regimes. In a future implementation of the multiscale 3DVAR, these scale-dependent vertical physics can be used in each of their corresponding steps of the multiscale 3DVAR.

Methodology: To begin, we require a way to derive observation- and model-based vertical physics in each of the two horizontal regimes used in the multiscale 3DVAR. This was done by leveraging work from two projects: NASA's Sub-Mesoscale Ocean Dynamics (S-MODE) and ONR's "Towards Full-Spectrum Ocean Prediction using Submesoscale Covariances." Corresponding with the sampling performed by S-MODE, 10 Naval Oceanographic Office (NAVO) gliders were deployed in the California Current System (CCS) off of San Francisco (Fig. 1). Global Heterogenous Observation System (GHOST) automation was used to drive the gliders utilizing the model to direct the glider platforms to areas where model errors were large. Over the course of two months, the gliders made multiscale observations of the region. Using those observations, we were able to convert the glider time series to distance series. Using the distance series, we calculated the horizontal scale down to which the model was tenable and used this value to partition the glider temperature and salinity into large- and small-scale components. The corresponding model data were sampled at the glider locations and were partitioned in the same way. With these data, we then calculated scale-dependent vertical physics.

Results: Scale-dependent temperature depth-depth cross-correlations are shown in Fig. 2. The "constrained" column shows the large-scale results and the "unconstrained" are the small-scale results. The top row is for observations and the bottom row is for the model. The large-scale correlations are highly similar between the observation- and model-based results. There is primarily a two-layer structure: a shallow layer corresponding with the mixed layer and a deeper layer corresponding with the thermocline. The small-scale results are also highly similar between the observations and the model. There is primarily a one-layer structure with weak off-diagonal elements, suggesting low correlation between any two depths.

DoD Impact/Significance: These results can be used to develop a multiscale, multiphysics 3DVAR system. This is in contrast with the current operational version of the multiscale 3DVAR that uses the same vertical physics in each of the two steps of the assimilation. This is expected to produce a better analysis, particularly for the smaller scales. This is important because smaller scales begin to approach "tactical" scales that are important for Navy operations that include search and rescue, drift prediction, and acoustic transmission.

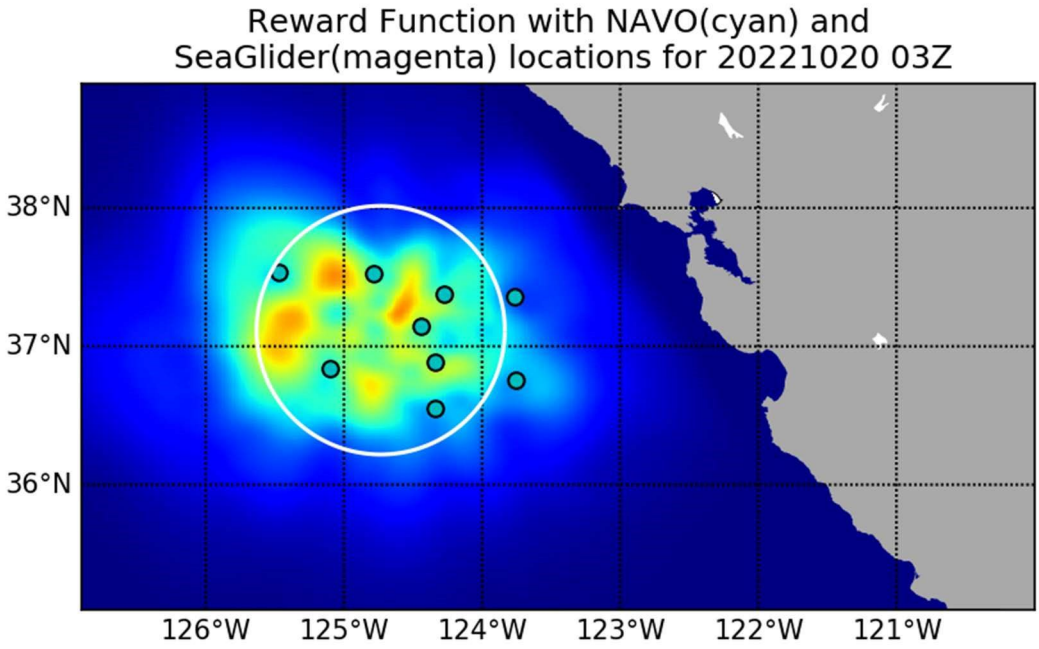


Figure 1. GHOST-based sampling of the California Current System during the 2022 S-MODE deployment. The color shows the reward function (where the gliders are incentivized to go) and the magenta dots show the glider locations for the given day.

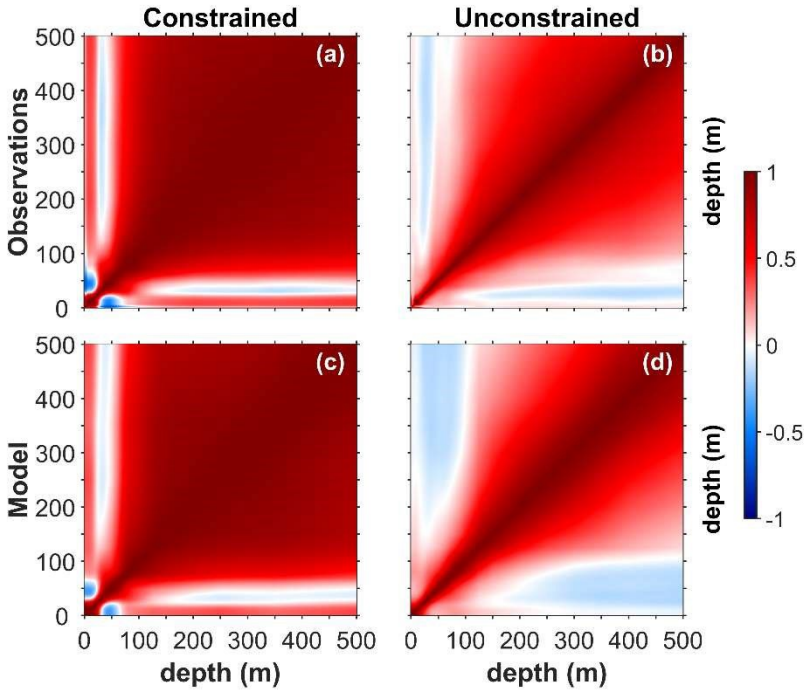


Figure 2. Temperature depth-depth cross-correlations in the (left column) constrained and (right column) unconstrained bands. (a) and (b) Glider-derived constrained and unconstrained temperature depth-depth cross-correlations. (c) and (d) Model-derived constrained and unconstrained temperature depth-depth cross-correlations.

Title: Ocean Data Assimilation – NCODA-4DVAR
Authors: M. Carrier,[1] S. Smith,[1] J. D'Addezio,[1] H. Ngodock,[1] J.J. Osborne,[1] I. Souopgui,[2] V. Montiforte,[3] C. Amos,[3] and C. Rowley[1]
Affiliations: [1]U.S. Naval Research Laboratory, Stennis Space Center, MS; [2] University of New Orleans, Stennis Space Center, MS; [3]American Society for Engineering Education, Stennis Space Center, MS
CTA: CWO

Computer Resources: Cray Shasta, HPE SGI 8600 [NAVY, MS]

Research Objectives: A four-dimensional variational (4DVAR) data-assimilation system is in transition to operations at the Fleet Numerical Meteorology and Oceanography Center (FNMOC). This 4DVAR capability differs from the currently operational three-dimensional variational (3DVAR) system in that, in addition to the spatial variation of the model and observations, the analysis takes the temporal variation into account as well. This allows for assimilating observations over a time window rather than all at once, thereby allowing more observations to influence the analysis.

Methodology: The Navy Coupled Ocean Data Assimilation system (NCODA) 4DVAR system employs a four-dimensional background error covariance, which allows the system to incorporate the spatial-temporal variability of the forecast model and observations while also preserving and enforcing specific dynamical balance constraints on the resulting ocean analysis that is produced. This not only allows for the assimilation of many more observations, but also reduces initialization shocks that can occur when the forecast model is adjusted by observations through data assimilation. The four-dimensional background error covariance is modeled, rather than explicitly computed, by employing the use of two model operators: the tangent linear and adjoint models, both of which are based directly on an ocean model (in this case, the Navy Coastal Ocean Model, or NCOM). These models are used in concert with each other during the analysis procedure to spread observation information through the ocean model domain in both time and space and they also act to impose dynamical balance constraints on the final ocean analysis.

Results: The NCODA-4DVAR system is tested in a real-data experiment within the Northeast Atlantic domain during a three-month period from June 2019 through August 2019. During this time period, there is a substantial amount of spatially and temporally dense observations that are available for assimilation and forecast verification. The NCODA-4DVAR system is run parallel with the operational NCODA-3DVAR system during this time period and the resulting 24-hour forecast from each analysis is compared to available observations. It is found that both systems perform in a statistically similar manner when compared to the sparse ARGO profiling float observations, but that 4DVAR significantly outperforms 3DVAR when compared to the temporally and spatially dense glider observations (Figs. 1 and 2).

DoD Impact/Significance: With the expectation of more temporally and spatially dense observations becoming available over the next few years, it is vital that the Navy take full advantage of these data sets in order to constrain and improve their ocean model forecasts. The NCODA-4DVAR system will allow for using more of this data in a dynamically consistent manner that will help to improve the ocean model analysis and resulting forecast as well. The 4DVAR method will also allow for the assimilation of new data types (e.g., velocity, direct assimilation of sea surface height) that will help to continue to improve the Navy ocean model forecast accuracy.

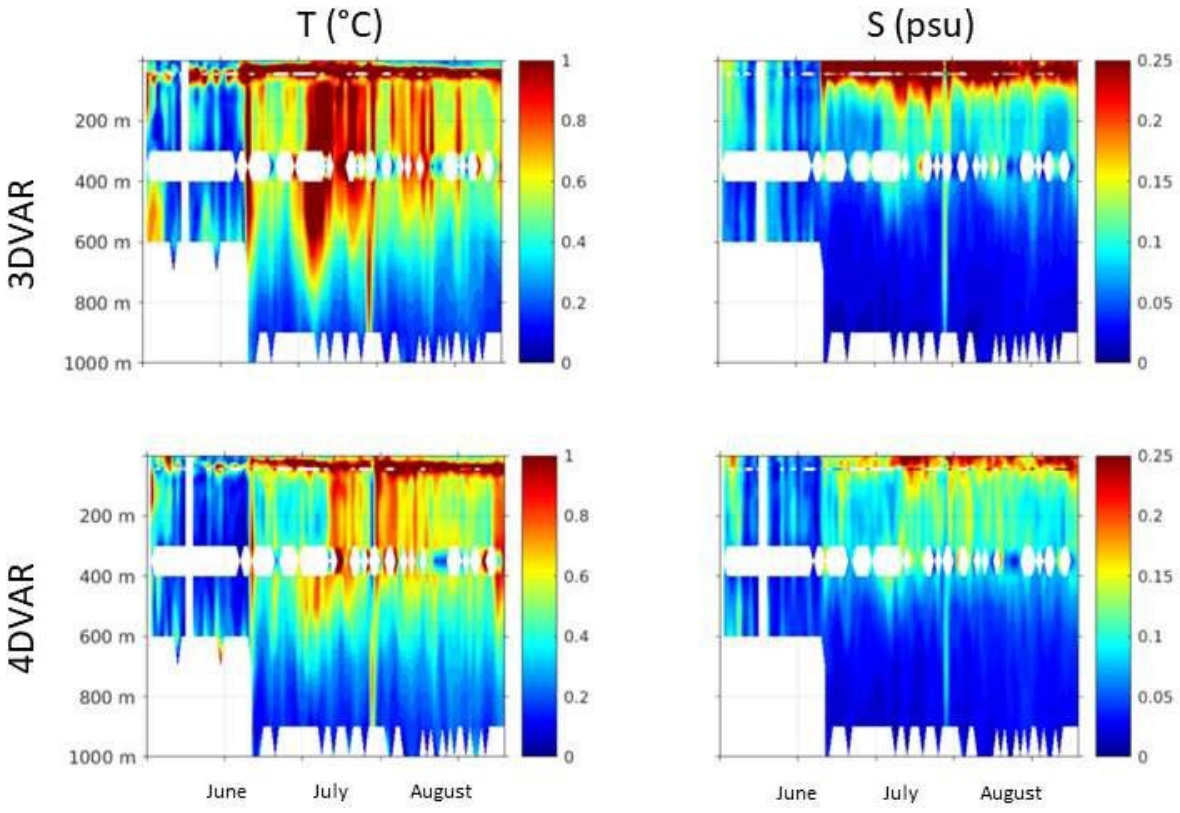


Figure 1. Daily profile root mean square error (RMSE) between the 24-hour forecast from 3DVAR (top panels) and 4DVAR (bottom panels) for temperature (left panels) and salinity (right panels) as compared to in-situ ocean profile observations.

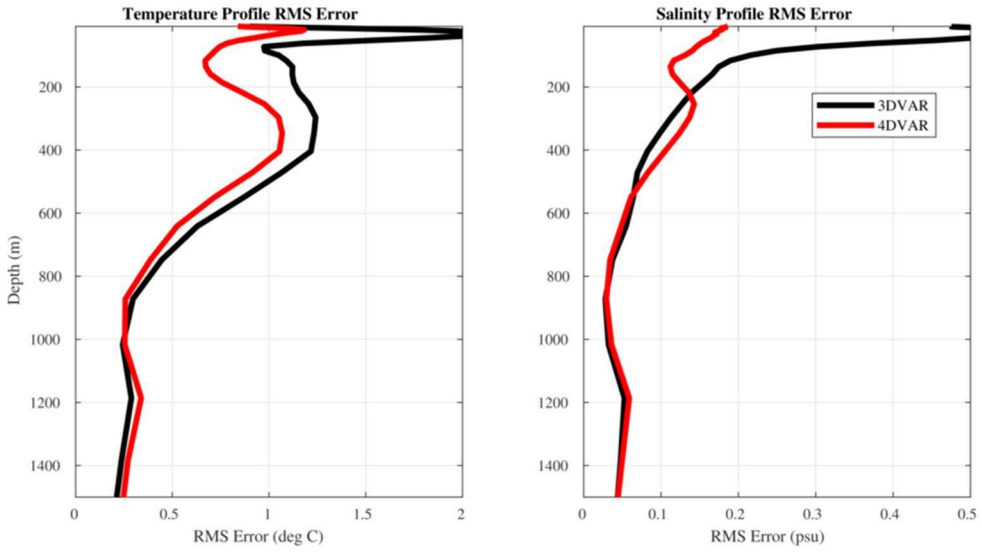


Figure 2. Overall profile RMSE in temperature (left panel) and salinity (right panel) for 24-hour forecast from 3DVAR (black line) and 4DVAR (red line) as compared to in-situ ocean profile observations from 1 June through 31 August, 2019.

Title: Ocean Data Assimilation – NCODAv5 and ALPS
Author(s): J. D'Addezio,[1] S. Smith,[1] G. Jacobs,[1] M. Carrier,[1] J.J. Osborne,[1] I. Souopgui,[2] H. Ngodock,[1] V. Montiforte,[3] and C. Rowley[1]
Affiliation(s): [1]U.S. Naval Research Laboratory, Stennis Space Center, MS; [2] University of New Orleans, Stennis Space Center, MS; [3]American Society for Engineering Education, Stennis Space Center, MS
CTA: CWO

Computer Resources: Cray Shasta, HPE SGI 8600 [NAVY, MS]

Research Objectives: A multiscale 3DVAR is currently being transitioned to Navy operations. The operational implementation performs only two analysis steps, thereby only correcting for two ocean horizontal scales. However, ocean horizontal scales are an unbroken continuum with the largest energy weighted toward the largest of scales. In order to better correct this continuum of scales, this project endeavors to add more than two analysis steps to the current multiscale system. This is expected to provide an initial ocean state that is both more accurate and more consistent with the scales present in the true ocean.

Methodology: At the time of this writing, NASA's Surface Water Ocean Topography (SWOT) satellite is still not operational. Therefore, to conduct this experiment, we created a controlled experiment called an observing system simulation experiment (OSSE). This demands a "truth" to sample and assimilate into parallel but significantly different simulations. The "truth" was taken as a near-real-time run of the California Current System (CCS) southeast of San Francisco (Fig. 1). That simulation was sampled at real observation locations and times for the observation types we have available at the time of this writing. Those include nadir altimeters, satellite sea surface temperature (SST), and in-situ profiles of temperature and salinity. The "truth" was also sampled by the Jet Propulsion Laboratory's (JPL) SWOT simulator to generate realistic sampling based on the path SWOT will fly when operational (Fig. 1). These simulated observations were then assimilated into simulations starting from different initial conditions than the "truth." Finally, we utilized the in-transition NCODAv5 code to perform data assimilation in both single- and multiscale configurations.

Results: The results of three experiments are shown here: A single-scale assimilation of observations available at the time of this writing, a single-scale assimilation of observations available at the time of this writing and SWOT, and finally, a multiscale, two-step assimilation of observations available at the time of this writing and SWOT. Because the "truth" is known, we can calculate errors in space and at all times. Analysis and forecast time root mean square errors (RMSE) of temperature at 100 m are shown in Fig. 2. As was shown in experimentation and a recent validation test report, the magnitude of errors is reduced going from the single-scale experiment with only the available observations to the multiscale assimilation of SWOT (Fig. 2). This provides a baseline set of experiments for the simulations we intend to perform in FY23: multiscale assimilation of SWOT data with many more assimilation steps, specifically, up to nine, which is expected to fill in for the spatial scales missed when running only two analysis steps.

DoD Impact/Significance: The experiments are expected to chart a way forward for the future of Navy ocean multiscale assimilation methods. If successful, NRL will recommend that Navy operations run as many multiscale steps as is feasible based on computational restrictions. Increased analysis skill has consistently been shown to improve the placement and representation of fronts and eddies that are essential for making accurate predictions for search and rescue, drift prediction, and acoustic transmission.

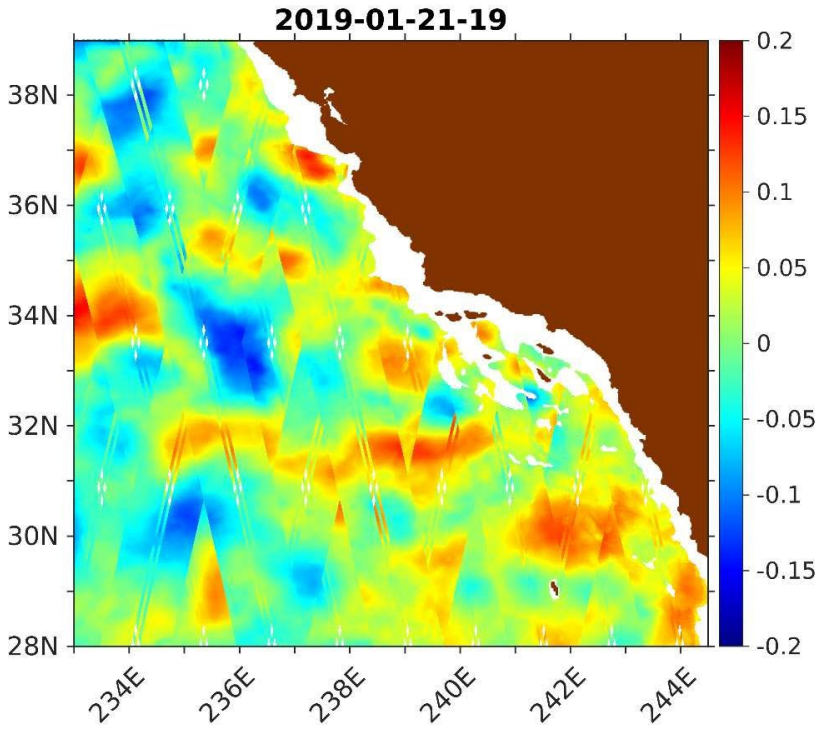


Figure 1. Simulated SWOT sampling of the California Current System (CCS).

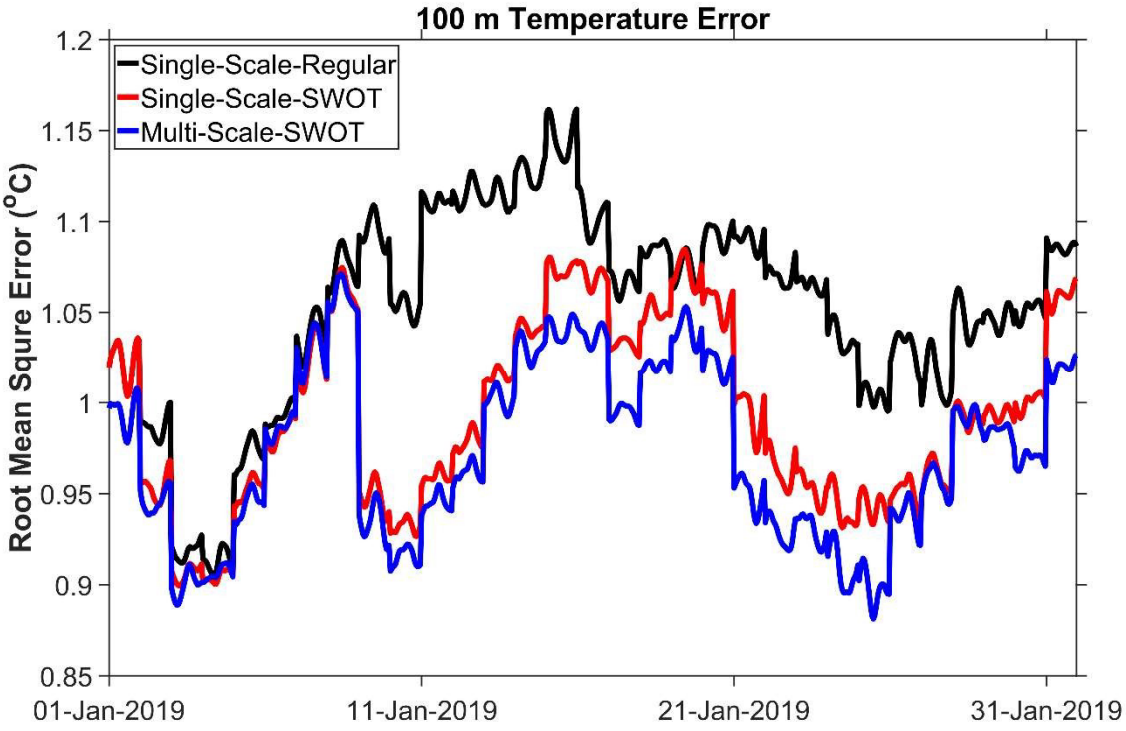


Figure 2. 100 m temperature root mean square error (RMSE) for three different OSSE experiments. SingleScale-Regular only assimilates the currently available observations. Single-Scale-SWOT includes simulated SWOT observations. Multi-Scale-SWOT is a two-step, multiscale assimilation of all data.

Title: Ocean Data Assimilation
Author(s): S. Smith,[1] J. D'Addezio,[1] J.J. Osborne,[1] I. Souopgui,[2], V. Montiforte,[3] M. Carrier,[1] G. Panteleev,[1] T. Townsend,[1] C. Amos,[3] S. DeRada,[1] L. Smedstad,[1] M. Phelps,[4] J. May,[1] R. Linzell,[4] E. Carr,[4] H. Ngodock,[1] and C. Rowley[1]
Affiliation(s): [1]U.S. Naval Research Laboratory, Stennis Space Center, MS; [2] University of New Orleans, Stennis Space Center, MS; [3]American Society for Engineering Education, Stennis Space Center, MS; [4] Peraton, Inc. Stennis Space Center, MS
CTA: CWO

Computer Resources: Cray Shasta, HPE SGI 8600 [NAVY, MS]

Research Objectives: The scope of this project is to advance the analysis-and-prediction capability of the Navy's environmental modeling and forecasting systems through the improvement of the assimilation software used to merge incoming observations with model forecast fields. Twelve funded NRL projects used this subproject in FY22 to perform experiments that went toward either using, adding, improving, or validating various capabilities of ocean data assimilation. In this report, we will focus on just two of these efforts: The 6.4 Determination of Asset Requirements (EDI) and the 6.1 Atlantic Ocean Deep Water Origins projects. Other efforts that were conducted in this project, such as those involving the 4D variational assimilation, multiscale 3DVAR, and the TFO projects, will be presented in separate reports.

Methodology: The purpose of the EDI project was to perform a series of high-resolution simulated assimilation experiments assimilating different distributions of float observations with the 3DVAR system. These experiments were performed in the northern Atlantic Ocean in a region that is very dynamic due to meandering eddies shedding off from the Gulf Stream. Collecting observations can be very difficult and expensive in this region; therefore, determining the optimal number and placement of profile observing platforms to produce an accurate prediction of mixed layer depth is beneficial. Another effort that was performed in the northern Atlantic Ocean as part of the Atlantic Ocean Deep Water Origins project was to examine how ice melt runoff affects the circulation along the eastern Greenland shelf. Sources of fresh, cold water were added to the model along the Greenland coast to represent the melting of ice during the warm months. Very-high-resolution experiments were performed with and without this runoff to determine if the inclusion of runoff produces the dynamics necessary to cause deep-water formation in this region.

Results: For the EDI project, a number of simulated experiments were performed on the DSRC assimilating a varying distribution of floats within a specific area of interest in the northern Atlantic Ocean. Figure 1 shows the time series of mixed layer depth (MLD) RMS error for December 2019 (top panel), January 2020 (middle panel), and February 2020 (bottom panel) within the area of interest for the nonassimilative run (solid black) and each of the four float deployment experiments. These results show that there is an overall improvement when more floats are used, but not by much, and it may not be worth the extra cost. For the Atlantic Ocean Deep Water Origins project, high-resolution experiments were performed on the DSRC to examine the runoff from ice melt along the Greenland coast. Figure 2 shows the concentration of a tracer field added at the runoff sources with and without runoff 2.5 months into the run. Comparison shows that the runoff causes a significant difference in circulation.

DoD Impact/Significance: The assimilation experiments tested under this project went toward improving the Navy's capability of forecasting the ocean environment and directly addresses Navy priorities as outlined in the following documents: OPNAVN2N6E FY 2021 RDT&E Priorities Letter 3062, Ser N2N6E/20U119707 (March 26, 2020), and the NRL ocean modeling road map developed in consultation with the Navy operational modeling centers NAVOCEANO and FNMOC.

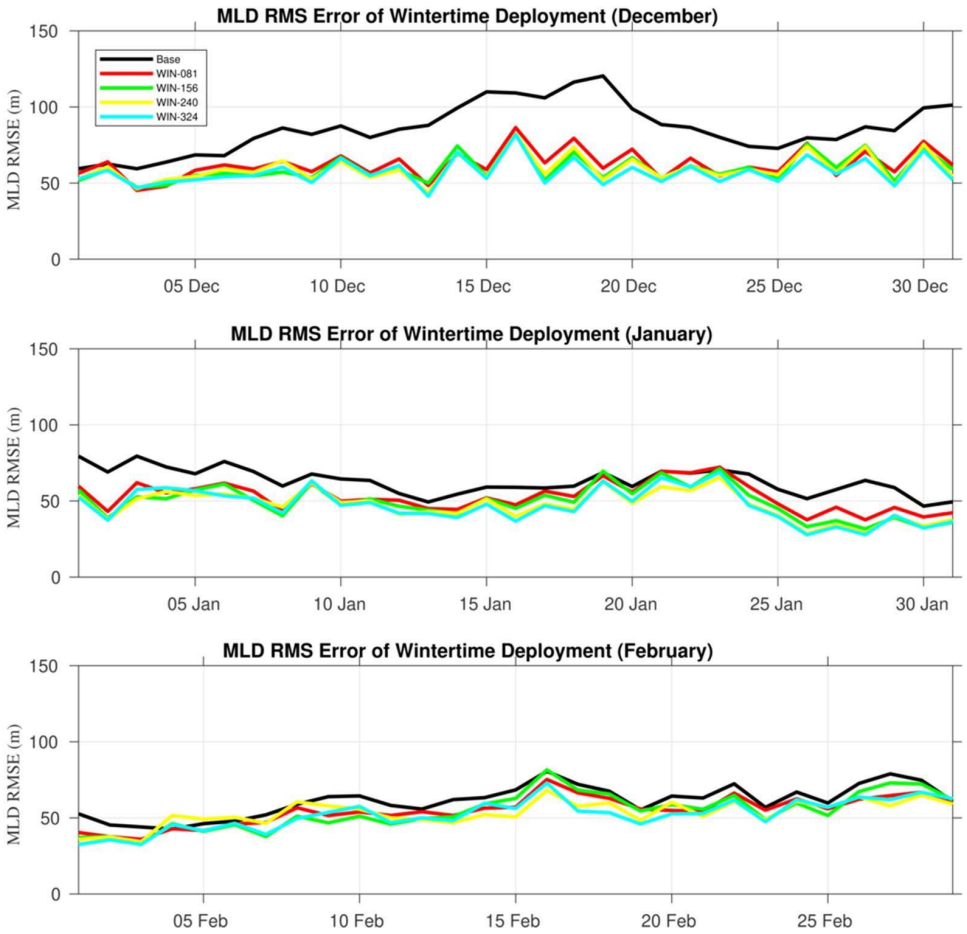


Figure 1. Mixed layer depth (MLD) root mean square error (RMSE) from 1 December 2019 through 29 February 2020 for the nonassimilative run (solid, black line) and each of the wintertime float deployment experiments (color lines).

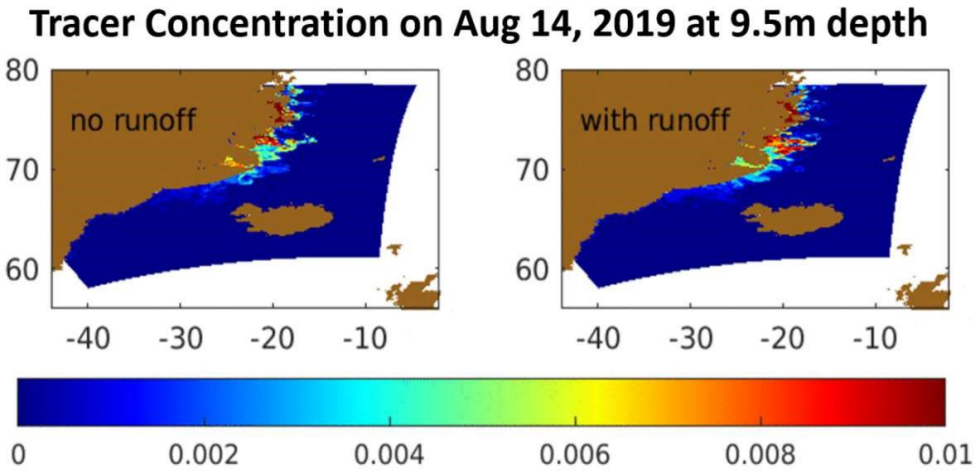


Figure 2. Tracer concentration at 9.5 m depth and 2.5 months after adding tracer fields to the model along the Greenland coast. The left panel is without any additional source of water from ice melt and the right panel does have additional source of water from ice melt.

Title: Data Assimilation Studies Project
Author(s): J. Tsu and W.F. Campbell
Affiliation(s): U.S. Naval Research Laboratory, Monterey, CA
CTA: CWO

Computer Resources: HPE Cray Shasta [AFRL, OH]; Cray Shasta, HPE SGI 8600 [NAVY, MS]

Research Objectives: Our objective is to improve the quality of Numerical Weather Predictions (NWP) by leveraging vast quantities of observations. Data assimilation (DA) corrects model analyses of the atmosphere, the ocean, or the surface using a nonhomogenous collection of observations. This project develops, tests, and improves 1) our 4D-Var assimilation system, which is coupled to the atmospheric global model NAVGEM (Navy Global Environmental Model) and is used by the Navy Earth System Prediction Capability (ESPC), 2) fully ensemble-based data assimilation, now including the ionosphere, 3) hybrid ensemble/4D-Var data assimilation, 4) 4D-Var data assimilation for the COAMPS® meteorological forecast model, 5) adjoint, tangent linear, and forecast sensitivity to observations, 6) coupled DA (atmosphere, ocean, sea ice, etc., together), 6) preparation for and test assimilation of new data types, both satellite and conventional, and 7) a new 3D-Var assimilation system compatible with the Navy Environmental Prediction System Utilizing the NUMA Core (NEPTUNE). Our goal is to assimilate traditional data (generally in situ, e.g., weather balloons, ship, aircraft, or buoy reports) as well as data from a variety of new sources (often spaceborne) efficiently and effectively to provide the best atmospheric analysis and ultimately to improve numerical weather forecast performance.

Methodology: A variety of experimental setups are used to develop and test our global and regional models and data-assimilation systems, as well as large datasets of in-situ and satellite-based observations for several summer and winter months.

Results: Since DA has a multitude of applications, numerous types of research takes place under this project using the Navy's latest global (Hybrid Ensemble NAVGEM, NEPTUNE) and mesoscale (COAMPS®) models, along with our global (NAVDAS-AR, hybrid NAVDAS-AR, and coupled hybrid NAVDAS-AR, JEDI) and mesoscale (COAMPS-AR) data assimilation systems. Results from FY22 research include 1) assimilating high-frequency radar wind retrievals into the COAMPS® model to improve coastal wind forecasts, 2) developing a unified observing system assimilation to generate new naval capabilities, 3) utilizing NAVGEM to explore the role of tropical cyclone (TC) synthetic observations on analysis and track forecasts, 4) development of an ionosphere data-assimilation technique using the SAMI3 ionosphere prediction model, 5) development of a cycling ensemble Kalman filter (EnKF) data-assimilation system for the SAMI3 ionosphere forecast model, 6) development of another EnKF but used in the Ensemble Navy Aerosol Analysis Prediction Systems (ENAAPS); this work will transition to operations at the DSRC in FY23, 7) development and evaluation of a 19-year-long high-resolution (T681L100) meteorological reanalysis and a ¼-degree, 3-hourly global multispectral reanalysis product for a broad spectrum of Navy applications, and 8) development of machine learning technique to dynamically assign observation errors to satellite observations and to improve NAVGEM forecast error.

DoD Impact/Significance: The computing platforms provided by HPCMP offer incredible computational resources which make possible the running of experiments involving millions of observations. These resources also provide a common environment for collaboration and the rapid development of NRL's multiple data assimilation systems. Large common datasets can be stored and accessed by many researchers, greatly facilitating collaboration between NRL scientists at different locations (Monterey, Stennis, and DC) and scientists in academia, government, and other laboratories. The advancements of NEPTUNE, JEDI, NAVDAS-AR, NAVGEM, and COAMPS-AR systems would not have been possible without the HPCMP systems. The core and future of Navy data-assimilation capabilities are being developed mostly, and in many cases solely, by using the resources provided by HPCMP. In summary, the ability to access the HPCMP resources is critical to prepare technology for successful transfer to operations.

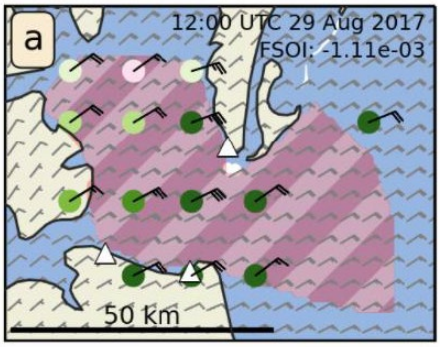


Figure 1. Pink, hatched area is footprint of the radar signal and black wind barbs are the quality-controlled HF radar wind retrievals on August 29, 2017, at 12:00 UTC. Green dots indicate these observations were beneficial to the COAMPS® model forecasts at 12-hour lead time. Gray wind vectors are from the COAMPS® model analysis.

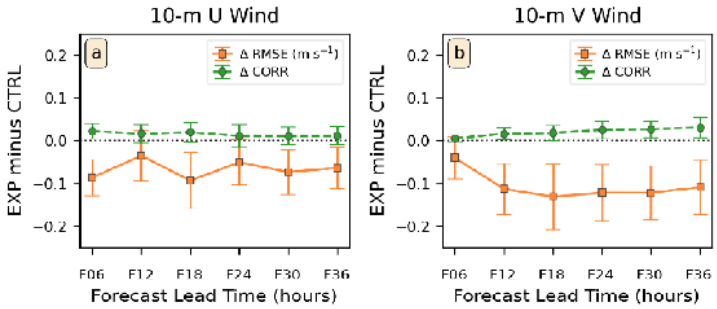


Figure 2. Assimilating HFR winds in COAMPS® model led to lower root-mean-square error and higher correlation coefficient in the forecasted *u* and *v* winds in the Chesapeake Bay domain.

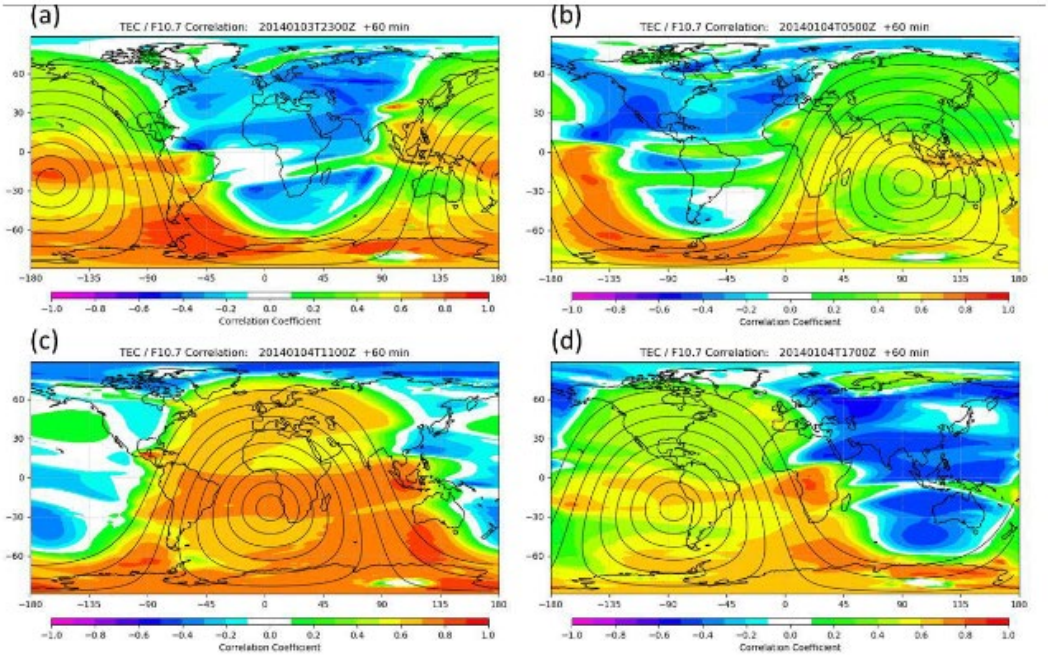


Figure 3. Prior ensemble correlation between vertical electron count (vTEC) and solar forcing parameter F10.7 on 1 Jan 2014 at (a) 0015Z, (b) 016Z, (c) 1215Z, and (d) 1815Z (shaded colors). Closed contours show the solar zenith angle between 0° and 80° , in increments of 10°. Highest correlations occur in the daylight section of the Earth.

Title: Atmospheric Process Studies
Author(s): T. Whitcomb,[1] N. Barton,[2] J. Christophersen,[3] W. Crawford,[1] M. Flatau,[1] K. Hansen,[3] M. Janiga,[1] M. Liu,[2] J. McLay,[1] J. Moskaitis,[1] C. Reynolds,[1] J. Ridout,[1] S. Rushley,[3] K. Viner,[2] S. Yang,[1] G. Carl,[4] and W. Davis[5]
Affiliation(s): [1]U.S. Naval Research Laboratory, Monterey, CA; [2]Departed/Retired from Naval Research Laboratory, Monterey, CA; [3]National Research Council, Monterey, CA; [4]SAIC, Monterey, CA; [5]DeVine Consulting, Monterey, CA
CTA: CWO

Computer Resources: HPE Cray Shasta [AFRL, OH]; Cray XC40/50 [ERDC, MS]; Cray Shasta, HPE SGI 8600 [NAVY, MS]

Research Objectives: The research objectives of this project are to improve our understanding of the fundamental dynamical and physical processes that operate in the atmosphere and to develop and test a state-of-the-art global atmosphere-prediction system that includes data assimilation and ensembles.

Methodology: Our methods and approach leverage the Navy Global Environmental Model (NAVGEM) in both stand-alone and coupled configurations. Our complementary approach is designed to simultaneously advance our R&D capability as well as the operational capability of U.S. Navy meteorological prediction. Improving the spatial resolution of the forecast model and improving the physical parameterizations to capture subgrid-scale processes enables improved fidelity of our predictive simulations. Postprocessing enables us to address persistent errors, yielding products with improved predictive skill. Coupled modeling allows us to exploit sources of predictability in the ocean and to better understand the role of air/sea interactions on atmospheric circulations. Ensemble forecasts provide us the capability to provide probabilistic guidance and to understand the uncertainty inherent in the prediction of the chaotic atmosphere.

Results: Our results in FY22 spanned from basic research to validation and verification in preparation for operational transition. We used HPC resources to explore the relationship between equatorially trapped Rossby waves in the ocean with atmospheric convection, developing diagnostic tools to evaluate the feedback processes associated with the waves. These analyses demonstrated model deficiencies in the air-sea coupling. We began diagnostics of physical parameterizations within the NAVGEM model to identify the source of persistent model biases in preparation for the next model upgrade and supported our operational partner with their operational implementation of the FY21 model upgrade.

We demonstrated that in an ensemble context, the analysis correction-based additive inflation (ACAI) is very effective at reducing model biases throughout the forecast. For postprocessing efforts, we were able to develop and validate a calibration prototype for the probability of turbulence severity. A key result was to identify that the postprocessing performed best when processing turbulence probabilities directly rather than postprocessing the constituent components (e.g., multiple levels of wind data).

DoD Impact/Significance: Improved models lead to improved forecasts. Improved forecasts provide better guidance for warfighters and decision makers to execute their mission. The Navy operates at the air/sea interface, and understanding the unique forecast challenges of this demanding environment allows naval operations to proceed safely with maximum mission effectiveness.

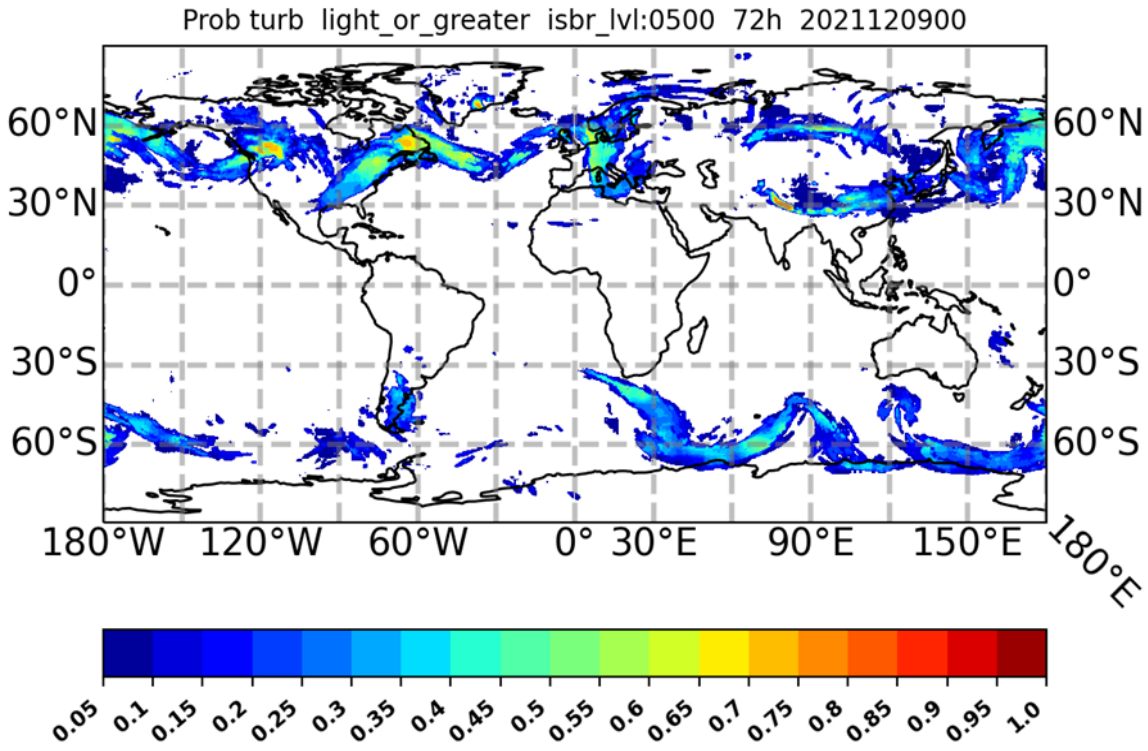


Figure 1. Calibrated (postprocessed) NAVGEM ensemble T+72h forecast probability of 500 hPa turbulence severity ≥ light category initialized 00UTC 09 Dec. 2021. The structure of the probability pattern reflects the underlying presence of vertical wind shear (associated with jet streaks and frontal zones) as well as zones of synoptic-scale deformation and convergence.

THIS PAGE INTENTIONALLY LEFT BLANK

SIP

Signal Image Processing

SIP covers the extraction of useful information from sensor outputs in real time. DoD applications include surveillance, reconnaissance, intelligence, communications, avionics, smart munitions, and electronic warfare. Sensor types include sonar, radar, visible and infrared images, and signal intelligence (SIGINT) and navigation assets. Typical signal-processing functions include detecting, tracking, classifying, and recognizing targets in the midst of noise and jamming. Image-processing functions include the generation of high-resolution, low-noise imagery and the compression of imagery for communications and storage. The CTA emphasizes research, evaluation, and testing of the latest signal-processing concepts directed toward these embedded systems. Usually, such processors are aboard deployable military systems and hence require hefty packaging and minimum size, weight, and power. System affordability is expected to improve by an order of magnitude through the development of scalable codes running on flexible HPC systems. This will enable the traditional expensive military-unique “black boxes” required to implement high-speed signal/image processing to be replaced by COTS HPC-based equipment.

Title: Applying Physics-based Machine Learning to Navy Problems
Author(s): L.N. Smith
Affiliation(s): U.S. Naval Research Laboratory, Washington, DC
CTA: SIP

Computer Resources: HPE Cray Shasta [AFRL, OH]

Research Objectives: The primary objective of our Physics-based Acoustic machine Learning for In-Situ Applications (PALIS) project in FY22 was the fast emulation of NRL's acoustics modeling simulations of transmission loss (TL). The secondary objective was compression of the input ocean acoustics field data for limited communication situations. Our technical approach made substantial progress with both objectives.

Methodology: This year's methodology was based on adapting the deep-learning method for computer vision known as image-to-image translation. In our acoustics domain, the input "image" represents undersea physical properties that impact how sound travels in the ocean. The output "image" is the TL predicted by the acoustics simulator. Since this type of emulation had never been done before in acoustics, our efforts included numerous aspects of the problem, such as the implementation approach, data preparation, data issues, performance measurements/metrics, neural network architecture, loss functions, hyperparameter optimization, data augmentation, intensity imbalance issues, and estimating the mean-square-error (MSE) of the predicted TLs.

Results: Our emulator obtained a speedup of over 500 times compared to the acoustic simulator. Specifically, the acoustic simulator required an average of 105 seconds over 13,000 runs, with a significant variance from one run to another (i.e., a minimum execution time of 1 second and a maximum of 3,700 seconds). On the other hand, inference with our emulator required only 0.20 seconds per sample for 1,676 samples, with the secondary benefit of essentially no variation in execution time from one run to another since the number of floating-point operations is independent of the input.

In addition, our approach (e.g., a variant of image-to-image translation) uses a generator architecture (e.g., U-net), which contains an input encoder. This encoder compresses the input into a series of feature vectors that the decoder contained in the generator uses to predict the TL. In our experiments, the compression of the encoder reduced to a fourth of its original size. We obtained this compression benefit without any effort on our part to balance the trade-off between compression and TL prediction performance. In FY23, we plan to investigate the Pareto optimality between compression and performance.

DoD Impact/Significance: Our work demonstrates that applying machine learning to acoustic problems is sound. We are now applying machine learning methods to solve other challenges in the acoustics domain in order to enable substantially improved environmental and situational understanding by our fleet. In addition, the understanding gained by the experiments on the HPC GPU servers builds on all the previous understanding gained from previous experiments, and this understanding is crucial for our future progress in the field.

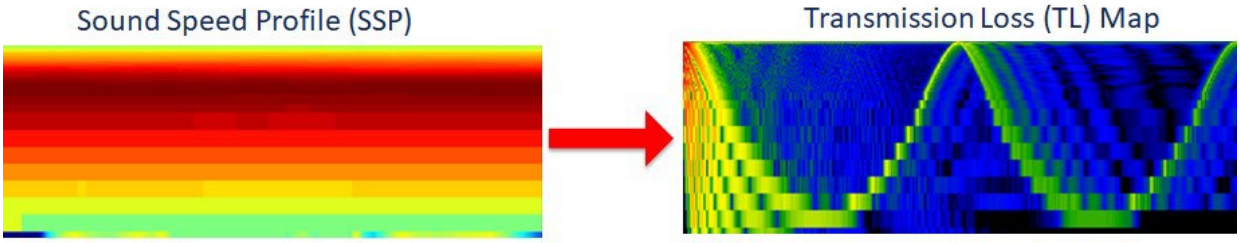


Figure 1. Our deep neural network (DNN) emulator of NRL's acoustic simulator is able to correctly predict the transmission loss (TL) from the simulator from the sound speed profile (SSP) but with a 500x speedup.

THIS PAGE INTENTIONALLY LEFT BLANK

SAS

Space and Astrophysical Science

Space and Astrophysical Sciences (SAS) research and development advance understanding, specification and prediction of the Earth's atmospheric and space domains to exploit the extended operational environment for military advantage and to minimize environmental impacts on military operations. The SAS Computational Technology Area (CTA) embodies the use of mathematics, computational science, and engineering in the analysis, design, identification, modeling, and simulation of the space and near-space environment and of all objects therein, whether artificial or natural. The SAS CTA encompasses foundational discovery research to study the atmospheres of the Sun and the Earth, including solar activity and its effects on the Earth's atmosphere and ionosphere and near-Earth space, and the unique physics and properties of celestial sources. SAS employs an extensive array of physical and empirical models and analysis tools to integrate observations and theoretical understanding for ever-improving DoD enterprises within, and exploitation of, the extended operational environment. The CTA melds the strengths of a broad range of physical sciences — atomic and molecular physics, materials science, plasma physics, applied optics, radiation survivability, electronic warfare, directed-energy technology, astronautics and space propulsion, orbital mechanics, space situational awareness, and remote sensing — into a structure that helps the DoD multiply force combat effectiveness.

Title: Electromagnetic Pulses from Hypervelocity Impacts on Spacecraft
Author(s): A. Fletcher
Affiliation(s): U.S. Naval Research Laboratory, Washington, DC
CTA: SAS

Computer Resources: SGI ICE X [ARL, MD]

Research Objectives: The objective of this project is to use large-scale simulations to understand electromagnetic pulses (EMPs) and other electrical effects that are associated with hypervelocity impacts (HVIs) on spacecraft and develop mitigation strategies.

Methodology: Hypervelocity impacts are simulated with two physical models: 1) a continuum mechanics approach for the formation of the crater and plasma, and 2) a kinetic electromagnetic plasma approach for microscale physics and emission of radiation. ALEGRA, a hydrocode from Sandia National Laboratories, is used for the continuum dynamics regime. VPIC, a particle-in-cell from Los Alamos National Laboratory, is used for the kinetic plasma regime. We run simulations to compare to both our theoretical predictions, in particular the generation of electromagnetic waves and interaction with the spacecraft potential, and to compare to experimental data from Van de Graaff experiments and NASA's Parker Solar Probe.

Results: This year, we applied the ALEGRA hydrocode to impacts that occur on NASA's Parker Solar Probe. Due to the speed of the probe and the meteoroids, the impacts are approximately two orders of magnitude larger than debris or meteoroid impacts on spacecraft surfaces in Earth orbit. This made the computation significantly more difficult because the grid must be larger and the time step is more restricted. We were able to calculate the plasma produced by these impacts, which provides an estimate for the measured electric field signals in the probe instruments. The simulations also provided distributions of dust ejecta from impact, which we are also attempting to correlate to images from the imager on the probe. Additionally, we simulated the motion of a charged impactor in space plasma in support of the design of a future in situ impact experiment. Under certain conditions, charged impactors can create solitons (which are solitary waves similar to shock waves in fluids) that can be used for diagnosis of debris and meteoroid properties. We showed that the solitons predicted by theory do appear in the simulation. The simulation also showed some of the two-dimensional (2D) and three-dimensional (3D) behavior that the theory cannot describe, which will be of use in designing the experiment.

DoD Impact/Significance: Protection of critical DoD space assets from this threat is necessary to ensure uninterrupted C4ISR capability, which is critical for operational success as envisioned in the Navy's S&T strategic plan for information dominance. Countermeasures against hypervelocity impacts of microprojectiles on DoD space assets depend on the knowledge of the electromagnetic power and frequency spectrum of the impact-associated EMPs.

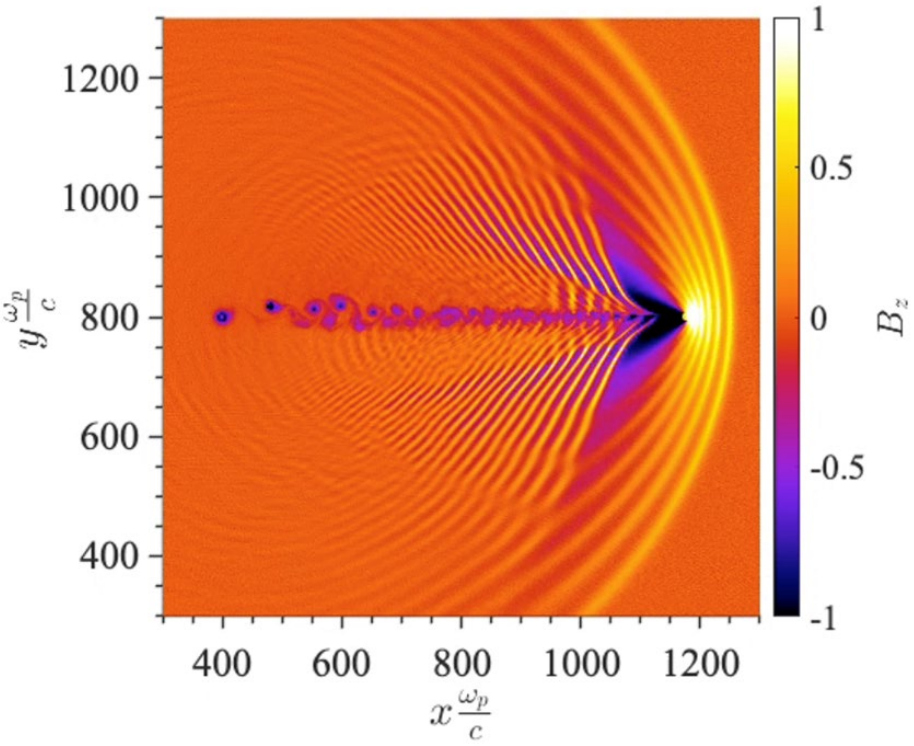


Figure 1. Magnetic field (out of the plane) created by a charged piece of debris moving at 110% of the Alfven speed of the background plasma. The debris is located at approximately (x,y) = (1150,800) and moving to the right. There are five precursor solitons propagating ahead of the debris. There is interesting behavior in the wake, including more structures and vortices in the perpendicular plane. The simulation is 8,000x8,000 grid cells and ~12 billion plasma particles.

Title: Global Kinetic Simulations of Space Plasma Waves and Turbulence
Author(s): A. Fletcher
Affiliation(s): U.S. Naval Research Laboratory, Washington, DC
CTA: SAS

Computer Resources: SGI ICE X [ARL, MD]; Cray Shasta [NAVY, MS]

Research Objectives: The objectives of this project are 1) to support an NRL and DARPA sounding rocket experiment program, SMART (space measurement of a rocket-released turbulence, whose launch has moved from fall 2021 to summer 2023), by helping to choose mission parameters and understanding the data from the experiment, and 2) to develop the capability to simulate near-Earth space plasmas on a global scale while including kinetic effects.

Methodology: We use a combination of four codes: 1) ALEGRA, a continuum dynamics code from Sandia National Laboratories, 2) VPIC, a particle-in-cell (PIC) code from Los Alamos National Laboratory 3) an NRL-built direct simulation Monte Carlo (DSMC) code, and 4) WICKED, a wave-in-cell (WIC) code developed at NRL. We will determine the density and optical/radar signature of the barium cloud, the amplitude and spectrum of the electrostatic and electromagnetic waves, and the rate of particle precipitation from the radiation belts. WIC, which could simulate the entire process, will need validation via comparable PIC runs. WIC will then be used to simulate as much of the cascade as possible within one simulation.

Results: This year, we performed a series of large three-dimensional (3D) PIC simulations of the ion ring instability using VPIC. These simulations were one of the primary goals of the project. The simulations verified the physics underpinning the SMART experiment. We found multiple pieces of evidence supporting the presence of nonlinear scattering, which is the key physics being tested by the rocket experiment in situ. Furthermore, we performed additional simulations varying the intensity of the instability and the background conditions (plasma beta). The behavior of the waves as the parameters changed also matched the theoretical predictions based on nonlinear induced scattering. We discovered new physics in the simulations as well. A key question was where the energy in the barium beam goes. We were able to partition the energy between the plasma waves and the thermal energy lost to the background. It was found that the electrons heat thermally (as expected) but the ions do not. The ions gain a non-Maxwellian distribution function, likely due to stochastic heating. We have implemented additional diagnostics to study the particle-wave interaction mechanism in more detail.

DoD Impact/Significance: The SMART experiment and associated simulations will study turbulence in the ionosphere coupling to waves in the magnetosphere. Given the DoD/Navy reliance on spaceborne assets, understanding the space environment is critical to assure uninterrupted C4ISR capability and maintain information dominance.

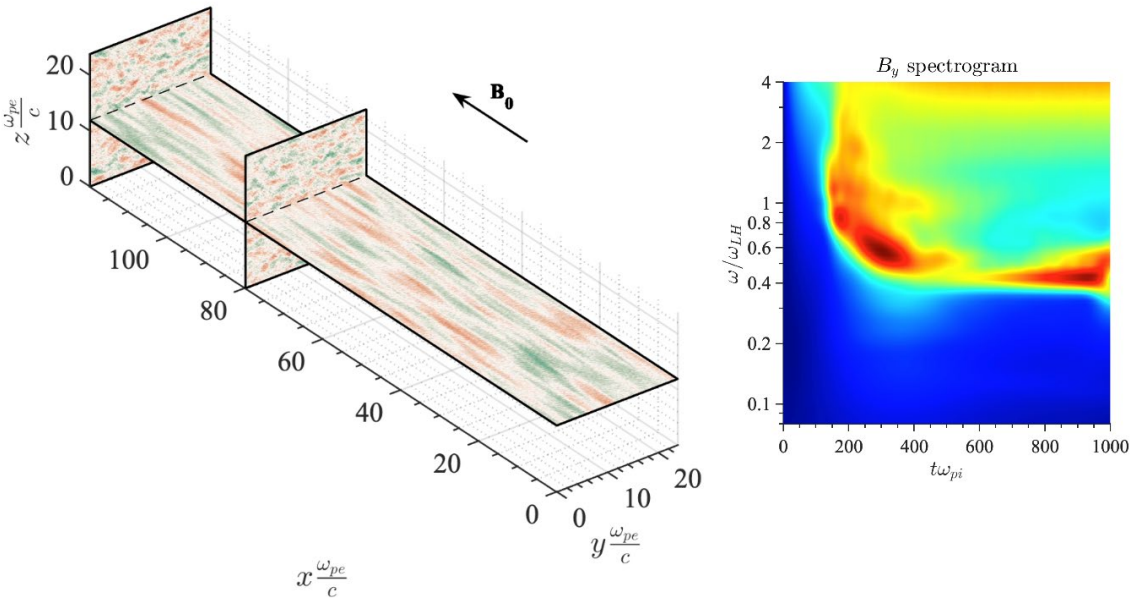


Figure 1. Snapshot of the magnetic field (in the y direction) from a three-dimensional (3D) VPIC simulation of the ion ring instability is on the left. One can see short-wavelength waves in the perpendicular plane (y-z plane) and long wavelengths parallel to the background magnetic field in x. The spectrogram of this field for the entire simulation is shown on the right. This spectrogram helps verify the theory that underpins the SMART sounding rocket experiment. Two sets of electrostatic waves near the lower hybrid frequency are visible at early times, with nonlinear scattering from the higher-frequency wave to the lower-frequency waves. At later times, there is an electromagnetic wave at lower frequency. This is the wave that will be measured far away from the source region in the experiment.

Title: Modeling Propagation of Ionospheric Disturbances Initiated by Magnetospheric Substorms
Author(s): J. Haiducek and J. Helmboldt
Affiliation(s): U.S. Naval Research Laboratory, Washington, DC
CTA: SAS

Computer Resources: HPE SGI 8600 [AFRL, OH]

Research Objectives: This program aims to develop a data-assimilation capability to enable simulation of traveling ionospheric disturbances (TIDs) using the NRL-developed SAMI3 (SAMI3 is Another Model of the Ionosphere). We aim to assimilate total electron content (TEC) observations collected by the Very Large Array (VLA) Low-Band Ionosphere and Transient Experiment (VLITE), a joint effort by NRL and the National Radio Astronomy Observatory. VLITE provides exceptionally high-fidelity TEC observations that have been shown to capture TIDs in detail. These observations will be complemented by GNSS TEC observations that provide global coverage, but at lower precision and spatial resolution than VLITE. By assimilating both datasets into an ensemble of SAMI3 simulations, we aim to develop an improved understanding of ionospheric dynamics, including TIDs.

Methodology: To assimilate TEC observations into SAMI3, we have developed a parallel data-assimilation tool called LightDA. LightDA provides extensible interfaces to support ensemble data assimilation in a model-agnostic manner. This allows us to test the data-assimilation algorithms separately from the specific model, enabling rapid testing of the framework before it is applied to the larger problem of TEC assimilation with SAMI3. On top of the basic interfaces of LightDA, we implemented an ensemble Kalman filter based on code from the Parallel Data Assimilation Framework (PDAF), testing it with a one-dimensional (1D) advection solver before applying it to SAMI3. We implemented a forward operator that computes vertical TEC from the SAMI3 state. We use cylc to manage the overall process of executing the SAMI3simulations, fetching data for assimilation, and invoking LightDA to update the SAMI3 ensemble.

Results: We conducted parallel scaling tests of LightDA on Mustang, as shown in Fig. 1. We obtained linear speedup for the overall system for up to a few hundred MPI processes, with limited improvement beyond that point (upper left panel). When we looked at the assimilation filter alone without including the time for other tasks, we found a linear speedup to 5,000 processes (upper right panel). The overall speedup was limited by less robustly parallelized tasks, such as disk i/o to read and write the SAMI3 ensemble states (lower right panel). Figure 2 shows the assimilated TEC observations and the corresponding values predicted by SAMI3. Across the two-hour period shown, the assimilation system kept the ensemble mean within a few TECU of the observed values and reproduced the downward trend seen in the observations.

DoD Impact/Significance: TIDs can influence the production of equatorial spread F, which can significantly degrade the accuracy of GNSS-based positioning. Even in the absence of secondary effects, TIDs can impact GNSS applications requiring centimeter-level precision. The assimilative modeling capabilities developed by this program will contribute to predictive capabilities that can be used to provide advance notice of TIDs and other ionospheric processes and their impact on navigation and communications.

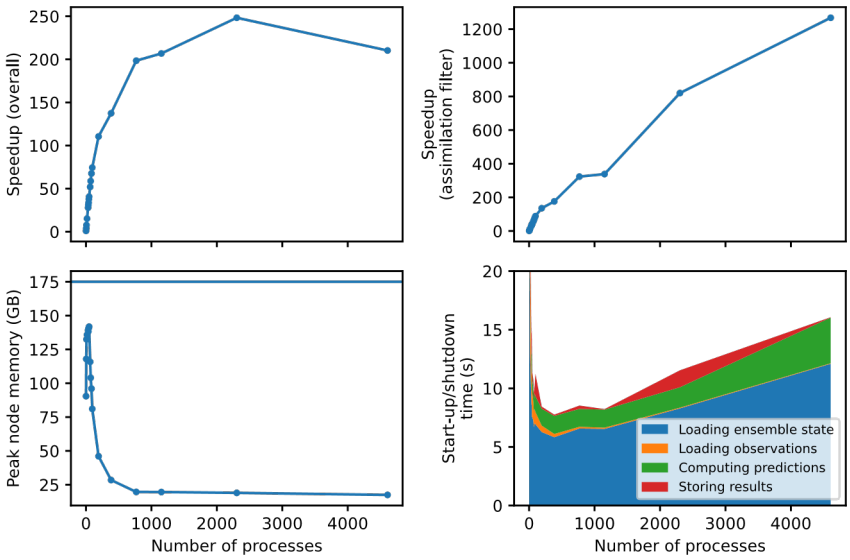


Figure 1. Scaling test results for 4,000 to 5,000 MPI processes. Upper left: speedup of the overall LightDA system. Upper right: speedup of the ensemble Kalman filter. Lower left: maximum per-node memory usage, with a horizontal line denoting the 175 GB per-node memory limit. Lower right: time required for other tasks (excluding the filter itself).

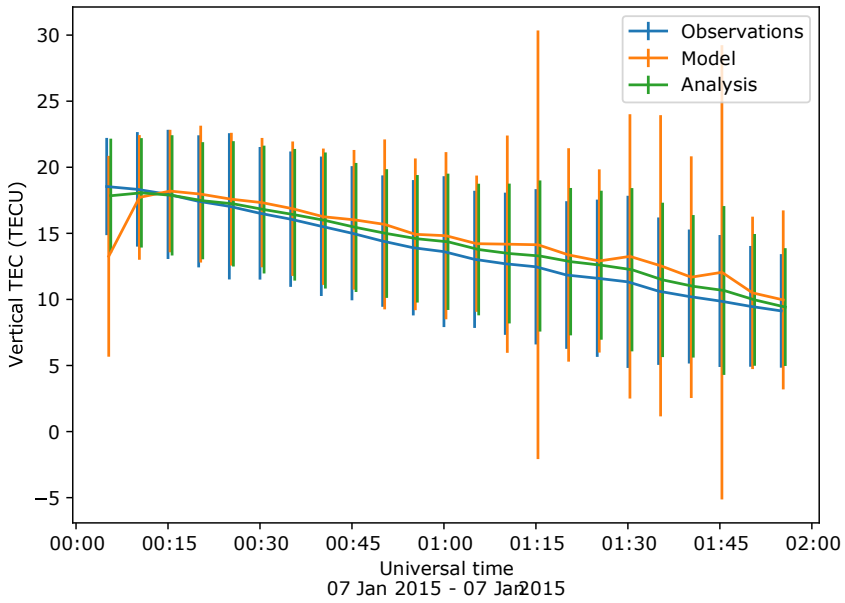


Figure 2. Time-series of vertical TEC. Blue curve shows the mean of observations assimilated into the ensemble, orange curve shows the mean of the ensemble TEC predictions before assimilation, and green curve shows the ensemble mean after assimilation. Error bars depict the standard deviation of each dataset.

Title: Navy Ionosphere Model for Operations
Author(s): S.E. McDonald,[1] C.A. Metzler,[1] F. Sassi,[1] J.L. Tate,[2] M.R. Burleigh,[1] D. Hodyss[1]
Affiliation(s): [1]U.S. Naval Research Laboratory, Washington, DC; [2]Computational Physics, Inc., Springfield, VA
CTA: SAS

Computer Resources: Cray XC40/50 [ERDC, MS]; Cray Shasta, HPE SGI 8600 [NAVY, MS]

Research Objectives: The objective of this effort is to develop a physics-based ionosphere model coupled to an ionospheric data-assimilation system that provides global and regional electron density specifications and short-term forecasts (0 to 24 hours). This capability forms the basis of a future Navy operational ionospheric forecasting system, running at multiple resolutions and fully coupled to operational atmospheric forecast models. In FY22, the main objectives were to continue to improve our understanding of the lower atmospheric effects on the ionosphere using SAMI3 coupled to whole atmosphere models, including the Whole Atmosphere Community Climate Model Extended (WACCM-X), and to perform model tuning and validation of the Next-generation Ionosphere Model for Operations (NIMO).

Methodology: The Next-generation Ionosphere Model for Operations (NIMO) consists of a physics-based ionosphere model, SAMI3, and a three-dimensional variational (3DVAR) data-assimilation system (IDA4D) that can ingest a wide variety of ionospheric datasets. NIMO also includes couplers that use the Earth System Modeling Framework (ESMF) for interpolating the ionosphere and data assimilation grids. In the context of NIMO, SAMI3 uses an empirical thermosphere, MSIS 2.0. To explore the influence of the lower atmospheric weather on the ionosphere, we have developed and continue to refine an interface to external thermosphere models, including WACCM-X, a whole-atmosphere model that can be nudged with lower atmospheric data to simulate specific days.

Results: In FY22, we have used HPC resources to perform forecast simulations with NIMO in order to benchmark the current skill of the system. In these simulations, the SAMI3 forecasts are initialized with the assimilated ionospheric electron densities, and then the simulation runs unconstrained. Due to the highly driven nature of the ionosphere, the forecasts return to climatology within a few hours of the forecast. These results underline the need for skillful thermospheric forecasts that can be used in place of an empirical thermosphere model in order to improve the forecast skill of NIMO. We have continued to improve the coupling of SAMI3 to external thermosphere models and used these systems to investigate the influence of lower atmospheric weather on ionospheric structure. In particular, we have run SAMI3 with a high-resolution version of WACCM-X (0.47°×0.625° in latitude and longitude) for several different time periods. The longitudinal resolution of SAMI3 is 0.6° from ~63.6° to 136.5°W and 4° at the other longitudes. Figure 1 highlights variations in the appearance of depletions in total electron density (TEC) in the nighttime ionosphere west of South America that are aligned with the magnetic field. These depletions are very strong for the simulation of 24 October 2020, but were nonexistent the day before. The day-to-day variability demonstrated in the simulations is consistent with observations of such depletions. Further analysis of these results will advance our understanding of the drivers of ionospheric variability.

DoD Impact/Significance: Development of an operational ionospheric forecast model will aid in the numerical forecasting of high-frequency (HF) radio wave propagation through the Earth's atmosphere and ionosphere across the range of conditions relevant to DoD/Navy operations.

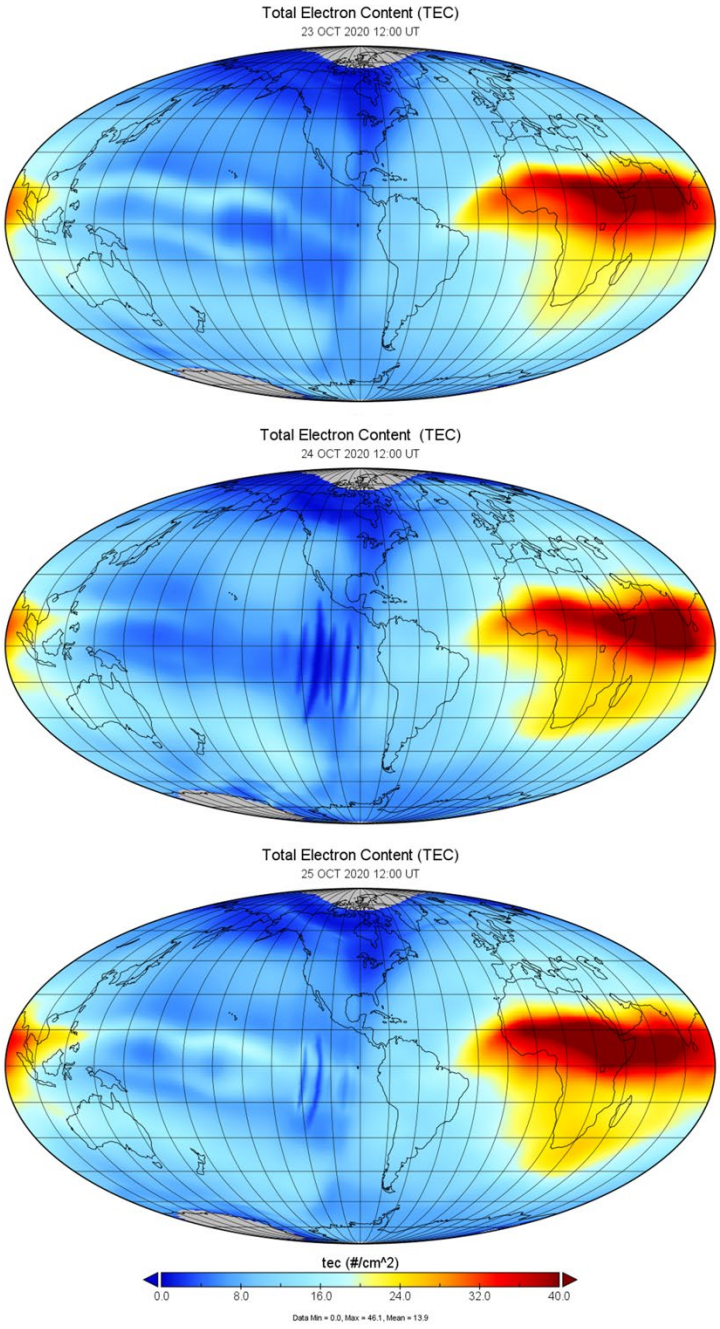


Figure 1. SAMI3/WACCM-X simulations of ionospheric global total electron content (TEC) shown at 12:00 UT on three consecutive days (23–25 October 2020). These simulations show day-to-day variability in the formation of large longitudinally aligned depletions in TEC west of South America during local nighttime. There are no depletions on 23 October, but they are present in the subsequent days. Such large-scale depletions in electron density can disrupt communication systems that transmit signals through impacted regions.

Title: Searches for Millisecond Pulsars and Pulsar Emission Modeling
Author(s): P.S. Ray[1] and J. Deneva[2]
Affiliation(s): [1]U.S. Naval Research Laboratory, Washington, DC; [2]George Mason University, resident at Naval Research Laboratory, Washington, DC
CTA: SAS

Computer Resources: Cray XC40/50 [ERDC, MS]

Research Objectives: The first goal of this project is to search for millisecond pulsars in radio observations made with the Robert C. Byrd Green Bank Telescope (GBT) in West Virginia. These searches require high-performance computing resources because of the massive parameter spaces that must be searched. The second goal of the project is to model the X-ray emission of pulsars based on data from the NICER X-ray telescope that is currently on the International Space Station.

Methodology: We use custom codes to search for pulsations in our radio data sets. These correct for frequency-dependent delays caused by interstellar dispersion and variable Doppler shifts caused by orbital acceleration in a binary system, then search over a broad range of candidate frequencies using very large Fourier transforms and harmonic summing. We split up the trials over a set of nodes on the cluster. We use another custom code to model pulsar emission. This is an iterative, computationally intensive process involving multithreaded calculations of the Bayesian likelihood of a number of model parameters.

Results: We used Onyx to fit several emission models of PSR J1231-1411. Each model includes known pulsar parameters, like the rotation period and pulse shape, and unknown parameters, like the pulsar's mass and radius, and the locations and shapes of the hot spots on the pulsar's surface that produce the X-ray emission. We built on our previous work by using NICER data in conjunction with data from XMM (the X-ray Multi-Mirror telescope, a spacecraft operated by the European Space Agency). While NICER is optimized for very precise time stamping of X-ray photons, XMM is optimized for collecting aggregate spectral data. This combined data set allowed us to more accurately model the emission of PSR J1231-1411. We also processed GBT data on six candidate sources near the Galactic center. These sources have pulsar-like radio spectra and are located in an area of excess gamma-ray emission detected by *Fermi.* One of the leading hypotheses for the origin of this emission is a large population of millisecond pulsars. While we did not detect any pulsations from the six sources, the observations allow us to place limits on their pulsed radio emission.

DoD Impact/Significance: The main goal is to find millisecond pulsars that are very stable rotators and therefore are useful for detecting gravitational waves with a pulsar timing array (PTA). Among the ~3,300 known pulsars, only 35 fit this criterion and any addition to this set is a significant contribution to the nanohertz gravitational wave detection effort as it improves the sensitivity of the PTA. A detection of these low-frequency gravitational waves will set the ultimate stability of pulsars as clocks.

The objective of modeling pulsar light curves is to obtain measurements of neutron star masses and in order to constrain the equation of state of ultradense matter, with densities twice that of nuclear matter, that cannot be reproduced in a laboratory.

This work is important because millisecond pulsars can be used as a basis of a GPS-independent navigation and timekeeping system for spacecraft and these studies will assess the limiting accuracy of such systems. This supports the goals of the NRL Space Focus Area and addresses needs in the 2017 Naval Research and Development Framework and the DON 30 Year Research and Development Plans. This work will also maintain NRL leadership in this technical area and will provide expertise useful to USNO and other government partners.

*This work was supported by NASA and ONR

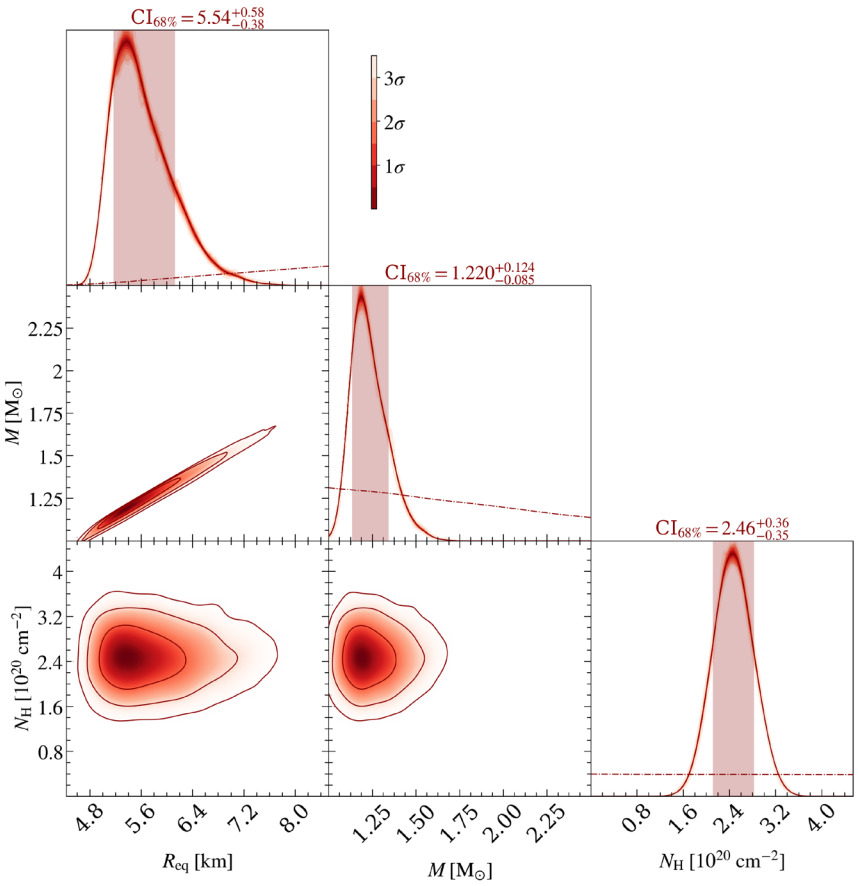


Figure 1. Results from one of our maximum likelihood models of the X-ray emission of PSR J1231-1411based on NICER and XMM data. The emission was modeled as coming from two hot spots with independent shapes and locations on the pulsar's surface. The plot shows contours of the posterior distributions of some of the main parameters: radius, mass, and hydrogen column density along the line of sight to the pulsar. In the top panel in each column, dashed lines represent the prior for each parameter, a solid line shows the posterior distribution, and a shaded region represents the 68% posterior confidence interval.

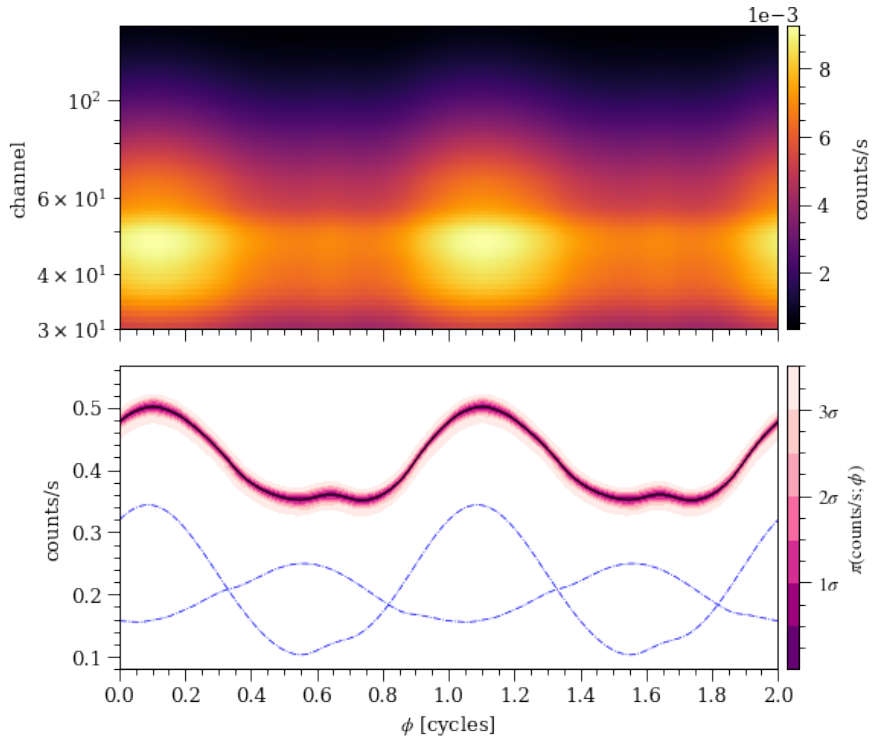


Figure 2. Top: NICER counts per second vs. energy channel and pulse phase. The brighter areas of the plot indicate more emission; the main pulse occurs at phase 0.0 to 0.2 and a small interpulse is visible at phase 0.5 to 0.6.

Bottom: The maximum likelihood light curves of the two modeled hot spots (blue) and the combined light curve (purple) vs. counts per second and pulse phase.

Title: Dynamic Phenomena in the Solar Atmosphere
Author(s): J.E. Unverferth
Affiliation(s): National Research Council Postdoctoral Fellow, U.S. Naval Research Laboratory, Washington, DC
CTA: SAS

Computer Resources: Cray XC40/50 [ERDC, MS]

Research Objectives: The goal of this HPC program is to investigate the mechanisms behind space weather events that influence and impact both DoD and civilian navigation and communication systems. This program focuses on eventually predicting the occurrence and behavior of the solar events that drive space weather. The two solar events of interest are coronal mass ejections (CMEs) and solar flares. Both of these phenomena are tied to the evolution of the magnetic field in the solar atmosphere after it emerges from the solar interior. The fundamental process we are investigating is how energy is released from the magnetic field after being driven by the interior.

Methodology: Our work focuses on the evolution of magnetic fields in the solar atmosphere after they have emerged from the solar interior, with the goal of understanding the energy release from a current sheet in the corona. This year, we performed three-dimensional (3D) numerical simulations of a model current sheet. We used this simulation to investigate the evolution of magnetic flux as it underwent magnetic reconnection through the current sheet. The goal of this investigation is to determine how one-dimensional (1D) simulations of individual flux elements can be improved if driven by a 3D model instead of *ad hoc* initial conditions based on inferred characteristics. For these studies, we use the 3D MHD code LARE3D.

Results: This year, we have studied the evolution of magnetic flux undergoing reconnection mediated by a current sheet placed in the low solar atmosphere. We have developed tracking to ensure that we are tracking similar field lines as they reconnect and change the connectivity. We have created the framework to take the evolution of a field line from the LARE3D simulation and to extract the necessary information to pass into a 1D simulation as the initial condition.

This effort addresses how the magnetic field in a solar eruptive event can influence the splitting of released energy into different forms. Capturing the correct split of energy into phenomena like electron beams, bulk motion, and local heating is vital to being able to reproduce these events.

DoD Impact/Significance: The simulations that this investigation is creating are helping to understand the energy release mechanism involved in solar events. Understanding the reconnection mechanism and how it partitions energy between various effects is important to being able to predict the onset and effects of solar phenomena.

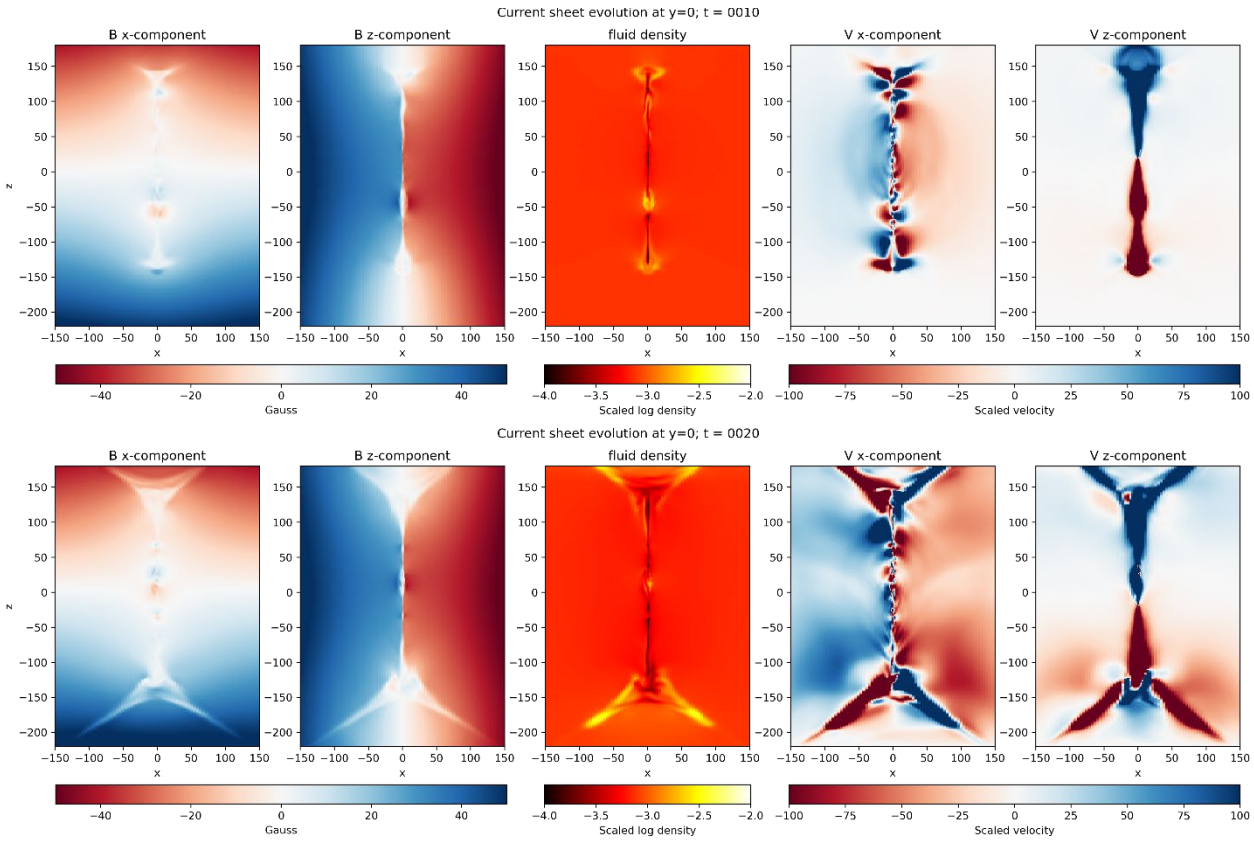


Figure 1. Evolution of the current sheet viewed edge on. The top row displays the current sheet at 10 seconds and the bottom at 20 seconds. From left: horizontal magnetic field, vertical magnetic field, fluid density, horizontal velocity, vertical velocity. In the middle panel, the brighter the color, the denser the fluid. In the other panels, blue represents a positive value, red a negative, with darker colors representing stronger values.

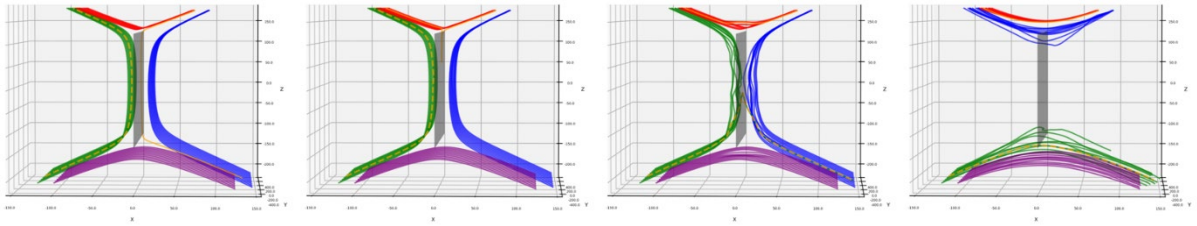


Figure 2. Magnetic field lines, colored by their initial connectivity, displayed around the current sheet in gray. These reconnect through the current sheet, changing from four distinct groupings into two over tens of seconds.

Title: Particle-in-Cell Simulations of Plasma Waves and Turbulence
Author(s): A.R. Soto-Chavez
Affiliation(s): U.S. Naval Research Laboratory, Washington, DC
CTA: SAS

Computer Resources: HPE Cray Shasta [AFRL, OH]; Cray Shasta [NAVY, MS]

Research Objectives: The objectives of this project are: 1) to support the U.S. Naval Research Laboratory and Defense Advanced Research Projects Agency SMART sounding rocket experiment program by developing the capability to simulate near-Earth space plasmas on a kinetic scale in order to predict and assess possible scenarios, 2) to be able to choose mission parameters and to understand the data from the experiment, 3) to gain deeper understanding of the nonlinear induced scattering process in a turbulent plasma, 4) to support the U.S. Naval Research Laboratory Space Chamber Experiments by performing nonlinear simulations of plasma-beam instabilities, and 5) to apply the understanding of turbulence gained from the SMART experiment to the turbulence in the solar wind (SW). Note the SMART experiment launch has moved from 2021 to sometime in the summer of 2023. Also, the SW studies will be performed in the fall of 2023.

Methodology: We used the Tristan-MP code, which is a massively parallel (MP) particle-in-cell (PIC) code that has been tested in HPC systems. Tristan-MP has been used successfully to simulate magnetosphere "chorus" and "whistlers" space plasma waves by the PI.

Results: This year, we conducted several large two-dimensional (2D)-PIC simulations of ion-ring instability leading to the successful excitation and creation of whistler waves. The whistler waves are the result of a nonlinear phenomenon in plasmas that we call nonlinear induced scattering. This nonlinear scattering is at the heart of the SMART experiment and is something that we needed to test. Some of the major results we found were:

1) The confirmation of the generation of whistler waves by the nonlinear scattering mechanism, Fig.1. (Although the nonlinear scattering is expected to be faster in three dimensions (3D), there is a slower version of the scattering that persists in 2D).
2) The observation, for the first time in a PIC code, of the quasi-modes (nonlinear density perturbations, see Fig. 2 below) that arise due to the nonlinear scattering process. These quasi-modes had been predicted theoretically but had never been seen to come out directly of a PIC simulation.
3) We varied parameters, such as ion-to-electron mass ratios, and temperatures, with the objective of testing theory, experiment, and other PIC simulations results. In all cases, we are able to find the excitation of the whistler waves.

DoD Impact/Significance: The SMART experiment and associated simulations will ultimately demonstrate the formation of turbulence and its coupling between the ionosphere and the magnetosphere. Given the DoD and U.S. Navy reliance on spaceborne assets, understanding kinetic-scale processes in the space environment gives the Navy new capabilities to predict, prepare for, respond to, and recover from space weather events.

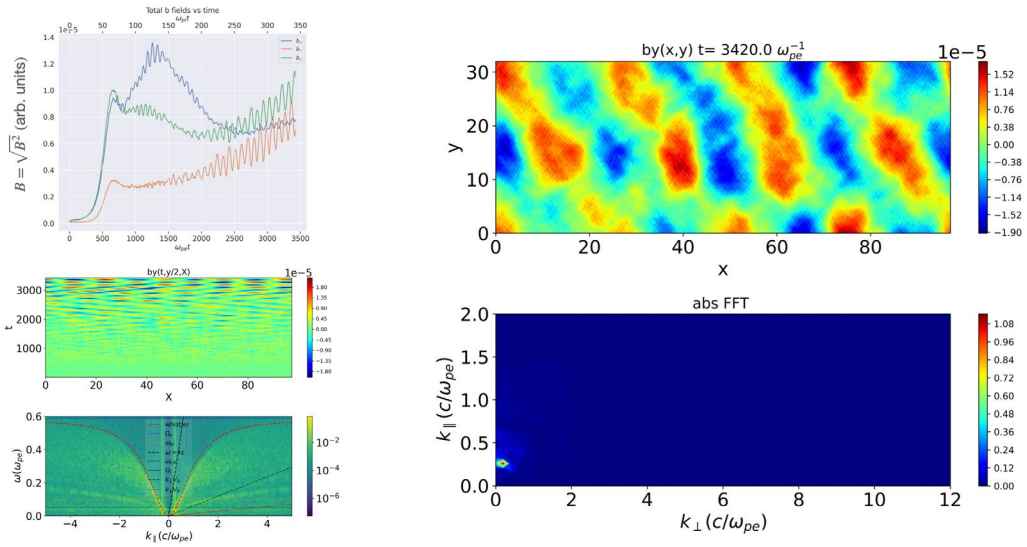
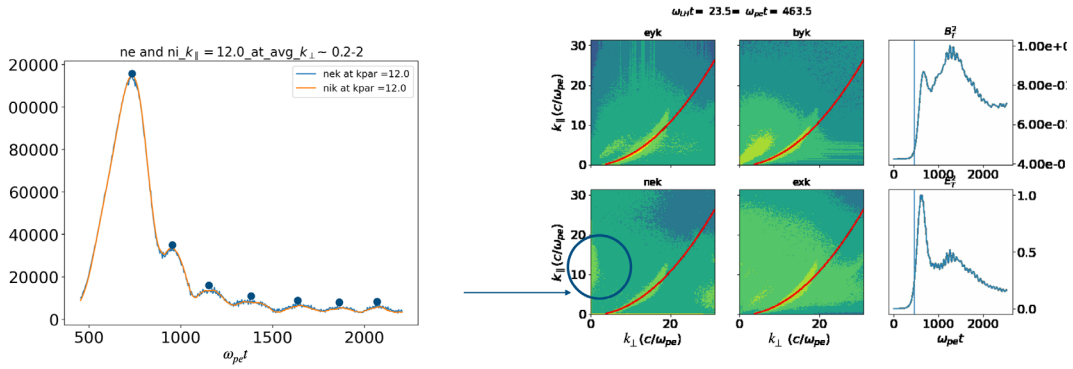


Figure 1. The whistler waves generation snapshot from a 2D PIC simulation. Top left: the three magnetic field magnitudes time histories. Bottom left: The whistler wave fronts as a function of time (middle panel) and their dispersion relation (bottom). Right: The whistler waves in real space and k-space (top and bottom respectively) at the indicated time. This confirms the generation of whistler waves.



$$\frac{\Delta\omega}{\Delta k_\parallel} = 1.4\times10^{-3}c \lesssim \theta_e = 6.3\times10^{-3}c$$

Figure 2. Left: The electron (and ion) density perturbations as a function of time (a.k.a. quasi-modes). Right: Snapshot of the fields' FFT and density perturbations (nek). The blue circle indicates the quasi-modes propagating down in k-space. This region is then enlarged and plotted as a function of time on the left. This confirms the nonlinear perturbation due to the nonlinear scattering.

Title: Thermosphere & Ionosphere Numerical Models and Ensemble Methods
Author(s): D.P. Drob, M. Jones, and J. Emmert
Affiliation(s): Naval Research Laboratory, Washington, DC
CTA: SAS

Computer Resources: HPE Cray Shasta, HPE SGI 8600 [AFRL, OH]; Cray Shasta, HPE SGI 8600 [NAVY, MS]

Research Objectives: This effort seeks to specify the weather of Earth's ionosphere and thermosphere for high-frequency (HF) radio wave applications. Accurate and computationally efficient numerical models are needed to specify and forecast the density, ion-neutral composition, winds, and temperatures of the near-Earth space environment. This environment is perturbed from below by solar-heating-driven tides and internal waves, and from above by ionizing extreme ultraviolet solar radiation from sunspot variations, as well as fluctuations in the solar wind that interact with the Earth's magnetic field.

Methodology: A number of first-principles thermosphere and ionosphere numerical models are utilized for this effort. The National Center for Atmospheric Research (NCAR) Thermosphere Ionosphere Mesosphere Electrodynamics - General Circulation Model (TIME-GCM) provides a means to investigate the influence of lower atmospheric perturbations on the ionosphere-thermosphere system. A whole-atmosphere configuration of the Navy Environmental Prediction System Utilizing a Non-hydrostatic Engine (NEPTUNE) model is being coupled to the NRL SAMI3 (Sami is Another Model of the Ionosphere – version 3) ionosphere model to also investigate these effects in tandem. Version 4 of the SAMI model, with improved physics and operational forecast capabilities, is also being developed as part of this effort.

Results: Numerical experiments were performed with the TIME-GCM by specifying the lower atmosphere perturbations with observation analysis from the high-altitude version of the Navy Operational Global Atmospheric Prediction System (NAVGEM-HA). A series of 72-hour forecast experiments was also performed by coupling the NEPTUNE and SAMI3 models to explore the two-way exchanges of mass, momentum, and energy between the thermospheric and ionospheric state variables. For the SAMI4 model, stochastic ensemble Kalman filter (EnKF) data-assimilation methods were improved to update the initial forecast model state variables, as well as uncertain model parameters, to improve short- (< 6-hrs) and medium-range (6- to 72-hrs) ionospheric forecast skill. Figure 1 shows the root mean square error (RMSE) for 6-hour SAMI4 forecasts (green) and the default untuned SAMI4 model (blue) against objective observational analysis between ± 65° geomagnetic latitude. Lower RMSE values are better. The frequency at maximum electron density (FoF_2) is shown (top) and the total electron content of the ionosphere < 480 km altitude bTEC is shown (below). To achieve these improvements, Fig. 2 shows the natural logarithm of scaled SAMI4 model parameters from a 48-member ensemble (0 = unperturbed default scalar, 0.1 = ~10% adjustment), (top) secondary photoelectron production efficiency, (middle) [O+]-[O] momentum coupling efficiency, (bottom) and secondary photoelectron heating efficiency. For these numerical experiments, these are only three of the nine forecast model parameters that are dynamically corrected every three hours, utilizing the prior six hours of available observations and the previous forecasts in order to improve the forecast model skill as shown in Fig. 1.

DoD Impact/Significance: The coupled physical-based thermosphere-ionosphere model validation studies performed here address the DoD/Navy's long-term need for environmental prediction of space weather effects for tactical planning purposes, as well as the maximization of DoD HF and space systems performance though adaption to the variable environment (ref: SECNAVINST 2400.2A).

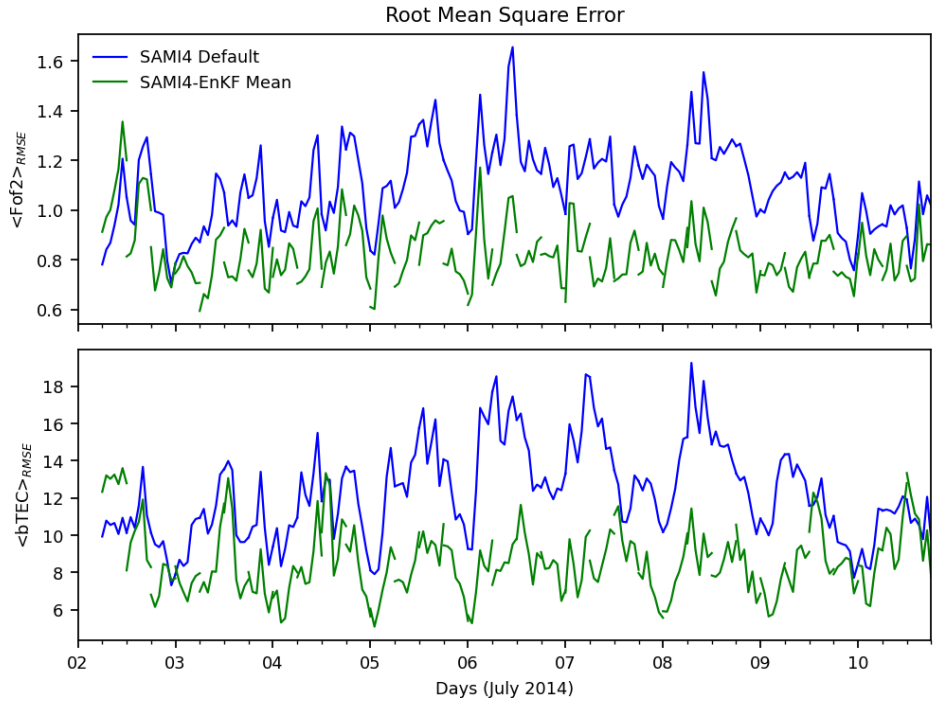


Figure 1. RMSE for 6-hour SAMI4-EnKF forecasts (green) and the default SAMI4 model (blue) against objective observational analysis between ± 65° geomagnetic. Lower RMSE values are better. (Upper) plasma frequency at maximum altitude of electron density (FoF_2), (lower) bottom side total integrated electron density content < 480 km (bTEC).

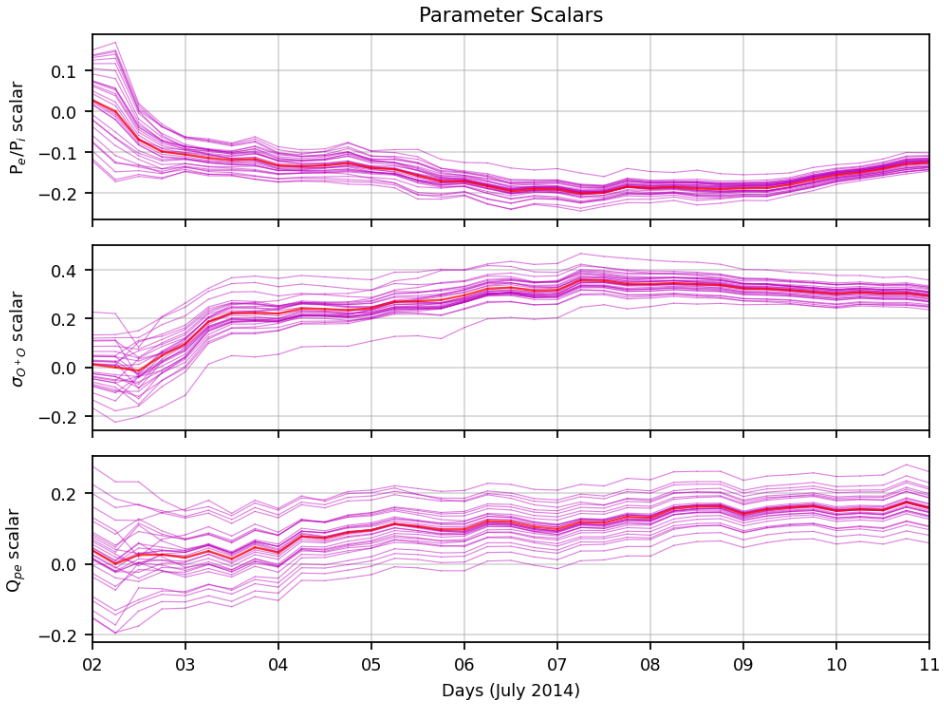


Figure 2. Ensemble estimates (from a 48-member ensemble) of natural logarithm of scaling factors applied to SAMI4 model physics parameters; (top) secondary photoelectron production efficiency, (middle) $[O^+]$-[O] momentum coupling efficiency, and (bottom) secondary photoelectron heating efficiency.

THIS PAGE INTENTIONALLY LEFT BLANK



Other

Work that is not easily categorized as one of the other computational technology areas.

Title: Simulation of High Energy-Radiation Environments
Author(s): J. Finke and W. Duvall
Affiliation(s): U.S. Naval Research Laboratory, Washington, DC
CTA: OTH

Computer Resources: Cray XC40/50 [ERDC, MS]; Cray Shasta [NAVY, MS]

Research Objectives: (1) Apply three-dimensional (3D) Monte Carlo methods to simulate the transport of high-energy particles for use in space applications and for modeling detection systems, radiation environments, and the operational concepts relevant to the detection of special nuclear materials and other radiological/nuclear materials in maritime and urban scenarios of interest to DoD and other civilian agencies. (2) Create an improved model of the extragalactic background light (EBL) useful for the study of extragalactic sources by a number of instruments, including the Fermi Gamma-ray Telescope and the future Cherenkov Telescope Array.

Methodology: (1) We use three industry-standard ionizing radiation transport codes: two 3D Monte Carlo packages, Geant4 (CERN) and Monte Carlo N-Particle (MCNP) from Los Alamos National Lab (LANL), and one discrete ordinates package, Denovo (Oak Ridge National Lab). We use an NRL-developed front-end package called SoftWare for Optimization of Radiation Detectors (SWORD) to quickly prototype geometries and radiation environments for running our simulations. (2) We use a model of the EBL created by Co-PI Finke and fit it with a Markov chain Monte Carlo (MCMC) to a wide variety of data from the literature to determine model parameters and strongly constrain a number of quantities of astrophysical significance and of use to observations of extragalactic gamma-ray sources.

Results: (1) Several SWORD simulation runs contributed to an ongoing effort to validate the Nuclear Detection Figure of Merit (NDFOM) simulation environment from LANL. In this case, Monte Carlo results for specific detectors run on HPC resources were compared to the semi-analytical results from NDFOM. This work was done as part of the Data Mining Analysis and Modeling Cell (DMAMC), a program of the Department of Homeland Security/Countering Weapons of Mass Destruction (DHS/CWMD) Office. SWORD 7 also was released in FY22 and was installed onto the HPC system. Some of the HPC time was used to validate SWORD 7. In addition, SWORD runs on the HPC systems were used to study atmospheric gamma-ray propagation from terrestrial gamma-ray emission as part of the Surveying Ingress Pathways for Energetic Radiation Background (SUPERB) program, also for DHS/CWMD. (2) Co-PI Finke's research has led to the measurement and constraints on a number of interesting quantities of astrophysical interest. This includes the mean metallicity and mass density evolution of the universe across cosmic time and the cosmic star formation rate (SFR). The 68% constrain from the MCMC fit to luminosity density data is shown in Fig. 1 from an MCMC fit with our EBL model. The model provides a good fit to the data.

DoD Impact/Significance: (1) Our 3D Monte Carlo radiation modeling allows us to provide timely answers to the questions posed by DHS/CWMD, the Defense Threat Reduction Agency (DTRA), the National Aeronautics and Space Administration (NASA), the DoD, and other government sponsors about radiation environments and detectors. The science addressed by ionizing radiation simulations such as the studies described above is often impractical or not cost effective to study in any manner other than simulation. (2) The EBL absorbs gamma rays from extragalactic objects, and thus, understanding the EBL is crucial to studying these types of high-energy sources. Understanding how high-energy particles are accelerated and produce ionizing radiation in these sources helps researchers understand the high-energy radiation environment that can affect DoD space assets.

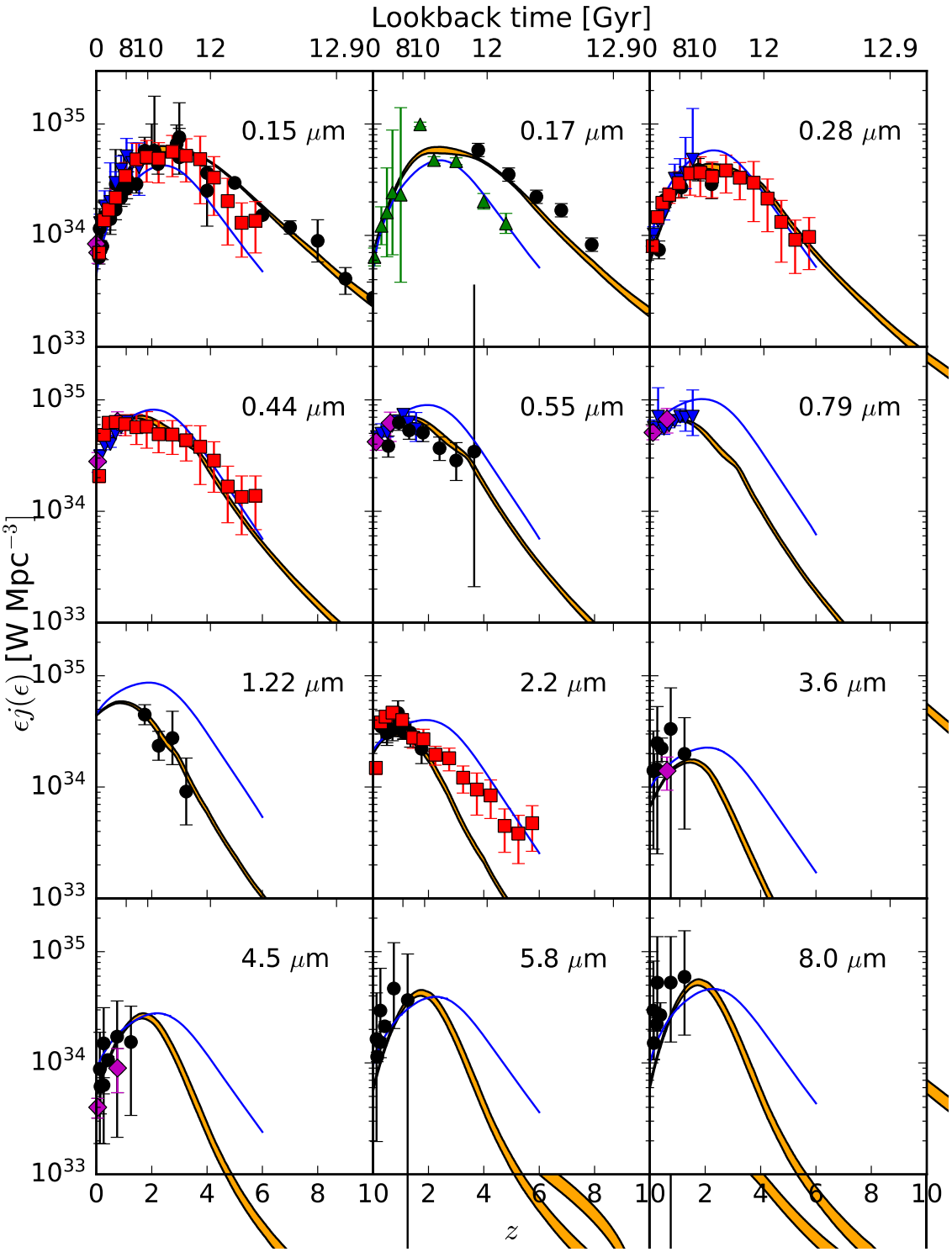


Figure 1. The luminosity as a function of redshift, or equivalently, lookback time, for several wavelengths. The orange shaded regions represent the 68% confidence intervals from MCMC fits to the gamma-ray and luminosity density data. The black, red, and violet points represent measurements from galaxy sky surveys. The blue curves represent the model by Co-PI Finke published in 2010.

THIS PAGE INTENTIONALLY LEFT BLANK

Author Index

Adams, I. ---------- 36
Adamson, P.E. ---------- 88, 90
Alatishe, J. ---------- 92
Allard, R. ---------- 106
Allen, D.R. ---------- 108
Amos, C.M. ---------- 140, 144, 148
Antillon, E. ---------- 2
Arcari, A. ---------- 8

Barron, C. ---------- 142
Barton, C.A. ---------- 108
Barton, N. ---------- 152
Bateman, S.P. ---------- 36
Bates, J.W. ---------- 12
Bernstein, N. ---------- 50
Bird, L.J. ---------- 56
Bojko, B.T. ---------- 20, 40
Burleigh, M.R. ---------- 166

Calantoni, J. ---------- 36
Campbell, T. ---------- 106, 114
Campbell, W.F. ---------- 150
Carl, G. ---------- 152
Carr, E. ---------- 148
Carrier, M. ---------- 142, 144, 146, 148
Cayula, S. ---------- 138
Champlain, J.G. ---------- 82
Christophersen, J. ---------- 152
Colston, S.M. ---------- 56
Compton, J.R. ---------- 56
Cooley, K.A. ---------- 82
Crawford, W. ---------- 152
Crout, J. ---------- 142

D'Addezio, J. ---------- 142, 144, 146, 148
Davis, W. ---------- 152
DeHaan, C. ---------- 142
Deneva, J. ---------- 168
deRada, S. ---------- 148
Douglass, E. ---------- 106, 122
Doyle, J.D. ---------- 110
Drob, D.P. ---------- 174
Duvall, W. ---------- 178

Eckermann, S.D. ---------- 108
Edwards, K. ---------- 32, 36, 106

Fabre, J.P. ---------- 94
Fan, Y. ---------- 112
Finke, J. ---------- 178
Flatau, M. ---------- 114, 152
Fletcher, A. ---------- 160, 162
Foster, J.C. ---------- 88
Fragiadakis, D. ---------- 80

Gamezo, V.N. ---------- 14
Gatling, G.R. ---------- 102
Giles, I.D. ---------- 58
Goodwin, G. ---------- 16

Haiducek, J. ---------- 164
Hansen, K. ---------- 152
Harrison, S. ---------- 32
Hebert, D. ---------- 106, 130
Helber, R. ---------- 126
Hellberg, C.S. ---------- 52
Helmboldt, J. ---------- 164
Herrera, M.A. ---------- 108
Hervey, W.J. ---------- 54, 56
Hess, A.M. ---------- 20
Hodyss, D. ---------- 166
Hoppel, K.W. ---------- 108
Huba, J.D. ---------- 42

Imler, G.H. ---------- 58

Jacobs, G.A. ---------- 140, 142, 146
Janiga, M. ---------- 152
Jensen, T. ---------- 106, 114
Johannes, M. ---------- 60
Johnson, R.F. ---------- 18, 20
Jolliff, J.K. ---------- 116

Kearney, W.S. ---------- 36
Kelly, J.F. ---------- 108
Kessler, D.A. ---------- 20
Khine, Y. ---------- 22, 30, 118

Author Index

Komaromi, W.A. ---------- 120
Krall, J. ---------- 42
Kuhl, D.D. ---------- 108
Kuna, L.P. ---------- 6, 8
Kushto, G. ---------- 78

Ladner, S. ---------- 116
Lambrakos, S. ---------- 62
Leary, D.H. ---------- 56
Linzell, R. ---------- 142, 148
Liu, J. ---------- 24, 26
Liu, M. ---------- 152
Luecke, C. ---------- 114
Lyons, J.L. ---------- 64

Ma, J. ---------- 108
Matt, S. ---------- 28
May, J. ---------- 130, 148
McDonald, S.E. ---------- 166
McLay, J. ---------- 152
Metzger, E.J. ---------- 124, 126, 128, 132
Metzler, C.A. ---------- 166
Meyer, J.R. ---------- 96
Michopoulos, J.G. ---------- 8
Montiforte, V. ---------- 144, 146, 148
Moskaitis, J. ---------- 152
Mott, D.R. ---------- 30

Ngodock, H. ---------- 142, 144, 146, 148

Obenschain, K. ---------- 12
Orzech, M. ---------- 136
Osborne, J.J. ---------- 140, 144, 146, 148
Ouellette, J.D. ---------- 100

Panteleev, G. ---------- 148
Penko, A.M. ---------- 32, 36
Penta, B. ---------- 138
Perkins, F.K. ---------- 84
Petrov, G.M. ---------- 98
Phelps, M. ---------- 106, 130, 148
Phillip, R. ---------- 32, 36
Phillips, M. ---------- 66
Poludnenko, A.Y. ---------- 14
Povolotskyi, M. ---------- 96

Ramamurti, R. ---------- 38, 44
Ray, P.S. ---------- 168
Reinecke, P.A. ---------- 120
Reinecke, T.L. ---------- 68
Reynolds, C. ---------- 152
Rhodes, T. ---------- 108
Ridout, J. ---------- 152
Rittersdorf, I.M. ---------- 90
Rosenberg, A. ---------- 78
Rowley, C. ---------- 144, 146, 148
Rushley, S. ---------- 152
Rydbeck, A. ---------- 106, 114

Sassi, F. ---------- 166
Saunders, R.N. ---------- 4, 6, 8
Schoenauer, S. ---------- 32, 36
Schweigert, I.V. ---------- 70, 72
Schwer, D.A. ---------- 34, 46
Shabaev, A. ---------- 62
Sharp, C.H. ---------- 84
Shriver, J.F. ---------- 126
Shulman, I. ---------- 138
Simeonov, J.A. ---------- 36
Sletten, M.A. ---------- 100
Smedstad, L. ---------- 142, 148
Smith, L.N. ---------- 156
Smith, S. ---------- 142, 144, 146, 148
Smith, T. ---------- 106, 116
Soto-Chavez, A.R. ---------- 172
Souopgui, I. ---------- 142, 144, 146, 148
Swanekamp, S.B. ---------- 88, 90

Tan, X.G. ---------- 4
Tate, J.L. ---------- 166
Teferra, K. ---------- 6
Tejero, E.M. ---------- 102
Thoppil, P. ---------- 134
Toporkov, J.V. ---------- 100
Townsend, T. ---------- 130, 148
Tschirhart, T. ---------- 56

Author Index

Tsu, J. ---------- 150

Unverferth, J.E. ---------- 170

Veeramony, J. ---------- 32, 36, 106
Viner, K. ---------- 152
Viswanath, K. ---------- 38
Vora, G.J. ---------- 54, 56
Vurgaftman, I. ---------- 96

Wang, D. ---------- 114
Wang, Z. ---------- 56
Weber, B.V. ---------- 90
Welland, I. ---------- 68
Whitcomb, T. ---------- 152
Whitener, K. ---------- 74
Wickramaratne, D. ---------- 76
Wijesekera, H. ---------- 114
Wimmer, S.A. ---------- 8

Yang, S. ---------- 152
Yu, Z. ---------- 132

Zamudio, L. ---------- 124, 128

Division/Branch Index

Systems Directorate (Code 5000)

Radar Division (Code 5300)

Surveillance Technology (Code 5340) 92

Information Technology Division (Code 5500)

Navy Center for Applied Research In Artificial Intelligence (Code 5510) 156

Optical Sciences Division (Code 5600)

Optical Physics (Code 5610) 78, 96

Materials Science and Component Technology Directorate (Code 6000)

Laboratories for Computational Physics and Fluid Dynamics (Code 6040).....12, 14, 18, 20, 22, 24, 26, 30, 34, 38, 40, 44, 46, 118

Chemistry Division (Code 6100)

Materials Chemistry and Dynamics (Code 6120)..... 80
Center for Corrosion Science and Engineering (Code 6130) 8
Surface Chemistry (Code 6170) 74
Navy Technology Center for Safety and Survivability (Code 6180) 70, 72

Materials Science and Technology Division (Code 6300)

Multifunctional Materials (Code 6350) 4, 6, 8
Materials and Sensors (Code 6360) 62
Center for Materials Physics and Technology (Code 6390)..... 2, 8, 50, 52, 60, 62, 64, 66, 76

Plasma Physics Division (Code 6700)

Laser Plasma (Code 6730)..... 12
Charged Particle Physics (Code 6750) 42, 102, 160, 162, 172
Pulsed Power Physics (Code 6770) 42, 88, 90
Beam Physics (Code 6790)..... 98

Electronics Science and Technology Division (Code 6800)

Senior Scientist for Nanoelectronics (Code 6803)..... 68
Quantum and Optoelectronics (Code 6810) 68

Electromagnetic Technology (Code 6850) 82
Power and Advanced Materials (Code 6880) 84

Center for Biomolecular Science and Engineering (Code 6900)

Principal Scientist for Biotechnology (Code 6904) 54, 56
Laboratory for Bio/Nano Science and Technology (Code 6910) 54, 56, 58
Laboratory for Biomaterials and Systems (Code 6920) 56
Laboratory for Molecular Interfaces (Code 6930) 58

Ocean and Atmospheric Science and Technology Directorate (Code 7000)

Acoustics Division (Code 7100)

Acoustics Simulation, Measurements, and Tactics (Code 7180) 94

Remote Sensing Division (Code 7200)

Radio/Infrared/Optical Sensors (Code 7210)..... 164
Remote Sensing Physics (Code 7220) 100, 108, 166
Image Science and Applications (Code 7260)..... 100

Ocean Sciences Division (Code 7300)

Ocean Dynamics and Prediction (Code 7320).... 32, 36, 106, 112, 114, 116, 122, 124, 126, 128, 130, 132, 134, 136, 140, 142, 144, 146, 148
Ocean Sensing and Processing (Code 7330) 28, 114, 116, 138, 148
Seafloor Sciences (Code 7350)..... 32, 36

Marine Meteorology Division (Code 7500)

Senior Scientist for Mesoscale Meteorology (Code 7503)..... 110
Probabilistic Prediction Research Office (Code 7504)..... 152
Atmospheric Dynamics and Prediction (Code 7530) 114, 120, 150, 152
Meteorological Applications Development (Code 7540) 152

Space Science Division (Code 7600)

Special Projects Office for High Altitude Numerical Weather Prediction (Code 7604) 108
Geospace Science and Technology (Code 7630)..... 108, 166, 174
High-Energy Space Environment (Code 7650) 168, 178
Solar and Heliospheric Physics (Code 7680)..... 170

Naval Center for Space Technology (Code 8000)

Spacecraft Engineering Division (Code 8200)

Design and Verification (Code 8220) 16

Site Index

DSRCs

AFRL	2, 4, 6, 8, 12, 14, 18, 20, 22, 24, 26, 30, 36, 38, 42, 44, 50, 52, 54, 56, 60, 62, 64, 66, 68, 70, 72, 74, 78, 80, 82, 84, 88, 92, 96, 100, 118, 150, 152, 156, 164, 172,174
ARL	20, 28, 30, 38, 52, 58, 62, 64, 66, 70, 76, 80, 120, 160, 162
ERDC	2, 6, 14, 20, 22, 24, 30, 36, 38, 42, 50, 52, 54, 56, 58, 60, 62, 64, 66, 68, 90, 100, 108, 110, 118, 120, 124, 128, 132, 152, 166, 168, 170, 178
NAVY	4, 6, 8, 14, 16, 20, 22, 24, 26, 30, 32, 34, 36, 38, 40, 46, 52, 62, 64, 70, 72, 80, 82, 88, 90, 92, 94, 96, 98, 100, 102, 106, 108, 110, 112, 114, 116, 118, 120, 122, 124, 126, 128, 130, 132, 134, 136, 138, 140, 142, 144, 146, 148, 150, 152, 162, 166, 172, 174, 178

THIS PAGE INTENTIONALLY LEFT BLANK